



Univerzita Tomáše Bati ve Zlíně

Centrum polymerních systémů

Disertační práce

Polymerní kompozitní materiály pro nositelnou elektroniku

Polymer composite materials for wearable electronic

Autor: **Ing. Romana Štěpančíková**

Studijní program: Nanotechnologie a pokročilé materiály (P3972)

Studijní obor: Nanotechnologie a pokročilé materiály (3942V006)

Školitel: Prof. Ing. Petr Slobodian, Ph.D.

Konzultant: Ing. Robert Olejník, Ph.D.

Externí zkoušející:

Zlín, Prosinec 2024

© Romana Štěpančíková

Vydala **Univerzita Tomáše Bati ve Zlíně** v edici **Disertační práce**.
Publikace byla vydána v roce 2024.

Klíčová slova v češtině: Polymerní kompozity; uhlíkové nanotrubicice; nositelná elektronika; chytré textilie; chytrá obuv; piezoresistivní senzory; piezoelektrické senzory; vodivé cesty; funkcionalizace.

Klíčová slova v angličtině: Polymer composite; carbon nanotubes; wearable electronic; smart textile; smart shoe; piezoresistive sensors; piezoelectric sensors; conductive paths; functionalization.

Plné znění disertační práce je k dispozici v knihovně UTB ve Zlíně.

PODĚKOVÁNÍ

Chtěla bych upřímně poděkovat svému školiteli profesoru Petru Slobodianovi, PhD. za jeho vedení, podporu a povzbuzení v mém doktorském studiu.

Dále děkuji za přínosné rady a vedení v experimentální části od mého konzultanta Ing. Roberta Olejníka, Ph.D. a Ing. Jiřího Matyáše, Ph.D.

Děkuji všem spoluautorům mých publikací, že se se mnou podělili o své zkušenosti a odborné rady. Děkuji Ing. Lukáši Münsterovi, Ph.D. za zaškolení na rastrovacím skenovacím mikroskopu. Děkuji Ing. Milanu Masařovi, Ph.D. za odborné konzultace v oblasti mikroskopie.

Další poděkování směřuje panu profesoru Ivu Kuřitkovi, Ph.D. za vstřícnost a odborné konzultace v oblasti nanomateriálů a nanotechnologií.

V neposlední řadě patří poděkování mé celé rodině za podporu a naslouchání během mého studia. Zejména bych ráda poděkovala svému manželovi Lud'kovi a dcerám Elišce a Kláře za pomoc podporu pochopení a trpělivost.

ABSTRAKT

Popularita nositelné elektroniky a nositelných technologií stále roste. V budoucnu se očekává, že se nositelné technologie stanou nepostradatelnou součástí našeho každodenního života. I potenciální aplikace naznačují, že budoucnost bude s nositelnými technologiemi bezpečnější, jednodušší, zdravější, rychlejší a zábavnější.

Zařízení pro nositelnou elektroniku musí splňovat následující parametry jako flexibilita, snadná implementace, jednoduchá vyrobiteľnosť a nízka cena. Na tyto všechny parametry byl v naší práci kladen velký důraz. Pro aplikaci senzorů byly vybrány komerčně dostupné předměty, jako sportovní tričko a obuv, do kterých byly zabudovány naše piezoresistivní senzory na bázi polymerních kompozitů a uhlíkových nanotrubic. Dále byla testována možnost uplatnění mechanoelektrické konverze principem piezoelektrickým pro konstrukci samonapájecích senzorů mechanického stimulu s zacílením na nositelnou elektroniku.

Bylo monitorováno několik charakteristik dýchání u jednotlivce i porovnání dýchání u dvou dobrovolníků. Naše piezoresistivní senzory jsou schopny monitorovat dýchání citlivě, vratně a opakovatelně. Senzory do stélky boty byly umístěny na plochu komerční stélky tak, aby snímaly tlak při chůzi a nenarušily integritu stélky. Obě naše řešení jak monitorování lidského dechu, tak detekce a měření došlapu se od základního materiálového výzkumu posunuly do oblasti vývoje a optimalizace komplexního řešení těchto aplikací.

ABSTRACT

The popularity of wearable electronics and wearable technology continues to grow. In the future wearable technology is expected to become an indispensable part of our daily lives. Even the potential applications suggest that the future will be safer, easier, healthier, faster, and more fun with wearable technology.

Wearable electronics as a field is developing considerably these days. Devices for wearable electronics require the following parameters such as flexibility, easy implementation, simple manufacturability, and low cost. A high impact was placed on all these parameters in this work. Commercially available objects, such as a sports T-shirt and shoes were selected for the application of the sensors, into which our piezoresistive sensors based on polymer composites and carbon nanotubes were built. Furthermore, the possibility of applying mechano-electrical conversion using the piezoelectric principle for the construction of self-powered mechanical stimulus sensors aimed at wearable electronics was tested.

Several characteristics of breathing in an individual were monitored as well as a comparison of breathing in two volunteers. Our piezoresistive sensors can monitor respiration sensitively, reversibly, and repeatably. Sensors in the insole of the shoe were placed on the surface of the commercial insole so that they sense the pressure during walking and do not disturb the integrity of the insole. Both of our solutions for human breath monitoring and footprint detection and measurement have moved from basic material research to the development and optimization of a comprehensive solution for these applications.

OBSAH

1	<u>ÚVOD</u>	8
2	<u>TEORETICKÁ ČÁST</u>	11
2.1	POLYMERŇÍ KOMPOZITY NA BÁZI UHLÍKOVÝCH TRUBIC	11
2.1.1	UHLÍKOVÉ NANOTRUBICE	11
2.1.2	METODY PŘÍPRAVY CNT POLYMERŇÍCH NANOKOMPOZITŮ	15
2.1.3	PIEZO REZISTIVŇÍ POLYMERŇÍ KOMPOZITY S CNT	15
2.2	POLYMERŇÍ KOMPOZITY S PIEZOELEKTRICKÝMI VLASTNOSTMI	17
2.2.1	POLYMERŇÍ SAMONAPÁJECÍ SENSORY MECHANICKÉHO STIMULU	18
2.2.2	PIEZOELEKTRICKÉ POLYMERŇÍ KOMPOZITY JAKO ZDROJ ENERGIE	18
2.3	NOSITELNÁ ELEKTRONIKA	19
2.3.1	UPLATŇĚŇÍ NOSITELNÉ ELEKTRONIKY	19
2.3.2	TECHNICKÁ OMEZENÍ V NOSITELNÉ ELEKTRONICE	22
2.3.3	VYŠÍVANÉ VODIVÉ CESTY	23
3	<u>CÍLE PRÁCE</u>	25
4	<u>EXPERIMENTÁLNÍ ČÁST</u>	27
4.1	MATERIÁLY	27
4.2	PŘÍPRAVA VZORKŮ	28
4.2.1	PŘÍPRAVA BUCKY PAPERU MWCNT	28
4.2.2	PŘÍPRAVA VZORKŮ PRO KRÍPOVÝ TEST	30
4.2.3	CHARAKTERIZAČNÍ TECHNIKY	30
4.3	METODY MĚŘENÍ	31
4.3.1	KRÍPOVÁ ZKOUŠKA	31
4.3.2	ZVÝŠENÍ CITLIVOSTI SENZORU	32
4.3.3	CHARAKTERISTIKA DÝCHÁNÍ	32
4.3.4	MĚŘENÍ PIEZOELEKTRICKÝCH CHARAKTERISTIK	33
4.3.5	ZATĚŽOVÁNÍ SENZORŮ VE STĚLCE BOTY	34
5	<u>VÝSLEDKY A DISKUZE</u>	36
6	<u>ZÁVĚR</u>	49

<u>REFERENCE</u>	<u>52</u>
<u>SEZNAM OBRÁZKŮ</u>	<u>59</u>
<u>SEZNAM SYMBOLŮ</u>	<u>61</u>
<u>CURRICULUM VITAE.....</u>	<u>63</u>
<u>SEZNAM PUBLIKACÍ.....</u>	<u>66</u>

1 ÚVOD

Kompozitní materiál je podle definice heterogenní systém složený ze dvou a více fází, které se liší složením nebo formou, zachovávající si své vlastní chemické a fyzikální vlastnosti a udržující rozhraní mezi jednotlivými složkami. Polymerní kompozitní materiály jsou pak většinou tvořeny spojitou polymerní maticí, v níž je distribuovaná druhá složka, o které podle vlastností, které přináší, můžeme hovořit jako o plnivu, výstuži, modifikátoru dalších vlastností matrice, může zlevňovat výsledný produkt a tak podobně. Polymerní matrice zajišťuje celistvost kompozitu a jeho tvar, dodává mu elastické vlastnosti a houževnatost. Plnivo pak pevnost, povrchovou tvrdost, elektrickou vodivost nebo třeba elektromagnetické stínění. Obecně aditiva do polymerů mohou představovat dvě základní skupiny materiálů. První s cílem ovlivnit nebo zlepšit zpracovatelské vlastnosti polymeru a druhá velká skupina látek, která se do polymeru přidává má cíl modifikovat, změnit, nebo zlepšit některé užité vlastnosti polymerního produktu. Mezi výše zmíněné procesní přísady mohou patřit modifikátory viskozity, látky ovlivňující stabilitu procesu nebo polymeru, nukleační přísady, příměsi například snižující tření produktu a hromadění nechtěné statické elektřiny ve vyrobené fólii a mnohé další a zůstávají tak i v produktu, často tak nechtěně vytvářejíce polymerní kompozit. Druhá skupina se pak přidává do produktu cíleně modifikovat užité vlastnosti. Mezi přísady, plniva, výztuže nebo jak je všechny vyjmenovat patří především materiály ovlivňující základní vlastnosti produktu jako jsou mechanické, elektrické, termické, optické, či chemické vlastnosti atd.

V současné době se vyrábí opravdu rozmanité druhy polymerních kompozitních materiálů jak z pohledu složení, struktury, technologie, ceny, ekologie nebo například i možné recyklace kompozitního odpadu. Přesto abychom mohli mluvit o kompozitním materiálu uvádí se většinou některá obecná kritéria pro jejich zařazení do této skupiny materiálů. Pokud pomíneme přesné vědecké definice kompozitu, jsou někdy tato tvrzení fádni a neurčitá a také se

mohou zásadně lišit případ od případu, od “vědeckého” úhlu pohledu či pohledu definovaného modifikovanou vlastností a funkcí kompozitu. Setkáváme se s tvrzeními, že kompozitní materiál je připravován mísením jednotlivých složek, objemový podíl vyztužující složky musí být alespoň, fyzikální, mechanické a chemické vlastnosti matrice a výztuže musí být značně odlišné atd. Je pravdou, že z pohledu modifikace polymerní matrice plnivem s ohledem na zlepšení mechanických vlastností matrice a mnohdy hledání i synergického spojení platí obecně výroky jako: vlastnosti výztuže i matrice kompozitu je nutné dokonale propojit na jejich rozhraní, zajistit co nejlepší přenos napětí při zatěžování celého kompozitu, jednotlivé složky kompozitního materiálu si zachovávají svoje charakteristiky, ale jako celek, respektive nový kompozit, dosahuje vlastností, které nejsou zdaleka tak dosaženy ani sečtením vlastností jednotlivých složek atd. Úkolem matrice je chránit výztuž před mechanickým a chemickým poškozením atd. Snahou tohoto popisu v úvodu disertační práce není zpochybňovat zažité zvyklosti, nabourávat používanou nomenklaturu nebo vytvářet „paralelní“ vědu, ale má podtrhnout myšlený cíl disertační práce. V podtitulu by mohlo být, hledání nových, přidaných či alternativních vlastností běžně používaných kompozitů. Nechceme popírat správnost, nutnost, efektivitu či znalosti dosažené výzkumem a zkušenostmi, ale naopak podívat se na tuto oblat s cílem dosažení u klasických řešení dalších, nových, mnohdy přidružených vlastností. Uveďme příklad. Použití uhlíkových trubic dispergovaných v polymerní matrici s cílem zvýšit mechanické vlastnosti matrice jsou primárním záměrem. Protože uhlíkové trubice jsou elektricky vodivé dochází také k modifikaci elektrických vlastností. A to od modifikace v oblasti antistatiky až po získání elektricky vodivého kompozitu. Takže plnivo přidáváme primárně pro modifikaci mechanických vlastností matrice. Výsledný kompozit tak ale současně může mít i další vhodné užité vlastnosti. Na kompozit může být nahlíženo z pohledu piezorezistivity. Mechanickým namáháním se mění rozměry kompozitního výrobku, rozložení plniva v matrici a pokud kompozit má měřitelnou elektrickou vodivost mění se

tato vlivem zmíněné deformace. Změna elektrické vodivosti se pak může stát mírou deformace kompozitu měřením jeho elektrické vodivosti. Uhlíkové plnivo primárně dispergované v polymerní matrici jako výztuž dodává současně i další užité vlastnosti. Kompozit má schopnost detekovat deformaci, můžeme být senzorem nebo můžeme třeba sledovat stav výrobku a jeho poškození.

Tato práce spadá do oblasti nositelné technologie, o kterou je během posledního desetiletí velký zájem. Nositelná technologie je interdisciplinární výzkumná oblast, která spojuje specialisty v oboru materiálů, výrobních technologií, elektroniky, informačních technologií, mikrosystémů atd. pro dosažení inovace ve vývoji nositelných elektronických produktů. Aplikační řešení práce se týká v použití kompozitních materiálů se schopností detekce aplikovaného mechanického stimulu. Jsou řešeny dva principiálně odlišné přístupy detekce. První je využití *piezorezistivních* vlastností polymerního kompozitu. Měřenou veličinou je zde elektrická vodivost, která se vlivem deformace kompozitu mění a stává se tak mírou deformace. Druhá oblast je využití *piezoelektrického* jevu, který představuje generování elektřiny deformací materiálu.

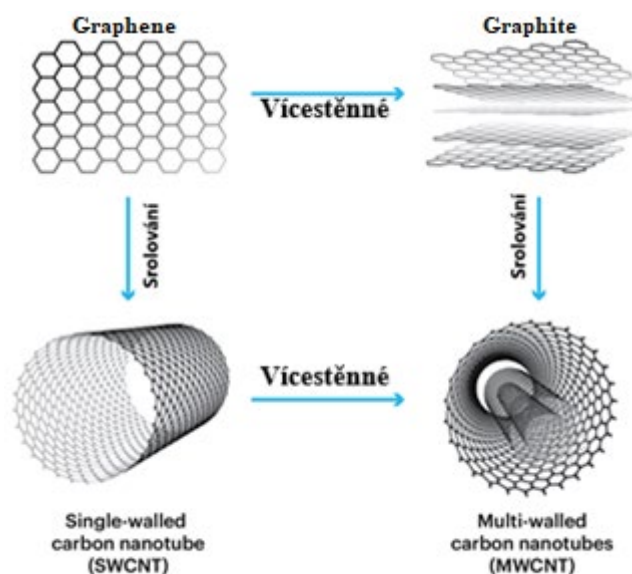
2 TEORETICKÁ ČÁST

2.1 Polymerní kompozity na bázi uhlíkových trubic

Pro naši aplikační oblast nositelné elektroniky jsou zkoumány polymerní nanokompozity s dispergovanými uhlíkovými trubicemi. Nanokompozit je obecně charakterizován přítomností dostatečně dispergovaného plniva, které má alespoň jeden rozměr menší než 100 nm. Mimořádné fyzikální vlastnosti CNTs spojené se snadno přizpůsobitelnými charakteristikami polymeru vedou k novým a všestranným nanokompozitům. V této práci je základním požadavkem dosažení elektrické vodivosti kompozitu. Tyto materiály pak mohou vykazovat **piezorezistivní vlastnosti**. Mohou tedy při vytvoření jejich vhodné struktury a zabezpečení dalších nutných věcí jako je sběr signálu a jeho zpracování být aplikovány jako senzory mechanického stimulu.

2.1.1 Uhlíkové nanotrubic

Uhlíkové nanotrubic (carbon nanotubes, CNTs) jsou válcovité uhlíkové struktury, které jsou myšleně tvořeny stočenou vrstvou grafenu. Mohou být jedностěnné (Single-Walled Carbon Nanotubes, SWCNTs), které sestávají z jednoho stočeného grafenového plátu a víceštěnné (Multi-Walled Carbon Nanotubes, MWCNTs), u kterých je koaxiálně složeno soustředně více trubic různých průměrů, Obr. 1 [1]. SWCNTs mají obvykle průměr mezi 0,7 až 2 nm a délku pohybující se mezi několika mikrony a až několika milimetry. V závislosti na směru, ve kterém je grafenový list srolován, je možné mít různou chiralitu (ta je definovaná chirálním úhlem mezi uhlíkovými šestiúhelníky a osou trubice), která spolu s průměrem ovlivňuje elektrickou vodivost nanotrubic [2,3]. CNT mají obecně velmi dobré mechanické vlastnosti jako je mechanický modul a pevnost, nízkou hmotnost a s vysokou elektrickou a teplotní vodivostí.



Obrázek č.1: Ilustrace rolování jednoho grafenového plátu - jednotěnné uhlíkové nanotrubic (SWCNT) a rolování více průměrů grafenových plátů - vicestěnné uhlíkové nanotrubic (MWCNT) [16].

Metody syntézy CNT

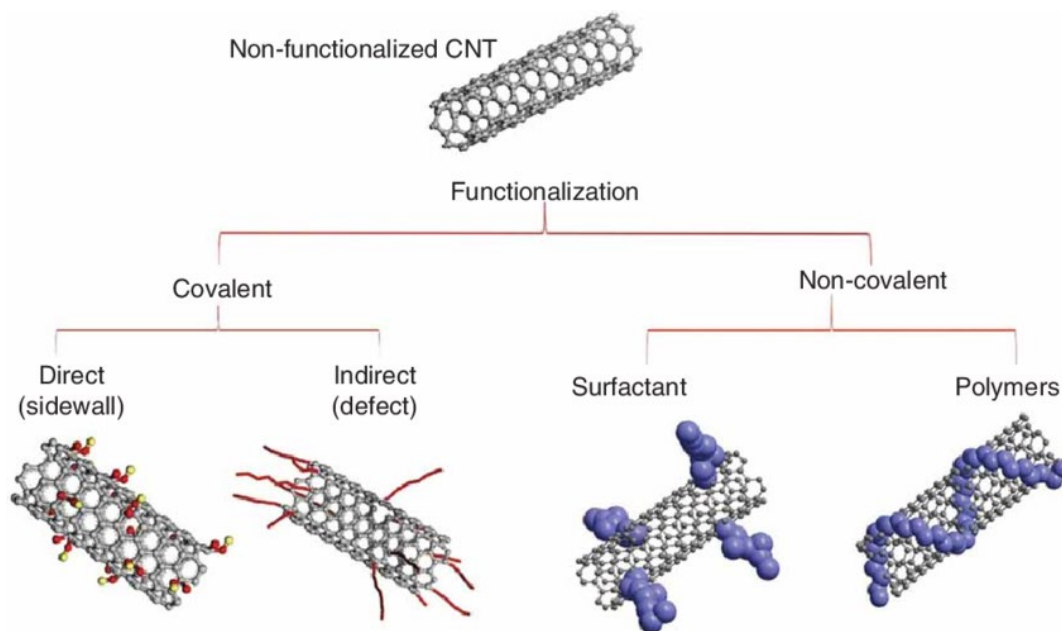
Existují tři hlavní metody syntézy CNT jako je využití plazmového obloukového výboje, laserové odpařování (pulzní laserová ablace) a metody chemické depozice par (CVD). První metoda je založena na obloukovém výboji, který je generován mezi dvěma grafitovými elektrodami v atmosféře helia nebo argonu a za přítomnosti kovového katalyzátoru jako železo, nikl nebo kobalt [4]. Laserová ablace je založena na laserem indukované sublimaci směsi grafitu a kovového katalyzátoru (Fe, Ni, Co). Proces se provádí v křemenném trubkovém reaktoru vloženém do pece a zahřátém na teplotu 2 700 - 3 200 °C v atmosféře helia nebo argonu. Tok plynu podporuje ukládání uhlíku a částic katalyzátoru na kolektor při nižší teplotě. Změnou teploty chlazení kolektoru, tak i průtokem plynu je možné řídit růst nanotrubic [5]. Chemická depozice par je pak jednou z hlavních metod pro průmyslovou výrobu CNT. Průměr nanotrubic souvisí s velikostí kovových částic katalyzujících růst. Kovové částice katalyzátoru zůstávají zachyceny uvnitř vytvořených CNT, a to buď ve špičce nebo na základně, v závislosti na síle adheze mezi částicemi katalyzátoru a substrátu [6].

Funkcionalizace CNT

Dokonalé CNT neobsahují mřížkové defekty. Vady a poruchy, které mohou být přítomny v mřížce z různých důvodů, souvisejí především se syntézou CNT a expozicí právě vyrobených trubic okolní atmosféře vlivem oxidace kyslíkem. Obrovský počet defektů vede k poškození CNT a tím se zásadně snižují teoretické hodnoty vlastností jako je pevnost, elektrická a teplotní vodivost. Na druhou stranu jsou defekty nutné pro funkcionalizaci CNT a taky dobrou dispergovatelnost CNT v polárních médiích. V prvním případě velmi chemicky inertní CNT nespodně tvoří kovalentní vazby s reakčními činidly. Využití defektů ve stěnách CNT nebo otevřených konců CNT poskytuje možnost, jak provést snadněji funkcionalizaci CNT. S tím je také spojena možnost zlepšit dispergovatelnost CNT. Chemické reakce, jakými jsou především oxidace mohou vést k nakrácení CNT a tím snaží deaglomeraci v polární matrici, nebo navázané funkční skupiny zvýší vzájemnou afinitu hydrofóbního povrchu CNT s polárním médiem. Asi nejprogresivnější metodou se zdá být proces oxidace CNT [7,8] vedoucí k vytvoření karboxylových a hydroxylových skupin, které se stávají vazebným prvkem pro různé polymerní molekuly [9-12].

Prostřednictvím funkcionalizace je možné tedy modifikovat fyzikálně-chemické vlastnosti, jako zvýšit disperzi, reaktivitu, manipulaci a zpracovatelnost [13]. Existuje mnoho metod pro modifikaci CNT, které lze rozdělit do čtyř hlavních skupin: kovalentní funkcionalizace, nekovalentní funkcionalizace, vnější dekorování anorganickými materiály a endoendrická výplň (Obrázek č.2) [14]. Kovalentní funkcionalizace se dělí na přímou kovalentní funkcionalizaci s připojením funkčních skupin, jako je např. fluorace a hydrogenace a nepřímou kovalentní funkcionalizaci s využitím karboxylových skupin na povrchu CNT pro další derivatizace CNT [15-18]. Karboxylace a další derivatizace představují čištění CNT zahrnující odstranění kovových částic nebo amorfního uhlíku ze surového materiálu oxidačními metodami v silně kyselém prostředí. Za těchto podmínek se konce nanotrubiček otevírají a tvoří karboxylové skupiny a na

koncích a na bočních stěnách hydroxilové funkční skupiny vhodné pro další derivatizaci. Pro provádění funkcionalizace CNT oxidací může být použit jako oxidační činidlo například manganistan draselný v přítomnosti kyseliny sírové [19-21]. Nekovalentní funkcionalizace spočívá v adsorbci nebo obalení povrchu CNT různými funkčními molekulami. Zaměřuje se na dosažení dispersibility CNT exfoliací svazků za účelem získání jednotlivých CNT, které je jinak velmi obtížné homogenně dispergovat v roztoku. Použité ultrazvukové míchání vytváří prostředí s vysokým smykovým namáháním [22,23]. Povrchově aktivní látky se také používají k interakci s CNT, kdy dochází k orientaci hydrofilní části povrchově aktivních látek směrem do rozpouštědla a hydrofobní části jsou adsorbovány na povrch nanotrubičky, což zabraňuje agregaci CNT. Používá se řada aniontových, kationtových a neiontových aktivních látek. Povrchově aktivní látkou s jednoduchým alkylovým řetězcem je například často používaný dodecylsulfát sodný [24].



Obrázek č.2: Hlavní metody funkcionalizace – kovalentní (přímá a nepřímá), nekovalentní (za pomoci surfaktantu a polymeru) [15].

2.1.2 Metody přípravy CNT polymerních nanokompozitů

Byl zmíněn velký teoretický potenciál při použití CNT jako plniva pro modifikaci polymerních matic. Existují však základní obtíže jak těmto předpovědím dostát, a to především protože je velmi obtížné připravit homogenní polymerní kompozit s dispergováním plniva až na úroveň jednotlivých trubic. To je způsobeno CNT špatnou schopností dispergovatelnosti v organických látkách spolu se silnými van der Waalsovými interakcemi mezi jednotlivými CNT s tendencí k jejich aglomeraci. Další komplikací je fakt že CNT ve formě aglomerátů produkuje již jejich syntéza a také to, že někteří výrobci pro zlepšení přepravních parametrů CNT dále CNT granulují do mikropuletek [25,26]. Následně kompozity připravené klasickými metodami míchání v tavenině často mají jen určitý a velmi nedostatečný stupeň disperze plniva s agregáty dosahujícími až mikrometrických rozměrů [27-29]. Tyto aglomeráty výrazně snižují štíhlostní poměr CNT v matrici a tím i vyztužující efekt [30]. Kromě toho je schopnost přenášet napětí z matrice na výztuž výrazně snížena, když je mnohem snazší vytáhnout jednotlivou trubici z aglomerátu CNT, kdy trubice snadno klouže po grafenovém povrchu CNT, kdy stačí vynaložit mnohem menší síly, než jaké by vedly k porušení trubice jako efektivní výztuže [31,32]. V současnosti se pro překonání těchto nedostatečností inovují techniky a používá se například zpracování v roztoku polymeru s intenzivním mícháním například sonikací. Míchání v tavenině představuje metody s aplikací vysokého smykového namáhání. Nebo se používají různé in-situ polymerační techniky se současnou funkcionalizací a dispergací CNT v polymerní matrici.

2.1.3 Piezo rezistivní polymerní kompozity s CNT

Získáním elektrické vodivosti polymerního kompozitu přidavkem CNT získáváme také vlastnost, kdy tato vodivost může být ovlivněna mechanickým působením a deformací kompozitu. Kompozit pak může detekovat deformaci nebo dokonce může být považován za senzor různých druhů mechanických

napjatostí jako je namáhání v tlaku či tahu. Může se jednat o kompozity kdy se CNT používají jako částicové plnivo, nebo se integrují do polymerních matric jako „bucky papers“, uhlíkové sítě z volně zapletených CNT. Tyto se dají výhodně použít jako flexibilní snímače deformace s relativně vysokou citlivostí na deformaci a nízkými výrobními náklady. CNT filmy se většinou fixují na silnější pružný polymerní substrát, který působí jako mechanická podpora přenášející mechanický podnět na vrstvu citlivou na namáhání [33–35]. Pro přípravu uhlíkového papíru se často používá vodná disperze CNT filtrována přes filtrační membránu a výsledný filtrační koláč jako propletená síť CNT je použit jako součást kompozitu [1,4-6]. Pro sledování deformace lze síť CNT připevnit k povrchu deformovaného kompozitu epoxidovou pryskyřicí [37] nebo ji lze zapouzdřit uvnitř kompozitu [38]. V našich předchozích pracích byla síť z MWCNT zapouzdřena do termoplastického polyuretanu (TPU) [34,35]. Výsledný kompozit byl elektricky vodivý i při 400% deformaci (konvenční kovové tenzometry mohou být přitom deformovány maximálně do ~5 %). Při infiltraci polyuretanového pojiva do CNT pramenců (CNT forests) byly připraveny senzory schopné měřit deformaci s vysoce reprodukovatelnou změnou měrného odporu kompozitu při elongační deformaci až 40 % [39]. Vrstva CNT vložená do silikonové matrice může měřit mechanické napětí až do deformace kompozitu 280 % [40] a vrstva CNT vložená do přírodního kaučuku dokonce až do 620 % [41].

Citlivost tenzometru se obvykle určuje jako citlivostní faktor (gauge factor-GF), který je definován jako relativní změna elektrického odporu k relativní deformaci, $GF = (R/R_0)/\varepsilon$. Komerční snímače napětí mají hodnotu GF asi 2-5 a schopnost pružné deformace je v jednotkách %. Ale například elastický kompozit ze sítě nanotrubiček v polyuretanu natažený na 400 % má GF téměř 69 [35].

2.2 Polymerní kompozity s piezoelektrickými vlastnostmi

Piezoelektrický jev je výsledkem namáhání piezoelektrického prvku za účelem vytvoření náboje nebo napětí. Piezoelektrický jev je lineární. Velikost generovaného náboje je úměrná velikosti napětí působícího na piezoelektrický materiál. Tento efekt je reverzibilní. Aplikace náboje na piezomateriál generuje mechanickou odezvu na pulz. Výsledkem je, že piezoelektrické komponenty nacházejí uplatnění v aplikacích pro produkci a detekci zvuku, generování napětí a frekvence v mnoha měřících systémech. Piezoresistivní jev zahrnuje také tlak nebo napětí. Změny elektrického odporu napříč piezomateriálem jsou však produktem, nikoliv nábojem. Jedná se o změnu elektrického odporu polovodičového materiálu v důsledku mechanického namáhání [42].

Piezoelektrické materiály mají schopnost přeměňovat mechanickou energii na elektrickou energii a naopak. Piezoresistivní zařízení přeměňují mechanickou energii na hodnoty elektrického odporu. Mezi běžně používanými materiály jako je piezoelektrická keramika, polymery a polymerní kompozity se stále více uplatňují. Je to tím, že mají oproti mnohdy drahé, křehké a zdravotně závadné keramice výhodné vlastnosti jako je například flexibilita, nízká hmotnost, efektivní zpracovatelnost polymerů, přizpůsobivost v designu. Flexibilita a přizpůsobivost činí polymerní kompozity zvláště vhodnými pro aplikace, jako jsou senzory a zařízení pro získávání energie [42-46]. Senzory vyrobené z těchto materiálů vykazují citlivost na mechanické podněty a lze je integrovat jako samonapájecí systémy a chytrá zařízení v různých technických aplikacích [43], včetně lékařské diagnostiky [44], monitorování poškození konstrukcí [45] a nositelných technologiích [46]. Flexibilita polymerních kompozitů dále umožňuje vývoj účinných piezoelektrických zařízení schopných zachytit okolní, odpadní nebo parazitní mechanickou energii a efektivně ji ukládat pro využití jako zdroj elektrické energie.

2.2.1 Polymerní samonapájecí sensory mechanického stimulu

Piezoelektrické senzory pracují nezávisle od vnějšího zdroje elektrické energie, kdy je detekovaný signál generován vzorkem přímo prostřednictvím mechano-elektrického převodu. Koncept piezoelektrických polymerních materiálů může představovat použití čistě piezoelektrického polymeru, jako je například poly(vinylidenfluorid) (PVDF) [47,48] či jeho kopolymerů, jako je poly(vinylidenfluorid-trifluorethylen) (P(VDF-TrFE)) [49] nebo poly(vinylidenfluorid-co-hexafluorpropylen) (P(VDF-HFP)) [50]. Mimo to může být piezoelektrický polymer použit ve směsi s nepiezoelektrickým polymerem pro zlepšení flexibility a dobrou detekci stimulů, jako je ohýbání, prudký ráz a vibrace [51]. Další možností je příprava piezoelektrických kompozitů sestávajících z piezoelektrických keramických částic distribuovaných v polymerní matici [52]. Polymerní matrice může představovat jak piezoelektrický polymer s přidanými piezoelektrickými částicemi, tak běžný ne-piezoelektrický polymer s piezoelektricky aktivními částicemi. První skupina může být reprezentována PVDF maticí s $\text{Cs}_2\text{AgBiBr}_6$ částicemi [53], nebo nanostrukturovanými částicemi $\text{Zn-Fe}_2\text{O}_3$ [54]. Druhá skupina pak například polymerní senzor vyrobený z polyamidu-6 matrice s piezoelektrickou keramikou PZT [55], nebo PZT/polyuretanový kompozit [42], či také draslíkem modifikovaná olovnatá titaničitanová keramika a termoplastický polymer polyetherketonketon [56].

2.2.2 Piezoelektrické polymerní kompozity jako zdroj energie

Generovaná piezoelektrická elektrická energie může být použita jako zdroj energie. Piezoelektrické generátory, známé jako PENG, běžně používané v různých odvětvích slouží pro získávání energie a současnou detekci deformací. Anglicky „harvesting“ systémy na bázi polymerů mohou představovat tenké filmy PVDF [49] nebo také elastické ultratenké PVDF-TrFE fólie aplikované jako nositelné vzdálené zařízení pro monitorování pohybů lidského těla [57]. Polymerní kompozity lze také aplikovat jako flexibilní a snadno zpracovatelné s

částicemi BaTiO₃ s polymerní matricí PVDF-TrFE, tento senzor poskytuje výstupní napětí 59,5 V a výstupní proud 6,52 μA generátoru PENG [58].

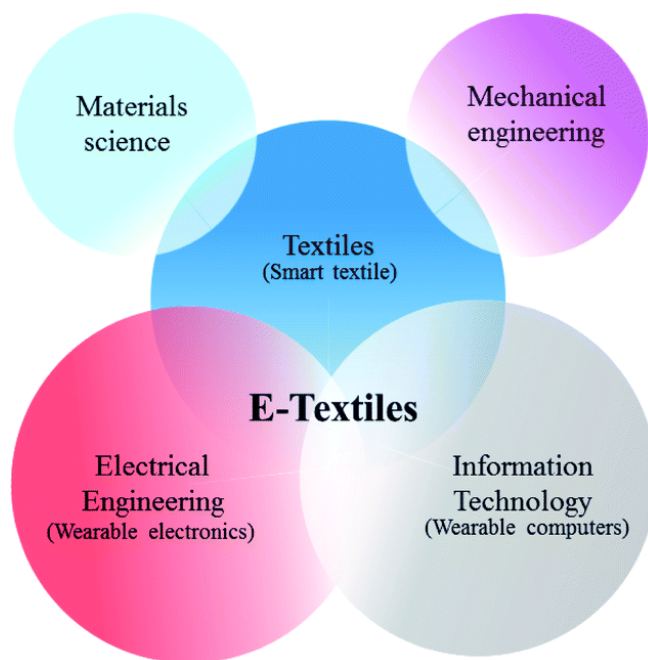
2.3 Nositelná elektronika

Nositelná elektronika je jedním z nejatraktivnějších trendů v digitálním světě a senzory jsou jejími klíčovými prvky. Sensory detekují změnu prostředí, která může být fyzikální, chemická nebo jakákoliv jiná forma, ke které je určena. Jsou funkčními členy odesílající informaci o změně měřené veličiny do externího zařízení. Tyto elektronické senzory jsou často vyrobeny z anorganických materiálů, kovů nebo polymerních kompozitů a často jsou samonosné nebo zapouzdřené v pevných pouzdrech, nebo se implementují přímo do textilních materiálů. U kovových a anorganických materiálů je slabinou jejich malá elasticita a nízký rozsah aplikované deformace. Nejsou flexibilní, nedají se prát a mají malou odolnost vůči dynamickému a únavovému mechanickému namáhání. Navíc mohou vyvolat nepohodlí při vlastním nošení, jestliže jsou součástí oděvu. Tato omezení a některé další související technické problémy vyvolaly potřebu vyvinout nové materiály a inženýrské techniky pro spojení obou oborů, elektroniky a textilu [59].

2.3.1 Uplatnění nositelné elektroniky

Počítače a chytré telefony změnilý náš každodenní život. Přenáší obrovské množství dat, která nás spojují s okolním prostředím. Tato chytrá elektronická zařízení se stávají nositelnými a přibližují komunikaci a výpočetní techniku blíže lidskému tělu. Základní předpoklady pro její aplikovatelnost stimulovaly růst technologické konvergence, nejvýrazněji ovlivnily mechanickou vhodnost, dále pak integraci elektroniky a schopnosti komunikace, které generují koncept nositelné elektroniky (Obrázek č.3) [60]. Nositelná elektronika nebo chytré textilie (E-textilie) jsou schopny plnit elektronické funkce. Jsou vnímány jako

způsob přidávání funkcí do běžných nositelných textilií a budují výhody konkurenceschopnosti na trhu. Tyto technologie umožňují komplexní pohled na pohyb a mobilitu jedince. Potenciálně podporují zdravý životní styl a doplňují lékařskou diagnostiku a sledování terapeutických výsledků [61-63].



Obrázek č.3: Multidisciplinární prostředí pro E-textilie, které zahrnují chytré textilie, nositelnou elektroniku, počítače, vědu o materiálech a strojírenství [60].

Chytré tričko

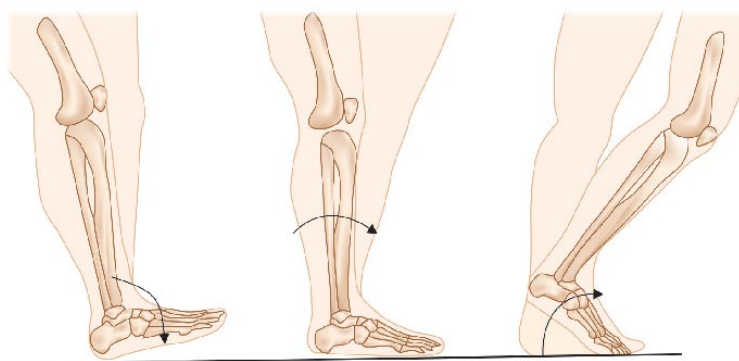
První zmínkou k chytrému oblečení byla v roce 1985 uvedena mikina od Britského vynálezce Harryho Wainwrighta s barevnou kreslenou animací, která používala optická vlákna, vodiče a mikroprocesor. V roce 1998 byla započata průmyslová výroba na trh. V roce 1996 následoval další výzkum chytrého oblečení na základě chytré lékařské košile vyvinuté společností Georgia Tech Wearable Motherboard (GTWM). Tato košile byla vyrobena z optických vláken a speciálních senzorů pro detekci střelných poranění a sledování fyziologických signálů v bojovém prostředí. Na ni navazovali další společnosti, které se zabývaly vývojem chytrého trička, jako Cityzen Sciences. Ta vyrobila tričko ze speciální tkaniny s vetkanými sensory zaznamenávající srdeční frekvenci uživatele, polohu

GPS, trasu, rychlost a nadmořskou výšku. Aplikace chytrého oblečení se již neomezuje pouze na armádu, ale široce se využívá v letectví, požární ochraně, medicíně, fitness a dalších oborech [64-67].

Jednou ze zajímavých a důležitých věcí, které je zapotřebí sledovat, je určitě detekce a sledování lidského dechu. Frekvence, intenzita dýchání a způsob dýchání jsou detekované jako vertikální rozložení parametrů dechu na lidském těle [68].

Chytrá stélka do boty

Chůze je ideální cílový parametr, protože definuje mobilitu a autonomii jako hlavní aspekty kvality života. Právě abnormality chůze jsou spojeny s klinickými případy, jako je výskyt nádorů, Parkinsonova choroba nebo dětská mozková obrna. Monitorováním a nepřetržitou analýzou chůze, respektive mapováním aktivit tlaků působících po celé ploše chodidla, je možné předcházet těmto anomáliím nebo zlovykům v podobě pohybu s nevyváženou zátěží vzhledem ke středu páteře. K analýze chůze je důležité přesně identifikovat chůzi s došlapem paty a odražení špičky (Obrázek č.4) [69,70].



Obrázek č.4: Popis fáze došlapu chodidla při chůzi [70].

Bota se nazývá „chytrá“, když je v ní integrován alespoň jeden akční člen nebo senzor. Akční členy mohou být elektronické nebo mechanické. Dosahovaná

přesnost pomocí chytrého snímače by měla být v ideálním případě více než 90 %. U chytrých bot lékařské třídy by přesnost měla překročit 99,5 % [71].

V polovině 80. let byly v obuvi představeny dva nové technologické pokroky. První pokrok mohl elektronicky měřit vzdálenost, průměrnou rychlost a kalorie spotřebované sportovcem. Druhým pokrokem byla počítačově založená bota s vestavěným krokoměrem, který mohl sledovat ušlou vzdálenost a kalorie spotřebované sportovcem. Jako první začaly tuto technologii implementovat do běžeckých bot firma Adidas a posléze Puma. Jednalo se o první elektronickou inteligentní botu, která dokázala měřit běžcovu vzdálenost, průměrnou rychlost a spotřebu kalorií se schopností uložit celkovou trasu, kterou běžec urazil [72].

2.3.2 Technická omezení v nositelné elektronice

Je zapotřebí věnovat pozornost vyřešení všech technických omezení, zejména přesnosti a spolehlivosti měřených údajů, také snížení šumu, dále spolehlivosti, bezpečnosti a zabezpečení přenosu údajů, trvanlivosti včetně omyvatelnosti a dlouhodobé přesnosti výrobku [73-75].

Trhu s chytrým textilem stále chybí vyspělost. Současné systémy potřebují zlepšení z hlediska spolehlivosti, jako je přesnost, opakovatelnost a reprodukovatelnost. Je třeba reagovat na riziko interference nositelné elektroniky s komunikačními a dalšími elektronickými systémy, jako jsou například kardiostimulátory. Navíc vnitřní a vnější podmínky prostředí, jako je silné pocení nebo déšť, mohou také narušovat správné fungování chytrých textilií. Komunikační systémy v elektronických textiliích, jako je Bluetooth, umožňují připojení textilie k dalším inteligentním zařízením pro vizualizaci a analýzu dat získaných v reálném čase. S tím souvisí bezpečnost a zabezpečení citlivých uživatelských informací, která se shromažďují v nositelných zařízeních. Taková zařízení mají schopnost zachytit a přenášet informace i o okolí uživatele [76,77].

Chytré textilie jsou během používání vystaveny silnému ohýbání, kroucení a roztahování. Senzory na bázi textilu jsou náchylné k poškození během praní. Je důležité hledat ekonomickou, funkční a spolehlivou metodu výroby vysoce vodivých a odolných senzorů s vynikající citlivostí, které mají fungovat v náročných podmínkách použití [77, 78].

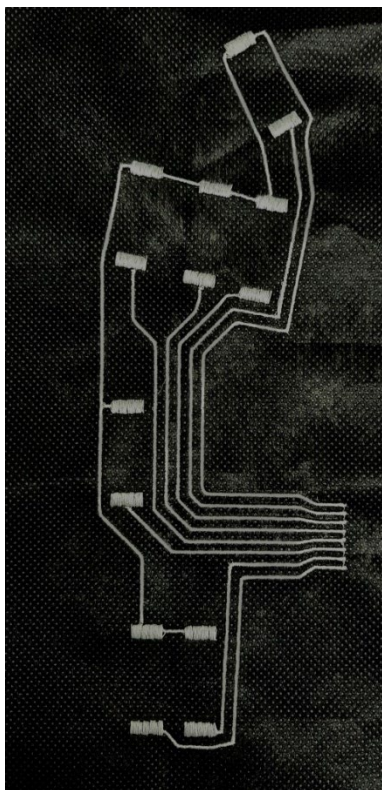
2.3.3 Vyšívání vodivé cesty

Textilní substráty mohou být vyrobeny různými výrobními technikami. Textilii se rozumí jakýkoliv druh textilního materiálu vyrobeného tkaním, pletením nebo netkanými technikami. Přímé použití elektricky vodivých přízí do výrobních procesů tkaní a pletení, šicích nebo vyšívacích systémů jsou možnými výrobními cestami pro e-textilie [70-72].

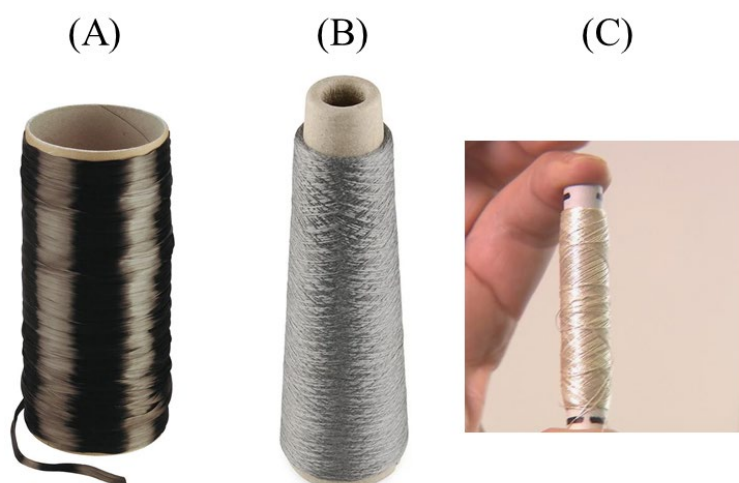
Výšivka je definovaná jako dekorativní uspořádání přízí, šňůr, korálů na tkanině pro získání požadované konfigurace na povrchu. Flexibilitu procesu výšivky lze snadno kombinovat s vysoce užitnými vlákny a vytvářet vysoce funkční materiály šité na míru. Digitální vyšívací vzory navíc umožňují kombinovat elektronické součástky na textilním povrchu, tj. vodivé příze mohou být vyšívány s konvenčními přízemi nebo bez nich, aby se na textiliích vytvořil prvek elektrické vodivosti tak, aby proud procházel vyšívaným vzorem (Obrázek č.5). Vyšívání příze lze také použít jako elektrodu nebo jako nositelnou anténu [73-75].

Vodivé příze jsou dostupné ve formě drátu, staplových vláken nebo multifilamentů (Obrázek č.6). Lze je získat z elektricky vodivých materiálů, jako je uhlík, měď, hliník, titan apod. nebo je lze získat potahováním a plněním nevodivých vláken elektricky vodivými materiály. Nitě na bázi kovu mají lepší elektrickou vodivost než přirozeně vodivé polymerní nitě. Z tohoto důvodu jsou kovová vlákna preferována jako vodivé plnivo s konvenčními přízemi a

tkaninami. Na druhou stranu je šití kovových přízí ve srovnání s elektricky vodivými polymerními přízemi poměrně obtížné [76-78].



Obrázek č.5: Vyšité cesty vodivými nitěmi pro chytrou stélku do boty na polypropylenovou tkaninu.



Obrázek č.6: (A) uhlíkové vlákno, (B) vodivá nit, (C) vodivá hybridní nit Cu/Ag 54 [76].

3 CÍLE PRÁCE

Prvořadým cílem disertační práce bylo vytvoření komplexního systému nositelné elektroniky pro chytré tričko a chytrou stélku do boty. Chytré tričko mělo sloužit k monitorování lidského dechu. Jednalo se o běžně dostupné komerční tričko, do kterého byly integrovány polymerní senzory. Chytrá stélka do obuvi měla sledovat pohybové aktivity, monitorovat tlaková rozhraní po celé ploše stélky. K tomuto cíli bylo nutné se dopracovat jednotlivými úkoly:

- 1) Zhotovení nanokompozitních uhlíkových materiálů se specifickými materiálovými vlastnostmi. Tyto materiály vynikají tím, že jsou elektricky vodivé a vysoce elastické. Pro tento účel byly použity uhlíkové nanotrubic jako plnivo. Z nanotubic byla vytvořena síť pomocí vakuové filtrace a následně tato vzniklá samostatná vrstva byla dále použita k vytvoření kompozitního materiálu pro výrobu elastického a flexibilního snímače napětí.
- 2) Komplexní analýza vlastností a optimalizace senzorů. Síť MWCNT byla upevněna na polyuretanové těleso pro zkoušku krípu. Tyto senzory byly deformovány v širokém rozsahu deformací hrudníku (deformace při dýchání se pohybuje v rozmezí jednotek procent až cca 14 %). Výrazné zvýšení citlivosti senzorů bylo pomocí chemické funkcionalizace.
- 3) Zaměření se na senzory pro získání elektrické energie. Vytypování materiálů. Obalový odpad jako zdroj obnovitelné energie.
- 4) Integrace senzorů do komerčního sportovního trička i do stélky obuvi. Zapouzdření aktivní vrstvy k zamezení styku s okolím. Vytvoření systému sběrných elektrod a vodivých cest technikou vyšívání. Elektronika pro sběr dat byla řešena ve spolupráci s externistou panem Ing. Martinem Adámkem PhD.
- 5) Testování systému na tričku a v botě v běžných podmínkách. Porovnání u dvou uživatelů.

V budoucnu je možné zvážit použití tohoto systému pro sportovní a fitness oblečení, kdy bude senzor zaznamenávat údaje o tělesných aktivitách, vyhodnocovat tato data pro uživatele, což může vést ke zlepšení těchto činností, výkonu sportovců a každodenních aktivit jednotlivce.

Z hlediska financování by nebylo možné samotný projekt provést bez podpory projektů IGA (Interní grantová agentura). Další spolupráce byla s externí firmou MioMove s finanční podporou Ministerstva průmyslu a obchodu České Republiky v rámci projektu (EG17_107/0012417).

4 EXPERIMENTÁLNÍ ČÁST

4.1 Materiály

Víceštěnné uhlíkové nanotrubičky (MWCNT) byly nakoupeny od společnosti Sun Nanotech Co. (Čína). Byly syntetizovány metodou chemické depozice par (CVD). Jako prekurzor byl použit acetylen. MWCNT mají tyto vlastnosti: průměr 10 - 30 nm, délka 1 – 10 μm , elektrický odpor 0,12 Ωcm a čistota > 90 %. Transmisní elektronovou mikroskopií (TEM, JEOL Ltd., Tokio, Japonsko) byl zjištěn průměr jednotlivých nanotrubiček mezi 10 a 60 nm a jejich délka od 3 do 10 μm . Maximální štíhlostní poměr stran byl 300 [79].

Netkané polyuretanové (PU) porézní membrány pro filtraci disperzí MWCNT byly připraveny elektrostatickým zvlákňováním z PU roztoku ve spolupráci s firmou SPUR a.s. se sídlem ve Zlíně. Složení roztoku: dimethylformamid/methylisobutylketon (DMF/MIBK, 1:3).

Jako materiál pro polymerní filtrační membrány byl použit termoplastický polyuretan (TPU) Desmopan DP 385 S (Bayer Material Science, Leverkusen, Berlín, Německo). Použitý TPU je vysoce elastický elastomerní polyuretan s maximální tažností 400 %. Slouží jako elastický podklad pro senzoričnou vrstvu z MWCNTs. Je tedy nedílnou součástí snímače, který se skládá z těchto dvou funkčních vrstev.

Vodivé nitě s označením CU/Ag 54 byly zakoupeny od společnosti Clever Tex® (VÚB a.s. Ústí nad Orlicí). Jedná se o postříbřenou měď s parametry: jemnost 38 tex, el. odpor 8,60 Ω/m , pevnost za sucha 30,72 cN/tex, tažnost za sucha 12,73 %.

Dále byl použit ethyl vinyl acetát (EVA) elastomerní kopolymer, který základem pro pružné a měkké materiály na bázi pryže. Tato pěna je využita jako tlumící výplň naší vložky do boty. Materiál je velmi pružný, lehký a ohebný.

Výborně chrání proti nárazům a je mechanicky odolný. Má nepromokavé vlastnosti a je odolný vůči UV záření.

První komerční tričko bylo vybráno od české sportovní značky Moira CZ (Strakonice, Česká Republika) se složením 97 % polypropylen značky Moira a 3 % elastan. Další sportovní tričko bylo zakoupeno ve sportovním řetězci Decathlon pod označením Kipsta spodní funkční prádlo se složením 69 % polyester, 28 % polyamid a 3 % elastan. Jedná se o kombinaci těsnějšího a volnějšího úpletu. Aby byl materiál plně funkční, musí přiléhat k tělu dobrovolníka.

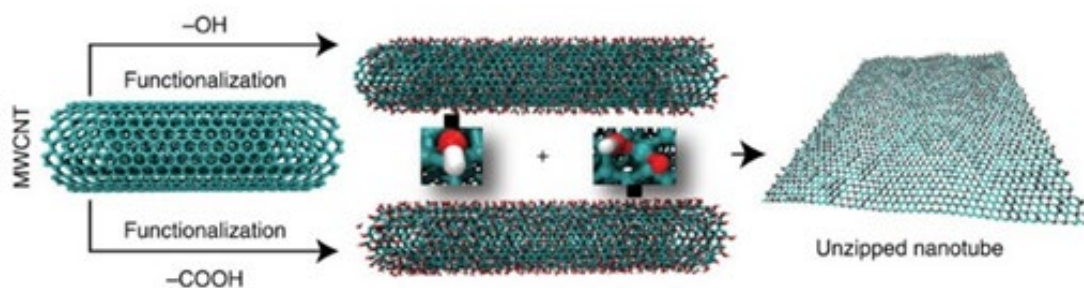
Polyesterový mezivrstvý proužek je nezbytný pro nažehlení senzoru. Jedná se o mřížkovou strukturu, která se teplem roztaví a stává se pojivem mezi senzorem a tkaninou. Tuto vlastnost neztrácí ani po opakovaném praní. Proužek byl zakoupen v běžné galanterii.

Dvousložková silikonová pryž GMS 2628 od Dawex Chemical s.r.o. (Česká Republika, Zlín) se Shore tvrdostí 26 – 28 A a s vysokou elasticitou byla použita pro finální překrytí našeho CNT senzoru. Pryž sloužila jako ochranný film senzoru proti jeho mechanickému poškození vlivem vysokých tlaků.

4.2 Příprava vzorků

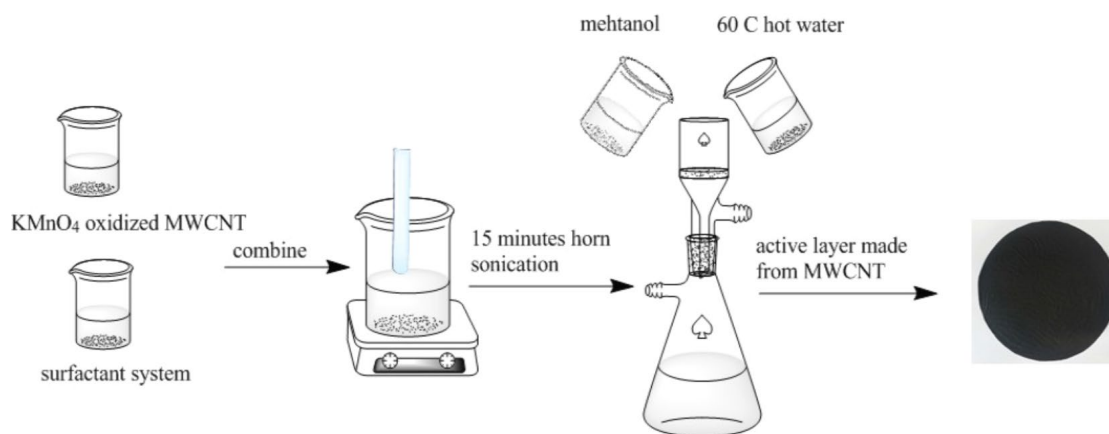
4.2.1 Příprava Bucky paperu MWCNT

Prvním krokem přípravy byla funkcionizace MWCNT pomocí KMnO_4 . Cílem oxidace bylo zkrácení řetězců MWCNT a zvýšení obsahu kyslíkatých skupin kovalentně vázaných na CNT, jako karboxylové, karbonylové a hydroxylové skupiny (Obrázek č.7). Byla zvolena metoda karboxylace pomocí roztoku KMnO_4 s 0,5 M H_2SO_4 při teplotě 85 °C po dobu 11 hodin. Následovala filtrace a promytí kyselinou chlorovodíkovou (HCl) a destilovanou vodou. Takto připravené MWCNT byly sušeny při pokojové teplotě a rozetřeny v třecí misce.



Obrázek č.7: Schéma odzipování MWCNT při syntéze [80].

Druhým krokem procesu byla interakce funkcionalizovaných MWCNT se surfaktantovým systémem, který obsahoval SDS (Sodium Dodecil Sulfát), 1 M hydroxid sodný (NaOH), penthanol a destilovanou vodu. Cílem bylo podpoření dispergace a zabránění agregace MWCNT do svazků. Vodná disperze MWCNT byla připravena sonikací v přístroji UP 400 S od Dr. Hielscher GmbH, Stuttgart, Německo (ultrazvukový trn S7, amplituda 88 μm , výkon 300 W a frekvence 24 kHz, Stuttgart, Německo) po dobu 15 minut při pokojové teplotě. Koncentrace MWCNT v suspenzi byla 0,3 hm.%. Dále byl přidán roztok NaOH pro úpravu pH na 10. Pro vytvoření propletené sítě MWCNT byla použita porézní polyuretanová membrána za pomoci vakuové filtrace. Kdy 30 ml homogenizované disperze bylo přefiltrováno přes nálevku o průměru 90 mm. Připravená síť MWCNT byla několikrát promyta deionizovanou 60 °C horkou vodou, poté methanolem in situ a sušena mezi dvěma filtračními papíry po dobu 24 hodin. Takto je připraven jeden „Buckypaper“, ze kterého se následně stříhají proužky o daném rozměru senzoru (Obrázek č.8) [81].



Obrázek č.8: Příprava uhlíkového papíru z funkcionalizovaných MWCNT pomocí vakuové filtrace vodné disperze MWCNT za účasti oxidovaných MWCNT pomocí $KMnO_4$ a systému surfaktantu, které byly sonikovány a následně promyty methanolem a horkou vodou .

4.2.2 Příprava vzorků pro kríkový test

Pro kríkový test byly vybrány sítě MWCNT čisté a MWCNTs oxidované. Kompozitní pásy 55 mm x 10 mm (D x Š) byly nalisovány na polyuretanová tělesa ve tvaru oboustranných lopatek.

4.2.3 Charakterizační techniky

Připravené struktury byly charakterizovány instrumentálními metodami:

Rentgenová fotoelektronová spektroskopie na přístroji TFA XPS Physical Electronics (PHI-TFA, Physical Electronics Inc., Chanhassen MN, USA) při základním tlaku v komoře asi 6×10^{-8} Pa. Vzorky byly excitovány rentgenovým zářením na ploše 400 μm s monochromatickým zářením Al $K_{\alpha 1,2}$ při 1486,6 eV. Fotoelektrony byly detekovány pomocí hemisférického analyzátoru umístěného pod úhlem 45° vzhledem k normále k povrchu vzorku. Survey-scan spektra byla vytvořena při průchozí energii 187,85 eV, energetický krok byl 0,4 eV. Jednotlivá spektra s vysokým rozlišením pro C1s byla vzata při propustné energii 23,5 a energetickém kroku 0,1 eV. Koncentrace prvků byla stanovena z průzkumných spekter pomocí software MultiPak v7.3.1 od společnosti Physical Electronics.

Následovala metoda Diferenční skenovací kalorimetrie na přístroji DSC 1 Star System (Metler Toledo, USA). První ohřev byl nastaven tak, aby vymazal tepelnou historii z 25 na 180 °C (rychlost ohřevu 10 °C.min⁻¹), pomocí 5 minutové izotermy, poté ochlazení ze 180 na -60 °C (rychlost chlazení 10 °C.min⁻¹), izoterma při -60 °C po dobu 5 min. Druhý cyklus ohřevu byl od -60 do 250 °C (10 °C.min⁻¹) a byl určen pro analýzu testovaného materiálu [82].

Skenovací (rastrovací) elektronová mikroskopie Nova NanoSEM 450 (FEI Company, Hillsboro, Oregon, USA) s bodovým rozlišením ≤ 1.0 nm při 15 kV, ≤ 1.4 nm při 1 kV, v nízkovakuovém modu ≤ 2 nm při 3 kV byla použita k pozorování vzorků MWCNTs jak čistých, tak oxidovaných, a také polotovaru filtrace, finálních kompozitů TPU/MWCNTs a ostatních použitých materiálů.

Skenovací transmisní elektronová mikroskopie STEM (FEI Company, Hillsboro, Oregon, USA) s rozlišením $\leq 0,8$ nm při 30 kV byla použita k pozorování vzorků MWCNTs čistých i oxidovaných.

4.3 Metody měření

4.3.1 Kríповá zkouška

Jednalo se o zatěžování konstatním napětím s následným měřením deformace a elektrického odporu vzorku v čase. Senzory MWCNT čisté a oxidované byly deformovány tahovým napětím od 0,167 do 1,066 MPa v šesti cyklech protažení/relaxace, kdy po 5-ti minutách zatížení následovala 5-ti minutová relaxace v nezátíženém stavu. V nezátíženém stavu došlo včas ke zpětnému krípu. Vzorek byl poté zatížen odpovídajícím vyšším napětím. Protažení vzorku vedlo ke zvýšení makroskopického elektrického odporu kompozitu a reverzibilnímu poklesu odporu, když byl vzorek ve stavu bez zatížení a mechanické napětí se uvolnilo. Snímač je pak citlivý na deformaci a tato odezva je vratná.

4.3.2 Zvýšení citlivosti senzoru

Principem snímání a zvýšení citlivosti senzoru je ve vytvoření mikrotrhlin a snížení počtu kontaktů v CNT síti, což vede ke zvýšení makroskopického elektrického odporu. Když se kompozit uvolní, mikrotrhlina se uzavře, což vede k reverzibilnímu snížení el. odporu. Oxidace zahrnuje více funkčních okysličených skupin chemicky navázaných na povrch CNT, a to má za následek prudké zvýšení el. odporu během deformace a citlivější sensor namáhání. Předpětí vede ke vzniku trhliny, která se v dalších cyklech snadněji otevírá a zvyšuje opět citlivost senzoru.

4.3.3 Charakteristika dýchání

Senzor byl aplikován na komerční tričko ke sledování lidského dechu u dvou dobrovolníků (mužů). Jednalo se o několik dýchacích charakteristik jako hluboké dýchání, zrychlené a se zadržným dechem. Stabilizační účinek na cykly v elektrickém odporu a zbytková normalizovaná změna el. odporu byly konstatní po pěti cyklech. Čili při prvních deformacích získala síť CNT strukturu, která zůstala víceméně stejná bez ohledu na počet deformačních cyklů. Tato mechanická stabilizace je výhodná pro použití snímače jako prvku pro snímání deformace hrudníku při dýchání.

K *měření obvodu hrudníku* jsme použili krejčovský metr, který jsme přiložili na záda těsně pod lopatky, vpředu probíhal u mužů nad prsními bradavkami, u žen přes střed hrudní kosti. Maximální obvod hrudníku se zjišťuje při maximálním vdechu. Dobrovolník se zhluboka nadechne, zadrží dech a v tomto okamžiku se odečítá maximální (inspirační) obvod hrudníku. Následně se změří obvod hrudníku při maximálním výdechu. Dobrovolník s nejvyšším úsilím provede výdech a na okamžik zadrží dech. Odečítá se tak minimální (expirační) obvod hrudníku. Rozdíl mezi maximálním a minimálním obvodem se nazývá respirační amplituda. Obvod hrudníku je tím větší, čím zdatnější jsou dýchací

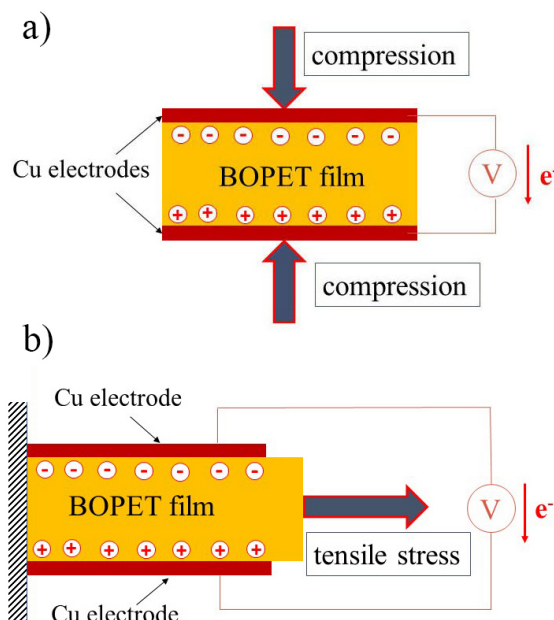
svaly. Průměrné hodnoty respirační amplitudy u mužů jsou 6 – 9 cm. U žen je to kolem 5 cm [83].

4.3.4 Měření piezoelektrických charakteristik

Pro měření piezoelektrifikace byly použity dva druhy materiálů a to PVDF membrána vyrobená procesem elektrostatického zvlákňování neboli elektrospinningem. Elektrospinning vyniká vysokou účinností a nízkými výrobními náklady. Jako semikrystalický polymer obsahuje PVDF čtyři druhy krystalických fází, které byly pojmenovány α , β , γ ad.. Piezoelektrická vlastnost PVDF závisí hlavně na β fázi [84]. Byla vytvořena ultrajemná nanovlákna, která byla použita jako funkční vrstva ve flexibilních senzorech.

Jako druhý testovaný materiál by vzorek Tenolan® biaxiálně orientovaná polyethylentereftalát fólie (BOPET) o tloušťce 50 μm , byla získána od společnosti Fatra as, Česká republika. Obrázek č.9 znázorňuje schéma experimentálního uspořádání navrženého pro mechanoelektrickou piezoelektrifikaci prostřednictvím tlakového a tahového zatížení fólie BOPET. Tlakové pulsy byly iniciovány přístrojem pro měření odrazové pružnosti pryže (Polymer Test, Versta, Zlín, Česká republika). V rámci tohoto experimentu byla fólie BOPET umístěna mezi dvě měděné elektrody 25 \times 25 mm. Aplikovaná nárazová energie byla 0,5 J a nárazová rychlost byla 2,1 m/s. Tenzometr (L6D-C3-40kg, Zemic Europe B.V., Etten-Leur, Nizozemsko) integrovaný do přístroje účinně měřil sílu působící během nárazu kyvadla. Tenzometr byl napájen analogovým převodníkem (TZA11410, VTS Zlín sro, Zlín, Česká republika) s výstupem $\pm 20\text{mA}$ a napájením 24V DC. Pro sledování generovaného piezoelektrického napětí byl použit osciloskop (Infinivision 1000 x-series, 4ch, 100 MHz, DSOX1204A, Keysight, Santa Rosa, CA, USA) s vstupní impedancí 1 M Ω . Pro výpočet zkratového proudu byl použit Ohmův zákon pro jeden cyklus vybití přes elektrickou odporovou zátěž 10 k Ω , měřeno osciloskopem připojeným paralelně k zátěži. Nakonec byl měřen náboj generovaný za jeden cyklus pomocí

elektroskopu (snímač náboje GRG-BTA) připojeného k systému rozhraní LabQuest (Vernier, Edu-for sro, Praha, Česká republika).



Obrázek č. 9: Schematické znázornění snímacího systému pro měření piezoelektrické odezvy filmu BOPET na piezoelektrickou deformaci mechanickými tlakovými podněty (a) a tahovými pulzy (b) [90].

4.3.5 Zatěžování senzorů ve stélce boty

Zatěžování senzorů spočívalo v zaměření se na aplikaci snímačů tlaku zabudovaných do flexibilní vložky boty. Principem byla simulace chůze, respektive vyvíjení tlaků na senzory. Pro zkoušku bylo zvoleno zařízení v podobě páky, na kterou bylo nakládáno závaží o dané hmotnosti v pravidelném časovém intervalu. Stélka obsahuje sedm tlakových senzorů, které jsou rozmístěny po celé ploše stélky. Rozměry senzorů ve stélce odpovídají rozměrům senzorů použitých do trička. Kompozitní proužky byl nažehleny spolu polyesterovou (PES) mřížkou na elastickou PES tkaninu. Sensory byly překryty silikonovou ochrannou vrstvou.

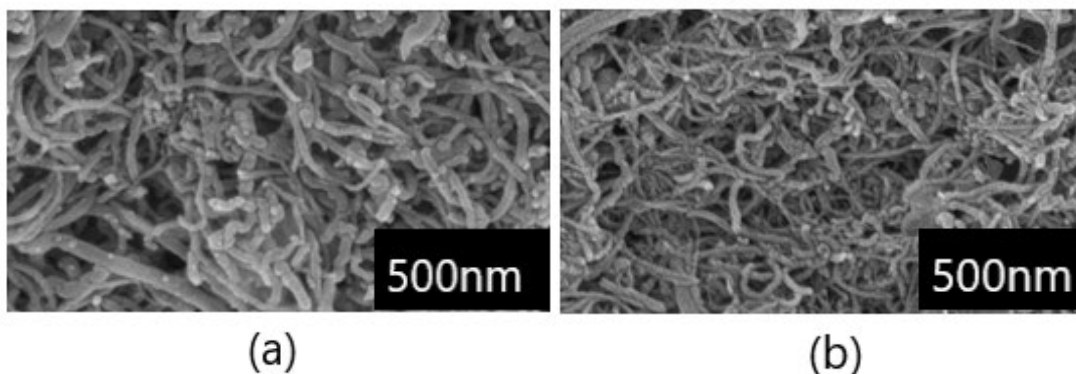
Stélka se senzory byla následně vložena mezi dvě vrstvy EVA a tvořila tak sendvičovou strukturu (Obrázek č.10).



Obrázek č.10: Materiál EVA jako sendvičová ochranná spodní a vrchní vrstva stélky, uvnitř je stélka se senzory, vyšitými vodivými cestami a elektrodami.

5 VÝSLEDKY A DISKUZE

Pro tuto disertační byly použity dva typy MWCNT a testovány jako čisté a oxidované. Na základě výsledků kríkové zkoušky byl vybrán vzorek oxidovaných MWCNT (KMnO_4) a porovnán s hodnotami MWCNT (původní dodané výrobcem). Síť MWCNT (původních) se skládala z dlouhých propletených trubek (obrázek č. 11a), zatímco síť MWCNT (KMnO_4) byla zkrácena v důsledku předchozí oxidace (obrázek č. 11b). Takto byl počet vodivých kontaktů Proto byl počet kontaktů MWCNT maximalizován, což vedlo k vysoké citlivosti senzoru na změny napětí/deformace.

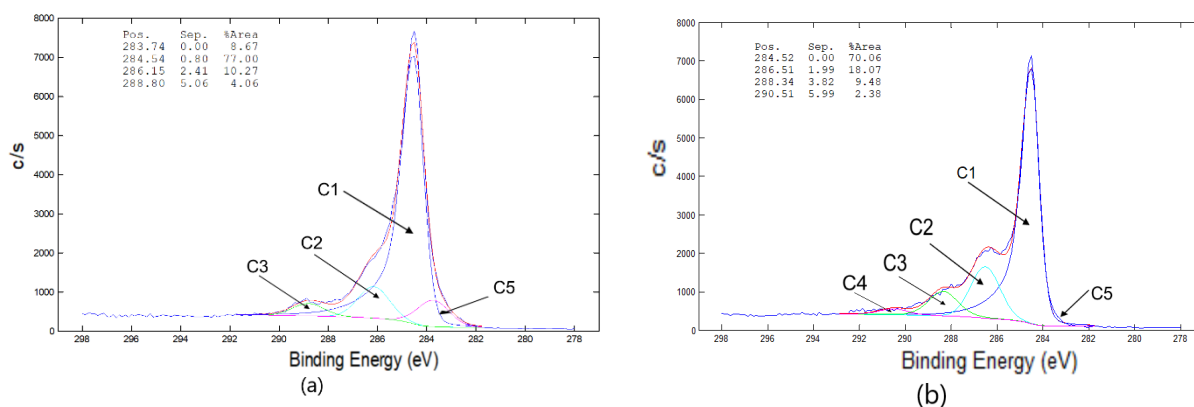


Obrázek č.11. Mikrosnímek sítě uhlíkových nanotrubic z rastrovacího elektronového mikroskopu (SEM). Horní povrch sítě propletených uhlíkových nanotrubic připravený filtrační metodou z vícečetných uhlíkových nanotrubic (MWCNT; čisté) a oxidovaných MWCNT (KMnO_4). **(a)** SEM mikrofotografie MWCNT (čisté). **(b)** SEM mikrofotografie MWCNT (KMnO_4).

Podle našich výsledků XPS MWCNT byl celkový obsah kyslíku stanoven na $18,8 \text{ hm } \%$ pro původní MWCNT a $21,4 \%$ pro oxidované CNT. Poměr uhlíku sp^3/sp^2 byl $2,50$ a $1,69$ pro původní MWCNT a oxidované KMnO_4 (obrázek č.12), v tomto pořadí [85-87].

Měrný elektrický odpor těchto sítí byl naměřen $0,084 \pm 0,003 \Omega\text{cm}$ pro síť vyrobenou z původních MWCNT a $0,156 \pm 0,003 \Omega\text{cm}$ pro síť z oxidovaných trubek KMnO_4 [88].

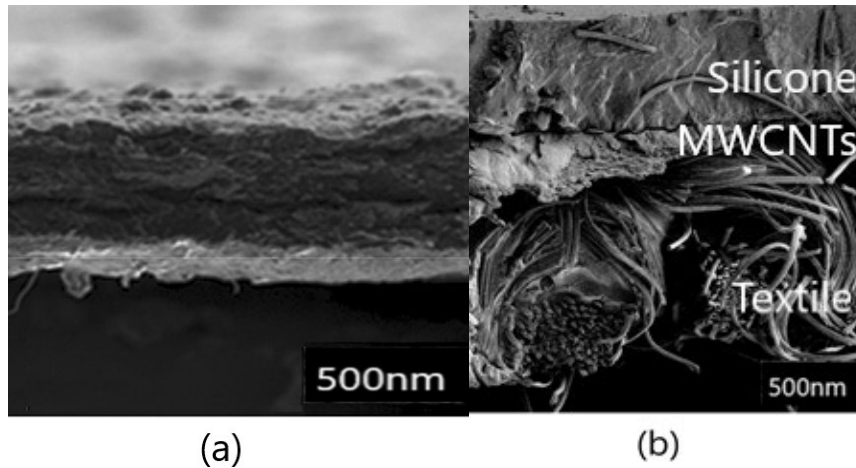
Porozity dvou hlavních sítí byly vypočteny na 0,67 a 0,56 pro původní a oxidovanou síť [89].



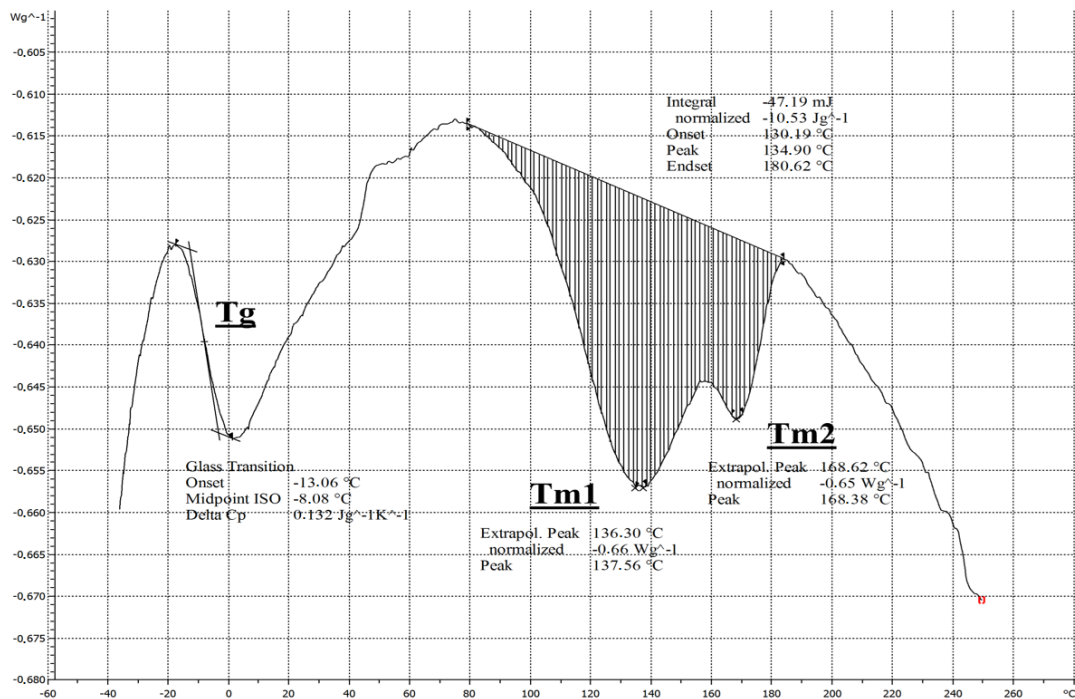
Obrázek č.12: Rentgenová fotoelektronová spektroskopie (XPS) pro CNT/PU a CNT/PU $KMnO_4$. (a) Proložení křivky uhlíkového spektra C1s MWCNT (původní). (b) Proložení křivky uhlíkového spektra C1s MWCNT ($KMnO_4$).

Podstatou snímání deformace změnou elektrického odporu sítě je na principu redukce kontaktů mezi jednotlivými nanotrubičkami a vytváření trhlin v uhlíkovém papíru. Když jsou kompozity prodlužovány, počet kontaktů klesá, což vede k růstu makroskopického odporu senzorké vrstvy [39]. Naopak při relaxaci kompozitu se počet kontaktů zvyšuje, což vede k reverzibilnímu snížení odporu kompozitu. Jak bylo demonstrováno, oxidace vede k tvorbě kyslíkových funkčních skupin vytvořených na povrchu CNT, což způsobuje zvýšení kontaktního odporu v přechodech CNT, a také zvýšení odporů těchto kontaktů v síti CNT. Výsledkem je zvýšení citlivosti snímače na namáhání při pozorování procentuální změny odporu při deformaci [89]. Morfologii připraveného kompozitu působícího jako deformační senzor lze demonstrovat na obrázku č. 13. V principu se jedná o kompozit tvořený třemi vrstvami jako komerční triko, vrstvou na rozhraní CNT/TPU a dvousložkovou silikonovou pryží [81].

Obrázek č. 14 charakterizuje DSC analýzu netkané termoplastické PUR membrány. Byl změřena teplota skelného přechodu (T_g) elastomerní složky, $T_g = -8,08 \text{ }^\circ\text{C}$. Je také možné sledovat dvě po sobě jdoucí oblasti tavení materiálu (endotermický proces) $T_{m1} = 137,56 \text{ }^\circ\text{C}$ a $T_{m2} = 168,38 \text{ }^\circ\text{C}$.



Obrázek č.13: (a) Průřez filmu MWCNT (nahore) a podpůrné TPU filtrační membrány (dole). (b) Průřez kompozitu MWCNT po nalisování v tavenině TPU.



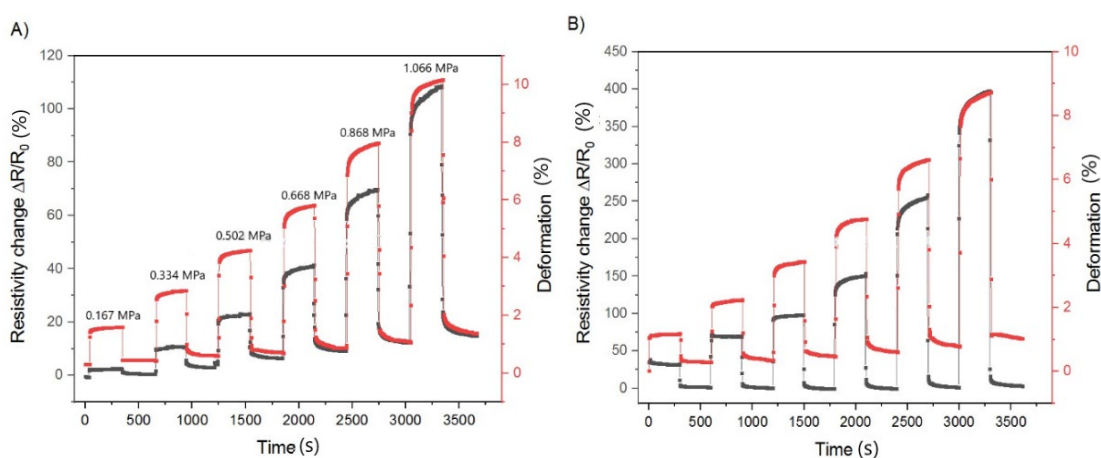
Obrázek č.14: Diferenční skenovací kalorimetrie (DSC) netkané polyuretanové membrány z TPU.

Senzory MWCNT (čisté) a oxidované MWCNT (KMnO₄) byly deformovány tahovým napětím od 0,167 do 1,066 MPa v šesti cyklech protažení/relaxace a byly porovnány. Výsledky jsou znázorněny na obrázku č.15 jako procentuální změna relativního odporu,

$$\Delta R/R_0 = (R - R_0)/R_0 \quad (3)$$

kde R_0 je elektrický odpor měřeného vzorku před prvním protažením a R je odpor během protažení, deformace je relativní změna délky vzorku.

Doby prodloužení, kdy bylo napětí v rozsahu od 0,167 do 1,066 MPa a relaxace po odstranění zátěže, byly 300 s (obrázek č.15). Maximální změny odporu MWCNT (čisté) byly 110 % a deformace byla 10 %. Maximální změny odporu MWCNT (KMnO₄) byly 400 % a deformace byla 9 %, což představuje čtyřnásobné zvýšení citlivosti.

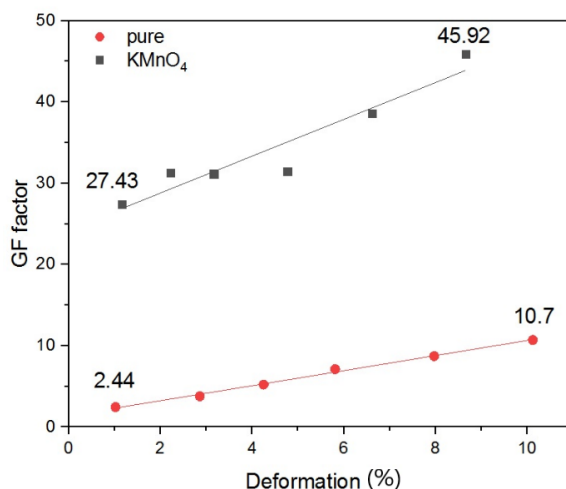


Obrázek č.15: Porovnání změny relativního odporu vs. deformace pro snímač MWCNT (čistý) (A) a MWCNT (KMnO₄) (B) v šesti cyklech protažení/relaxace vyvolaných tahovým napětím (od 0,167 do 1,066 MPa). Tahová napětí jsou pro obě měření stejná. Deformace je označena červenými kroužky, relativní odpor představují černé kroužky.

Dále je citlivost na aplikované prodloužení, deformace ε , definována Gauge faktorem (GF)

$$GF = (\Delta R/R_0)/\varepsilon \quad (4)$$

Deformace představuje relativní změnu délky vzorku jako poměr mezi změnou délky vzorku ΔL vzhledem k počáteční délce L_0 , $\varepsilon = \Delta L/L_0$. Obrázek č. 16 ukazuje závislost citlivostního faktoru GF na deformaci ε .



Obrázek č.16: Závislost citlivostního faktoru (GF) s rostoucí deformací pro snímače MWCNT (čisté) a oxidované MWCNT ($KMnO_4$).

Jednalo se o křipovou zkoušku, což znamená zatěžování konstantním tahovým napětím s následným měřením deformace a elektrického odporu vzorku v čase. Po 5 minutách zatížení následovala relaxace v dalších 5 minutách v nezatíženém stavu, kdy došlo k relaxaci deformace. Vzorek byl poté zatížen odpovídajícím vyšším napětím. Výsledkem bylo šest po sobě jdoucích cyklů zatížení/odlehčení. Protážení vzorku vedlo ke zvýšení makroskopického odporu kompozitu a reverzibilnímu poklesu odporu, když byl vzorek ve stavu bez zatížení a mechanické napětí se uvolnilo. Obecně je pak snímač citlivý na deformaci a tato odezva je vratná. Naměřená hodnota GF dosáhla hodnoty 11 pro MWCNT (původní) a 46 pro MWCNT ($KMnO_4$)

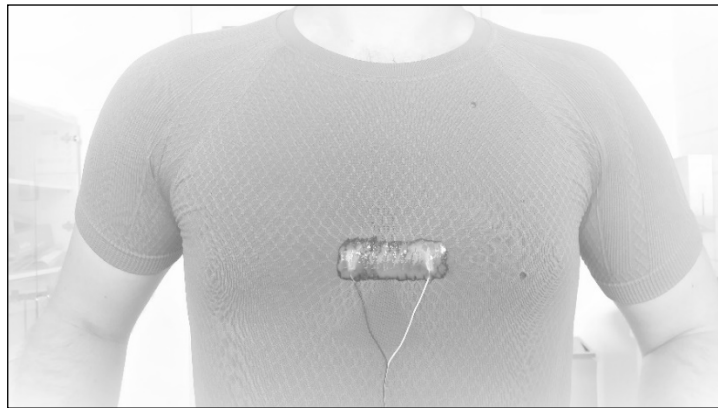
při aplikované deformaci cca 10 % (Obrázek č.16). Princip snímání je ve vytvoření mikrotrhlin a snížení počtu kontaktů v CNT síti, což vede ke zvýšení makroskopické elektrického odporu. Když se kompozit uvolní, mikrotrhlina se uzavře, což vede k reverzibilnímu snížení odporu. Oxidace zahrnuje více funkčních oksličených skupin chemicky navázaných na povrch CNT, což vede k prudšímu zvýšení odporu během deformace a citlivějšímu senzoru na namáhání. Předpětí vede ke vzniku trhliny, která se v dalších cyklech snadněji otevírá, což opět vede k vyšší citlivosti senzoru [81]. V další části je popsána aplikace senzoru ke sledování lidského dechu u dvou dobrovolníků. Následně byly pozorovány různé typy dýchání, a to hluboké a normální dýchání. Jak je znázorněno na obrázku č.17, tento integrovaný senzor MWCNT (KMnO_4) byl upevněn na tričku. Dva dobrovolníci A a B byli vybráni k testování normálního a hlubokého dýchání. Maximální deformace hrudníku dobrovolníka (A) byla 5 % při hlubokém dýchání a změna elektrického odporu byla 30 %. U dobrovolníka (B) byla maximální deformace obvodu hrudníku 7 % pro hluboké dýchání a změna elektrického odporu byla 65 % (obrázek č.18).

Odezva senzoru změnou elektrického odporu byla tedy velmi citlivá na deformaci. Senzor byl reverzibilní a dokázal detekovat dýchání v reálném čase.

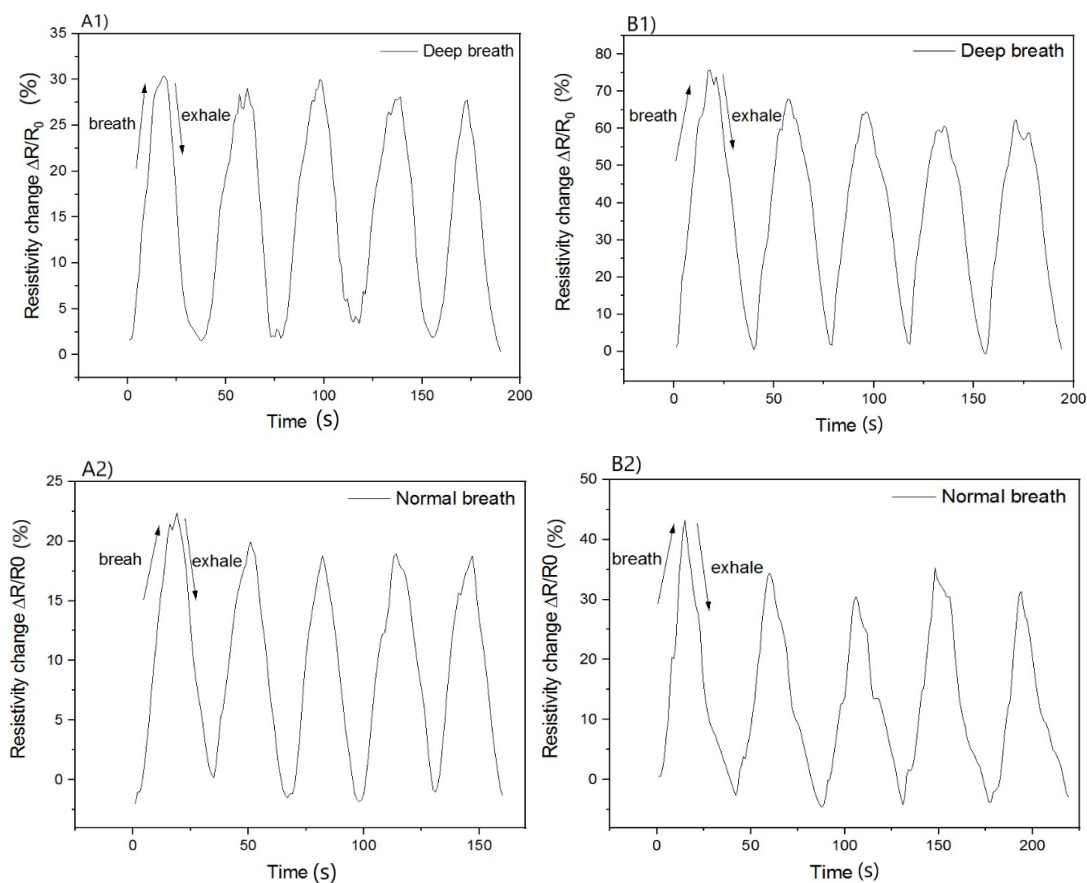
Stabilizační účinek na cykly prodloužení v elektrickém odporu a zbytková normalizovaná změna odporu byly konstantní po přibližně pěti cyklech. Čili při prvních deformacích získala síť nanotrubiček strukturu, která zůstala víceméně stejná bez ohledu na počet dalších deformačních cyklů. Tato mechanická stabilizace je výhodná pro použití snímače jako prvku pro detekci zatížení v mnoha se po sobě opakujících cyklech.

Po otestování jednoho senzoru na tričko byly na tričko Kipsta nažehleny čtyři senzory (Obrázek č.19) a následně otestovány. Presentovaný vývoj rozšiřuje a vylepšuje dosavadní výsledky. Na obrázku č.20 jsou již uvedeny

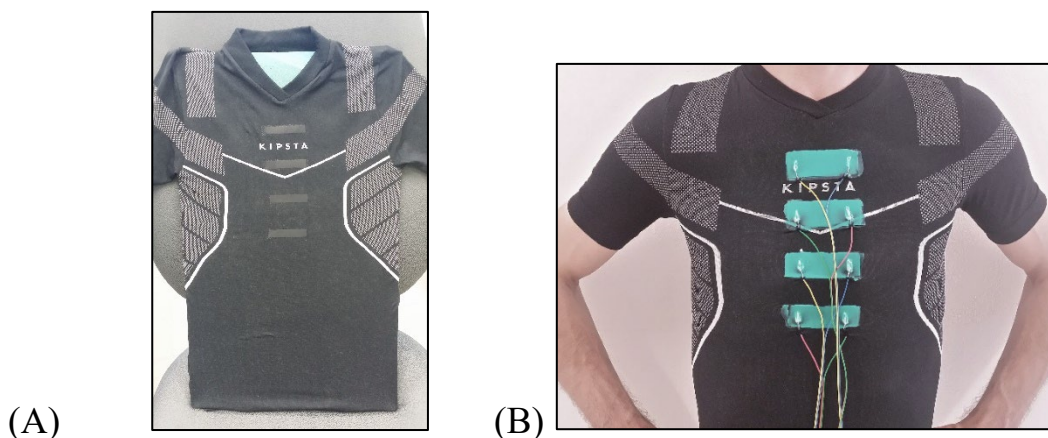
výsledky všech měření ze čtyř senzorů. Je zde zaznamenáno dýchání a hluboké dýchání se zadržením dechu.



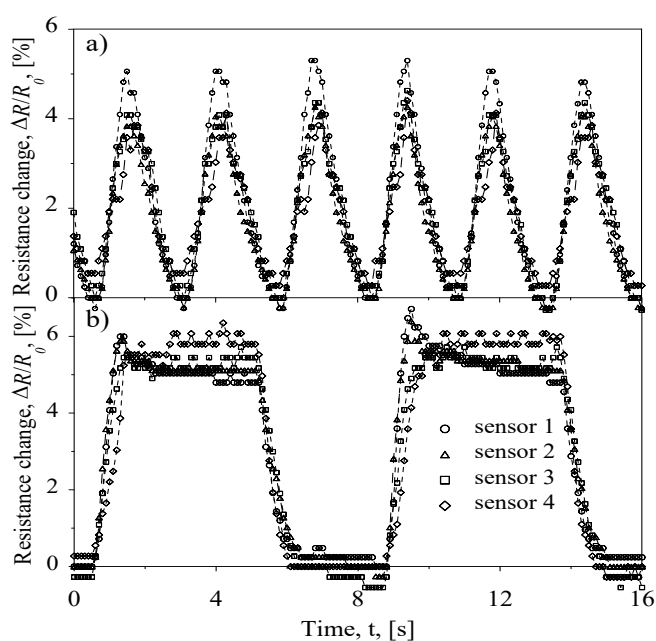
Obrázek č.17: Umístění jednoho senzoru na tričko pro praktickou aplikaci monitorování lidského dechu.



Obrázek č.18: Odezva na deformaci na změnu relativního odporu $\Delta R/R_0$ senzorů uhlíkových nanotrubic ($MWCNTs/KMnO_4$) integrovaných do trička pro monitorování lidského dechu. Porovnání hlubokého a normálního dechu u obou dobrovolníků (A, B).

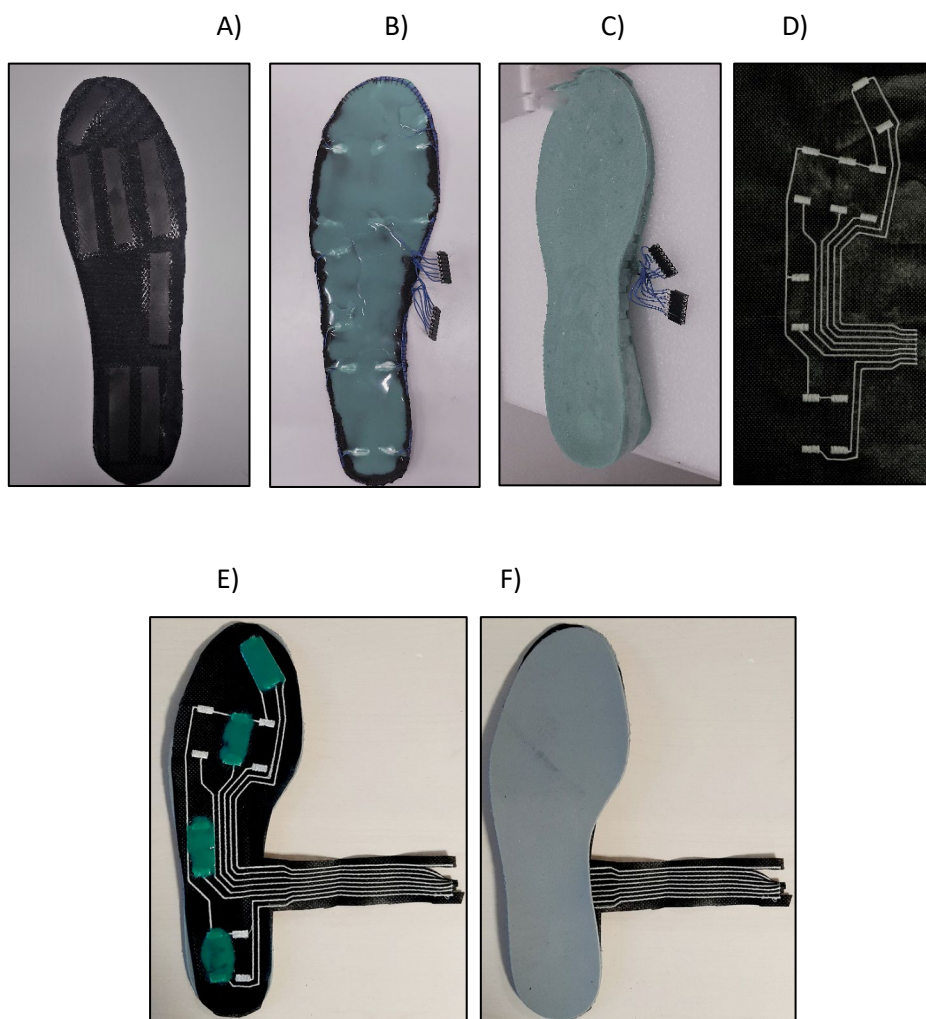


Obrázek č.19: Umístění senzorů na tričko. (A) senzory jsou nažehleny na tričko. (B) prezentace oblečeného trička na dobrovolníkovi se zapouzdřenými senzory silikonovým povlakem a opatřenými elektrodami.



Obrázek č.20: Charakteristiky měření dechu se čtyřmi senzory na tričku. Charakteristika hlubokého dýchání (a), charakteristika hlubokého dýchání se zadržením dechu (b).

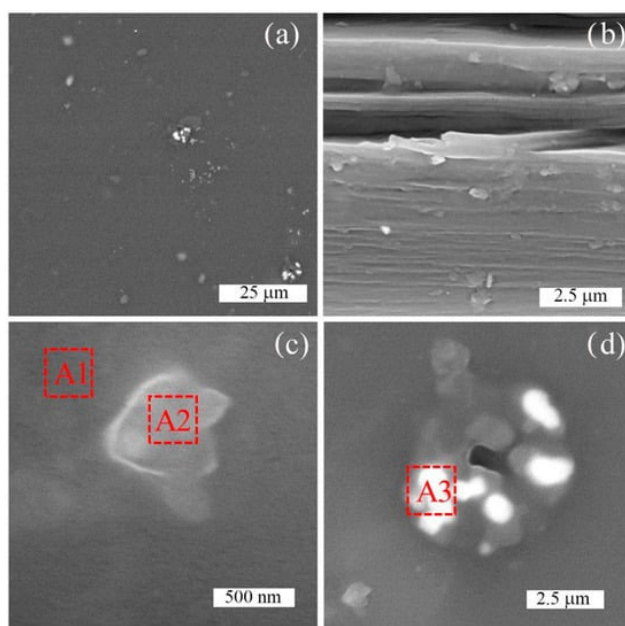
Dále se přesuneme k výsledkům testování senzorů pro detekci chůze, k chytré stélce s integrovanými MWCNT senzory. Na jednotlivých obrázcích č.21 je možné vidět vývojovou posloupnost jednotlivých stélek do boty. S rozmístěním jednotlivých senzorů po celé ploše stélky.



*Obrázek č.21: Vývojové kroky chytré stélky do boty: **A)** Umístění tlakových senzorů MWCNT na elastickou PES tkaninu. **B)** Stélka se senzory a elektrodami překrytá dvousložkovým silikonovým povlakem. **C)** Tvar pružné vložky do boty vyrobené ve formě, **D)** Vyšité vodivé cesty, **E)** Stélka obsahující senzory, **F)** Finální sendvičová struktura chytré stélky.*

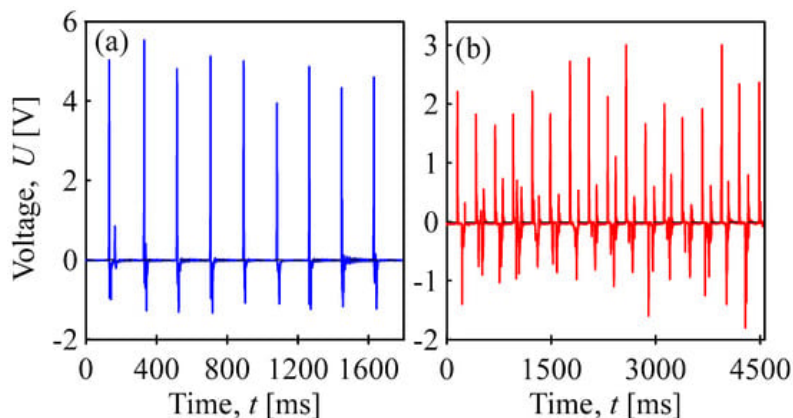
Biaxiálně orientovaná PET obalová fólie (BOPET) byla testována jako piezoelektrický materiál s dalším uplatněním jako samonapájecí senzor deformace pro aplikace v nositelné elektronice, jako je poklep prstem či došlap chodidla. Analýza SEM identifikovala distribuované částice pomocné látky ve filmu BOPET, zatímco analýza EDAX byla použita ke stanovení jejich chemického složení. Částice plniva na povrchu filmu BOPET byly pozorovány jako světlé skvrny (obrázek č.22 a). Různé intenzity emitovaného světla ukazují

na různé chemické vlastnosti rozptýlených částic. Mají širokou distribuci průměrů, od jednotek mikrometrů do přibližně 500 nm. Konkrétní pevné částice byly také pozorovány v jeho příčném řezu (obrázek č.22 b), byly tedy distribuovány ve hmotě a byly přimíchány do polyesterové taveniny. Podrobnosti o dvou typech částic nalezených ve filmu BOPET jsou uvedeny ve spodních částech obrázku č.22 c,d. První představuje jednu pevnou částici, která odpovídá čisté polymerní matici a druhý je aglomerát vytvořený shlukováním menších částic, kde je obsažen křemík jako důkaz SiO_2 . Třetí oblast představují další procesní složky, jako jsou antiblokátory a kluzné přísady, jako jsou vosky, stejně jako jsou povrchově aktivní látky pro lepší kluzné vlastnosti. Z hlediska piezoelektrických vlastností lze tedy BOPET považovat za polymerní kompozit obsahující piezoelektrické částice SiO_2 distribuované v polymerní matici polyesteru.



Obrázek č.22: SEM analýza (a) povrchu, (b) příčného řezu a (c, d) detailní pohledy na dvě částicová plniva identifikovatelná v polymerní matici. Červeně očíslované čtverečky ukazují místa, kde byla provedena analýza EDAX.

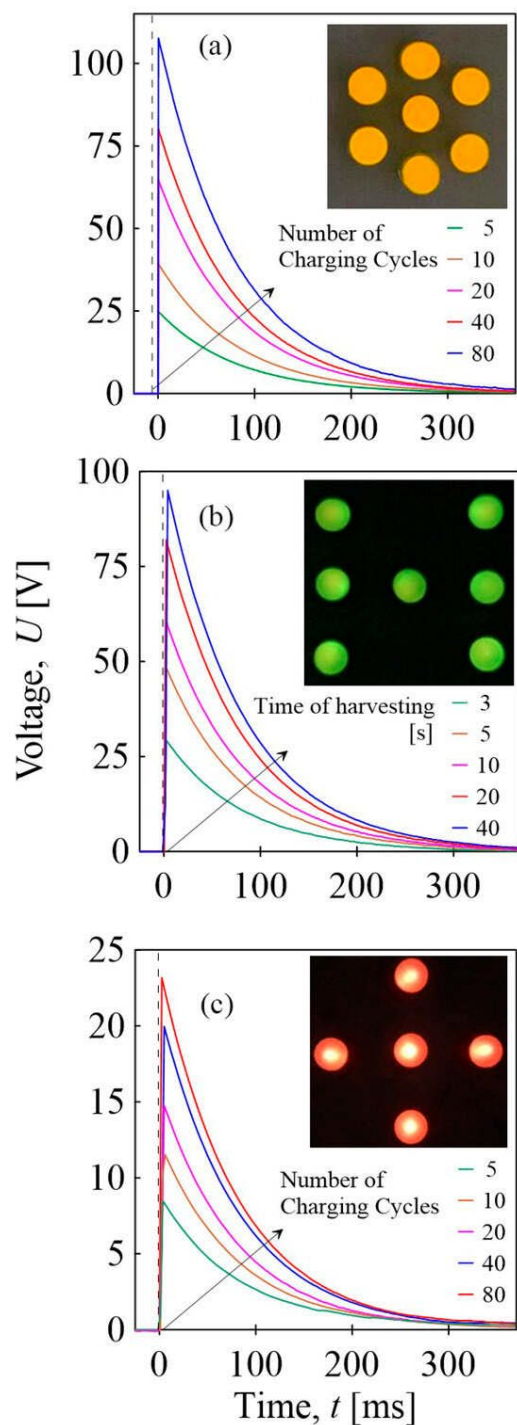
Vlastní testování BOPET senzorů je presentováno na obrázku č. 23. Odezva senzoru na klepnutí prstu je citlivá a vratná, maximální generované elektrické napětí je přibližně $5V$. Při krocích se snímačem umístěným pod patou se generuje napětí větší než $2V$. Podrobný popis dalších výsledků je uveden v článku [90].



Obrázek č.23: Elektromechanická konverze BOPET fólií jako samonapájecího polymerního senzoru transformujícího mechanické podněty na odpovídající elektrické signály aplikované v oblasti nositelné elektroniky: (a) klepání prstem, modrá, (b) kroky detekované piezoelektrickým senzorem umístěným pod patou, červená.

Náraz kyvadla na film BOPET a vibrace vyvolané síťovou analýzou byly převedeny na elektrický signál. Vzniklé piezoelektrické napětí je ve formě střídavého proudu a pro efektivní využití je nutné jej usměrnit na stejnosměrný proud. To bylo dosaženo pomocí usměrňovače Graetz Bridge. Konečný stejnosměrný náboj může být následně uložen do kondenzátoru. Po nabití kondenzátoru může dojít ke ztratu. Obrázek č.24 ukazuje závislost napětí na čase, které bylo uloženo v kondenzátoru pro různé doby trvání detekce/konverze vibrací síťového analytického zařízení. Dále pak pro různé počty tlakových pulzů a pulzy tahového napětí. Po zkratu dosáhne napěťová odezva významného maxima a poté se v průběhu času exponenciálně snižuje na nulu. Doby vybíjení pro všechny sběry se pohybovaly po zkratu až 350 ms . Nejnižší hodnoty byly získány pro pulzy tahového napětí (nad 20 V po 80 cyklech). Velikost vrcholů se

zvyšovala s počtem nárazů kyvadla a dosáhla přibližně $107 V$ na 80 cyklů nárazu a doba trvání vibrace síťové analýzy byla $40 s$ s výstupním napětím $95 V$. Demonstrování potenciálního využití akumulované energie je patrná v blikání sedmi žlutých LED diod zapojených do série pro nárazové cykly, sedmi zelených LED diod pro energii z vibrací a pěti červených LED diod pro tahové impulsy s dobou svícení přibližně $10 ms$.



Obrázek č.24: Zkratované napětí nabitého kondenzátoru: (a) tlakovými pulzy po dopadu kyvadla na fólii BOPET, (b) vibracemi dodávanými zařízením pro síťovou analýzu a (c) pulzy tahového napětí. Světelný záblesk sedmi žlutých LED diod zapojených do série po 10 cyklech nárazu, sedmi zelených po 10s sběru vibrací a pěti červených diod po 80 cyklech tahového impulsu [90] .

6 ZÁVĚR

Tato disertační práce zahrnuje širokou oblast výzkumu. V první části byl představen vysoce elastický deformovatelný a piezoresistivní senzor složený ze sítě elektricky vodivých zapletených uhlíkových nanotrubiček. Ty byly zapouzdřeny elastickým silikonem do elastického komerčního trička. Podstatným krokem byla implementace senzorů na komerční tričko pomocí PES mřížky, která se zahřátím roztavila a působila jako spojovací člen mezi senzorem a tričkem. Tento celý sendvičový prvek byl dostatečně citlivý na to, aby byl použit k monitorování charakteristik lidského dýchání. Aplikace senzoru neovlivnila žádnou lidskou činnost. Byly porovnány respirační charakteristiky u dvou dobrovolníků. Sledování dechu fungovalo na principu změny elektrického odporu kompozitních senzorů. Možná aplikace senzoru v elastickém tričku může být například pro sportovce nebo pro potřeby rehabilitace.

V druhé části byl výzkum zaměřen na stélku do boty. Na testování materiálů, které budou vhodné pro nažehlení senzorů a vyšití vodivých cest. Klíčovou částí bylo testování stélky do boty samostatně mimo botu. Byly provedeny tlakové zkoušky i rázové zkoušky pomocí kyvadla. Důležitým krokem bylo vyšití vodivých cest, testování různých technik výšivek a ukotvení vodivých cest pro výstup do měřicího zařízení.

V poslední části se naše práce zaměřuje na získávání energie. Přináší důležité zjištění o polymerních obalových materiálech, které mohou mít neočekávané vlastnosti a jejich odpad je možné dále využít v oblasti senzorů a získávání energie. Právě myšlenka, že polymerní obalový odpad může být použit ke generování elektrické energie, by měla být chápána jako způsob výroby obnovitelné energie. V souvislosti s tím byly zvažovány různé druhy odpadů, zejména ty, které vedou k mechanoelektrické konverzi s potenciálem použití jako samonapájecí senzory deformace a harvestery. Byl zmíněn polyvinylidenfluorid (PVDF), který sloužil jako piezoelektrický sběrač energie. Dále byl zvolen

BOPED, protože se jedná o nezávadný materiál určený pro styk s potravinami. Tyto flexibilní materiály mohou sloužit jako samonapájecí senzory pro signalizaci vnějších podnětů. Díky své flexibilitě je právě vhodný pro použití v oblasti nositelné elektroniky.

PŘÍSPĚVEK PRO VĚDU A PROBÍHAJÍCÍ VÝZKUM

Prací byly sledovány možnosti přípravy elektricky vodivých kompozitů, jejichž deformací dochází ke změně jejich makroskopického elektrického odporu. Při vhodném uspořádání experimentu se tato změna může použít pro vlastní detekci mechanického stimulu a v dalším kroku pro jeho kvantifikaci. Při vyřešení dalších převážně technických výzev se takto polymerní kompozit stává senzorem deformace. Takto může sloužit jako aktivní člen pro monitorování lidských aktivit, jako součást nositelné elektroniky nebo elektronického textilu. Je opět nutné zmínit, že konečné aplikační řešení je velmi komplexní a spojuje mnoho rozdílných oblastí techniky a technologie. Vlastní práce přináší podle našich nejlepších vědomostí velmi dobrý základ. A pro další pokrok jsou cíle jasné, a to je komerčně využitelné řešení. To, že bylo dosaženo významných výsledků z oblasti základního výzkumu dokumentují publikované práce. Velký projekt MIOMOVE poukazuje dále na realizovaný přesun z materiálového výzkumu do aplikovaného výzkumu a experimentálního vývoje, chytré boty a chytrého trička.

REFERENCE

- [1] https://www.nanowerk.com/nanotechnology/introduction/introduction_to_nanotechnology_22.php.
- [2] X. Lu, Z. Chen. *Curved pi-conjugation, aromaticity, and the related chemistry of small fullerenes*. Chem. Rev., 105 (2005), pp. 3643-3696, doi: 10.1021/cr030093d.
- [3] A. Bhatt, A. Jain, E. Gurnany, R. Jain, A. Modi, A. Jain. *17-Carbon nanotubes: a promising carrier for drug delivery and targeting*. A.M. Holban, A.M. Grumezescu (Eds.), Nanoarchitectonics Smart Deliv. Drug Target., William Andrew Publishing (2016), str. 465-501, doi: 10.1016/B978-0-323-47347-7.00017-3.
- [4] W.S. Hummers, R.E. Offeman. *Preparation of graphitic oxide*. J. Am. Chem. Soc., 80 (1958), doi: 10.1021/ja01539a017.
- [5] S. Iijima. *Helical microtubules of graphitic carbon*. Nature, 354 (1991), str. 56-58, doi: 10.1038/354056a0.
- [6] X. Lu, Z. Chen. *Curved pi-conjugation, aromaticity, and the related chemistry of small fullerenes*. Chem. Rev., 105 (2005), pp. 3643-3696, doi: 10.1021/cr030093d.
- [7] Rasheed A, Howe JY, Dadmun MD, Britt PF, *The efficiency of the oxidation of carbon nanofibers with various oxidizing agents*, CARBON 45 (2007) 1072-1080.
- [8] Hernadi K, Siska A, Thien-Nga L, Forro L, Kiricsi I., *Reactivity of different kinds of carbon during oxidative purification of catalytically prepared carbon nanotubes*. SOLID STATE IONICS 141 (2001) 203-209.
- [9] T. Ramanathan, H. Liu, L.C. Brinson, *Journal of Polymer Science: Part B-Polymer Physics*, **43** 3269 (2005).
- [10] Kim MH, Hong CK, Choe S, Shim SE, *Synthesis of polystyrene brush on multiwalled carbon nanotubes treated with KMnO4 in the presence of a phase-transfer catalyst* JOURNAL OF POLYMER SCIENCE PART A-POLYMER CHEMISTRY 45 (2007) 4413-4420.
- [11] Ha JU, Kim M, Lee J, Choe S, Cheong IW, Shim SE, *A novel synthesis of polymer brush on multiwall carbon nanotubes bearing terminal monomeric unit*, JOURNAL OF POLYMER SCIENCE PART A-POLYMER CHEMISTRY 44 (2006) 6394-6401.
- [12] Xiong J.W., Zheng Z., Qin X.M., Li M, Li H.Q., Wang X.L., CARBON 44 (2006) 2701-2707.
- [13] Ramanathan T, Fisher FT, Ruoff RS, Brinson LC, CHEMISTRY OF MATERIALS 17 (2005) 1290-1295.

- [14] K.A. Wepasnick, B.A. Smith, K.E. Schrote, H.K. Wilson, S.R. Diegelmann, D.H. Fairbrother. *Surface and structural characterization of multi-walled carbon nanotubes following different oxidative treatments.* Carbon, 49 (2011), str. 24-36, doi: 10.1016/j.carbon.2010.08.034.
- [15] Mahdi Karimi, Navid Solati, Mohammad Amiri, Hamed Mirshekari, Elmira Mohamed, Mahdiar Taheri, Mahshid Hashemkhani, Ahad Saeidi, Mehrdad Asghari Estiar, Parnian Kiani, Amir Ghasemi, Seyed Masoud Moosavi Basri, Amir R Aref, and Michael R Hamblin. *Carbon nanotubes part I: preparation of a novel and versatile drug-delivery vehicle.* Expert Opin Drug Deliv. 2015 July doi:10.1517/17425247.2015.1003806.
- [16] Bekyarova, E., Sarkar, S., Wang, F., Itkis, M.E., Kalinina, I., Tian, X., Haddon, R.C. *Effect of covalent chemistry on the electronic structure and properties of carbon nanotubes and graphene.* Acc. Chem. Res. 46, 2013, doi: 10.1021/ar300177q.
- [17] Gonzalez, A.B., Mendoza, E., Pellicer, E., Alsina, F., Fernandez-Sanchez, C., Lechuga, L.M.: *Discriminating the carboxylic groups from the total acidic sites in oxidized multi-wall carbon nanotube by means of acid–base titration.* Chem. Phys. Lett. 462, 2008, doi: 10.1016/j.cplett.2008.07.071.
- [18] Zhao Z, Yang Z, Hu Y, Li J, Fan X. *Multiple functionalization of multi-walled carbon nanotubes with carboxyl and amino groups.* Appl Surf Sci 2013, doi: 10.1016/j.apsusc.2013.03.119.
- [19] PX Hou, S. Bai, QH Yang, C. Liu a HM Cheng. *Multi – step purification of carbon nanotubes.* Carbon, 2002, doi: 10.1016/S0008-6223(01)00075-6.
- [20] H. Hiura, TW Ebbesen a K. Tanigaki. *Opening and purification of carbon nanotubes in high yields.* Adv. Mater., 1995, doi: 10.1002/adma.19950070304.
- [21] N. Zhang, J. Xie a VK Varadan. *Functionalization of carbon nanotubes by potassium permanganate assisted with phase transfer catalyst.* Smart Mater. Struct., 2002, doi: 10.1088/0964-1726/11/6/318.
- [22] Di Crescenzo, A., Ettore, V., Fontana, A. *Non-covalent and reversible functionalization of carbon nanotubes.* Beilstein J. Nanotech. 5, 2014, doi: 10.3762/bjnano.5.178.
- [23] Strano, M.S., Moore, V.C., Miller, M.K., Allen, M.J., Haroz, E.H., Kittrell, C., Hauge, R.H., Smalley, R.E.: *The role of surfactant adsorption during ultrasonication in the dispersion of single-walled carbon nanotubes.* J. Nanosci. Nanotechnol. 3, 2003, doi: 10.1166/jnn.2003.194.
- [24] Bilalis, P., Katsigiannopoulos, D., Avgeropoulos, A., Sakellariou, G.: *Non-covalent functionalization of carbon nanotubes with polymers.* RSC Adv. 4, 2014, doi: 10.1039/C3RA44906H
- [25] Thess A., Lee R., Nikolaev P., Science, 273 (1996) 483.
- [26] Kathyayini H., Willems I., Fonseca A., Catal. Commun. 7 (2006) 140.
- [27] Manchado M. A. L., Valentini L., Biagiotti J., Kenny J. M., Carbon 43 (2005) 1499.
- [28] McNally T., Potschke P., Halley P., Murphy M., Martin D., Bell S. E. J., Brennan G. P., Bein D., Lemoine P., Quinn J. P., Polymer 46 (2005) 8222.

- [29] Meincke O., Kaempfer D., Weickmann H., Friedrich C., Vathauer M., Warth H., *Polymer* 45 (2004) 739.
- [30] Zhang Q. H., Rastogi S., Chen D. J., Lippits D., Lemstra P. J., *Carbon* 44 (2006) 778.
- [31] Ajayan P. M., Schadler L. S., Giannaris C., Rubio A., *Advanced Materials* 12 (2000) 750.
- [32] Schadler L. S., Giannaris S. C., Ajayan P. M., *Applied Physics Letters* 73 (1998) 3842.
- [33] O. Kanoun et al., *Flexible carbon nanotube films for high performance strain sensors*, *Sensors*, vol. 14, no. 6, pp. 10042-10071, 2014.
- [34] Slobodian, P. Riha and P. Saha, *A highly-deformable composite composed of an entangled network of electrically-conductive carbon-nanotubes embedded in elastic polyurethane*, *Carbon*, vol. 50, no. 10, pp. 3446-3453, 2012.
- [35] P. Slobodian, P. Riha, R. Olejnik, U. Cvelbar and P. Saha, *Enhancing effect of KMnO₄ oxidation of carbon nanotubes network embedded in elastic polyurethane on overall electro-mechanical properties of composite*, *Compos. Sci. Technol.*, vol. 81, pp. 54-60, Jun. 2013.
- [36] I. Kang, M. J. Schulz, J. H. Kim, V. Shanov and D. Shi, *A carbon nanotube strain sensor for structural health monitoring*, *Smart Mater. Struct.*, vol. 15, no. 3, pp. 737-748, 2006.
- [37] P. Dharap, Z. Li, S. Nagarajaiah and E. V. Barrera, *Nanotube film based on single-wall carbon nanotubes for strain sensing*, *Nanotechnology*, vol. 15, no. 3, pp. 379-382, 2004.
- [38] M. D. Rein, O. Breuer and H. D. Wagner, *Sensors and sensitivity: Carbon nanotube buckypaper films as strain sensing devices*, *Compos. Sci. Technol.*, vol. 71, pp. 373-381, Feb. 2011.
- [39] M. K. Shin, J. Oh, M. Lima, M. E. Kozlov, S. J. Kim and R. H. Baughman, *Elastomeric conductive composites based on carbon nanotube forests*, *Adv. Mater.*, vol. 22, no. 24, pp. 2663-2667, 2010.
- [40] T. Yamada et al., *A stretchable carbon nanotube strain sensor for human-motion detection*, *Nature Nanotechnol.*, vol. 6, pp. 296-301, Mar. 2011.
- [41] S. Tadakaluru, W. Thongsuwan and P. Singjai, *Stretchable and flexible high-strain sensors made using carbon nanotubes and graphite films on natural rubber*, *Sensors*, vol. 14, no. 1, pp. 868-876, 2014.
- [42] Sapatti, K.; Bhadra, S. *Piezoelectric Polymer and Paper Substrates: A Review*. *Sensors*. 2018, <https://doi.org/10.3390/s18113605>.
- [43] Khanbareh, H.; De Boom, K.; Van Der Zwaag, S. A Groen, W. A. *Highly sensitive piezo particulate-polymer foam composites for robotic skin application*. *Ferroelectrics*. 2017, pp. 25-33. <https://doi.org/10.1080/00150193.2017.1360101>.
- [44] Ali, F.; Koc, M. *3D Printed Polymer Piezoelectric Materials: Transforming Healthcare through Biomedical Applications*. *Polymers*. 2023, pp 15, 23. <https://doi.org/10.3390/polym15234470>.
- [45] Ghadarah, N.; Ayre, D. *A Review on Acoustic Emission Testing for Structural Health Monitoring of Polymer Based Composites*. *Sensors*. 2023, pp 23, 15. <https://doi.org/10.3390/s23156945>.
- [46] Chang, S.-M.; Hur, S.; Park, J.; Lee, D.-G.; Shin, J.; Kim, H.S.; Song, S.E.; Baik, J.M.; Kim, M.; Song, H.-C.; Kang, C.-Y. *Optimization of piezoelectric polymer composites and 3D*

- printing parameters for flexible tactile sensors*. Additive Manufacturing. **2023**, 67, 103470. <https://doi.org/10.1016/j.addma.2023.103470>.
- [47] Slobodian, P.; Olejnik, R.; Matyas, J.; Hausnerova, B.; Riha, P.; Danova, R.; Kimmer, D. *Electrical Detection of Vibrations of Electrospun PVDF Membranes*. International Journal of Molecular Science 2022;14322. <https://doi.org/10.3390/ijms232214322>.
- [48] He, Z.; Mohsenzadeh, E.; Zhang, S.; Rault, F.; Salaün, F. *Development of high-sensitive piezoelectric nanogenerators of all-organic PVDF multilayer nanofibrous membrane with innovative 3D structure via electrohydrodynamic processes*. Journal of Polymer Research 2023, <https://doi.org/10.1007/s10965-023-03776-6>.
- [49] Li, S.; Crovetto, A.; Peng, Z.; Zhang, A.; Hansen, O.; Wang, M.; Li, M.; Wang, F. *Bi-resonant structure with piezoelectric PVDF films for energy harvesting from random vibration sources at low frequency*. Sensors and Actuators A: Physical 2016, 247, 547-554.
- [50] Oh, S.R.; Yao, K.; Zhang, L.; Tay, F.E.H. *Asymmetric electrode design for significant performance enhancement of piezoelectric P(VDF-TrFE) polymer microcantilevers*. Smart Materials and Structures. 2015, 24, <https://doi.org/10.1088/0964-1726/24/4/045035>.
- [51] Zhou, Z.; You, C.; Chen, Y.; Xia, W.; Tian, N.; Li, Y.; wang C.K. *Piezoelectric sensing performance of flexible P(VDF-TrFE)/PBDMS porous polymer materials*. Organic Electronics 2022. 105, 106491.
- [52] Lushcheikin, G. A. *New polymer-containing piezoelectric materials*. Physics of the Solid State 2006, 48, 6, 1023-1025. 1063-7834. doi.org/10.1134/S1063783406060011.
- [53] Wang, M.; Wang, X.; Xu, Y.; Chai, S.; Zhao, Z.; Li, Q.; We, J.; Chen, J.; Zhu, Z.; Bae, B.S.; Tala-Ighil, R.; Zhou, J.; Zhu, Y.; Lei, W. *Enhanced nanogenerator by embedding lead-free double perovskite Cs₂AgBiBr₆ in polymer matrix for hybrid energy harvesting*. Journal of Materials Chemistry C 2023, 1, 207-220. ISSN 2050-7526. doi.org/10.1039/D3TC03314G.
- [54] Yempally, S.; Magadia, P.; Ponnamma, D. *Effect of Zn-Fe₂O₃ nanomaterials on the phase separated morphologies of polyvinylidene fluoride piezoelectric nanogenerators*. RSC Advances 2023, pp. 33863-33874. ISSN 2046-2069. doi.org/10.1039/D3RA03745B.
- [55] Van Den Ende, D.A.; Groen, W.A. A Van Der Zwaag, S. *Development of temperature stable charge based piezoelectric composite quasi-static pressure sensors*. Sensors and Actuators A: Physical 2010, 163, 1, 25-31. ISSN 09244247.
- [56] Marin-Franch, P.; Martin, T.; Tunnicliffe, D.L. A Das-Gupta, D.K. *PTCa/PEKK piezo-composites for acoustic emission detection*. Sensors and Actuators A: Physical 2002, 99, 3, pp 236-243. [doi.org/10.1016/S0924-4247\(01\)00789-0](https://doi.org/10.1016/S0924-4247(01)00789-0) [cit.2023-12-28].
- [57] Bae, J.; Song, J.; Jeong W. et al. *Multi - deformable piezoelectric energy nano-generator with high conversion efficiency for subtle body movements*. Nano Energy 2022, 97.
- [58] Cho, Y., JEONG, J.; Choi, M. et al. *BaTiO₃@PVDF-TrFE nanocomposites with efficient orientation prepared via phase separation nano-coating method for piezoelectric performance improvement and application to 3D-PENG*. Chemical Engineering Journal 2022, 427.
- [59] Nauman A. Choudhry, Lyndon A., Abher R., Imtiaz A. Khan, Lujing Wang. *Textronics- A Review of Textile-Based Wearable Electronics*. (2021) Doi: 10.1002/adem.202100469.
- [60] J. Foroughi, F. Mokhtari, Z. X. Cheng, R. Raad and J. Xi, J. Mater. *Piezofibers to smart textiles: a review on recent advances and future outlook for wearable technology*. Chem. A, 2020, DOI: 10.1039/D0TA00227E.

- [61] J. S. Heo, J. Eom, Y.-H. Kim and S. K. Park. *Recent Progress of Textile-Based Wearable Electronics: A Comprehensive Review of Materials, Devices, and Applications*. Small, 2018, doi:10.1002/sml.201703034.
- [62] S. K. Bahadir and U. K. Sahin, *A Wearable Heating System with a Controllable e-Textile-Based Thermal Panel*. Wearable Technologies, 2018, doi:10.5772/intochopen76192.
- [63] Y. J. Yun, W. G. Hong, D. Y. Kim, H. J. Kim, Y. Jun and H.-K. Lee. *E-textile gas sensors composed of molybdenum disulfide and reduced graphene oxide for high response and reliability*. Sensors and Actuators B: Chemical, 2017, doi:10.1016/j.sn.b.2016.12.028.
- [64] www.retail-insight-network.com/comment/smart-clothing-timeline
- [65] Park, S.; Gopalsamy, C.; Rajamanickam, R. *The Wearable Motherboard: A Flexible Information Infrastructure or Sensate Liner for Medical Applications*. Stud. Health Technol. Informovat. 1999.
- [66] Hertleer, C.; Odhiambo, S.; Lieva, V.L. *Protective clothing for firefighters and rescue workers*. Elsevier: Amsterdam, The Netherlands, 2013, doi: 10.1016/B978-0-85709-056-0.50012-1.
- [67] Scataglini, S.; Moorhead, A.; Feletti, F. *A Systematic Review of Smart Clothing in Sports: Possible Applications to Extreme Sports*. Muscles Ligaments Tendons J. 2020, doi: 10.32098/mltj.02.2020.19.
- [68] Danoudis, M.; Ganesvaran, G.; Iansek, R. *Disturbances of automatic gait control mechanisms in higher level gait disorder*. Gait Posture 2016, doi: 10.1016/j.gaitpost.2016.04.026.
- [69] Thomas, M.J.; Roddy, E.; Zhang, W.; Menz, H.B.; Hannan, M.T.; Peat, G.M. *The population prevalence of foot and ankle pain in middle and old age: A systematic review*. Pain 2011, doi: 10.1016/j.pain.2011.09.019.
- [70] I. Almuteb, R. Hua, Y. Wang. *Smart insoles review (2008-2021): applications, potentials, and future*. Smart Health 2022, doi: 10.1016/j.smhl.2022.100301.
- [71] Crea, M. Donati, S. De Rossi, C. Oddo, N. Vitiello. *A wireless flexible sensorized insole for gait analysis*. Sensors 2014, doi: 10.3390/s140101073.
- [72] Kymissis, C. Kendall, J. Paradiso, and N. Gershenfeld. *Parasitic power harvesting in shoes. Digest of Papers*. Second International Symposium on Wearable Computers (Cat. No.98EX215), 1998, doi: 10.1109/ISWC.1998.729539.
- [73] E. Ismar, S. Zaman, SK Bahadir, F. Kalaoglu, V. Koncar. *Seam Strenght and Washability of Silver Coated Polyamide Yarns*. IOP Conf. Ser.: Mater. Sci. Ing. 2018, doi: 10.1088/1757 - 899X/460/1/012053.
- [74] Y. T. Tsukada, M. Tokita, H. Murata, Y. Hirasawa, K. Yodogawa, Y. Iwasaki, K. Asai, W. Shimizu, N. Kasai, H. Nakashima, S. Tsukada. *Validation of Wearable textile electrodes for ECG monitoring*. Heart Vessels 2019, doi: 10.1007/s00380-019-01347-8.
- [75] Ezgi Ismar, Senem Kurşun Bahadir, Fatma Kalaoglu, and Vladan Koncar. *Futuristic Clothes: Electronic Textiles and Wearable Technologies*. Wiley online Library, 2020, doi: 10.1002/gch2.201900092.

- [76] Nauman A. Choudhry, Lyndon Arnold, Abher Rasheed, Imtiaz A. Khan, and Lijing Wang. *Textronics—A Review of Textile-Based Wearable Electronics*. Wiley online Library, 2021, doi:10.1002/adem.202100469.
- [77] Tang, L.P.S. *Recent developments in flexible wearable electronics for monitoring applications*. Trans. Inst. Meas. Control 2007, doi: 10.1177/0142331207070389.
- [78] Jiang, Y.; Pan, K.; Leng, T.; Hu, Z. *Smart textile integrated wireless powered near field communication body temperature and sweat sensing system*. IEEE J. Electromagn. RF Microw. Med. Biol. 2019, doi: 10.1109/JERM.2019.2929676.
- [79] Slobodian P., Riha P., Saha P. *A highly-deformable composite composed of an entangled network of electrically-conductive carbon-nanotubes embedded in elastic polyurethane*. Carbon doi: 2012.50:3446-3453.
- [80] Mohamad A. Kabbani, Chandra Sekhar Tiwary, Pedro A.S. Autreto, Gustavo Brunetto, Anirban Som, K.R. Krishnadas, Sehmus Ozden, Ken P. Hackenberg, Yongi Gong, Douglas S. Galvao, Robert Vajtai, Ahmad T. Kabbani, Thalappil Pradeep, Pulickel M. Ajayan. *Ambient solid-state mechano-chemical reactions between functionalized carbon nanotubes*. Nature Communications 2014, doi:10.1038/ncomms8291.
- [81] Slobodian P., Daňová R., Olejník R., Matyáš J., Münster L., *Multifunctional flexible and stretchable polyurethane/carbon nanotube strain sensor for human breath monitoring*. 2019, doi: 10.1002/pat.4621.
- [82] Longteng Yu, Joo Chuan Zeo, Ren Hao Soon, Trifannz Zeo, Hong Hui Lee, Chwee Teck Lim. *Highly Stretchable, Weavable, and Washable Piezoresistive Microfiber Sensors*. ACS Appl. Mater. Interfaces 2018, doi: 10.1021/acsami.7b19823.
- [83] J.Klišťová, *Poruchy dechových funkcí u osob s Parkinsonovou chorobou a jejich ovlivnění pomocí respirační fyzioterapie*. Diplomová práce 2008, Univerzita Palackého v Olomouci.
- [84] Sanskruti Smaranika Dani, Bibekananda Sundaray, Sanjay Kimar Nayak, Smita Mohanty. *Electrospun PVDF and composite nanofiber: Current status and future prescription towards hybrid Piezoelectric nanogenerators*. March 2024, Materials Today Communication, doi:101016/j.mtcomm.2023.107661.
- [85] Ana M Grancaric, Ivona Jerkovic, Vladan Koncar, Cedric Cochrane, Fern M Kelly, Damien Soulat, Xavier Legrand. *Conductive polymers for smart textile applications*, Journals Permission sagepub (2017) doi: 10.1177/1528083717699368.
- [86] Zhang X., Tao X. *Smart textiles: Passive smart*. Text Asi 2001; 32: 45-49.
- [87] Oliveri, A., Maselli, M., Lodi, M., Storace, M., & Cianchetti, M.. *Model-based compensation of rate-dependent hysteresis in a piezoresistive strain sensor*. IEEE Transactions on Industrial Electronics (2018), doi:10.1109/tie.2018.2884204.
- [88] Walters DA, Casavant MJ, Quin XC, Huffman CB, Boul PJ, Ericson LM, Haroz EH, O'Connel MJ, Smith K, Colbert DT, Smalley RE (2001) Chem Phys Lett 338:14.
- [89] Benlikaya R., Slobodian P, Riha P. *Enhanced strain-dependent electrical resistance of polyurethane composites with embedded oxidized multiwalled carbon nanotube networks*. J Nanomater. 2013: Art. No. 327597;2013:1-10.

[90] Romana Štěpančíková, Robert Olejník, Jíří Matyáš, Milan Masař, Berenika Hausnerová, Petr Slobodian. *Pressure-Driven Piezoelectric Sensors and Energy Harvesting in Biaxially Oriented Polyethylene Terephthalate Film*. *Sensors* 2024: Art. No. 10.3390/s24041275.

SEZNAM OBRÁZKŮ

Obrázek č.1: Ilustrace jednotěnných SWCNT a víceštěnných uhlíkových nanotrubic MWCNT [16].

Obrázek č.2: Hlavní metody funkcionalizace – kovalentní (přímá a nepřímá), nekovalentní (za pomoci surfaktantu a polymeru) [15].

Obrázek č.3: Multidisciplinární prostředí pro E-textilie, které zahrnují chytré textilie, nositelnou elektroniku, počítače, vědu o materiálech a strojírenství [60].

Obrázek č.4: Popis fáze došlapu chodidla při chůzi [70].

Obrázek č.5: Vyšité cesty vodivými nitěmi pro chytrou stélku do boty na PES materiál.

Obrázek č.6: (A) uhlíkové vlákno, (B) vodivá nit, (C) vodivá hybridní nit Cu/Ag 54 [76].

Obrázek č.7: a) schéma odzipování MWCNT při syntéze, b) mechanismus odzipování zprostředkovaný vodíkovou vazbou: krok A tvorba vodíkové vazby, krok B exotermická reakce - rychlý přenos protonů, uvolněné teplo může způsobit přerušení vazeb uhlík-uhlík (žlutá oblast), krok C produkuje se H₂O a CO₂, přerušení vazeb uhlík-uhlík [80].

Obrázek č.8: Příprava uhlíkového papíru z funkcionalizovaných MWCNT pomocí vakuové filtrace vodné disperze MWCNT za účasti oxidovaných MWCNT pomocí KMnO₄ a systému surfaktantu, které byly sonikovány a následně promyty methanolem a horkou vodou .

Obrázek č.9: Schematické znázornění snímacího systému pro měření piezoelektrické odezvy filmu BOPET na piezoelektrickou deformaci mechanickými tlakovými podněty (a) a tahovými pulzy (b) [90].

Obrázek č.10: Materiál EVA jako sendvičová ochranná spodní a vrchní vrstva stélky, uvnitř je stélka se senzory, vyšitými vodivými cestami a elektrodami.

Obrázek č.11: Mikrosnímek sítě uhlíkových nanotrubic z rastrovacího elektronového mikroskopu (SEM). Horní povrch sítě propletených uhlíkových nanotrubic připravený filtrační metodou z víceštěnných uhlíkových nanotrubic (MWCNT; čistý) a oxidovaných MWCNT (KMnO₄). (a) SEM mikrofotografie MWCNT (čistý). (b) SEM mikrofotografie MWCNT (KMnO₄).

Obrázek č.12: Rentgenová fotoelektronová spektroskopie (XPS) pro CNT/PU a CNT/PU KMnO₄. (a) Proložení křivky uhlíkového spektra C 1s MWCNT (původní). (b) Proložení křivky uhlíkového spektra C 1s MWCNT (KMnO₄).

Obrázek č.13: (a) Průřez filmu MWCNT (nahore) a podpůrné TPU filtrační membrány (dole). (b) Průřez kompozitu MWCNT po nalisování v tavenině TPU.

Obrázek č.14: Diferenční skenovací kalorimetrie (DSC) netkané polyuretanové membrány z TPU.

Obrázek č.15: Porovnání změny relativního odporu vs. deformace pro snímač MWCNT (čistý) (A) a MWCNT (KMnO₄) (B) v šesti cyklech protažení/relaxace vyvolaných tahovým napětím (od 0,167 do 1,066 MPa). Tahová napětí jsou pro obě měření stejná. Deformace je označena červenými kroužky, relativní odpor představují černé kroužky.

Obrázek č.16: Závislost citlivostního faktoru (GF) s rostoucí deformací pro snímače MWCNT (čistý) a oxidované MWCNT (KMnO₄).

Obrázek č.17: Umístění jednoho senzoru na tričko pro praktickou aplikaci monitorování lidského dechu.

Obrázek č.18: Odezva na změnu relativního odporu $\Delta R/R_0$ senzorů uhlíkových nanotrubic (MWCNTs/KMnO₄) integrovaných do trička pro monitorování lidského dechu. Porovnání hlubokého a normálního dechu u obou dobrovolníků (A, B).

Obrázek č.19: Umístění senzorů na tričko. (A) senzory jsou nažehleny na tričko. (B) prezentace oblečeného trička na dobrovolníkovi se zapouzdřenými senzory silikonovým povlakem a opatřenými elektrodami.

Obrázek č.20: Charakteristiky měření dechu se čtyřmi senzory na tričku. Charakteristika hlubokého dýchání (a), charakteristika hlubokého dýchání se zadržením dechu (b).

Obrázek č.21: Vývojové kroky chytré stélky do boty: A) Umístění tlakových senzorů MWCNT na elastickou PES tkaninu. B) Stélka se senzory a elektrodami překrytá dvousložkovým silikonovým povlakem. C) Tvar pružné vložky do boty vyrobené ve formě, D) Vyšité vodivé cesty, E) Stélka obsahující senzory, F) Finální sendvičová struktura chytré stélky.

Obrázek č.22: SEM analýza (a) povrchu, (b) příčného řezu a (c, d) detailní pohledy na dvě částicová plniva identifikovatelná v polymerní matrici. Červeně očíslované čtverečky ukazují místa, kde byla provedena analýza EDAX.

Obrázek č.23: Elektromechanická konverze BOPET fólií jako samonapájecího polymerního senzoru transformujícího mechanické podněty na odpovídající elektrické signály aplikované v oblasti nositelné elektroniky: (a) klepání prstem, modrá, (b) kroky provedené se snímačem umístěným pod patou, červená.

Obrázek č.24: Zkratované napětí nabitého kondenzátoru: (a) tlakovými pulzy po dopadu kyvadla na fólii BOPET, (b) vibracemi dodávanými zařízením pro síťovou analýzu a (c) pulzy tahového napětí. Světelný záblesk sedmi žlutých LED diod zapojených do série po 10 cyklech nárazu, sedmi zelených po 10s sběru vibrací a pěti červených diod po 80 cyklech tahového impulsu [90].

SEZNAM SYMBOLŮ

C_{60}	Molekula s 60 atomy uhlíku
C_{960}	Molekula s 960 atomy uhlíku
CNT	Carbon Nano Tubes - uhlíkové nanotrubičky
SWCNT	Single-Walled Carbon Nanotubes – jedностěnné uhlíkové nanotrubičky
MWCNT	Multi-Walled Carbon Nanotubes víceštěnné uhlíkové nanotrubičky
nm	nanometr
sp^2	Dvojná chemická vazba mezi orbitaly
$KMnO_4$	Manganistan draselný
ΔL	Poměrné prodloužení
L_0	Délka vzorku na začátku měření
ε	Deformace měřeného vzorku
R	Elektrický odpor
R_0	Elektrický odpor při nulové teplotě
Δt	Rozdíl teplot
α	Součinitel tepla
PVDF	Polyvinylidenfluorid
kPa	kilo Pascal
ms	milisekunda
α	Krystalická fáze alfa
β	Krystalická fáze beta
γ	Krystalická fáze gama
δ	Krystalická fáze delta

GF	Gauge faktor – citlivostní faktor
%	procento
GTWM	Georgia Tech Wearable Motherboard
mm	milimetr
AFM	Mikroskopie atomárních sil
TEM	Transmisní elektronový mikroskop
SEM	Rastrovací elektronový mikroskop
DSC	Diferenciální skenovací kalorimetrie
IGA	Interní grantová soutěž pro studenty
XPS	Rentgenová fotoelektronová spektroskopie
μm	mikrometr
Al	hliník
eV	elektronVolt
CVD	Chemical Vapor deposition - Chemické napařování
Ω	ohm
PU	Polyuretan
DMF/MIBK	dimethylformamid/methylisobutylketon
TPU	Termoplastický polyuretan
°C	Stupeň Celsia
NaOH	Hydroxid sodný
MPa	Mega Pascal
ΔR	Změna relativního odporu
Cu	měď
Ag	stříbro
PES	Polyester

CURRICULUM VITAE

Osobní údaje

Jméno a příjmení	Romana Štěpančíková
Adresa	Mladotické nábřeží 370, 763 21
Kontakt	733 531 555
E-mail	stepancikova@utb.cz
Národnost	česká
Datum narození	6.9.1981

Vzdělání a odborná příprava

Datum	2024 – dodnes Schneider Electric
Pracovní pozice	Electronic Support engineer
Datum	2017–dodnes
Udělený titul	Doktorské studium – očekávané ukončení 2024
Hlavní zaměření	Polymerní kompozitní materiály pro nositelnou elektroniku
Organizace zajišťující vzdělání	Centrum polymerních materiálů – Univerzita Tomáše Bati ve Zlíně
Datum	2015–2017 Vybudování vlastního podnikání v oboru cukrářství
Datum	2014-2017 Mateřská dovolená
Datum	2012-2014 Obaly Adamec a.s.
Pracovní pozice	Vedoucí výrobního úseku a Manažer kvality
Náplň práce	- Zodpovědnost za 30 pracovníků

- Plánování zakázek
- Zajištění plynulého chodu výroby
- Vyhodnocování zakázek
- Řešení reklamací
- Nápravná opatření
- Vybudování prvků kvality
- Spolupráce na nových projektech
- Hledání úspor
- Optimalizace procesů

Datum **2011-2012**
Agentura Osma a.s.

Pracovní pozice Výkonný ředitel

Datum **2011-2011**
Agentura Osma a.s.

Pracovní pozice Manažer kvality

Datum **2007-2011**
Zálesí a.s.

Pracovní pozice Vedoucí kvality

Náplň práce

- ISO 9001
- Interní externí audity
- Zavádění čistých prostorů skupiny D
- Zkušenosti v oblasti mikrobiologie
- Hledání úspor
- Optimalizace procesů
- Kontrolní procesy

Datum **2002-2007**

Hlavní obor	Polymerní inženýrství
Organizace zajišťující vzdělání	Technologická fakulta – Univerzita Tomáše Bati ve Zlíně
Udělený titul	Inženýr
	Ing.
Název diplomové práce	- <i>Nanoplniva v PVC plastisolech pro automobilový průmysl</i>

SEZNAM PUBLIKACÍ

1. Slobodian, Petr, **Daňová, Romana**, Olejník, Robert, Matyáš, Jiří, Münster, Lukáš. *Multifunctional flexible and stretchable polyurethane/carbon nanotube strain sensor for human breath monitoring*. *Polymers* 2019, roč.30, č.7, <https://doi.org/10.1002/pat.4621>
2. Olejník, Robert, Goňa, Stanislav, Slobodia, Petr, Matyáš, Jiří, Moučka, Robert, **Daňová, Romana**. *Polyurethane-carbon nanotubes composite dual band antenna for wearable applications*. *Polymers* 2020, roč. 12, č. 11, s. 1-17. ISSN 2073-4360. <https://doi.org/10.3390/polym12112759>
3. **Daňová Romana**; Olejník Robert; Slobodian Petr; Matyáš Jiří, *The piezoresistive highly elastic sensor based on carbon nanotubes for the detection of breath*, *Polymers* 2020 12(3) 713, <https://doi.org/10.3390/polym12030713>
4. Slobodian, Petr; Olejník, Robert; Matyáš, Jiří; Hausnerová, Berenika; Říha, Pavel; **Daňová, Romana**; Kimmer, Dušan, *Electrical detection of vibrations of electrospun PVDF membranes*, *International journal of molecular sciences* 2022, 23(22) 14322, <https://doi.org/10.3390/ijms232214322>
5. Taiskang, Jamatia, Matyáš, Jiří, Olejník, Robert, **Daňová, Romana**, Maloch, Jaroslav, Škoda, David, Slobodian, Petr, Kuritka, Ivo, *Wearable and*

Stretchable SEBS/CB Polymer Conductive Strand as a Piezoresistive Strain Sensor. *Polymers* 2023, 15(7), <https://doi.org/10.3390/polym15071618>

6. **Romana Stepancikova**, Robert Olejnik, Jiri Matyas, Milan Masar, Berenika Hausnerova, Petr Slobodian, *From Waste to Power: Pressure-Driven Piezoelectric Sensors and Energy Harvesting in BOPET Film*, *Sensors* 2024 <https://doi.org/10.3390/s24041275>.

PŘEHLED OSTATNÍCH AKTIVIT

Konference:

DAŇOVÁ, Romana, SLOBODIAN, Petr, OLEJNÍK, Robert, MATYÁŠ, Jiří. Monitorování lidského dýchání pomocí flexibilního polyuretanového senzoru s integrovanou vrstvou uhlíkových nanotrubiček. *Plastko: sborník příspěvků z konference, 18. - 19. dubna 2018*, 2018,

SLOBODIAN, Petr, KARAKURT, Nuri, OLEJNÍK, Robert, **DAŇOVÁ, Romana**. Thermoelectrical Behaviour of Surface-Treated Multiwall Carbon Nanotube Filled Ethylene-Octene Polymer Composites. *Plastko 2018*. Zlín : Univerzita Tomáše Bati ve Zlíně, 2018, s. 193-200. ISBN 978-80-7454-727-0.

DAŇOVÁ, Romana, OLEJNÍK, Robert, SLOBODIAN, Petr, MATYÁŠ, Jiří, KARAKURT, Nuri. Human breath monitoring by flexible polyurethane sensor with integrated carbon nanotube layer. *11th International Symposium on Flexible Organic Electronics (ISFOE18), 2-5 July 2018, Thessaloniki, Greece*, 2018,

DAŇOVÁ, Romana, SLOBODIAN, Petr, OLEJNÍK, Robert, MATYÁŠ, Jiří. Carbon nanotubes composite pressure sensors integrated into flexible shoe insole for human movement monitoring. *ICSTWT 2019: International Conference on Smart Textiles for Wearable Technology, 22-23 July, Rome, Italy*, 2019,

DAŇOVÁ, Romana, SLOBODIAN, Petr, OLEJNÍK, Robert, MATYÁŠ, Jiří. A system based on polymer elastic composites for monitoring of human breath connected with mobile application. *ICSTWT 2019: International Conference on Smart Textiles for Wearable Technology, 22-23 July, Rome, Italy*, 2019,

SLOBODIAN, Petr, ŘÍHA, Pavel, OLEJNÍK, Robert, MATYÁŠ, Jiří, **DAŇOVÁ, Romana**, SCHLEDJEWSKI, Ralf. Self-sensing of strain in a fiber glass/epoxy composite by built-in stripe of carbon nanotubes with Ag nanoparticles. *19th World Congress on Materials Science and Engineering, June 11-13, 2018, Barcelona, Spain, 2018,*

OLEJNÍK, Robert, MATYÁŠ, Jiří, SLOBODIAN, Petr, **DAŇOVÁ, Romana**, KARAKURT, Nuri. High flexible and durable carbon nanotubes electrically conductive polymer base antenna for bluetooth. *AUTEX 2019: 19th World Textile Conference on Textiles at the Crossroads, 11-15 June 2019, Ghent, Belgium, 2019,*

DAŇOVÁ, Romana, AVVARI, Venkata Dinesh, OLEJNÍK, Robert, SLOBODIAN, Petr, MATYÁŠ, Jiří, KIMMER, Dušan. Enhanced PVDF electrospun nanofiber capacitive pressure sensor for wearable electronic. *15th IEEE International Conference on Nano/Micro Engineered and Molecular System, NEMS 2020. Piscataway, New Jersey : Institute of Electrical and Electronics Engineers Inc., 2020, s. 115-119. ISBN 978-1-72817-230-9.*

AVVARI, Venkata Dinesh, OLEJNÍK, Robert, **DAŇOVÁ, Romana**, MATYÁŠ, Jiří, SLOBODIAN, Petr, ADÁMEK, Martin, KIMMER, Dušan. Poly(vinylidene fluoride) electrospun non-woven nanofibers based piezoelectric nanogenerator. *15th IEEE International Conference on Nano/Micro Engineered and Molecular System, NEMS 2020. Piscataway, New Jersey : Institute of Electrical and Electronics Engineers Inc., 2020, s. 500-505. ISBN 978-1-72817-230-9.*

MATYÁŠ, Jiří, SLOBODIAN, Petr, OLEJNÍK, Robert, **DAŇOVÁ, Romana**. Polymerní samozhášivá mikro-chránička svazku optických kabelů se sníženým mechanickým třením.

MATYÁŠ, Jiří, SLOBODIAN, Petr, OLEJNÍK, Robert, **DAŇOVÁ, Romana**. Polymerní směs na výrobu samozhášivé mikrochráničky svazku optických kabelů. 2021,

SLOBODIAN, Petr, OLEJNÍK, Robert, MATYÁŠ, Jiří, HAUSNEROVÁ, Berenika, ŘÍHA, Pavel, **DAŇOVÁ, Romana**, KIMMER, Dušan. Electrical detection of vibrations of electrospun PVDF membranes. *International Journal of Molecular Sciences*, 2022, roč. 23, č. 22, s. nestránkováno. ISSN 1661-6596.

MATYÁŠ, Jiří, SLOBODIAN, Petr, OLEJNÍK, Robert, ADÁMEK, Martin, **DAŇOVÁ, Romana**. Elektronický monitorovací systém pro průběžnou detekci a signalizaci obsahu amoniaku v plynném prostředí. 2019,

Pracovní projekty:

IGA/CPS/2017/002 - Analýza kompozitních laminátů vyztužených skleněnými vlákny s integrovanou vrstvou uhlíkových trubiček dekorovaných Ag klastry pro detekci deformace

IGA/CPS/2018/005 - Vysoce citlivý polymerní kompozitní systém pro monitorování lidského dechu

IGA/CPS/2019/010 - Systém na bázi polymerních elastických kompozitů pro monitorování lidského dechu s provázáním na mobilní aplikaci

IGA/CPS/2020/008 - Vliv nanostrukturovaných karbonizovaných substrátů na užité vlastnosti ohebných tlakových senzorů

IGA/CPS/2021/003 - Piezorezistivita pokročilých materiálů

RP/CPS/2020/006 - Smart nanomateriály: od základů k aplikaci

08/1/2020/GAMA2 - TP01010006 - Inovovaná konstrukce mikro-chrániček svazků optických kabelů

02/2/2017/GAMA - TG03010052 - Senzor pro detekci amoniaku na bázi PANI

Dále jsem se podílela na projektu EG17_107/0012417: MIOMOVE

Pedagogické aktivity:

Spolupráce na laboratorním cvičení u následujících předmětů:

TCPM / TK8VV Výroba a vlastnosti obalů

TCPM / TP6TA Termická analýza materiálů

TCPM / TK7RP Recyklace plastů

TCPM / TP8NK Nanomateriály v kompozitech

Mobilita: březen 2020, místem konání byla firma Miomove s.r.o. ve Slavičíně.

NÁSLEDUJÍ PUBLIKACE



Article

Electrical Detection of Vibrations of Electrospun PVDF Membranes

Petr Slobodian^{1,2,*} , Robert Olejnik¹, Jiri Matyas¹ , Berenika Hausnerova^{1,3} , Pavel Riha^{3,4},
Romana Danova¹ and Dusan Kimmer¹

¹ Centre of Polymer Systems, University Institute, Tomas Bata University in Zlin, Trida T. Bati 5678, 760 01 Zlin, Czech Republic

² Polymer Centre, Faculty of Technology, Tomas Bata University in Zlin, Vavreckova 5669, 760 01 Zlin, Czech Republic

³ Department of Production Engineering, Faculty of Technology, Tomas Bata University in Zlin, Vavreckova 5669, 760 01 Zlin, Czech Republic

⁴ The Czech Academy of Sciences, Institute of Hydrodynamics, Pod Patankou 5, 166 12 Prague, Czech Republic

* Correspondence: slobodian@utb.cz; Tel.: +420-576-031-350

Abstract: We prepared electroactive PVDF membranes, which were subjected to mechanical as well as dual electro–mechanical signals and their responses were detected by the evoked electrical pulses. The aim was to obtain primarily electric energy that could be used for light signalling, sensing of the membrane properties and membrane motion detection. The obtained data showed the unique as well as usable properties of PVDF membranes. From this point of view, the gain and analysis of the electrical responses to combined electro–mechanical loads of PVDF membranes have been important in terms of identifying the mechanism. The detected electrical response of the PVDF membrane to their electro–mechanical pulses also indicated the possibility of using this phenomenon. Among others, it suggests monitoring of membrane fouling and use for a self-cleaning mechanism.

Keywords: PVDF; poly(vinylidene fluoride); electrospinning; piezoelectricity; sound sensor; electrical energy harvester; electrostriction



Citation: Slobodian, P.; Olejnik, R.; Matyas, J.; Hausnerova, B.; Riha, P.; Danova, R.; Kimmer, D. Electrical Detection of Vibrations of Electrospun PVDF Membranes. *Int. J. Mol. Sci.* **2022**, *23*, 14322. <https://doi.org/10.3390/ijms232214322>

Academic Editor: Marta Fernández-García

Received: 7 September 2022

Accepted: 5 November 2022

Published: 18 November 2022

Publisher's Note: MDPI stays neutral with regard to jurisdictional claims in published maps and institutional affiliations.



Copyright: © 2022 by the authors. Licensee MDPI, Basel, Switzerland. This article is an open access article distributed under the terms and conditions of the Creative Commons Attribution (CC BY) license (<https://creativecommons.org/licenses/by/4.0/>).

1. Introduction

Transmembrane pressure, resulting in the permeation of gases and liquids through electroactive elastic membranes, as well as acoustic or electrically-driven membrane vibrations, can be used as mechanical or electrical membrane control signals. In the former case, a mechanical loading is converted to an electrical one. In the latter, an electrical loading is converted into a mechanical one. Finally, in the combined case, e.g., an electrical loading result in mechanical deformation and this induces an electrical response or vice versa. Initial mechanical and electrical loadings are used to adjust, for instance, membrane selectivity towards different chemicals, to minimize membrane fouling, to provide energy for harvesting by converting mechanical energy into electrical energy and storing it for further use. Primarily, in the mentioned applications, semicrystalline Poly (vinylidene fluoride) (PVDF), $-\text{[CH}_2\text{-CF}_2\text{]}_n\text{-}$ membranes are used. The mechano–electric coupling manifests through piezoelectricity, which is the ability of PVDF to generate an electric charge in response to the deformation of covalent crystals of the β -PVDF crystalline face. These ferroelectric crystals, which have a zigzag/all-trans configuration, exhibit partial charges at the opposite sides of the zigzag chain [1,2], which create molecular dipolar orientation with positive hydrogen and negative fluoride leading to the spontaneous polarization of the atoms, orienting them in one direction [3]. When these covalent crystals are deformed, charge levels are shifted and electrical voltage is generated [3]. On the other hand, the electric–mechanical coupling manifests through the reverse effect of piezoelectricity, which is the ability of PVDF to generate strain and is caused by the displacement of ions in

the crystal (lattice) being exposed to an electric field. Accumulation of this displacement throughout the PVDF membrane results in an overall elongation in the direction of the field.

The covalent crystals are elastic, flexible, lightweight and soluble, which makes it possible to prepare electroactive PVDF membrane networks by electrospinning [2,4]. This is an advantage of using these membranes where, on the other hand, brittle piezoelectric crystalline or ceramic materials cannot be used. Consequently, numerous applications of PVDF membranes include flexible strain sensors, biomedical sensors [4] or permeable membranes with electrically controlled selectivity towards polluting chemicals. Other cases of PVDF membrane use are actuators, wearable electronics, soft robotics [1], microelectromechanical systems, storage memory devices and energy harvesters, when the produced charge in many mechanical cycles can be store to capacitor to increase electric power for further use [5,6]. As far as the electrostriction application of PVDF membrane is concerned, a representative example is the anti-fouling membrane whereby self-cleaning is carried out by the membrane vibration using induced AC electric signals [7]. Another promising application of the piezoelectric effect is an energy harvesting.

In the present work, the prepared electroactive PVDF membranes were subjected to mechanical as well as dual electro–mechanical signals and their responses were detected by the evoked electrical pulses. The aim was to obtain primarily electric energy that could be used for light signalling, sensing of the membrane properties and membrane motion detection. The obtained data showed the unique as well as usable properties of PVDF membranes. From this point of view, the gain and analysis of the electrical responses to combined electro–mechanical loads of PVDF membranes have been the focus of our effort. The detected electrical response of the PVDF membrane to their electro–mechanical pulses indicated the possibility of using this phenomenon. Among others, it suggests monitoring of membrane fouling and use for a self-cleaning mechanism.

2. Results

A PVDF non-woven fibre structure was prepared by technology of electrospinning from its dimethyl formamide solution. The main idea was to prepare free standing membrane structure susceptible to mechanical deformations. PVDF fibres were pulled out from solution of PVDF powder in dimethylformamide (DMF), stretched and dried in the process of spinning and collected on polypropylene (PP) substrate. The structure of membrane was investigated by SEM analysis and results are presented in Figure 1. The upper part of the figure (a) shows a surface view of the membrane consisting of entangled PVDF fibres of different diameters and (b) a detailed view of the fibres. Porosity of PVDF membrane ϕ was calculated using $\phi_{net} = 1 - \rho_{net}/\rho_{PVDF}$ [8], where ρ_{net} is the apparent density of PVDF network ($\rho_{net} = 0.402 \text{ g/cm}^3$, determined by membrane weighting and measuring dimensions) and ρ_{PVDF} bulk PVDF density ($\rho_{PVDF} = 1.780 \text{ g/cm}^3$). PVDF membrane has porosity 0.77%.

Membrane cross-section with a layered longitudinal fibre structure obtained by breaking it after cooling in liquid nitrogen is shown in Figure 1c. The distribution of measured diameters is presented in Figure 1d. Fibre diameters are approximately from 50 to 300 nm with average fibre diameter $182 \pm 51 \text{ nm}$. The average fibre diameter and fibre diameter distribution of prepared PVDF membrane were determined from 100 randomly selected fibres from SEM images.

The X ray diffraction analysis (XRD) was used to confirm the presence of β -phase crystals in PVDF electrospun fibres. Measured XRD spectra are presented in Figure 2, Part (a). Owing to the applied high voltage during fibre spinning, providing strong electrostatic force between electrodes and the stretching polymer chains, induced diffraction lines at $2\theta = 18.06^\circ$ and 20.3° , which indicate nonpolar α -phase crystals and polar β -phase crystals, respectively [9,10]. The crystallinity X_c of prepared PVDF electrospun nanofibres was calculated using

$$X_c = \frac{\sum A_{cr}}{\sum A_{cr} + \sum A_{amr}} \times 100 [\%] \quad (1)$$

where ΣA_{arm} and ΣA_{cr} are the total integral areas of amorphous halo and crystalline diffraction peaks, respectively [4]. According to this analysis, the crystallinity was about 50.8%.

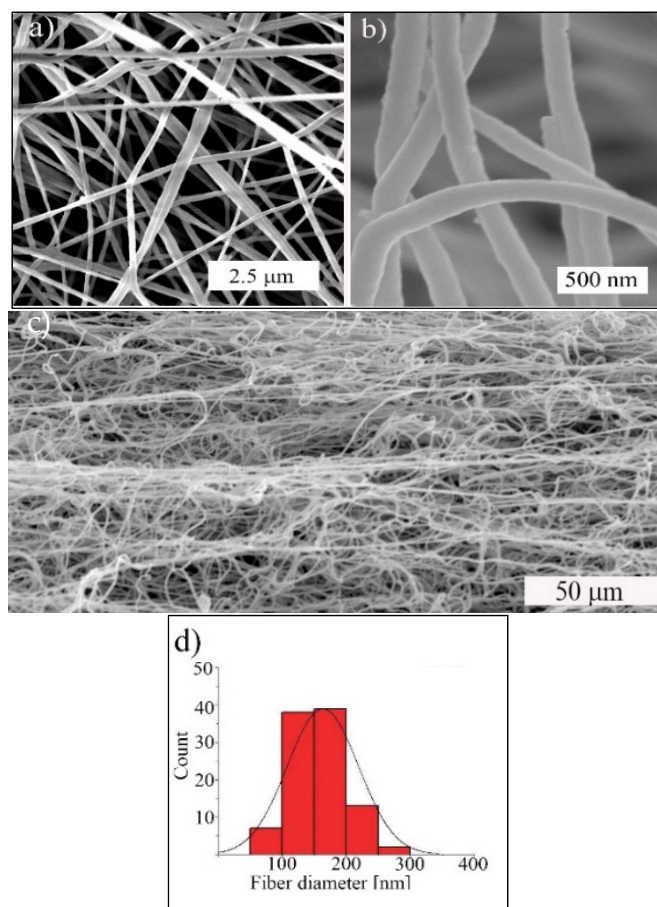


Figure 1. SEM micrographs of an electrospun PVDF membrane (a) shows a surface view of the membrane consisting of entangled PVDF fibres of different diameters, (b) a detailed view of the fibres, (c) membrane cross-section with a layered longitudinal fibre structure obtained by breaking it after cooling in liquid nitrogen, (d) the distribution of fibre diameters.

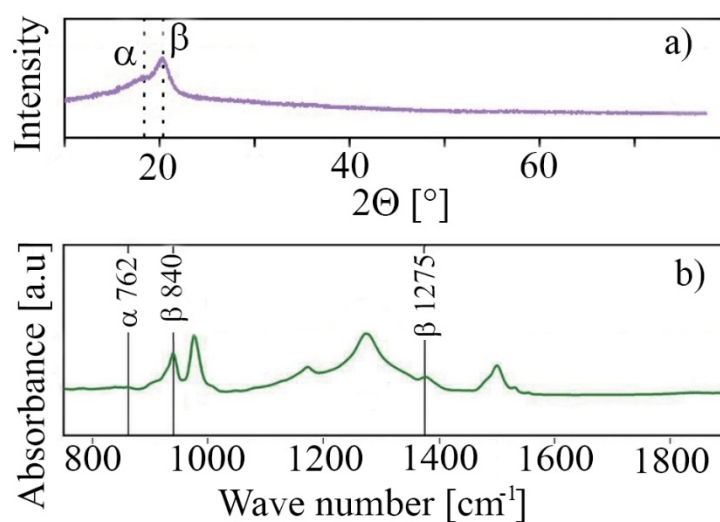


Figure 2. Part (a) represents XRD analysis and part (b) FT-IR analysis, both for electrospun PVDF fibre network.

The α and β -phase contents were determined by means of FT-IR spectra measured with a Fourier transform infrared spectrometer Figure 2b. The fraction of β -phase in fibres denoted $F(\beta)$ was calculated using the Lambert–Beer law [4,11]

$$F(\beta) = \frac{A_{\beta}}{\left(\frac{K_{\beta}}{K_{\alpha}}\right)A_{\alpha} + A_{\beta}} \quad (2)$$

where A_{α} and A_{β} represent the absorbance at 764 and 840 cm^{-1} and coefficients K_{α} and K_{β} represent the absorption coefficients at 764 and 840 cm^{-1} and had values $6.1 \times 10^4 \text{ cm}^2 \text{ mol}^{-1}$ and $7.7 \times 10^4 \text{ cm}^2 \text{ mol}^{-1}$, respectively. Portion of polar β -phase crystals β was determined using Equation (3) [12]

$$\beta = F(\beta) \times X_c [\%], \quad (3)$$

at a value of about 85%.

Piezoelectric response of PVDF membrane to pressure pulse at the surface (see schematic illustration Figure 3a from five identical pendulum impacts (Pendulum tester for evaluating impact resistance; POLYMERTEST, Zlin, Czech Republic). During the impact, the PVDF membrane was compressed and after the pendulum rebounded, the membrane regained its original thickness after in about five ms. The idea of this setup was to modulate mechanical vibrations on PVDF piezoelectric membrane and is potential for following energy harvesting if energy is generated in many cycles.

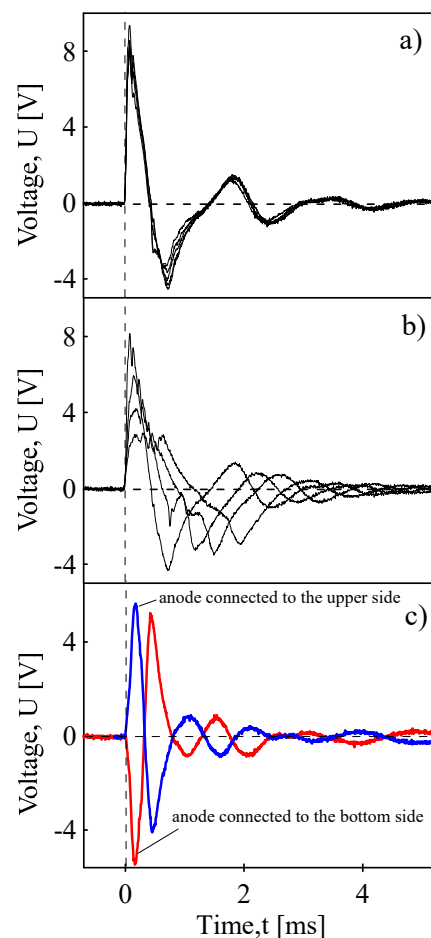


Figure 3. Piezoelectric response to a pressure pulse on the surface of PVDF membrane after pendulum impact. (a) Five impacts of the same mechanical energy, (b) response to impacts of pendulum when impacts were reduced by the absorbed impact energy from the previous cycle, (c) piezoelectric response when anode is connected to upper side or bottom side of membrane, respectively, demonstrating the polarity of the membrane.

Another experiment showed the piezoelectric response to the repeated faded pendulum impacts. The first impact cycle had full energy. The next one faded in intensity when impact was reduced by the absorbed impact energy in the previous cycle. It could be said that the first cycle had energy 100% (it means impact energy 0.5 J and velocity $2 \text{ m}\cdot\text{s}^{-1}$). The second impact after rebounding had 35% of the first cycle energy and so on. The third 20% and the fourth 15%, Figure 3b. As the impact energy successively decreased, the generated piezoelectric voltage decreased as well.

Figure 3c demonstrates the piezoelectric response when the anode of oscilloscope is connected to the upper side or bottom side of the membrane. It demonstrates polarity of the membrane during deformation. Without this phenomenon, any piezoelectric effect could not exist for the membrane made of randomly arranged fibres. Here the electric dipoles randomly oscillate and the total spontaneous polarization from the electric dipoles is constant and without the mechanical stimulus, no output current or voltage can be observed [13]. So, when the anode is connected to the upper side of the membrane, a positive piezoelectric signal is generated during compression (Figure 3c; blue curves). When the pendulum bounces, the fibre structure of the membrane relaxes to its original thickness and the piezoelectric signal starts to decrease and finally to be negative. When the polarity of the fabricated piezoelectric device is connected oppositely, in respect to the oscilloscope anode, the response is reversed and the electrical output curve is flipped (red curve). This “switching polarity” [14] depends on the connection of top/bottom electrodes and then in the direction of the flow of generated electrons. This radial piezoelectricity from randomly oriented electrospun PVDF nanofibres was also demonstrated in [15]. When the anode is connected to the upper electrode, electrons move to the anode and during this pressure loading, the upper surface starts to macroscopically be more positive. This can be caused by a larger deformation of the PVDF membrane in the upper layers, while the deformation of the lower layers is thus partially dampened.

As is well known, the impact loading of PVDF membranes can be used for a piezoelectric energy harvesting. We assembled an electrical circuit with Graetz bridge and a storage capacitor to show this phenomenon Figure 4a. The Graetz bridge serves to direct to convert the generated piezoelectric AC signal to a DC one which was stored in the capacitor. After usually 20 to 160 cycles of pendulum, the circuit was short circuited to measure the discharging time of stored energy or to light up three led diodes connected in series. Time-dependency of the discharge for different number of the pendulum bounces is shown in Figure 4b and lighting the diodes after 20 bounces in Figure 4c (duration of lighting is around 8 ms according to the data from Figure 4b). The increased number of harvesting cycles increased the short-circuit voltage by up to 30 V after the 160 impact cycles.

Sound waves, which produce pressure changes over the surface of the piezoelectric PVDF membrane, generate electricity that can be used for vibration sensing [16,17] to detect sound in cochlear implants [18] and abnormalities in the heart sound [19] or for sound energy harvesting [13].

In our sound detection test of the prepared PVDF membrane, the membrane was installed into the experimental setup. There were two rings between PVDF membrane, which was fixed and tensioned with screws. Sound pressure spectra were generated by speaker (Logitech, Speaker system Z 323) in a frequency range 100–3000 Hz. Generated sound was selected to be in discrete steps at 50 Hz to record the piezoelectric response as a peak-to-peak value. Figure 5a,b represents the membrane piezoelectric response to seven handclaps.

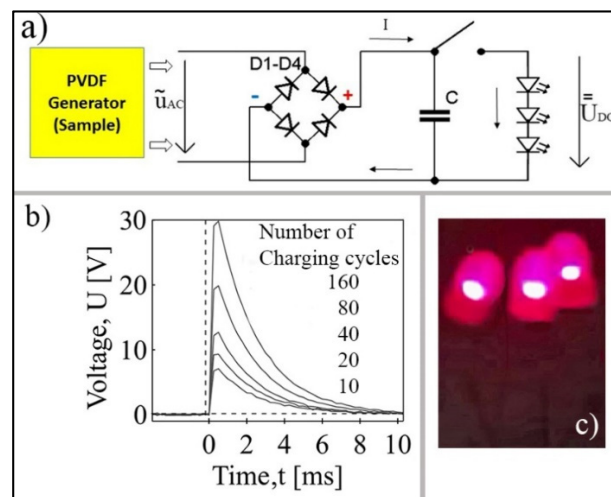


Figure 4. Energy harvesting. (a) Graetz bridge with storage capacitor, (b) discharge of stored voltage for different number of impact cycles, part (c) light flash of three LED diodes connected in a series after 20 impact cycles.

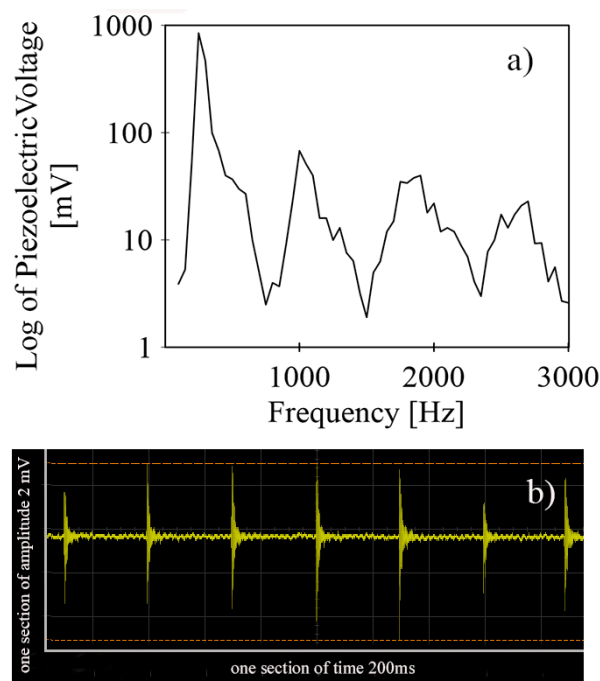


Figure 5. (a) Frequency spectra of generated piezoelectric voltage by a PVDF membrane as a response to sound generated by the speaker in a frequency range 100–3000 Hz, (b) membrane piezoelectric response to seven handclaps. (Note: one section is represented by the range between two grid lines on the graph background represented by thin white lines.)

As mentioned above, the piezoelectric response of the PVDF membrane to deformation depends on its coupling to electrical polarization. However, the effect is inherently reversible. A deformation can occur as a result of the displacement of ions in the crystals being exposed to an electric field. To show it, we prepared a membrane and the experimental setup whose membrane responded with mechanical deformation to the DC input denoted as U_{DC} . Then the inner electro–mechanical coupling induced the output voltage shown in Figure 6. If the AC voltage was applied, then the induced PVDF membrane mechanical vibrations generated a corresponding sine voltage delayed in degrees, as shown in Figure 7.

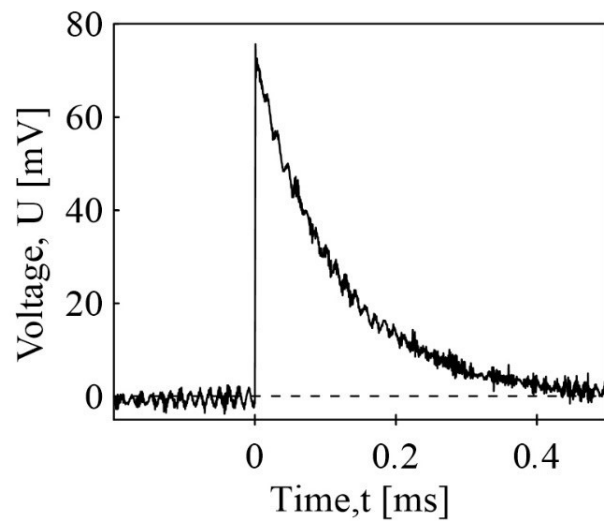


Figure 6. The electrospun PVDF membrane time dependent response to its mechanical deformation. The inner electro–mechanical coupling induced output voltage (~ 77 mV peak) from the membrane mechanical response to the input DC signal.

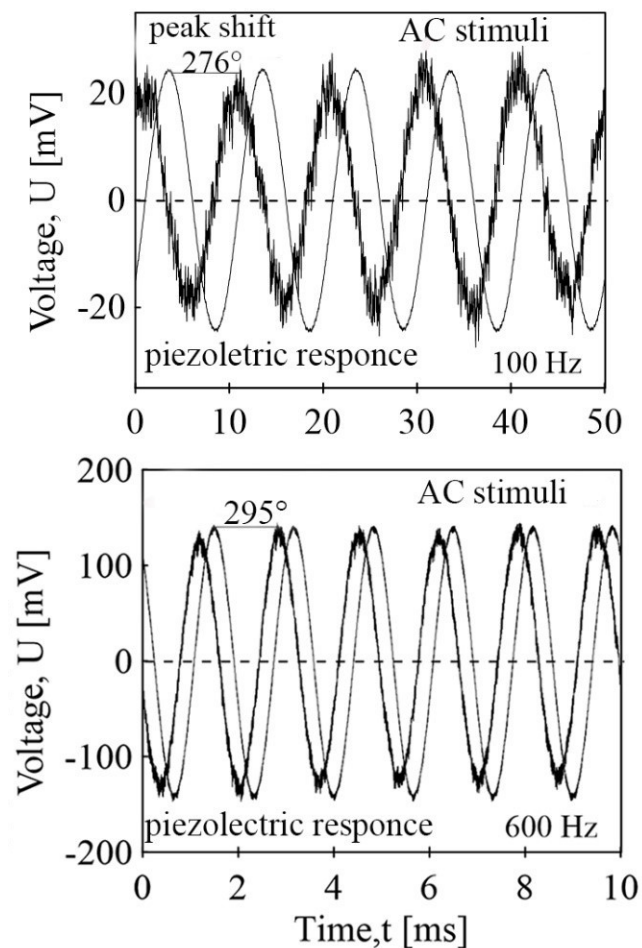


Figure 7. The electrospun PVDF membrane response to its mechanical vibrations. The input AC with a voltage ± 10 V and a frequency of 100 and 600 Hz, plotted with a thin smooth line, induced mechanical vibrations of a membrane. The inner electro–mechanical coupling induced an output voltage from the vibrating membrane plotted with a jagged line in the graph. There is significant delay between stimulated AC signal and piezoelectric response, indicated in figures in units of degree.

3. Discussion

This study introduced electroactive PVDF membranes whose electrospun structure manifested the mechano–electric coupling through piezoelectricity and electro–mechanical coupling through inverse piezoelectricity. When the PVDF membrane was under mechanical stress, deformation of the covalent crystals of the β -PVDF crystalline face generated an electric charge while the displacement of ions in the crystals of the β -PVDF crystalline face from an external electric field resulted in overall strain. The piezoelectric responses were detectable and measurable in units of volts, Figures 3 and 4. Figure 3c demonstrates the piezoelectric response when the anode of oscilloscope is connected to the upper side or bottom side of the membrane. It demonstrates polarity of the membrane during deformation. Without this phenomenon, any piezoelectric effect could not exist for the membrane made of randomly arranged fibres. Here the electric dipoles randomly oscillate and the total spontaneous polarization from the electric dipoles is constant and without the mechanical stimulus, no output current or voltage can be observed [13]. So, when the anode is connected to the upper side of the membrane, a positive piezoelectric signal is generated during compression (Figure 3c; blue curves). When the pendulum bounces, the fibre structure of the membrane relaxes to its original thickness and the piezoelectric signal starts to decrease and finally to be negative. When the polarity of the fabricated piezoelectric device is connected oppositely, in respect to the oscilloscope anode, the response is reversed and the electrical output curve is flipped (red curve). This “switching polarity” [14] depends on the connection of top/bottom electrodes and then in the direction of the flow of generated electrons. This radial piezoelectricity from randomly oriented electrospun PVDF nanofibres was also demonstrated in [14,15,20,21]. When the anode is connected to the upper electrode, electrons go to the anode and during this pressure loading, the upper surface starts macroscopically to be more positive. This can be caused by a larger deformation of the PVDF membrane in the upper layers, while the deformation of the lower layers is thus partially dampened. Finally, the charge generated in this way could be used for sufficient energy harvesting and sound detection. When collecting the energy (the energy harvesting) by means of an electronic circuit with the Graetz bridge and the storage capacitor voltage of 70 V, the collected charge was sufficient to blink three LED diodes connected in millivolts (Figure 5b).

The PVDF membrane loaded by sound pressure spectra in the frequency range 100 Hz–3000 Hz that was generated induced an electric response in mV units (Figure 5a). Since the membrane interfered at the same time with electro–magnetic waves, both from the electrical wires in the wall of the building (50 Hz, and intensity measured by the oscilloscope about 50 mV) and the waves generated by the speaker, the experimental setup was placed into the Faraday cage made of a special steel mesh constructed for the electromagnetic shielding (electro-smog shielding metallic fabric, mesh width 1.0 mm, wire diameter 0.16 mm, mesh thickness 0.32 mm, open area 70%, weight 260 g/m²). The shielding was capable of suppressing the AC 50 Hz voltage to intensity below about 150 μ V. The measured response to sound that was generated by clapping hands in the detected PVDF membrane response was in units of millivolts (Figure 5b).

The key results of our study were obtained as a reaction of our PVDF membranes to the electro–mechanical loading. If the AC voltage was applied and then induced, the PVDF membrane mechanical vibrations would generate the corresponding and significant sine piezoelectric voltage.

The data were collected simultaneously by oscilloscope, where from one channel of the AC generator with T-splitter for measurement of AC stimuli and from a second channel the generated piezoelectric response were connected to two different inputs of the oscilloscope. It can be expressed as a value of its amplitude and has significant signal delay as a peak shift in degrees (Figure 7). The AC stimuli of 20 V (peak-to-peak) and frequency 100 Hz generate sine mechanical deformation which induce piezoelectric voltage response with an amplitude of approximately 40 mV (peak-to-peak) and 100 Hz frequency and piezoelectric voltage with delay of 276°. In case of an input deformation, the AC

voltage of 10 V (peak-to-peak) and a frequency of 600 Hz, the amplitude of the piezoelectric response was 236 mV and the time delay of the piezoelectric response was 295°. The detected electrical response of the PVDF membrane to their electro-mechanical pulses indicated the possibility of using this phenomenon. The measurements also pose that it is not only the frequency of the stimulating AC voltage moderate phase shift of the piezoelectric signal, it also has a significant effect on the generated piezoelectric voltage, measured as the peak-to-peak amplitude value. A following paper will focus on this phenomenon and our preliminary results reporting that there is a piezoelectric response to AC frequency stimuli from mHz to an approximate size of MHz with two transitions at frequencies of around 60 Hz and 90 kHz. In addition, the maximal amplitude of generated piezoelectric voltage depends on units of AC stimuli voltage. It increases linearly on the AC voltage peak-to-peak from 3, 5, 10, 15 and 20 V reaching the maxima of 85, 137, 286, 408 and 557 mV, respectively, in plateau for between frequencies approximately 7–20 kHz. The response of the substances to the action of an electric field has two limiting cases. It is an irreversible change, a time-dependent transport of electrically charged particles that are present in the substance. An electric current is created, and substances are called electrical conductors. Alternatively, electrical displacement occurs due to the formation of induced dipoles, or dipoles already present in the substance, such as in PVDF covalent β crystals as C-F bonds (with partial charge δ^-) and C-H bonds (δ^+). This accumulation of energy is then reversible and disappears after the field has been extinguished. The electrical shift is generally time-dependent, and a phase shift is induced between the input stimulus and the response [22–24].

A future work will focus on the detection of the filtration process of aqueous solutions and dispersions (variables can be like change of solutions viscosity, electrical conductivity, filtration of dyes or steroids or particles such as kaolin and algae). Detection of filter fouling will be based both on the amplitude of the generated piezoelectric voltage and by changing the frequency spectrum of the AC stimulated membrane. Subsequently, experiments about the possibility of using electrostriction to clean the filter will start.

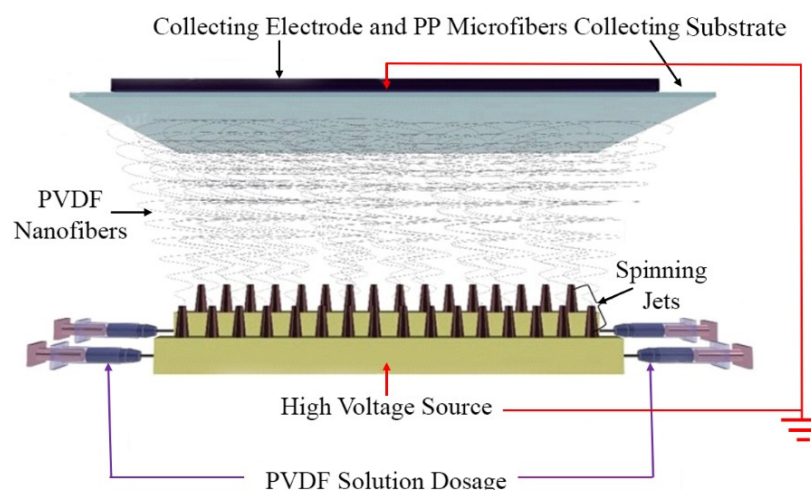
4. Materials and Methods

4.1. Electrospinning of PVDF Membrane

PVDF polymer was purchased from Arkema as a brand Kynar Flex[®] 2801, Zhejiang, China. It had a powder state and was dissolved in dimethylformamide (DMF) from Brenntag CR s.r.o, Chropyne, Czech Republic. Both were of analytical grade and no additional purification was necessary. PVDF in DMF was prepared as 20 wt. % PVDF solution by dissolving 2 g of polymer in 8 g DMF as solvent. The solution was then stirred with a magnetic stirrer at 340 rpm at 40° C for 2 hrs. The process of electrospinning was performed at room temperature (22–24 °C) and a relative humidity about 31–34%. The construction of electrospinning apparatus (Spin line 40, Zlin, Czech Republic, Scheme 1) was carried out with 32 static hollow stainless steel, each having an inner diameter of 1.5 mm. The voltage between needles and collecting electrode was 65 kV, at a distance of 20 cm and a dosing volume of 2.3 cm³ per hour. Nanofibre networks were collected at two different times of 10 and 30 min of electrospinning process with a final thicknesses of 18 and 400 μ m, respectively. PVDF nanofibres were collected during processing on spun-bond prepared non-woven polypropylene, collected in the capacity of 30 g/m².

4.2. Analysis

The structure of prepared PVDF network was analyzed using the scanning electron microscope—SEM (NOVA NanoSEM 450, FEI Co., Hillsboro, OR, USA) at an accelerating voltage of 10 kV. The average nanofibre diameter and fibre diameter distribution were analyzed from the obtained SEM pictures using Digimizer, version 5.4.4, MedCalc Software, Ostend, Belgium and one hundred measurements of randomly selected parts of fibres.



Scheme 1. Experimental setup of PVDF nanofibre network fabrication by electrospinning technology.

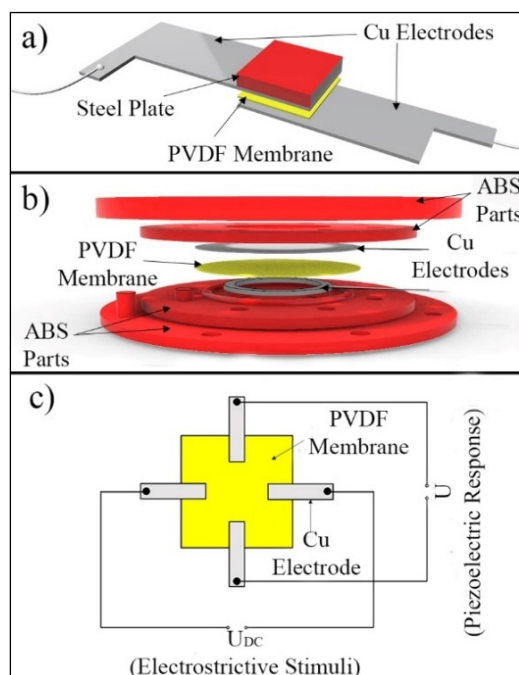
The crystalline content was calculated from data obtained by X-ray diffraction—XRD (MiniFlex™ diffractometer, Malvern Panalytical, Malvern, UK) with CoK_{β} radiation operated at 40 kV and 15 mA. The samples were scanned in a 2θ range of $10\text{--}90^{\circ}$. The collected data using cobalt source were converted to copper source using the program 15 PowDLL software [25,26].

Fourier transform infrared (FT-IR) spectrometer (NICOLET iS5, Fisher, Thermo Scientific, Waltham, MA, USA) was used to check the content of β phase fraction in the prepared PVDF fibres. The apparatus worked in attenuated total reflection (ATR) mode using a diamond crystal in the wavenumber range of $400\text{--}4000\text{ cm}^{-1}$ at a resolution of resolution 4 cm^{-1} .

4.3. Piezoelectric and Electrostriction Measurements

Several measurements to prove and quantify piezoelectric and electrostriction performers for the prepared PVDF polymer membrane structure composed of electrospun fibres were performed. An oscilloscope (Infinivision 1000 x-series, 4ch, 100 MHz, DSOX1204A, Keysight, Santa Rosa, CA, USA) was used to measure the generated piezoelectric voltage. In this course, three types of experimental setups with incorporated PVDF electrospun non-woven membrane were prepared, as presented in Scheme 2. Part (a) of the schematic illustration represents the experimental setup for mechanical loading on the top surface of the PVDF membrane by pressure pulses using an instrument for the impact flexibility of rubbers (Polymer test, Versta, Zlin, Czech Republic). There are two copper electrodes to measure the generated piezoelectric potential, the electrodes made of Cuprexite (double layer structure containing Cu foil fixed by glass fibre epoxy plate) between which PVDF membrane is fixed with a thickness of $400\text{ }\mu\text{m}$. Finally, a steel plate ($18 \times 18\text{ mm}$) was placed on top of the membrane to avoid its destruction in the area of the pendulum impact. The energy of impact was 0.5 J with an impact velocity of 2 m/s .

Scheme 2a shows the experimental setup for the detection of sound. Sound pressure spectra were generated by speaker (Speaker system Z 323, Logitech, Newark, CA, USA) in a frequency range $100\text{--}3000\text{ Hz}$. Generated sound was selected to be in discrete steps 50 Hz to record piezoelectric response of mV as a peak-to-peak value from a distance of 20 mm and a sound intensity of 100 dB (Figure 5a). In Figure 5b, the plot shows the electrical response to clapping hands 30 cm from the top surface of fixed and tightened PVDF membrane. The diameter of the PVDF membrane was 50 mm with a thickness of $18\text{ }\mu\text{m}$. The membrane was fixed with the help of plastic three-dimensional (3D) printed acrylonitrile butadiene styrene (ABS) parts. The sound of clapping creates sound pressure waves that vibrate the stretched membrane, which generate an electric voltage detected and measured with help of an oscilloscope.



Scheme 2. Three types of experimental setups with incorporated PVDF electrospun non-woven membrane to detect and measure piezoelectric and electrostriction responses (a) to mechanical loading by pressure pulse, (b) detection of the sound of clapping hands, (c) conversion of electrostriction to piezoelectric response.

Scheme 2c represents the experimental setup for proving and demonstrating the electro–mechanical response. There are two electrical circuits. The first causes electrostrictive stimuli by direct current (DC) of 30 V with the help of power supply Metex AX 502 (AEMC Instruments, Dover, NH, USA). When the power supply was turned on, it led to electrostriction of PVDF membrane (30 × 30 mm and thickness 400 μm). The deformation of PVDF membrane by DC stimuli was measured by the perpendicular pair of electrodes creating the second electric circuit as the piezoelectric response following deformation by electrostriction.

5. Conclusions

A PVDF membrane was prepared by the technology of electrospinning from polymer solution. When fibres were solidified under tension, it led to the formation of the molecular dipolar orientation of polymer chains with zigzag/all-trans configuration. The representative data of membrane ability to generate electricity in response to mechanical deformation as well as to electro–mechanical deformation have been shown. In particular, the detected electrical response of the PVDF membrane to their electro–mechanical pulses suggested the possibility of using this phenomenon. Among others, e.g., for monitoring of membrane fouling and use for a self-cleaning mechanism. For instance, induced membrane mechanical vibrations can prevent particles from fouling the membrane and thus cleaning it.

Author Contributions: Conceptualization, validation, formal analysis, investigation, writing—original draft preparation, writing—review and editing, P.S.; investigation and resources, R.O.; investigation and resources, J.M.; writing—review and editing and supervision, B.H.; writing—original draft preparation, writing—review and editing, P.R.; resources, R.D.; resources, D.K. All authors have read and agreed to the published version of the manuscript.

Funding: This research was funded by Ministry of Education, Youth and Sports of the Czech Republic DKRVO (RP/CPS/2022/007).

Data Availability Statement: The data presented in this study are available on request from the corresponding author, P.S.

Acknowledgments: This work was supported by the Ministry of Education, Youth and Sports of the Czech Republic DKRVO (RP/CPS/2022/007, and also by the internal grants of TBU in Zlin No. IGA/CPS/2020/008 and IGA/CPS/2021/003 funded from the resources of the Specific University Research.

Conflicts of Interest: The authors declare no conflict of interest.

References

1. Li, J.; Meng, Q.; Li, W.; Zhang, Z. Influence of crystalline properties on the dielectric and energy storage properties of poly(vinylidene fluoride). *J. Appl. Polym. Sci.* **2011**, *122*, 1659–1668. [CrossRef]
2. Zhu, G.; Zeng, Z.; Zhang, L.; Yan, X. Piezoelectricity in beta-phase PVDF crystals: A molecular simulation study. *Comput. Mater. Sci.* **2008**, *44*, 224–229. [CrossRef]
3. Jaffe, B.; Roth, R.S.; Marzullo, S. Piezoelectric properties of lead zirconate-lead titanate solid-solution ceramics. *J. Appl. Phys.* **1954**, *25*, 809–810. [CrossRef]
4. Che, J.; Neri, W.; Ly, I.; Poulin, P.; Zakri, C.; Yuan, J. Waterborne Nanocomposites with Enhanced Breakdown Strength for High Energy Storage. *ACS Appl. Energy Mater.* **2020**, *3*, 9107–9116. [CrossRef]
5. Lombardi, G.; Lallart, M.; Kiziroglou, M.; Yeatman, E.M. A piezoelectric self-powered active interface for AC/DC power conversion improvement of electromagnetic energy harvesting. *Smart Mater. Struct.* **2020**, *29*, 117002. [CrossRef]
6. Bandyopadhyay, S.; Saha, N.; Brodnjak, U.V.; Saha, P. Bacterial cellulose based greener packaging material: A bioadhesive polymeric film. *Mater. Res. Express* **2018**, *5*, 115405. [CrossRef]
7. Zednicek, T.; Faltus, R.; Jane, M. Storage Capacitor Properties and Their Effect on Energy Harvester Performance. PCIM Europe Conference Proceedings, International Exhibition and Conference for Power Electronics. 2012, pp. 1523–1531. Available online: <https://www.kyocera-avx.com/docs/techinfo/Tantalum-NiobiumCapacitors/EnergyHarvesting.pdf> (accessed on 6 September 2022).
8. Lang, C.; Fang, J.; Shao, H.; Ding, X.; Lin, T. High-sensitivity acoustic sensors from nanofibre webs. *Nat. Commun.* **2016**, *7*, 11108. [CrossRef]
9. Tohluebaji, N.; Putson, C.; Muensit, N. High Electromechanical Deformation Based on Structural Beta-Phase Content and Electrostrictive Properties of Electrospun Poly(vinylidene fluoride- hexafluoropropylene) Nanofibers. *Polymers* **2019**, *11*, 1817. [CrossRef]
10. Sencadas, V.; Gregorio, R.; Lanceros-Méndez, S. α to β Phase Transformation and Microstructural Changes of PVDF Films Induced by Uniaxial Stretch. *J. Macromol. Sci. Part B* **2009**, *48*, 514–525. [CrossRef]
11. Low, Y.K.A.; Tan, L.Y.; Tan, L.P.; Boey, F.Y.C.; Ng, K.W. Increasing solvent polarity and addition of salts promote β -phase poly(vinylidene fluoride) formation. *J. Appl. Polym. Sci.* **2013**, *128*, 2902–2910. [CrossRef]
12. Xu, F.; Yang, J.; Dong, R.; Jiang, H.; Wang, C.; Liu, W.; Jiang, Z.; Zhang, X.; Zhu, G. Wave-Shaped Piezoelectric Nanofiber Membrane Nanogenerator for Acoustic Detection and Recognition. *Adv. Fiber Mater.* **2021**, *3*, 368–380. [CrossRef]
13. Luo, G.; Luo, Y.; Zhang, Q.; Wang, S.; Wang, L.; Li, Z.; Zhao, L.; Teh, K.S.; Jiang, Z. The Radial Piezoelectric Response from Three-Dimensional Electrospun PVDF Micro Wall Structure. *Materials* **2020**, *13*, 1368. [CrossRef]
14. Yang, R.; Qin, Y.; Li, C.; Dai, L.; Wang, Z.L. Characteristics of output voltage and current of integrated nanogenerators. *Appl. Phys. Lett.* **2009**, *94*, 022905. [CrossRef]
15. Fang, J.; Zhu, Y.; Lin, T. Electrical power generator from randomly oriented electrospun poly (vinylidene fluoride) nanofibre membranes. *J. Mater. Chem.* **2011**, *21*, 11088–11091. [CrossRef]
16. Hwang, S.H.; Han, C.M.; Yoon, H.N.; Jung, D.W.; Lee, Y.J.; Jeong, D.-U.; Park, K.S. Polyvinylidene fluoride sensor-based method for unconstrained snoring detection. *Physiol. Meas.* **2015**, *36*, 1399–1414. [CrossRef] [PubMed]
17. Park, S.; Guan, X.; Kim, Y.; Creighton, F.; Wei, E.; Kymissis, I.; Nakajima, H.H.; Olson, E.S. PVDF-Based Piezoelectric Microphone for Sound Detection Inside the Cochlea: Toward Totally Implantable Cochlear Implants. *Trends Hear.* **2018**, *22*, 2331216518774450. [CrossRef] [PubMed]
18. Liu, B.; Han, L.; Pan, L.; Li, H.; Zhao, J.; Dong, Y.; Wang, X. Flexible Multiscale Pore Hybrid Self-Powered Sensor for Heart Sound Detection. *Sensors* **2021**, *21*, 4508. [CrossRef]
19. Chen, F.; Wu, Y.; Ding, Z.; Xia, X.; Li, S.; Zheng, H.; Diao, C.; Yue, G.; Zi, Y. A novel triboelectric nanogenerator based on electrospun polyvinylidene fluoride nanofibers for effective acoustic energy harvesting and self-powered multifunctional sensing. *Nano Energy* **2019**, *56*, 241–251. [CrossRef]
20. Ahmed, A.; Jia, Y.; Huang, Y.; Khoso, N.A.; Deb, H.; Fan, Q.; Shao, J. Preparation of PVDF-TrFE based electrospun nanofibers decorated with PEDOT-CNT/rGO composites for piezo-electric pressure sensor. *J. Mater. Sci. Mater. Electron.* **2019**, *30*, 14007–14021. [CrossRef]
21. Ahmed, A.; Jia, Y.; Deb, H.; Arain, M.F.; Memon, H.; Pasha, K.; Huang, Y.; Fan, Q.; Shao, J. Ultra-sensitive all organic PVDF-TrFE E-spun nanofibers with enhanced β -phase for piezoelectric response. *J. Mater. Sci. Mater. Electron.* **2022**, *33*, 3965–3981. [CrossRef]
22. Yousry, Y.; Yao, K.; Chen, S.; Liew, W.H.; Ramakrishna, S. Mechanisms for Enhancing Polarization Orientation and Piezoelectric Parameters of PVDF Nanofibers. *Adv. Electron. Mater.* **2018**, *4*, 1700562. [CrossRef]

23. Yadav, V.S.; Sahu, D.K.; Singh, Y.; Kumar, M.; Dhubkarya, D.C.; Ao, S.-I.; Katagir, H.; Xu, L.; Chan, A.H.-S. Frequency and Temperature Dependence of Dielectric Properties of Pure Poly Vinylidene Fluoride (PVDF) Thin Films. *AIP Conf. Proc.* **2010**, *1285*, 267–278. [[CrossRef](#)]
24. Da Silva, A.B.; Wisniewski, C.; Esteves, J.V.A.; Gregorio, R. Effect of drawing on the dielectric properties and polarization of pressed solution cast β -PVDF films. *J. Mater. Sci.* **2010**, *45*, 4206–4215. [[CrossRef](#)]
25. Patwa, R.; Saha, N.; Saha, P. Magnetic hydrogel based shoe insoles for prevention of diabetic foot. *J. Magn. Magn. Mater.* **2020**, *514*, 167153. [[CrossRef](#)]
26. Slobodian, P.; Riha, P.; Lengalova, A.; Svoboda, P.; Saha, P. Multi-wall carbon nanotube networks as potential resistive gas sensors for organic vapor detection. *Carbon* **2011**, *49*, 2499–2507. [[CrossRef](#)]

Multifunctional flexible and stretchable polyurethane/carbon nanotube strain sensor for human breath monitoring

Petr Slobodian  | Romana Danova  | Robert Olejnik  | Jiří Matyas  | Lukas Münster 

Centre of Polymer Systems, University
Institute, Tomas Bata University, Zlin, Czech
Republic

Correspondence

Petr Slobodian, Centre of Polymer Systems,
University Institute, Tomas Bata University, Tr.
T. Bati 5678, 760 01 Zlin, Czech Republic.
Email: slobodian@utb.cz

Funding information

European Regional Development Fund (ERDF);
Ministry of Education, Youth and Sports of the
Czech Republic - Program NPU I, Grant/Award
Number: LO1504; TBU, Grant/Award Number:
IGA/CPS/2018/005

Flexible and stretchable polyurethane/carbon nanotube composite with strain detection ability was used for human breath monitoring. The composite material consisted of a network of multiwalled carbon nanotubes and thermoplastic high elastic polyurethane. It was found that elongation of the composite led to a macroscopic increase in electrical resistance, which can be used as a principle for applied strain detection. This detection was reversible, durable, and sensitive with gauge factor reaching very promising value, as, for example, ~ 46 at applied deformation of 8.7%. Further, the composite could be elongated to very large extend of deformation without discontinuity in measured resistance change reaching gauge factor ~ 450 at composite mechanical break at $\sim 300\%$ of strain. Sensor durability was also confirmed by sine wave deformation cycling when any decrease in the sensor properties for more than 10^3 cycles was observed. Simultaneously, the prepared composite possessed other utility properties also and was considered as multifunctional when it was tested as an organic solvent vapor sensor, an element for Joule heating and finally as a microstrip antenna.

KEYWORDS

carbon nanotubes, conductive polymer composites, flexible and stretchable strain sensor, flexible electronics

1 | INTRODUCTION

Currently, an electrically conductive and elastic polymer composite materials or conductive polymer composites are in focus of material scientists all over the world. It is their special attention for technology of sensors mainly for deformation detection, which is very topical. An excellent deformation capability compared to the traditional rigid metallic strain gauges and conductors predetermines them for new and beneficial applications.¹⁻¹⁴ These composite materials are usually composed as two component systems using electrically conductive filler (nanowires² or metal particles,³ but mainly carbon-based materials like carbon nanotubes [CNTs],⁴⁻⁹ carbon nanofibers,¹ carbon black [CB],¹⁰ graphite flakes,¹¹ graphite,¹² or graphene [GF]¹³) dispersed in a polymeric matrix or superimposed on polymer-based

support. The deformation of these polymer composite units results in a change in their electrical conductivity due to the piezoresistive properties of the CNT conductive network. Here, changes in the contacts and tunneling distances between the CNT junctions occur. Effects in composite microstructure finally lead to an increase in composite macroscopic resistivity, which becomes a means of measure of composite tensile or compressive strain deformation. Flexible and elastic polymers are often used as a support of functional electrically conductive structures or as a bulk polymeric matrix for electrically conductive particles distributed in it. These materials are able to detect deformation of large extent due to their high degree of elasticity and flexibility, which is significantly higher than the ability of conventional strain deformation sensors. Finally, they also have other very perspective functional properties such as high sensitivity to

deformation stimulus, reversibility of responses, durability, and detection capability over many cycles. These advantageous functional properties predestine them to be materials very asked for and required for arising areas of interests such as health monitoring,¹² human-friendly wearable interactive systems or human motion detection,^{5,6,8,9,14} human-machine interfaces,^{5,15} electronic skins,⁴ smart fabrics,^{15,16} soft and smart robotics,¹⁴ or athletic training.¹²

As straightforward examples of practical compositions, properties and applications of elastic polymer composite materials applied for mechanical strain detection can be summarized in the following paragraph.

Nanocomposites based on multiwalled CNTs (MWCNTs) dispersed in polymeric matrix (up to 8 wt. %) based on a high elastic form-stable phase change polymer prepared by mixing of polyethyleneglykol and polytetrahydrofuran poses excellent flexibility and outstanding stretchability.⁴ When tensile strain is applied, change in MWCNT conductive network occurs and nanocomposite is capable to detect sensitively and reversibly applied mechanical stimuli by a measure of its macroscopic resistance. Authors of the paper consider fabricated nanocomposite as a potential candidate for e-skin or wearable devices, which was demonstrated by application of nanocomposite film positioning onto index finger to monitor its periodical bending. Finally, nanocomposites are also multifunctional, exhibiting further, a response to infrared light and temperature.⁴ Another approach to make flexible sensors for deformation detection is from the field of printed electronics. Meniscus-guided printing of MWCNTs/PVP (polyvinylpyrrolidone) aqueous dispersion can make microlines printed on PI (polyimide) substrate with a width of 60 μm .⁵ This method is commercially viable and inexpensive, making the sensors really small, and fitting on exactly required positions. Prepared printed sensor is durable up to measured 1500 cycles at strain of 2.0%, with gauge factor (GF) of 12.87. This method can further be used to print functional MWCNTs/PVP layer also on nonflat substrates. The above mentioned strain sensors belong to a group of so-called microcrack sensors characterized by deformation of the CNT/PVP network-induced crack formation. It leads to an increase in the distance between the MWCNTs, in effect, decreasing the number of contacts between MWCNTs and increasing the tunneling distance between them. Gradually, this process leads to an increase in macroscopic resistance. When deformation relaxes, cracks are closed and resistance reversibly decreases.⁵ Finally, a gesture-based human-machine interface was developed by the resistance change of glove-mounted sensors while bending a finger.⁵ Another types of crack-based sensor were demonstrated for example in previous studies.^{6-8,17,18} In another case, polymer/graphite sensor was capable to detect very soft human movements such as pulses, respiration rates, and throat vibration.¹² In the next paper, polydimethylsiloxane (PDMS)-based composites were fabricated by using a solution mixing-casting molding method incorporating into matrix hybrid CNTs/CB nanofillers.¹⁴ Transmission electron microscopy (TEM) analysis confirmed that CB nanoparticles bridge the gaps between the neighboring CNTs, leading to a synergistic effect in electrical conductivity of the conductive networks inside the PDMS matrix, simultaneously with an improvement in the strain sensing

performance of CNTs-CB/PDMS sensor. It exhibited high stretchability when elongated up to a strain of $\sim 300\%$. Nice repeatability and durability were demonstrated when dynamical loading/unloading cycles were applied (2500 cycles) with GF of 13.1 at range of strain 255–300%. Last but not least, ability of elastic polymer composite materials for human body joint monitoring application, gesture recognition, or a glove for the motion detection of fingers was demonstrated with the help of a different composite concept. Here the strain sensor was prepared by the incorporation of highly conductive polyaniline, graphene nanoplatelets, and silicon rubber onto elastic Lycra fabric via a spin-coating method.¹⁵ The incorporation of polyaniline microparticles improved sensor sensitivity to approximately four times, reaching the GF of 67.3 for this fabric like strain sensor.

Surprisingly, layered nanocomposite materials exhibit simultaneous multifunctionality beyond conventional properties. This concept is followed by researchers such as capability of gas sensing, detection of applied strain or stress, thermoelectric phenomenon, selectivity for vapor permeation, interaction with electromagnetic field, or feasibility of Joule heating. Carbon-based materials, such as CNTs,^{6,19} graphene,^{20,21} or carbon nanowalls,^{22,23} generally called the carbon nanoallotropes, have been effectively used for gas sensing applications. Here, the change of surrounding environment leads to variation of semiconducting properties of the allotropes owing to the changed current carrier concentration by adsorbed molecules on carbon surface.^{21,22} Moreover, the electrical conductivity of interconnected carbon-based networks may be changed by a gas, which changes a contact resistance of the structure of the junction.^{6,19,23,24} These structures also simultaneously detect deformation or stress stimulus in elongation^{25,26} or compression,²⁷ which was found to be sensitive and reversible with sufficient durability in the dynamic loadings measured by a macroscopic electrical resistance change. The electrically conductive carbon allotrope/polymer composites possess thermoelectric properties.^{28,29} In our recent article, the flexible thermopile based on the polymeric composites filled with different types of carbon fillers was demonstrated.³⁰ Moreover, the authors in a very recent paper showed that the thermoelectric power of macroscopic graphene composite varies in a gas environment defined by the molecular mass of adsorbed gas molecules.³¹ In other areas such as gas permeation through the CNT membrane, the published data clearly showed that hydrocarbon gases exhibit higher permeability than noncarbohydrates.²¹ Our recent measurements further indicated that the permeation rate can be conveniently stimulated by an electric current. The electrically conductive materials composed of different carbon allotropes like CNTs or carbon nanowalls or their structural polymeric nanocomposites are capable to interact with electromagnetic field in the course of so-called passive microstrip antenna, which receives or broadcasts data signal.³² The resonance frequency and the gain rise up from the nanostructured hierarchy of the composite and its chemical nature. This nature can be further influenced by internal stimuli like change of chemical composition of the ambient gas³³ or by microstrip deformation. When electrical current is applied to the electrically conductive carbon based mats or polymeric

composites, their temperature increases. The Joule heating depends on the composite morphology and can be further stimulated by proper carbon functionalization.³⁴

In the present paper, we demonstrate the fabrication of flexible and stretchable polyurethane/CNT strain sensor, which is applied for human breath monitoring. Finally, it was found that this new polymer composite was multifunctional when other application were demonstrated such as use as gas sensor, an element for Joule heating and finally use as a microstrip antenna.

2 | EXPERIMENTAL

2.1 | Materials and sample preparation

The polyester-based thermoplastic polyurethane (TPU) Desmopan 385S was supplied by Bayer MaterialScience. MWCNTs as fillers were purchased from Sun Nanotech Co. (China) produced by chemical vapor deposition method from acetylene as precursor, electrical resistivity of 0.12 Ωcm , and purity >90%. We determined the diameter of individual nanotubes by TEM to be between 10 and 60 nm and their length from tens of micrometers up to 3 μm .²⁸ The maximum aspect ratio of the nanotubes was about 300.

Polyurethane nonwoven porous membranes, for MWCNTs, dispersion filtration was prepared by electrospinning from polyurethane dimethyl formamide/methyl isobutyl ketone (DMF/MIBK, 1:3) solution. The conditions of electrospinning were as follows: a PU concentration of 16 weight % was prepared. Electrical conductivity of the solution was adjusted to 20 $\mu\text{S/cm}$ using sodium chloride, an electric voltage of 75 kV (Matsusada DC power supply), a temperature of 20–25°C, and a relative humidity of 25–35% (for a detailed schematic of experimental equipment, see Kimmer et al³⁵). The TPU compression molding temperature was selected according DSC (Perkin-Elmer Pyris 1) measurement to be 175°C performed at a heating rate of 10°C/min.

KMnO₄ oxidation: Oxidized MWCNTs were prepared in a glass reactor with a reflux condenser filled with 250 mL of 0.5 M H₂SO₄, into which 5 g of potassium permanganate (KMnO₄) as oxidizing agent and 2 g of MWCNTs were added. The dispersion was sonicated at 85°C for 15 hours using thermostatic ultrasonic bath (Bandelin Electronic DT 103H). The dispersion was filtered, and then MWCNTs were washed with concentrated HCl to remove MnO₂ and then washed with water until the system attained a pH of 7.

2.2 | Polyurethane/MWCNT laminate

Aqueous dispersion of MWCNTs was prepared by sonication in an apparatus from Dr. Hielscher GmbH (ultrasonic horn S7, amplitude 88 μm , power density 300 W/cm², and frequency 24 kHz) for 15 minutes at room temperature. The nanotube concentration in the suspension was 0.3 wt. %. Dispersion also contained surfactants, namely, sodium dodecyl sulfate and 1-pentanol with concentration 0.1 and 0.14 M, respectively. Moreover, NaOH aqueous solution

was added to adjust pH to 10. For making an entangled MWCNT network, a porous polyurethane membrane and a vacuum filtration method was used. About 30 mL of homogenized dispersion was filtered through the funnel of diameter 90 mm. The prepared MWCNT network was washed several times with deionized water (65°C), afterwards by methanol in situ and dried between two filtration papers for 24 hours. Then the polyurethane filter with MWCNT network was melt welded (at 175°C) to the surface of pure TPU plate 1 and 0.3 mm thick made by compression molding from Desmopan 385S. Composite with thickness of 1 mm was tested in stress/relaxation tensile strain creep and reversible creep measurements. Composite with thickness 0.3 mm was welded onto a commercial sport T-shirt with a rubber elastic band to monitor human breathing.

2.3 | Measurements

MWCNTs were analyzed via TEM using the microscope JEOL JEM 2010 at the accelerating voltage of 160 kV. The structure of MWCNT network, PU filtering membrane, and MWCNT/PU composites were analyzed by scanning electron microscope (SEM) NOVA NanoSEM 450. For the observations, the regime of secondary electrons was chosen.

X-ray photoelectron spectroscopy (XPS) signals measured from pure and oxidized MWCNTs were recorded using a Thermo Scientific-Alpha XPS system (Thermo Fisher Scientific, UK) equipped with a microfocused, monochromatic Al α X-ray source (1486.6 eV).

The change in electrical resistance of CNT network/polyurethane laminates in extension/relaxation cycles was measured lengthwise by the two-point method using Multiplex datalogger 34980A with sampling frequency 10 Hz.

The MWCNT/TPU composite stripe 50 × 10 (L × W) with thickness of 1 mm was also tested as gas sensing material. The electrical resistance change was measured along the specimen length by the two-point technique using multimeter Sefram 7338. The strip was placed on a planar holder with Cu electrodes fixed on both sides of the specimen. Time-dependent electrical resistance measurements were performed during adsorption and desorption cycles. In the former case, the holder with the specimen was quickly transferred into an airtight conical flask full of vapors of the respective solvent.

Joule heating was tested using laboratory electrical source Metrix AX 502 when electrical potential was inserted onto opposite sides of the MWCNT/TPU strip sample. Temperature of MWCNT surface was measured in a center of MWCNTs/TPU composite strip 50 × 10 (L × W) using Pt100 connected to GHM 3250 digital thermometer.

Measurements of the prepared CNTs composite antenna were performed using N9912A FieldFox Handheld RF spectrum analyzer in frequency range from 2 MHz to 4 GHz. By means of this spectrum analyzer, the parameter S₁₁ was measured; this parameter determines the resonant frequency for the antenna. The size of the CNTs microstrip radiator layer was 50 × 10 mm. The ground plane of the antenna was made of FR-4 copper substrate sized 64 × 74 mm.

3 | RESULTS AND DISCUSSION

Analysis of individual MWCNTs was performed using TEM analysis. It is presented in Figure 1A, which clearly demonstrates a multilayer CNT structure when nanotubes consisted of 15 to 35 cylindrical layers. Oxygen content (at %) measured by XPS determined the oxygen involving functional groups (C=O, C—O, O—C=O) in amount of 13.0 and 21.7% for pure and KMnO₄ treated CNTs. Further, the ratio of sp³/sp² carbon atoms was found to be 2.50 and 1.69.⁸

Prepared aqueous MWCNT dispersion was in course of strain sensing polymeric composite fabrication filtered through TPU filtering membrane. Figure 1B represents SEM analysis of the membrane, which was prepared from TPU/DMF solution by electrospinning technology. It consisted of fibers of submicron diameters in the range of ~160 to ~840 nm. During the filtration of MWCNT dispersion, the individual tubes were collected by a filter. Nanotubes infiltrated into filter pores, which were finally blocked and filtering cake made of entangled CNT network, were created above the filter. SEM analysis of the upper surface of such layer of entangled CNTs is presented in Figure 1C. For this procedure, KMnO₄ oxidized tubes were used. It was on the basis of our previous work when higher sensitivity to the deformation stimulus was confirmed for oxidized tubes compared to pure tubes.^{7,8} This semiproduct, which consisted of thermoplastic TPU filtering membrane with deposited MWCNT network structure, was then welded onto surface of TPU dog-bone shape tensile test specimen by ironing at 175°C. During this process, the carbon layer was protected by means of PET foil. Figure 1D represents a photograph of final TPU dog-bone shape specimen with weld fixed stripe

of MWCNTs/PU composite (black). In the course of welding, TPU fibers were melted, which created adhesion layer, sticking dog-bone specimen to composite piezoresistive part. In fact, the cross section of final specimen demonstrated three-layer structure. There was 1-mm-thick TPU base followed by MWCNT/TPU nanocomposite layer created by melting of TPU filter with infiltrated nanotubes (thickness 3–5 μm) and finally, layer of entangled MWCNT network with thickness of about 15 μm.⁷ When TPU dog-bone shape specimen is elongated, this deformation is transferred directly to piezoresistive layers, which lead to its electrical resistance increase. Then the change in resistance is a measure of applied deformation. This kind of sensors is from area of so called crack sensors when during extension microcrack in structure appears, which oppositely recover in off load state.⁷ An example of microcrack structure at ~20% of longitudinal strain is demonstrated at Figure 1E (arrows indicate extension direction). As a practical demonstration of the applicability of such flexible and stretchable polyurethane/CNT composite as a unit for deformation detection, human breath monitoring was done. TPU/MWCNT sensor was placed on a sports T-shirt (Figure 1F). Electrodes for two-point resistance measurements were made by riveting. Further, for a uniform deformation of the sensor, the T-shirt was provided with a flexible belt surrounding the chest. The belt was based on rubber/textile ribbon.

The change of electrical resistance initiated by applied mechanical strain is usually expressed in terms as relative resistance change, $\Delta R/R_0$, where R_0 represents initial specimen resistance ΔR stands for the resistance change, $R-R_0$. Further, the sensitivity to applied strain, ϵ , is defined by GF, $GF = (\Delta R/R_0)/\epsilon$. Strain represents a relative change in

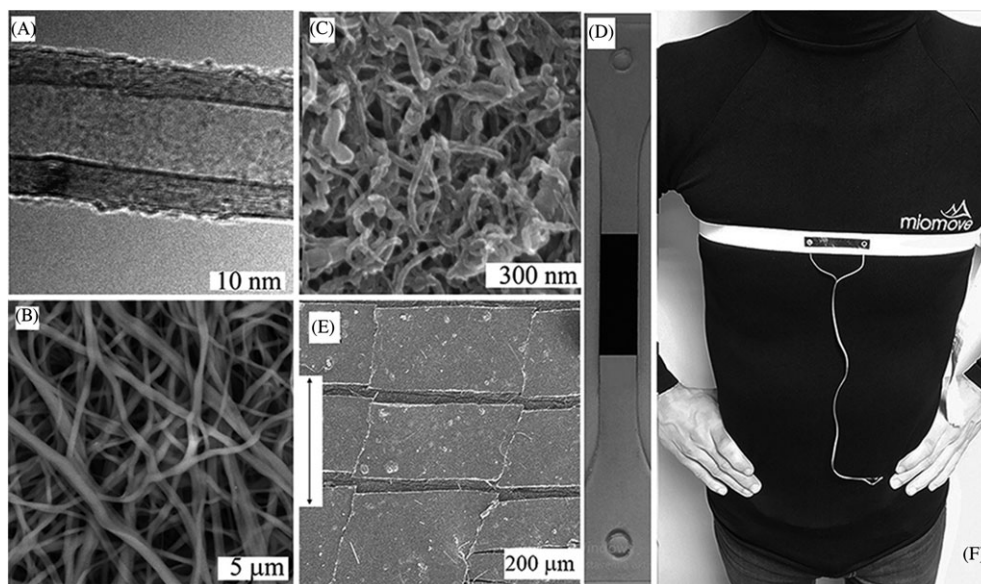


FIGURE 1 A, Transmission electron microscopy micrograph of individual multiwalled carbon nanotube (MWCNT). B, Scanning electron microscope (SEM) micrograph of polyurethane nonwoven filtering membrane prepared by technology of electrospinning. C, SEM micrograph of the upper surface of entangled carbon nanotube network prepared by filtering method from KMnO₄ oxidized MWCNTs. D, Photograph of PU dog-bone shape of tensile test specimen with the fixed stripe of MWCNT/PU piezoresistive composite (black). E, SEM micrograph demonstrating micro-cracking structure after ~20% longitudinal strain, (arrows indicate extension direction). F, Thermoplastic polyurethane/MWCNT-based composite fixed on a sports T-shirt for practical application of a human breath monitoring

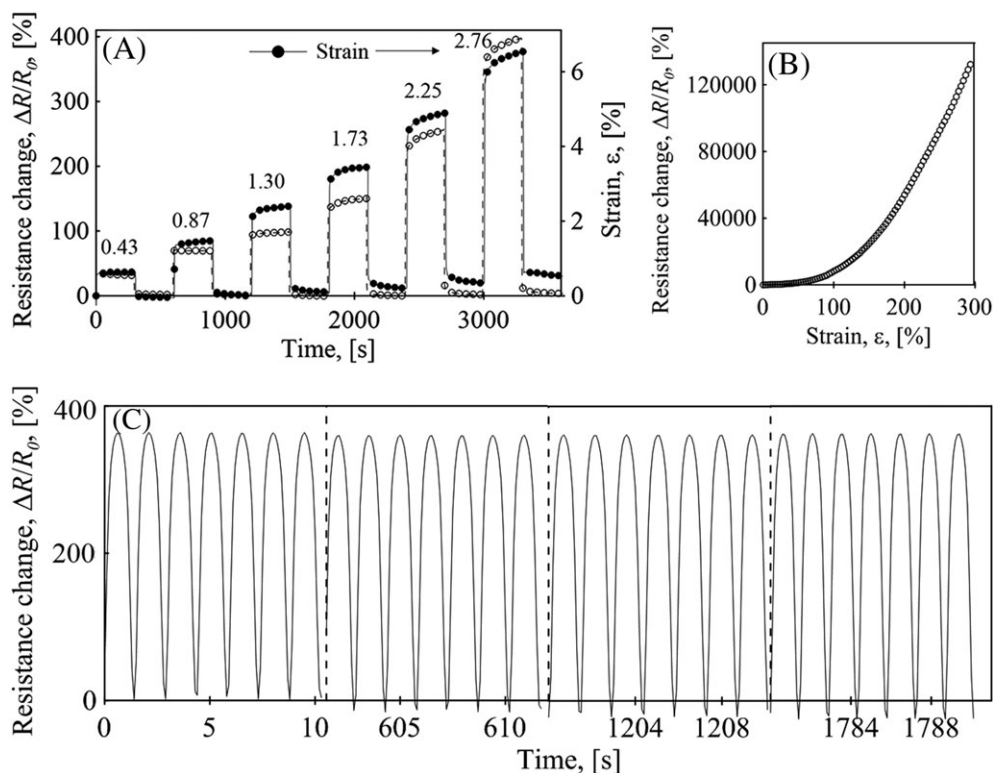


FIGURE 2 A, Six consecutive measurements of the relative resistance change, $\Delta R/R_0$, and the strain, ϵ , on time of creep and reversible creep experiments for multiwalled carbon nanotubes/thermoplastic polyurethane composite. The step increase of tensile strain was initiated by constant tensile stress (indicated about each curves in MPa). The strain values are denoted by solid circles; the relative resistance change by open circles. B, The measurement performed to high extends of deformations till fracture of the thermoplastic polyurethane/multiwalled carbon nanotubes dog-bond shape specimen at approx. $\sim 300\%$. C, Relative resistance change response to sin wave tensile deformation stimulus for more than 10^3 cycles, deformation reaching $\sim 6.5\%$ with frequency ~ 0.7 Hz

specimen length, as ratio between change of specimen length, ΔL , relative to initial length, L_0 , $\epsilon = \Delta L/L_0$. In Figure 2A, they represented the measurements of resistance change on mechanical deformation of the composite. It was set as creep test, which means loading by constant extension stress following by measurement of specimen deformation

and resistance in time. After 5 minutes of loading, it was followed by relaxation in another 5 minutes in off loaded state when reversible creep occurred in time. The specimen was then loaded with appropriate higher stress. Finally, there were six consecutive loading/unloading cycles. Elongation of the specimen led to an increase in composite

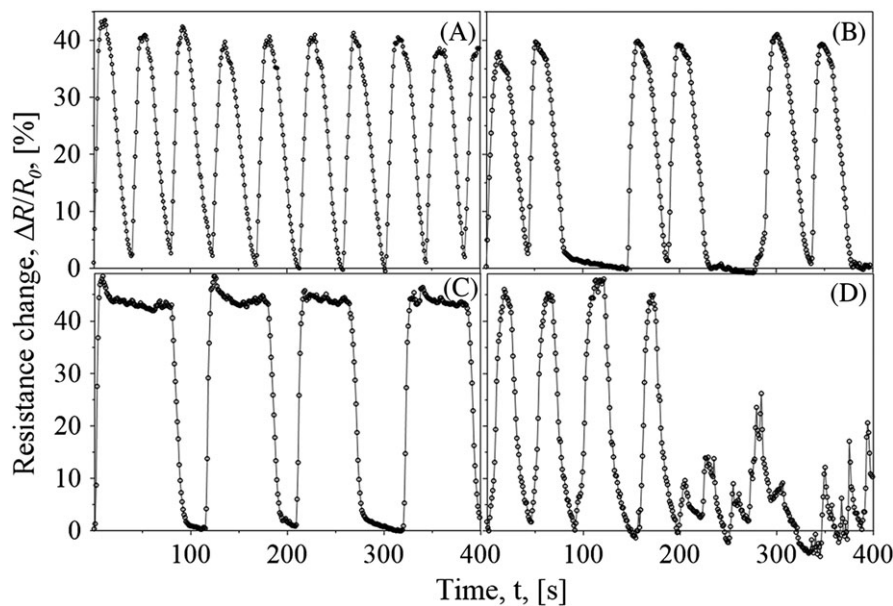


FIGURE 3 Response of the relative resistance change, $\Delta R/R_0$, of multiwalled carbon nanotubes/thermoplastic polyurethane composite sensor integrated on T-shirt at the chest of a volunteer for the human breath monitoring. A, Deep full breathing, B, twice a breath and exhale followed by breath holding, C, breath-breath holding-exhale, and finally D, deep full breathing followed by coughing

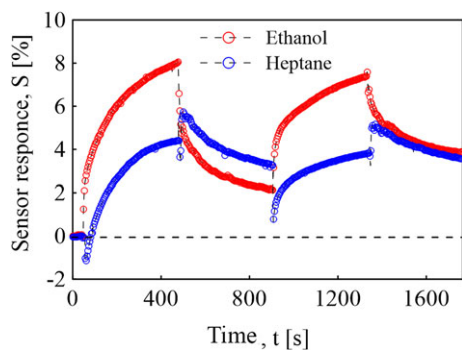


FIGURE 4 Two 5-minute-long adsorption/desorption cycles of multiwalled carbon nanotube/thermoplastic polyurethane composite strip on saturated vapors of ethanol and heptane [Colour figure can be viewed at wileyonlinelibrary.com]

macroscopic resistance and resistance reversible decrease when specimen was in load off state and the deformation relaxed. In general, the sensor is then sensitive to deformation and this response is reversible. There is some portion of irreversible deformation caused by plastic and viscoelastic deformation of TPU polymer. Achieved GF are very promising comparing to conventional for example metallic wire-based strain gauges with have typical values of GF between 2 and 5 and maximal possible applied deformation defined as strain in unit of percent. In case of MWCNT/TPU measured value of GF reaches for example value of ~ 46 at applied deformation 8.7%. Another advantage

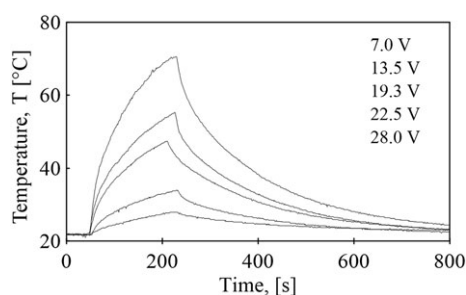


FIGURE 5 Time-dependent response of multiwalled carbon nanotube/thermoplastic polyurethane composite surface temperature increased by Joule heating for different applied DC electrical potentials and temperature decrease in the off state

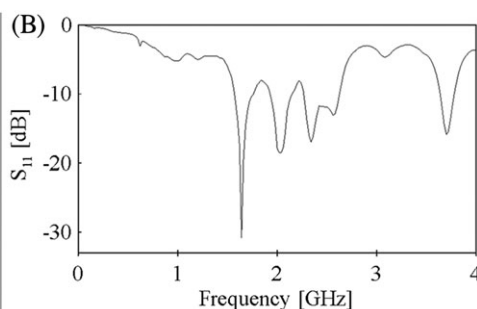
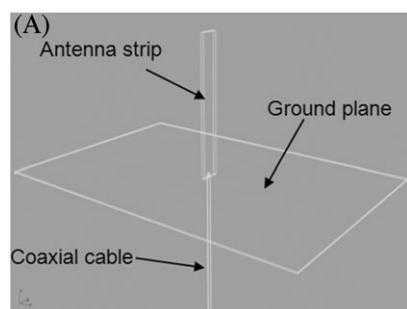


FIGURE 6 A, Schematic illustration of antenna set up with antenna composite strip connected with ground plane made of FR-4 copper substrate sized 64×74 mm and coaxial cable. B, S_{11} impedance of the proposed carbon nanotube composite antenna

of this solution for technology of sensors is that composite can be deformed at very large ranges of extension, hypothetically to maximal values of ultimate strain of TPU elastomer defined by producer as more than 400%. The measurement performed to such high extends of deformations is demonstrated in Figure 2B. Here, the change of resistance was measured until the specimen fracture occurred at strain $\sim 300\%$. The measurement was conducted in Instron tensile machine at elongation rate 10 mm/minute. Through the test, the resistance increased continuously without interruption of the electrical conductivity of the functional MWCNT/TPU layer. The relative resistance change at break reached relatively very high values of about $1.3 \times 10^5\%$ and also GF was high reaching some GF ~ 450 . The strain sensitive MWCNT/TPU composite was also durable when measured more than 10^3 cycles without any observed decreasing of the sensor properties (see Figure 2C). It was measured on creep instrument mounted with extender and electric drive motor applying to the specimen sine wave tensile deformation stimulus with maximal value of deformation reaching $\sim 6.5\%$ and with frequency ~ 0.7 Hz.

As a practical application of the polymeric composite strain sensor, monitoring of human breath was selected. Sensor with TPU part thick ~ 0.3 mm was fixed on T-shirt in the chest area of the volunteer by welding (by ironing). Then several different types of breathing were monitored. As shown in Figure 3, this integrated composite MWCNT/TPU sensor is capable of monitoring various breathing patterns. Response in electrical resistance is very sensitive for deformations occurring in this type and extends of deformations, which were in maximum of beep breath up to 7%. It is also reversible, and it is capable to detect breathing in real time.

In the next part of the present paper, different kinds of composite properties will be focused to demonstrate real multifunctionality of this flexible and stretchable CNT/polyurethane composite. The first will be demonstrated possible application as gas or vapor sensor. In Figure 4, there are two 5-minute-long adsorption/desorption cycles when composite was exposed to saturated vapors of two different solvents as ethanol and heptane. The results are presented as *Sensor response, S*, dependence on time of adsorption and desorption. *Sensor response* is defined as $S = \Delta R/R_0$, where ΔR stands the change of specimen resistance and R_0 as initial resistance of specimen. Exposure of specimen to ethanol vapors followed by absorption of ethanol molecules into composite structure led to an increase in its resistance. This shows that the composite is vapor-sensitive. On other hand, when the

composite was taken out of vapors, the resistance reversibly decreased. The mechanism of vapor detection can involve two kinds of principles. The first one can be caused by adsorption of analyte molecules into space of nanotubes crossing increasing contact resistance between them finally increasing composite macroscopic resistance. The second can be in swelling of MWCNTs/polymer nanocomposite layer causing its volume expansion and then less contact in MWCNT percolating network in TPU polymeric matrix. This behavior is very similar also in the case of heptane vapors. The difference was only at the beginning of both parts as adsorption/desorption started. An initial abrupt decrease in resistance was observed, followed by a decrease in adsorption part and conversely abrupt increase at the beginning of desorption. This can be caused also by another interaction of composite with analyte molecules as more complex interaction between sensor composite material and analyte molecules.

As a second practical use of the composite, Joule heating or resistive heating³⁶ was tested. Here, the electrical DC voltage was applied longitudinally to the specimen and the evolution of its surface temperature was measured as a function of time in both DC on followed by DC off states (Figure 5). The data clearly demonstrate possible use of that composite structure for self-heating by applied external voltage, which can be further utilized.

Finally, the MWCNT/TPU composite strip was tested as microstrip antenna. A schematic illustration of experimental measurement was set up in Figure 6A. Figure 6B demonstrates typical result of antenna measurements as a dependence of parameter S_{11} on frequency. Here the impedance of the MWCNT composite antenna is matched for frequencies of 1.6 GHz (-30.85 dB) and 3.7 GHz (-15.89 dB). The measured parameters show that the antenna operates in two frequency bands. The measured values at the frequencies of 1.6 GHz (-30.85 dB) and 3.7 GHz (-15.89 dB) make it possible for the CNT composite antenna to be used in various applications such as portable devices.

4 | CONCLUSIONS

In this work, we prepared flexible and stretchable polyurethane/CNT nanocomposite to demonstrate its multifunctional properties. First of all, this composite material was used as a unit, capable for application such as tensile strain sensor. Here the deformation of the composite increases its macroscopic electrical resistance. This change is reversible. The measurements to detect applied strain can be performed to really high extend of strains ~300% with reached very high GF with values of around 500 at specimen mechanical fracture. Prepared strain sensitive composite is also durable when measured more than 10^3 cycles without any observed decreasing of the sensor properties. The composite material is finally sensitive enough to be used for human breath monitoring. Furthermore, this material was tested for its other functional properties to be multifunctional such as gas or vapors sensor, element for Joule heating, and as the microstrip antenna.

ACKNOWLEDGEMENT

This project was supported by the internal grant of TBU in Zlin No. IGA/CPS/2018/005 funded from the resources of the Specific University Research. This work was also supported by the Ministry of Education, Youth and Sports of the Czech Republic - Program NPU I (LO1504) and with the support of the Operational Program Research and Development for Innovations co-funded by the European Regional Development Fund (ERDF) and the national budget of the Czech Republic, within the framework of the project CPS-strengthening research capacity (reg. number CZ.1.05/2.1.00/19.0409).

ORCID

Petr Slobodian  <https://orcid.org/0000-0003-4771-8928>

Romana Danova  <https://orcid.org/0000-0002-6690-2045>

Robert Olejnik  <https://orcid.org/0000-0003-0615-7992>

Jiří Matyas  <https://orcid.org/0000-0002-6554-4485>

Lukas Münster  <https://orcid.org/0000-0003-1643-2038>

REFERENCES


- Zhang F, Wu SY, Peng SH, Wang CH. The effect of dual-scale carbon fibre network on sensitivity and stretchability of wearable sensors. *Compos Sci Technol*. 2018;165:131-139.
- Amjadi M, Pichitpajongkit A, Lee S, Ryu S, Park I. Highly stretchable and sensitive strain sensor based on silver nanowire-elastomer nanocomposite. *ACS Nano*. 2014;8(5):5154-5163.
- Borghetti M, Serpelloni M, Sardini E, Pandini S. Mechanical behavior of strain sensors based on PEDOT:PSS and silver nanoparticles inks deposited on polymer substrate by inkjet printing. *Sens Actuators A*. 2016;243:71-80.
- Li M, Wang Y, Zhang Y, Zhou H, Huang Z, Li D. Highly flexible and stretchable MWCNT/HEPCP nanocomposites with integrated near-IR, temperature and stress sensitivity for electronic skin. *J Mater Chem C*. 2018;6(22):5877-5887.
- Wajahat M, Lee S, Kim JH, et al. Flexible strain sensors fabricated by meniscus-guided printing of carbon nanotube-polymer composites. *ACS Appl Mater Interfaces*. 2018;10(23):19999-20005.
- Slobodian P, Riha P, Saha P. A highly-deformable composite composed of an entangled network of electrically-conductive carbon-nanotubes embedded in elastic polyurethane. *Carbon*. 2012;50(10):3446-3453.
- Slobodian P, Riha P, Olejnik R, Cvelbar U, Saha P. Enhancing effect of KMnO₄ oxidation of carbon nanotubes network embedded in elastic polyurethane on overall electro-mechanical properties of composite. *Compos Sci Technol*. 2013;81:54-60.
- Benlikaya R, Slobodian P, Riha P. Enhanced strain-dependent electrical resistance of polyurethane composites with embedded oxidized multiwalled carbon nanotube networks. *J Nanomater*. 2013; Art. No. 327597;2013:1-10.
- Slobodian P, Riha P, Olejnik R, Matyas J, Machovsky M. Pre-strain stimulation of electro-mechanical sensitivity of carbon nanotube network/polyurethane composites. *IEEE Sens J*. 2016;16(15):5898-5903.
- Cochrane C, Koncar V, Lewandowski M, Dufour C. Design and development of a flexible strain sensor for textile structures based on a conductive polymer composite. *Sensors*. 2007;7(4):473-492.
- Tadakaluru S, Thongsuwan W, Singjai P. Stretchable and flexible high-strain sensors made using carbon nanotubes and graphite films on natural rubber. *Sensors*. 2014;14(1):868-876.

12. Li WG, Guo JH, Fan DL. 3D graphite-polymer flexible strain sensors with Ultrasensitivity and durability for real-time human vital sign monitoring and musical instrument education. *Adv Mater Technol.* 2017;2(6):Article Number: 1700070. <https://doi.org/10.1002/admt.201700070>
13. Boland CS, Khan U, Ryan G, et al. Sensitive electromechanical sensors using viscoelastic graphene-polymer nanocomposites. *Science.* 2016;354(6317):1257-1260.
14. Zheng Y, Li Y, Dai K, et al. A highly stretchable and stable strain sensor based on hybrid carbon nanofillers/polydimethylsiloxane conductive composites for large human motions monitoring. *Compos Sci Technol.* 2018;156:276-286.
15. Huang Y, Gao L, Zhao Y, Guo X, Liu C, Liu P. Highly flexible fabric strain sensor based on graphene nanoplatelet-polyaniline nanocomposites for human gesture recognition. *J Appl Polym Sci.* 2017;134(39):Article Number: 45340. <https://doi.org/10.1002/app.45340>
16. Castano LM, Flatau AB. Smart fabric sensors and e-textile technologies: a review. *Smart Mater Struct.* 2014;23:75-90.
17. Gallo GJ, Thostenson ET. Electrical characterization and modeling of carbon nanotube and carbon fiber self-sensing composites for enhanced sensing of microcracks. *Mat Today Comm.* 2015;3:17-26.
18. Kang D, Pikhitsa PV, Choi YW, et al. Ultrasensitive mechanical crack-based sensor inspired by the spider sensory system. *Nature.* 2014;516(7530):222-226.
19. Slobodian P, Riha P, Lengalova A, Svoboda P, Saha P. Multi-wall carbon nanotube networks as potential resistive gas sensors for organic vapor detection. *Carbon.* 2011;49(7):2499-2507.
20. Benlikaya R, Slobodian P, Riha P, Olejnik R. The enhanced alcohol sensing response of multiwalled carbon nanotube networks induced by alkyl diamine treatment. *Sens Actuator B-Chem.* 2014;201:122-130.
21. Huang SM, Kumar P. Effects of molecular adsorption on carrier transport properties of large-size graphene. *J Appl Phys.* 2015;117(2): Article Number: 025103. <https://doi.org/10.1063/1.4905944>
22. Novikov S, Lebedeva N, Satrapinski A. Ultrasensitive NO₂ gas sensor based on epitaxial graphene. *J Sens.* 2015; Article Number: 108581;2015:1-7.
23. Yu KH, Bo Z, Lu GH, et al. Growth of carbon nanowalls at atmospheric pressure for one-step gas sensor fabrication. *Nanoscale Res Lett.* 2011;6(1):Article Number: 202;202.
24. Yu KH, Wang PX, Lu GH, Chen KH, Bo Z, Chen JH. Patterning vertically oriented graphene sheets for nanodevice applications. *J Phys Chem Lett.* 2011;2(6):537-542.
25. Slobodian P, Riha P, Cavallo P, et al. Highly enhanced vapor sensing of multiwalled carbon nanotube network sensors by n-butylamine functionalization. *J Nanomat.* 2014;Article Number: 589627;2014:1-8.
26. Rein MD, Breuer O, Wagner HD. Sensors and sensitivity: carbon nanotube buckypaper films as strain sensing devices. *Compos Sci Technol.* 2011;71(3):373-381.
27. De la Vega A, Kinloch IA, Young RJ, Bauhofer W. Simultaneous global and local strain sensing in SWCNT-epoxy composites by Raman and impedance spectroscopy. *Compos Sci Technol.* 2011;71(2):160-166.
28. Slobodian P, Riha P, Lengalova A, Saha P. Compressive stress-electrical conductivity characteristics of multiwall carbon nanotube networks. *J Mater Sci.* 2011;46(9):3186-3190.
29. Hewitt AB, Kaiser S, Roth M, Craps R, Caroll DL. Varying the concentration of single walled carbon nanotubes in thin film polymer composites, and its effect on thermoelectric power. *Appl Phys Lett.* 2011;98:183110 1-183110 3.
30. Mahmoud L, Samad YA, Alhawari M, Mohammad B, Liao K, Ismail M. Combination of PVA with graphene to improve the Seebeck coefficient for thermoelectric generator applications. *J Electron Mater.* 2015;44(1):420-424.
31. Slobodian P, Riha P, Olejnik R, Kovar M, Svoboda P. Thermoelectric properties of carbon nanotube and nanofiber based ethylene-octene copolymer composites for thermoelectric devices. *J Nanomat.* 2013; Article Number: 792875;2013:1-7.
32. Holt JK, Park HG, Wang YM, et al. Fast mass transport through sub-2-nanometer carbon nanotubes. *Science.* 2006;312(5776): 1034-1037.
33. Kamyshny A, Magdassi S. Conductive nanomaterials for printed electronics. *Small.* 2014;10(17):3515-3535.
34. Matyas J, Olejnik R, Slobodian P, Vlcek K. Microwave antenna for use with organic vapor sensor integrated function. Patent Number: CZ304850-B6; CZ201300863-A3.
35. Kimmer D, Slobodian P, Petras D, Zatloukal M, Olejnik R, Saha P. Polyurethane/MWCNT nanowebbs prepared by electrospinning process. *J Appl Polym Sci.* 2009;111(6):2711-2714.
36. Prolongo SG, Del Rosario G, Urena A. Coupled thermal-electrical analysis of carbon nanotube/epoxy composites. *Polym Engin Sci.* 2014;54(9):1976-1982.

How to cite this article: Slobodian P, Danova R, Olejnik R, Matyas J, Munster L. Multifunctional flexible and stretchable polyurethane/carbon nanotube strain sensor for human breath monitoring. *Polym Adv Technol.* 2019;30:1891-1898. <https://doi.org/10.1002/pat.4621>

Article

The Piezoresistive Highly Elastic Sensor Based on Carbon Nanotubes for the Detection of Breath

Romana Daňová , Robert Olejnik, Petr Slobodian and Jiri Matyas

Centre of Polymer Systems, University Institute, Tomas Bata University in Zlin, 760 01 Zlin, Czech Republic; olejnik@utb.cz (R.O.); slobodian@utb.cz (P.S.); matyas@utb.cz (J.M.)

* Correspondence: danova@utb.cz; Tel.: +420-576-038-120

Received: 4 February 2020; Accepted: 18 March 2020; Published: 23 March 2020



Abstract: Wearable electronic sensor was prepared on a light and flexible substrate. The breathing sensor has a broad assumption and great potential for portable devices in wearable technology. In the present work, the application of a flexible thermoplastic polyurethane/multiwalled carbon nanotubes (TPU/MWCNTs) strain sensor was demonstrated. This composite was prepared by a novel technique using a thermoplastic filtering membrane based on electrospinning technology. Aqueous dispersion of MWCNTs was filtered through membrane, dried and then welded directly on a T-shirt and encapsulated by a thin silicone layer. The sensing layer was also equipped by electrodes. A polymer composite sensor is capable of detecting a deformation by changing its electrical resistance. A T-shirt was capable of analyzing a type, frequency and intensity of human breathing. The sensitivity to the applied strain of the sensor was improved by the oxidation of MWCNTs by potassium permanganate (KMnO₄) and also by subsequent application of the prestrain.

Keywords: elastic sensor; carbon nanotubes; wearable electronics; monitoring of breathing; strain sensor; polymer composite; CNTs

1. Introduction

Significant attention is devoted to wearable and flexible electronic technologies in the past decade. It is very important not to confuse the term “wearable technology” with “wearable device” or “smart device”. Wearable technology comes from describing the integration of electronics and computers into clothing or accessories that are comfortable on the body [1]. The research in an electronic textile has exposed to numeracy smart clothing applications for wearable electronic and healthcare monitoring. The base of success is an electrically conductive layer, which is flexible, stretchable, and lightweight [2].

Human breath is one of the basic natural bodily processes. Breathing can generally be divided into two basic types: diaphragm and thoracic. In the first case, the chest does not move, only the abdominal wall rises and falls. In the second type, in particular, the rib cage opens and contracts. [3].

The general trend of a healthy lifestyle is extended to areas that have the need to detect, record and analyze data from various human activities. There are already many advanced technologies that are also wearable but do not necessarily have integrated electronic or computing components. On the contrary, these belong to the range of smart textiles and clothing. Smart textiles are soft material with flexibility and drapability that are able to sense external conditions or stimulus, to respond and adapt to the behavior to them in an intelligent way. The stimulus that is detected by the smart textiles may have thermal, mechanical, chemical, electrical, magnetic and also optical properties. Similar formulations include intelligent, interactive, sensitive and adaptive. Smart textiles describe a novel category of textiles, which have the capability to detect and react to an external stimulus. In the current situation they can provide required information and help to master everyday life more effectively. They present a challenge in several fields of application such as health and sport. Among the first

areas in which they appeared is military and health care [4,5]. In contrast, ultra-strong fire-resistant or breathing fabrics are not considered smart functionalized materials. In terms of the degree of intelligence, it is possible to classify intelligent textiles according to whether they can perform one or more of the following functions:

- I. Passive smart textiles—ability to sense environmental conditions or an external element. The first generation of smart textiles that integrates sensors as conductive materials or optical fiber.
- II. Active smart textiles—ability to respond after capture. The textiles consist of sensors and actuators as membranes, hydrogels and chromatic materials that provide the ability to sense and actuate or move a part of their environment.
- III. Very smart textiles—ability to sense, react and adapt based on the learned experience from what it sensed and reacted to previously as thermo regulating clothing, space suits and health monitoring apparel for example [4,5].

Moreover, it is important to distinguish ‘intelligent’ clothing in terms of the degree of integration that relates to the extent to which the part that performs the intelligent function is embedded into the textile. At the lowest degree of integration, the smart material is attached to the surface of textile. In the second generation of intelligence, the material is integrated directly into the textile structure, for example, weaving or knitting conductive yarns to form a textile pressure sensor. The third generation of intelligence, which is the highest degree of integration is manifested innately as part of a yarn or fiber. It is thus able to be integrated much more discreetly without compromising user comfort. [1].

The term of electrically conductive fabrics are fabrics that can conduct electricity. They are designed for a wide range of textile fiber products woven from metal strands with very different specific electrical conductivity. This group includes conductive fibers, yarns, fabrics and finished products thereof [4].

One of the interesting and important things to be monitored is certainly the detection and monitoring of human breath. The frequency and intensity of respiration and the type of respiration are detected as a vertical distribution of breath parameters on the human body [6].

In addition, these new sensor technology materials have unique features such as high sensitivity, an ability to detect large-scale deformations and are flexible, lightweight and easy to manufacture. Moreover, in many cases they can be made multifunctional and have other utility properties. Sensitivity can also be successfully controlled. Their multifunctionality can be represented by the following properties: they can have thermoelectric properties, serve as a passive antenna element or a resistance heating element. Last but not least, they can be used to monitor the sensor fabrication process [7–9].

The first network of carbon nanotubes was made by Walters et al. in an attempt to vaporize graphite using a high energy laser, where the authors dispersed nanotubes into a liquid suspension and then filtered through fine filtration mesh. As a result, pure nanotubes stuck together to form a thin, free-standing, entangled structure that was later named Bucky Paper [9,10].

The aim of this article was a complex study of the electrical conductivity of multiwall carbon nanotube network both in the course of monotonic strain growth and also when loading/unloading cycles were imposed [8]. The multiwalled carbon nanotubes (MWCNTs) network was fixed on a polyurethane dog bond shape test specimen for the creep test. The current proposed solution of polymer composite highly elastic and elongation sensors brought a new generation of these deformation-electrically sensitive converters based on materials from the area of nanocomposite materials. These can be deformed in a wide range of deformations (chest deformation during breathing is in the range of units of percent to about 14%), then with high sensitivity, which can be significantly increased by chemical functionalization [11–15].

In the field of application, cooperation is underway, which leads to the prototype’s creation of a breath monitoring system including its own T-shirt integrated sensors, electronics with data transmission and subsequent visualization in a mobile application. In the future, it is possible to consider using this system for sports and fitness clothing, when the sensor will record biometric data,

analyze this data for users, which can lead to learning and performing these activities better, it can lead to improved performance of athletes, and the daily activities of the individual. In the present paper the fabrication of flexible and stretchable (carbon nanotubes: CNTs) strain sensor was demonstrated, which in general is applied for human breath monitoring [7].

The article was focused on both the areas, wearable electronics and preparation of highly elastic piezoresistive sensors for the detection of tensile deformation based on an elastic polymer and carbon filler such as carbon nanotubes (CNTs). A highly elastic sensor for a T-shirt was overlaying by the active layer to avoid contact with surroundings and development of the collecting electrode system [9]. The commonly used metal wire strain gauge, which is normally produced in the form of a wire with precise geometry in the elastic film. The ration between resistivity change and deformation is called the gauge factor (GF). The commercial strain sensor has a GF of about 2–5 and an elastic deformation capability in unit %. The sensitivity factor is given by the ability of the wire and foil to react to the applied deformation [11].

2. Materials and Methods

The following raw materials and applied manufacturing procedures were used to achieve the desired functionality.

The materials were also analyzed by X-ray photoelectron spectroscopy (XPS) on TFA XPS Physical Electronics instrument (PHI-TFA, Physical Electronics Inc., Chanhassen, MN, USA) [16,17] at the base pressure in the chamber of about 6×10^{-8} Pa. The samples were excited with X-rays over a 400 μm spot area with a monochromatic Al $K_{\alpha 1,2}$ radiations at 1486.6 eV. Photoelectrons were detected with a hemispherical analyzer positioned at an angle of 45° with respect to the normal to the sample surface. Survey-scan spectra were made at a pass energy of 187.85 eV, the energy step was 0.4 eV. Individual high-resolution spectra for C 1s were taken at a pass energy of 23.5 and 0.1 eV energy step. The concentration of elements was determined from survey spectra by MultiPak v7.3.1 software from Physical Electronics (Physical Electronics Inc., Chanhassen, MN, USA).

Purified multiwall carbon nanotubes (MWCNTs) were received from Sun Nanotech Co. (China). CNTs were synthesized by chemical vapor deposition method of acetylene (CVD). Acetylene was used as a precursor. MWCNTs has the following properties: a diameter of 10–30 nm, length of 1–10 μm , electrical resistivity of 0.12 Ωcm and purity more than 90%. By transmission electron microscopy (TEM, JEOL Ltd., Tokyo, Japan) the diameter of individual nanotubes was found to be between 10 and 60 nm and their lengths were from tens of micrometers up to 3 μm [14]. The maximum aspect ratio of the nanotubes was about 300 [13].

Non-woven polyurethane (PU) porous membranes for MWCNTs dispersion filtration were prepared by electrostatic spinning from a PU solution. Electrostatic spinning from polyurethane dimethyl form amide/methyl isobutyl ketone (DMF/MIBK, 1:3) solution was performed in cooperation with the SPUR a.s. company of the Czech Republic in Zlin. The conditions of electrospinning were as follows: a PU concentration of 16 wt %. Electrical conductivity of the solution was adjusted to 20 $\mu\text{S/cm}$ using sodium chloride, an electric voltage of 75 kV (Matsusada DC power supply, Matsusada, Shiga-ken, Japan) was applied. Temperature of 20–25 $^\circ\text{C}$, and a relative humidity of 25%–35% was controlled during the process (for a detailed schematic of experimental part, Kimmer et al. [12]). Thermal properties were measured by differential scanning calorimetry (DSC, Mettler Toledo, Columbus, OH, USA) on a Mettler Toledo DSC1 STAR System (Mettler Toledo, Columbus, OH, USA). The measurements were performed under nitrogen atmosphere. The first heating was set to erase the thermal history from 25 to 180 $^\circ\text{C}$ (heating rate 10 $^\circ\text{C}\cdot\text{min}^{-1}$) with a 5 min isotherm, then cooling from 180 to -60 $^\circ\text{C}$ (cooling rate 10 $^\circ\text{C}\cdot\text{min}^{-1}$), the isotherm at -60 $^\circ\text{C}$ for 5 min. The second heating cycle was from -60 to 250 $^\circ\text{C}$ (10 $^\circ\text{C}\cdot\text{min}^{-1}$) and was intended for analysis of the test material.

A thermoplastic polyurethane (TPU) Desmopan DP 385S (Bayer MaterialScience, Leverkusen, Berlin, Germany). The ultimate strength of TPU of 48.9 MPa, with the strain at break 442.2% and density of 1.20 g/cm^3 were specified by the supplier. Used TPU is high elastics elastomeric polyurethane with

an ultimate strength up to 400%. It serves as an elastic base for the MWCNT sensory layer. It is thus an integral part of the sensor, which consists of these two functional layers. By this process a high flexible and elastic sensor is prepared to be capable to measure deformations of a large extent. It is also important that the polymer is thermoplastic. The filter membrane then melts in the preparation process and becomes an adhesive layer between the two components. In conclusion, other polymeric elastomeric matrices can also be used.

KMnO₄ oxidation: Oxidized MWCNTs were prepared in a glass reactor with a reflux condenser filled with 250 mL of 0.5 M H₂SO₄, into which 5 g of potassium permanganate (KMnO₄) as an oxidizing agent and 2 g of MWCNTs were added. The dispersion was sonicated at 85 °C for 15 h using thermostatic ultrasonic bath (Bandelin Electronic DT 103H, Berlin, Germany). The dispersion was filtered, and then MWCNTs were washed with concentrated HCl to remove MnO₂ and then washed with water until the system attained a pH of 7.

Aqueous dispersion of MWCNTs was prepared by sonication in an apparatus UP 400S from Dr. Hielscher GmbH (ultrasonic horn S7, amplitude 88 µm, power 300 W and frequency 24 kHz, Stuttgart, Germany) for 15 min at room temperature. The nanotube concentration in the suspension was 0.3 wt %. Dispersion also contained surfactants, namely, sodium dodecyl sulphate and 1-pentanol with a concentration of 0.1 and 0.14 M, respectively. Moreover, NaOH aqueous solution was added to adjust the pH to 10. For making an entangled MWCNTs network, a porous polyurethane membrane and a vacuum filtration method was used. About 30 mL of homogenized dispersion was filtered through a funnel of diameter 90 mm. The prepared MWCNTs network was washed several times with deionized 60 °C hot water, afterwards by methanol in situ and dried between two filtration papers for 24 h.

The networks of MWCNTs (pure) and oxidized MWCNTs (KMnO₄) were selected for the creep test. The composite stripes 55 mm × 10 mm (L × W) were welded onto the polyurethane bodies and gradually loaded from 0.167 to 1.066 MPa.

A composite stripe of 55 mm × 10 mm with a thickness of 0.08 mm and weight was approximately 2.57 mg was directly welded onto a commercial sport T-shirt to monitor human breathing. The electrical resistance change was measured along the specimen length by the two-point technique using Multiplex datalogger 3498A. The electrodes for a two-point electrical resistance measurement were prepared from very thin Cu wires emailed to sensors with Ag conductive lacquer. The time for hardening of the Ag conductive lacquer after application on the sensor was 2 h. This mentioned technique does not affect the elasticity of the used T-shirt. The electrical resistance measurements as dependence on time were performed during breath and exhale cycles of breathing. The commercial sport T-shirt was chosen from a Czech sports brand (Moirá CZ a.s., Strakonice, Czech Republic), Moirá, with a composition of 97% polypropylene from the brand Moirá and 3% elastane. The T-shirt has to be tight in the entire upper half of the body therefore the size XS–S was chosen. The polyester interlayer strip is necessary for ironing the sensor on the T-shirt.

Two components silicone rubber GMS 2628 from Dawex Chemical s.r.o. (Zlín, Czech Republic) having a hardness score of 26–28 A and with high elasticity was also used to cover the final sensor.

The change in electrical resistance of the MWCNTs network in breath/exhale cycles was measured lengthwise by the two-point method using Multiplex datalogger 34980A (Keysight technologies, Santa Rosa, CA, USA) connected to a PC with a sampling frequency of 10 Hz.

Micrographs using scanning electron microscopy (FEI Nova NanoSEM 450, (FEI company, Hillsboro, OR, USA) were used to observe MWCNTs (pure) and MWCNTs (KMnO₄) samples and also a semi product of filtration and final TPU/MWCNTs composites. The samples were fixed with adhesive tape on the aluminum stub.

3. Results

Two types of MWCNTs were used for this article and tested as pure and oxidized, respectively. Based on the results of the creep test, a sample of oxidized MWCNTs (KMnO₄) was selected and with values of MWCNTs (pure) was compared. The network of MWCNT (pure) was composed of long

entangled tubes (Figure 1A) while the network of MWCNTs (KMnO_4) was shortened due to previous oxidation (Figure 1B). Therefore, the number of contacts was maximized, resulting in high sensor sensitivity to strain changes.

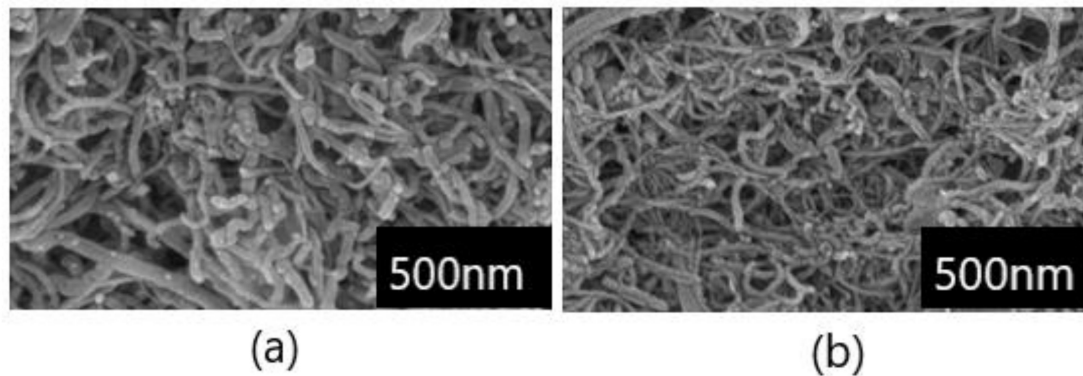


Figure 1. The scanning electron microscope (SEM) micrograph of carbon nanotubes network. The upper surface of entangled carbon nanotube network prepared by the filtering method from multiwalled carbon nanotubes (MWCNTs; pure) and oxidized MWCNTs (KMnO_4). (a) SEM micrograph of the MWCNTs (pure). (b) SEM micrograph of MWCNTs (KMnO_4).

The main binding energy peak (284.5 eV) in the XPS spectra of MWCNT was assigned to the $\text{C}1s\text{-sp}^2$, while the other ones were assigned to C-O (286.15 eV), C=O (287.1 eV), O-C=O (288.8–289 eV) and $\text{C}1s\text{-}\pi\text{-}\pi^*$ (291.1–291.5 eV). According to our XPS results of MWCNT the total oxygen content was determined to be 18.8 at % for pure MWCNT and 21.4 for the oxidized one. The sp^3/sp^2 carbon ratios were 2.50 and 1.69 for pure MWCNT and KMnO_4 oxidized ones (Figure 2), respectively [7].

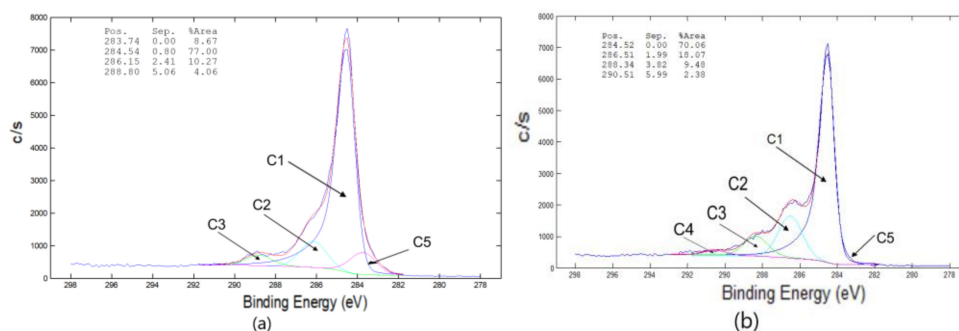


Figure 2. X-ray photoelectron spectroscopy (XPS) on CNT/PU and CNT/PU KMnO_4 . (a) Curve fitting of the C 1s carbon spectrum of the MWCNTs (pure). (b) Curve fitting of the C 1s carbon spectrum of MWCNTs (KMnO_4).

The resistivities of the network structures were measured to be $0.084 \pm 0.003 \Omega\text{cm}$ for the network fabricated from pure MWCNTs and $0.156 \pm 0.003 \Omega\text{cm}$ for the network made of KMnO_4 oxidized tubes [18].

Porosities of two principal networks were calculated to be 0.67 and 0.56, for pure and oxidized network respectively [18].

The principle of the sensing is in the reduction of intertube contacts and the creating of cracks. When the composites are elongated, the number of contacts decreases leading to macroscopic resistance of the sensory layer. Oppositely, when the composite relaxed, the number of contacts increases, which leads to a reversible decrease of the composite resistance. As was demonstrated elsewhere [19], oxidation leads to the formation of oxygenated functional groups detached to the CNT surface causing an increase of the contact resistance in CNT junctions. It finally increases sensor sensitivity to the strain when a sharper resistance change is observed when deformed.

Morphology of the prepared composite acting as a strain sensor can be demonstrated by Figure 3. In principle it is the composite created by the three layers as a commercial T-shirt, a CNT/TPU interface layer and two-component silicone rubber [19].

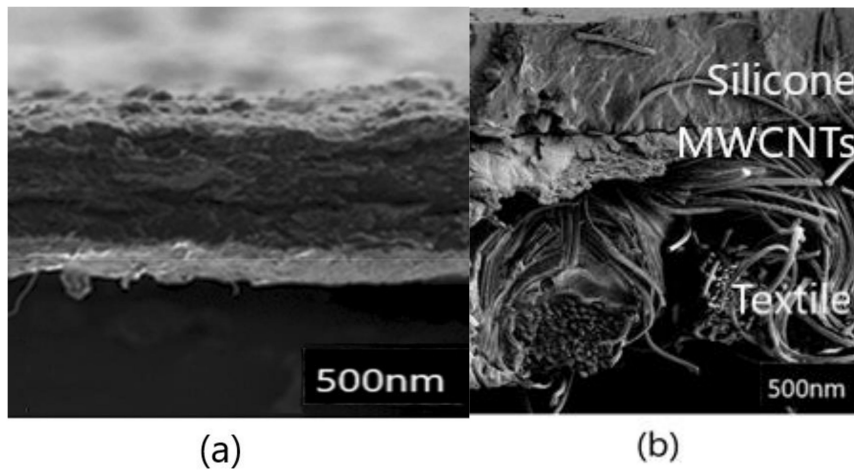


Figure 3. (a) The cross-section of a MWCNT film (above) and supporting TPU filtering membrane (underneath). (b) MWCNT composite cross-section after the melt welding.

Figure 4 characterizes the DSC analysis of the non-woven thermoplastic PUR membrane. A glass transition (T_g) of the elastomeric component was seen, $T_g = -8.08\text{ }^\circ\text{C}$. It is also possible to follow two successive areas melting of the material (endothermic process) $T_{m1} = 137.56\text{ }^\circ\text{C}$ and $T_{m2} = 168.38\text{ }^\circ\text{C}$.

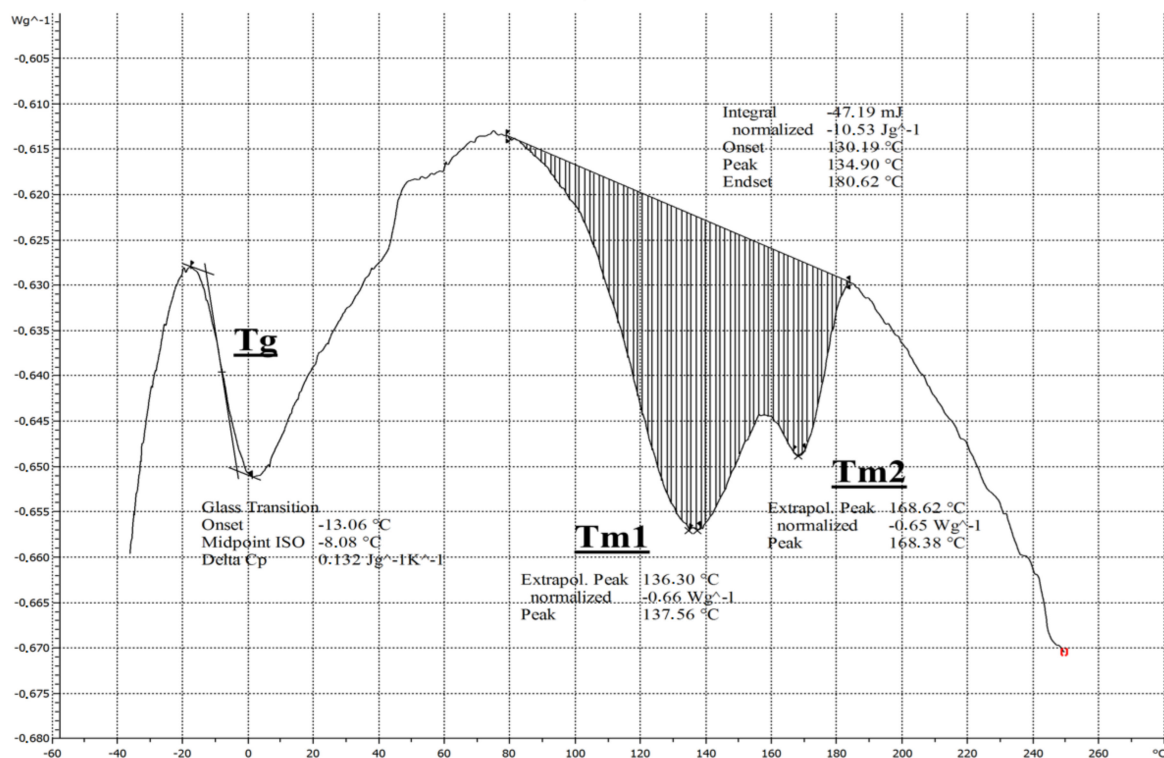


Figure 4. Differential scanning calorimetry (DSC) of a non-woven polyurethane membrane.

In the first case, the sensor of MWCNTs (pure) and oxidized MWCNTs (KMnO₄) were deformed by a tensile stress from 0.167 to 1.066 MPa in six extension/relaxation cycles and were compared. The results are shown in Figure 5 as a percentage change in the relative resistance,

$$\Delta R/R_0 = (R - R_0)/R_0 \tag{1}$$

where R₀ is the electrical resistance of the measured sample before the first elongation and R is the resistance during elongation, strain is the relative change in specimen length.

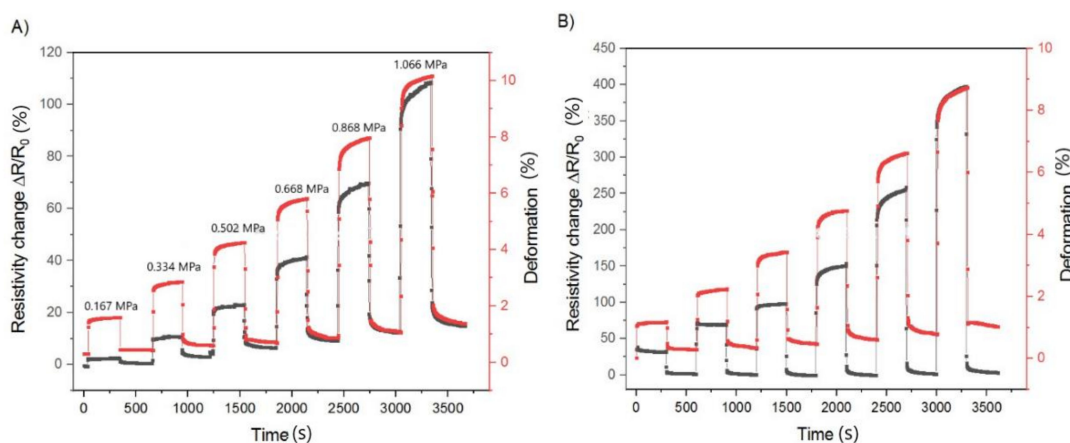


Figure 5. The comparison of the relative resistance change vs. the deformation for the MWCNTs (pure) (A) and MWCNTs (KMnO₄) (B) sensor in six extension/relaxation cycles induced by the tensile stress (from 0.167 to 1.066 MPa). The tensile stresses are the same for both measurements. The deformation is denoted by red circles, the relative resistance changes by black circles.

The elongation periods when the stress was in range from 0.167 to 1.066 MPa, and relaxation when the load was removed was 300 s (Figure 5). The maximum resistance changes of MWCNTs (pure) were 110% and the deformation was 10%. The maximum resistance changes of MWCNTs (KMnO₄) were 400% and the deformation was 9%, which implied a fourfold increase in sensitivity.

Further, the sensitivity to applied strain, deformation ϵ , is defined by the gauge factor (GF)

$$GF = (\Delta R/R_0)/\epsilon \tag{2}$$

Strain represents a relative change in specimen length, as the ratio between the change of specimen length, ΔL , relative to initial length, L_0 , $\epsilon = \Delta L/L_0$. Figure 6 shows the dependence of the gauge factor GF on deformation ϵ .

The issue was the creep test, which means loading by constant extension stress followed by measurement of the specimen deformation and resistance in time. After 5 min of loading, it was followed by relaxation in another 5 min in the off loaded state when the reversible creep occurred in time. The specimen was then loaded with an appropriate higher stress. Finally, there were six consecutive loading/unloading cycles. Elongation of the specimen led to an increase in composite macroscopic resistance and resistance reversible decrease when the specimen was in an off load state and the deformation relaxed. In general, the sensor is then sensitive to deformation and this response is reversible. The measured value of GF reached for the example value of 11 for MWCNTs (pure) and of 46 for MWCNTs (KMnO₄) at an applied deformation 10% (Figure 6). The principle of sensing is in the formation of a microcrack, which decreases the quantity of intertube contacts, which leads to the macroscopic resistance increase. When the composite relaxes, the microcrack close leading to a reversible resistance decrease. Oxidation incorporates more functional oxygenated groups chemically detached to the CNTs surface leading to a sharper increase of resistance during deformation and a

more sensitive sensor to strain. Prestrain leads to the formation of a crack, which is easier opened in the next cycles again leading to higher sensor sensitivity [19].

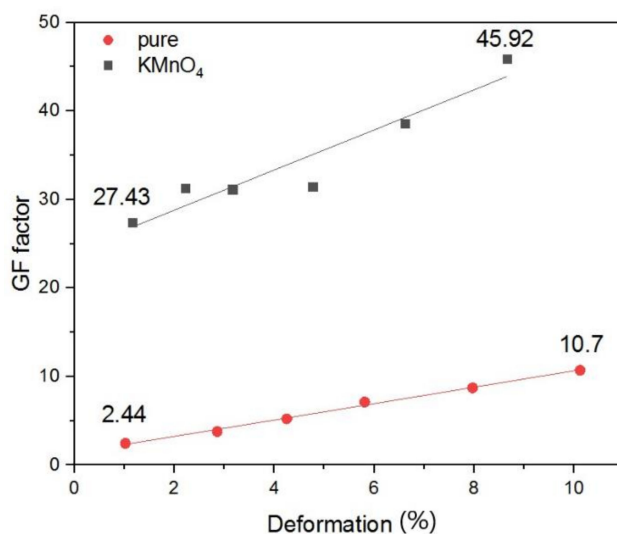


Figure 6. Dependence of gauge factor (GF) with increasing deformation for MWCNTs (pure) and oxidized MWCNTs (KMnO₄) sensors.

The next section describes the application of a strain gauge to monitor human breath in two volunteers. Subsequently, different types of breathing were observed, namely deep and normal breathing. As shown in Figure 7, this integrated MWCNTs (KMnO₄) sensor was fixed on a T-shirt. Two volunteers A and B were selected to test normal and deep breathing. The maximum deformation of the chest the volunteer (A) was 5% with deep breathing and the change in electrical resistance was 30%. In the volunteer (B), a maximum chest circumference deformation was 7% for deep breathing and a change in electrical resistance was 65% (Figure 8).

The response of the sensor to electrical resistance was therefore very sensitive to deformation. The sensor was reversible and was able to detect breathing in real time.

The stabilizing effect on the resistance extension cycles and the residual normalized resistance change was constant after approximately five cycles. That is, during the first deformations, the network of nanotubes acquired a structure that remained more or less the same regardless of the number of deformation cycles. This mechanical stabilization is advantageous for using the sensor as an elongation sensing element.



Figure 7. Sensor based of MWCNT (KMnO₄) fixed on a sports T-shirt for practical application of a human breath monitoring.

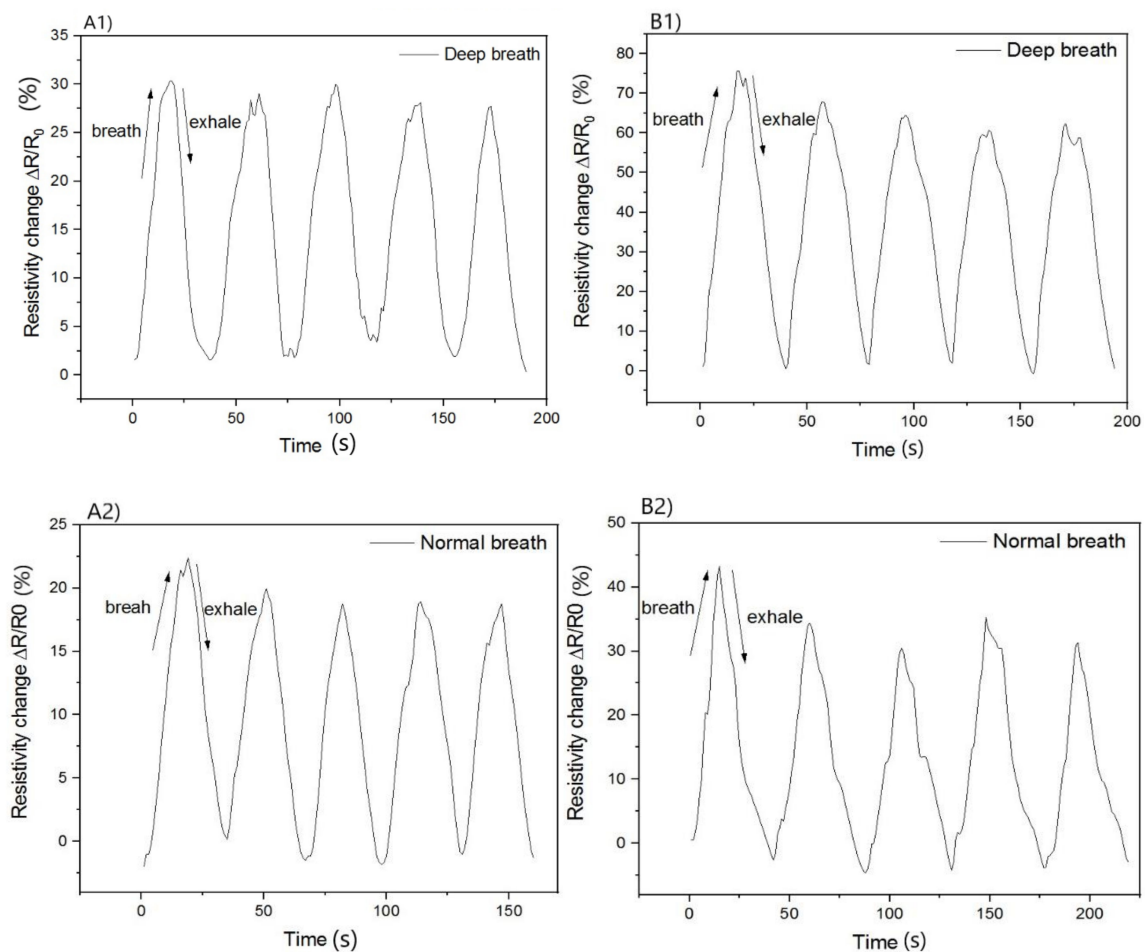


Figure 8. Response to a change in relative resistance, $\Delta R/R_0$, of carbon nanotube sensors (MWCNTs/ KMnO_4) integrated into the T-shirt to monitor human breath. The comparison of deep breath and normal breath for both volunteers (A1,A2,B1,B2).

4. Conclusions

A highly elastic deformable and piezoresistive sensor composed of a network of an electrically conductive entangled carbon nanotubes network built into the elastic commercial T-shirt and encapsulated by elastic silicone was introduced. This material was sensitive enough to be used to monitor human breath. It did not influence any human activity. Respiratory characteristics in two volunteers were compared. The monitoring of breath worked on the principle for the sensors electrical resistance change. Possible application of the sensor in an elastic T-shirt can not only be for athletes, but also for newborns with serious sleep disorders such as sleep apnoea, which can be used to prevent premature death.

Author Contributions: Resources, R.D.; Supervision, P.S., R.O. and J.M. All authors have read and agreed to the published version of the manuscript.

Funding: This research was funded by the Ministry of Education, Youth and Sports of the Czech Republic-Program NPU I (LO1504) and with the support of the Operational Program Research and Development for Innovations co-funded by the European Regional Development Fund (ERDF). The internal grant of TBU in Zlin No. IGA/CPS/2018/005 and IGA/CPS/2019/010 funded from the resources of the Specific University Research. The national budget of the Czech Republic, within the framework of the project CPS-strengthening research capacity (reg. number CZ.1.05/2.1.00/19.0409).

Acknowledgments: This project was supported by the internal grant of TBU in Zlin No. IGA/CPS/2018/005 and IGA/CPS/2019/010 funded from the resources of the Specific University Research. This work was also supported by the Ministry of Education, Youth and Sports of the Czech Republic-Program NPU I (LO1504) and with the support of the Operational Program Research and Development for Innovations co-funded by the European

Regional Development Fund (ERDF) and the national budget of the Czech Republic, within the framework of the project CPS-strengthening research capacity (reg. number CZ.1.05/2.1.00/19.0409).

Conflicts of Interest: The authors declare no conflict of interest.

References

1. Wu, J.X.; Li, L. An Introduction to Wearable Technology and Smart Textiles and Apparel: Terminology, Statistics, Evolution, and Challenges. 2019. Available online: <https://www.intechopen.com/books/smart-and-functional-soft-materials/an-introduction-to-wearable-technology-and-smart-textiles-and-apparel-terminology-statistics-evoluti> (accessed on 4 February 2020).
2. Yu, L.; Yeo, J.C.; Soon, R.H.; Yeo, T.; Lee, H.H.; Lim, C.T. Highly Stretchable, Weavable, and Washable Piezoresistive Microfiber Sensors. *ACS Appl. Mater. Interfaces* **2018**, *10*, 12773–12780. [[CrossRef](#)] [[PubMed](#)]
3. Available online: <https://www.walmark.cz/magazin/dychani-je-zivot> (accessed on 28 February 2018).
4. Grancarić, A.M.; Jerković, I.; Koncar, V.; Cochrane, C.; Kelly, F.M.; Soulat, D.; Legrand, X. Conductive polymers for smart textile applications. *J. Permis. Sagepub* **2017**, *48*, 612–642. [[CrossRef](#)]
5. Zhang, X.; Tao, X. Smart textiles: Passive smart. *Text Asia* **2001**, *32*, 45–49.
6. Oliveri, A.; Maselli, M.; Lodi, M.; Storace, M.; Cianchetti, M. Model-based compensation of rate-dependent hysteresis in a piezoresistive strain sensor. *IEEE Trans. Ind. Electron.* **2018**, *66*, 8205–8213. [[CrossRef](#)]
7. Benlikaya, R.; Slobodian, P.; Riha, P. Enhanced strain-dependent electrical resistance of polyurethane composites with embedded oxidized multiwalled carbon nanotube networks. *J. Nanomater.* **2013**, *2013*, 327597. [[CrossRef](#)]
8. Tadaluru, S.; Thongsuwan, W.; Singjai, P. Stretchable and Flexible High-Strain Sensors Made Using Carbon Nanotubes and Graphite Films on Natural Rubber. *Sensors* **2014**, *14*, 868–876. [[CrossRef](#)] [[PubMed](#)]
9. Slobodian, P.; Riha, P.; Saha, P. A highly-deformable composite composed of an entangled network of electrically-conductive carbon-nanotubes embedded in elastic polyurethane. *Carbon* **2012**, *50*, 3446–3453. [[CrossRef](#)]
10. Walters, D.A.; Casavant, M.J.; Quin, X.C.; Huffman, C.B.; Boul, P.J.; Ericson, L.M.; Haroz, E.H.; O’Connell, M.J.; Smith, K.; Colbert, D.T.; et al. In-plane-aligned membranes of carbon nanotubes. *Chem. Phys. Lett.* **2001**, *338*, 14–20. [[CrossRef](#)]
11. Allaoui, A.; Hoa, S.V.; Evesque, P.; Bai, J. Electronic transport in carbon nanotube tangles under compression: The role of contact resistance. *Scripta Materialia* **2009**, *6*, 628–631. [[CrossRef](#)]
12. Kimmer, D.; Slobodian, P.; Petras, D.; Zatloukal, M.; Olejnik, R.; Saha, P. Polyurethane/MWCNT nanoweb prepared by electrospinning process. *J. Appl. Polym. Sci.* **2009**, *111*, 2711–2714. [[CrossRef](#)]
13. Slobodian, P.; Daňová, R.; Olejník, R.; Matyáš, J.; Münster, L. Multifunctional flexible and stretchable polyurethane/carbon nanotube strain sensor for human breath monitoring. *Polym. Adv. Technol.* **2019**, *30*, 1891–1898. [[CrossRef](#)]
14. Slobodian, P.; Riha, P.; Lengalova, A.; Saha, P. Compressive stress-electrical conductivity characteristics of multiwall carbon nanotube networks. *J. Mater. Sci.* **2011**, *46*, 3186–3190. [[CrossRef](#)]
15. Yamada, T.; Hayamizu, Y.; Yamamoto, Y.; Yomogida, Y.; Izadi-Najafabadi, A.; Futaba, D.; Hata, K. A stretchable carbon nanotube strain sensor for human-motion detection. *Nat. Nanotechnol.* **2011**, *6*, 296–301. [[CrossRef](#)] [[PubMed](#)]
16. Cvelbar, U. Interaction of non-equilibrium oxygen plasma with sintered graphite. *Appl. Surf. Sci.* **2013**, *269*, 33–36. [[CrossRef](#)]
17. Cvelbar, U.; Markoli, B.; Poberaj, I.; Zalar, A.; Kosec, L.; Spaić, S. Formation of functional groups on graphite during oxygen plasma treatment. *Appl. Surf. Sci.* **2006**, *253*, 1861–1865. [[CrossRef](#)]

18. Slobodian, P.; Riha, P.; Lengálová, A.; Svoboda, P.; Sáha, P. Multi-wall carbon nanotube networks as potential resistive gas sensors for organic vapor detection. *Carbon* **2011**, *49*, 2499–2507. [[CrossRef](#)]
19. Slobodian, P.; Riha, P.; Olejnik, R.; Cvelbar, U.; Sáha, P. Enhancing effect of KMnO₄ oxidation of carbon nanotubes network embedded in elastic polyurethane on overall electro-mechanical properties of composite. *Compos. Sci. Technol.* **2013**, *81*, 54–60. [[CrossRef](#)]



© 2020 by the authors. Licensee MDPI, Basel, Switzerland. This article is an open access article distributed under the terms and conditions of the Creative Commons Attribution (CC BY) license (<http://creativecommons.org/licenses/by/4.0/>).

Article

Polyurethane-Carbon Nanotubes Composite Dual Band Antenna for Wearable Applications

Robert Olejník ^{1,*}, Stanislav Goňa ² , Petr Slobodian ¹, Jiří Matyáš ¹, Robert Moučka ¹ and Romana Daňová ¹ 

¹ Centre of Polymer Systems, University Institute, Tomas Bata University in Zlín, 76001 Zlín, Czech Republic; slobodian@utb.cz (P.S.); matyas@utb.cz (J.M.); moucka@utb.cz (R.M.); danova@utb.cz (R.D.)

² Faculty of Applied Informatics, Tomas Bata University in Zlín, 76005 Zlín, Czech Republic; gona@utb.cz

* Correspondence: olejnik@utb.cz; Tel.: +420-576-031-746

Received: 27 October 2020; Accepted: 16 November 2020; Published: 23 November 2020



Abstract: The design of a unipole and a dual band F-shaped antenna was conducted to find the best parameters of prepared antenna. Antenna radiator part is fully made of polymer and nonmetal base composite. Thermoplastic polyurethane (PU) was chosen as a matrix and multi-wall carbon nanotubes (MWCNT) as an electrical conductive filler, which creates conductive network. The use of the composite for the antenna has the advantage in simple preparation through dip coating technique. Minor disadvantage is the usage of solvent for composite preparation. Composite structure was used for radiator part of antenna. The antenna operates in 2.45 and 5.18 GHz frequency bands. DC conductivity of our PU/MWCNT composite is about 160 S/m. With this material, a unipole and a dual band F antenna were realized on 2 mm thick polypropylene substrate. Both antenna designs were also simulated using finite integration technique in the frequency domain (FI-FD). Measurements and full wave simulations of S_{11} of the antenna showed good agreement between measurements and simulations. Except for S_{11} , the gain and radiation pattern of the antennas were measured and simulated. Maximum gain of the designed unipole antenna is around -10.0 and -5.5 dBi for 2.45 and 5.18 GHz frequency bands, respectively. The manufactured antennas are intended for application in wearable electronics, which can be used to monitor various activities such as walking, sleeping, heart rate or food consumption.

Keywords: polymer antenna; composite material; carbon nanotubes; effective permittivity; effective permeability; effective conductivity; wearable electronics

1. Introduction

The rise of the Internet of Things (IoT) in the 21st century has seen a pressing need of developing easily incorporable electrochemical devices for acquiring real-time data. One segment of this field comprises smart clothing and wearable electronics, which is used for diverse ends ranging from activity monitoring bracelets, smart watches or glasses over GPS enabled shoes to life-saving devices used in healthcare [1,2]. IoT devices generally consist of a sensing unit collecting vital data and a transmitting unit, which sends the collected data to the processing or display unit. These are typically rigid, conventional electronic parts in the flexible plastic or elastic rubber substrates which presents some limitations in their seamless integration e.g., into clothing. Thus, developing and designing miniature and/or highly flexible IoT devices is highly desirable and currently draws a great deal of interest. Researchers have thus focused on developing wearable formats of electrochemical devices since they can play a vital role in the field of personalized IoT [3–6].

Antenna design which could be used in the segment of wearable electronics often features antennas with non-metallic radiators. If the radiator is to be made of a non-metallic material then this still has to

have sufficiently high conductivity at microwave frequencies to achieve sufficient radiation efficiency and consequently the highest possible gain. Therefore, conductive textiles, conductive polymers [7] or composite materials are mostly used. Conductive textiles are employed in fabric antennas, which are most frequently in the form of a patch antenna (a rectangular microstrip antenna). These antennas of good radiation characteristics typically consist of upper and lower conductive layers of antenna patch while the ground plane and the middle layer are made of dielectric substrate [8,9].

Another large group of materials used in antenna with non-metallic radiators is conductive polymers. First attempts in the field were made with polyaniline (PANI) composites [10]. Later researchers moved on to the usage of carbon nanotubes [11,12] or other very good conductors (silver and gold particles) to increase electrical conductivity [13,14]. The use of carbon nanotubes has led to technologies using PANI and carbon fibers (PANI-MWCNT) [15,16], technologies using polypyrrole (PPy), [17] and PPy combined with PEDOT materials [18,19]. Technologies using pure PANI exhibit DC conductivity around 4500 S/m [15,16]. Polypyrrole materials have conductivity about 2000 S/m [17] and are typically around 100 μm thick even though stacking of PPy layers into final thickness of several hundreds of microns is also possible. PEDOT materials have higher conductivity of about 10,000 S/m but their thickness is limited approximately to 10 μm . Small physical thickness and conductivity around 10,000 S/m results in DC sheet resistance of PEDOT materials being larger than the sheet resistance of PPy material [17]. All above-mentioned materials can be used in the design of an antenna having large radiation efficiency. PANI-MWCNT showed radiation efficiency around 60% [15]. PPy solution also shows radiation efficiency around 60% [17]. Antennas with PEDOT material have typically lower radiation efficiency of around 30% [17]. Recently, other approaches in preparation of conductive polymers with polyaniline have appeared in the literature. These approaches are represented by multifunction poly/amide-imid and polyaniline films [20] and highly conductive poly/amide-imid films [21].

Apart from conductive polymers, other non-metal materials can be used in radiating part of microwave antennas with large radiation efficiency. Most common case is the use of composites with long carbon fibers [22] or combination of long carbon fibers with carbon nanotubes [22]. Another solution is the use of pure nanotubes [23]. The approach described in [23] leads to a material with conductivity as high as 50,000 S/m, also known as buckypaper [23]. Conductivity measurement of carbon nanotubes at microwave frequencies was carried out in detail in [24]; conductivity of pure carbon nanotubes is around 160,000 S/m and conductivity of buckypaper is around 50,000 S/m [25]. Through mixing of carbon nanotubes with a dielectric matrix, the effective conductivity of the composite becomes lower than the conductivity of pure nanotubes and strongly depends on its concentration and spatial distribution of carbon nanotubes within the composite [7]. Examples of measurement of the conductivity of composite materials in waveguides can be found in [26,27].

In this paper, a novel approach to preparation of conductive composite material (using a “dip” technique) suitable for antenna’s radiator is presented together with an actual antennas design. The novel approach uses a composite comprising polyurethane mixed with multiwall carbon fibers (PU/MWCNT). The advantage of this approach lies in the simplicity of material preparation, which is comparable to polyaniline and polypyrrole, but is significantly less demanding than for PEDOT. As both thickness and conductivity of the PU/MWCNT composite is limited antenna radiators must be made from relatively thick layers (hundreds of microns), to achieve substantial radiation efficiency of antennas. Required thickness is realized by stacking several layers on top of each other. Although from an antenna construction viewpoint, it would be more appropriate to design a dual band antenna of other topology (e.g., a microstrip patch, a slot, or a variant of PIFA antenna), for the sake of simplicity, we decided to study a simple unipole and F-antenna over ground plane. Even though the gain of this approach is smaller, it is still acceptable for short range operating devices; typically, our antennas show gain of -10.0 and -5.5 dBi at 2.45 and 5.18 GHz frequency band, respectively. The resulting antenna is lightweight and small enough to fit into a pocket and although it is not fully flexible, it can tolerate certain bending; thus could be placed on upper arms or on a thigh, where minimum bending occurs.

2. Materials and Methods

2.1. Materials

All the chemicals used were of analytical grade. *N,N*-dimethylformamide 99.5%, analytical reagent grade was purchased from Fisher Chemical (Waltham, MA, USA). Purified multi wall carbon nanotubes (MWCNT) were produced by the chemical vapor deposition (CVD) of acetylene supplied by Sun Nanotech Co. Ltd., Nanchang, Jiangxi, China, China. According to the supplier, the nanotubes have diameters of 10–30 nm, length 1–10 μm , purity >90% and electrical resistivity 0.12 $\Omega\text{ cm}$.

A Thermoplastic polyurethane (PU) Desmopan DP 385S was purchased from Bayer MaterialScience, (Leverkusen, Berlin, Germany). According to supplier's specifications PU has following characteristic: strength of 48.9 MPa, with the strain at break of 442% and density of 1.20 g cm^{-3} . Polyurethanes (PU) Desmopan[®] is a thermoplastic block copolymer characterized by a wide range of properties. Its linear polymeric chains consist of alternating flexible, elastic segments. Polyurethane was used as a matrix and it was filled with MWCNT. It serves as an elastic base for the MWCNT antenna radiator layer.

2.2. Sample Preparation

Polyurethane solution 10 wt % in dimethylformamide (DMF) was prepared. The solution was mixed over night at 400 rpm and 90 °C. Subsequently carbon nanotubes were added to the solution and the dispersion was mixed using UP 400S ultrasonic homogenizer for 15 min, at power of 50% and at pulse of 50%. Then the dispersion was mixed mechanically using a magnetic stirrer for 30 min at 400 rpm. After that 30 wt % composite was made in the form of dispersion. The deep coating method was used for this layer preparation. PET foil was used as a substrate. After drying the desired shape of antenna (Figure 1) was cut out.

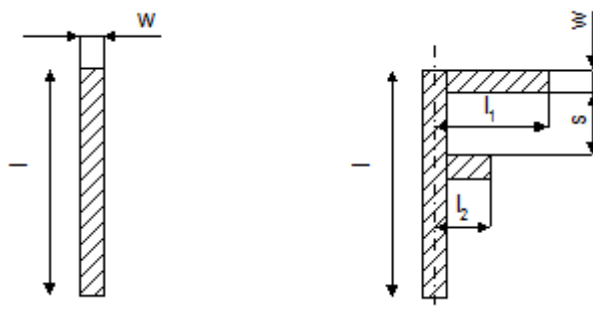


Figure 1. Topology and dimensions of the two studied antenna designs (on the left a dipole; on the right an F-antenna).

2.3. Methods

The scanning electron microscopy (SEM) observations were made using FEI Nova NanoSEM, scanning microscope (Waltham, MA USA). Sample was placed on SPI double side carbon tape substrates. All specimens were sputtered with gold/Pb before imaging to improve conductivity. After cryo-fractured in liquid nitrogen, the morphology of the failure surfaces (cross section) of PU/MWNT sample was observed.

The transmission electron microscopy (TEM) observations were made using TEM, JEOL Ltd., Tokyo, Japan microscope. The dispersions of the MWCNTs in acetone were cast on Cu grids.

The materials were also analyzed by X-ray photoelectron spectroscopy (XPS) on TFA XPS Physical Electronics instrument (Chanhassen, MN, USA) [28,29] at the base pressure in the chamber of about 6×10^{-8} Pa. The samples were excited with X-rays over a 400 μm spot area with a monochromatic Al $K\alpha_{1,2}$ radiations at 1486.6 eV. Photoelectrons were detected with a hemispherical analyzer positioned at an angle of 45° with respect to the normal to the sample surface. Survey-scan spectra were made at

a pass energy of 187.85 eV, the energy step was 0.4 eV. Individual high-resolution spectra for C 1s were taken at a pass energy of 23.5 and 0.1 eV energy step. The concentration of elements was determined from survey spectra by MultiPak v7.3.1 software from Physical Electronics (Chanhassen, MN, USA).

Thermogravimetric (TGA) studies were performed on a TGA Q500 (TA instruments, New Castle, DE, USA). The analysis was made under following conditions: temperature range from 25 to 1000 °C at 10 °C/min heating rate under nitrogen flow of 50 mL/min.

The conductivity of our composite material was measured on a 100 mm long and 10 mm wide sample made from polyethylene terephthalate (PET) substrate covered with a layer of PU/MWCNT composite. The composite and PET layers were 70 and 147 µm thick, respectively. DC resistance was measured in two-point set-up using Fluke 867B graphical multimeter (Eindhoven, The Netherlands); with probes located at the ends of the sample strip—good reproducibility of conductivity measurement was achieved.

Measurement of material properties of composite materials is typically done with the use of rectangular waveguides [26,27]. To measure the effective conductivity and the effective permittivity of the studied PU/MWCNT composite firstly the samples were placed inside the rectangular waveguides. These measurements relied on our previous work described in [30]. In the second measurement set-up, the samples were placed between the flanges of the rectangular waveguides. Finally, the third measurement of the effective conductivity were conducted on a microstrip test circuit.

For the design of the dual band antenna, two topologies were chosen. The first one was in the form of a simple unipole while the second in the form of an F-shaped antenna [31]. Dimensions of both antennas' designs are shown in Figure 1. Basic measurements of the antennas were performed in the anechoic chamber using the EMC 32 measurement software from Rohde Schwarz (Munich, Germany). Measurements of reflection coefficient S_{11} of antennas was done with the aid of the Keysight handheld spectrum analyzer N9912A (Santa Rosa, CA, USA) and with the Agilent vector network analyzer PNA-L-N5230A (Santa Rosa, CA, USA). The S_{11} measurements were performed in the frequency range from 0.1 to 7 GHz. The initial dimensions of the antennas were optimized in CST microwave studio to achieve low S_{11} over 2.45 and 5.18 GHz bands. CST microwave studio is a commercial simulation software used for analysis of electromagnetic structures through solving the Maxwell equations via finite integration technique (FI). An active (radiating) part of the antenna was made of a composite comprising polyurethane filled with multiwall carbon nanotubes (PU/MWCNT).

3. Results

3.1. Composite Material

Scanning electron microscopy showed homogenous dispersion of multi wall carbon nanotubes in thermoplastic polyurethane as a matrix. The layer was made by simple dipping of the PET foil (the substrate) into the carbon nanotubes dispersion. The uniform layer was created during drying process, by which the solvent was removed. The morphology shows a significant amount of multiwall carbon nanotubes and the polyurethane part around them (Figure 2A). The cross section after cryo-fracture in liquid nitrogen (Figure 2B) shows uniform distribution of carbon nanotubes in vertical and horizontal direction. Another cross-section SEMs (Figure 2C) after cryo-fracture in liquid nitrogen confirms uniform thickness and also double side coating of the substrate by the composite layer. SEM micrograph can be also used for determination of the composite layer thickness (Figure 2D).

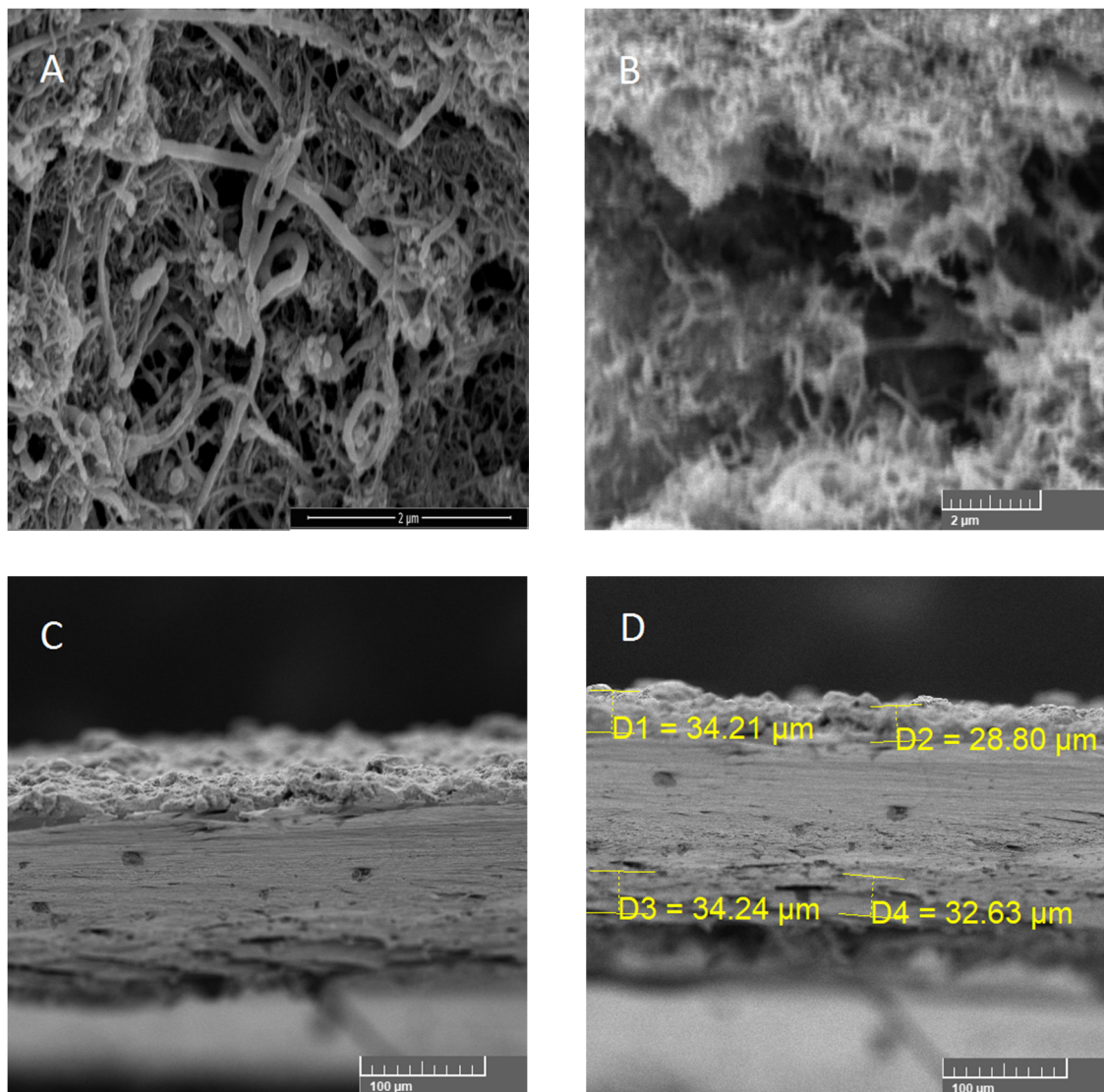


Figure 2. SEM pictures of prepared PU/MWCNT composite. (A) surface of PU/MWCNT composite. (B) cross section of prepared composite (upper part) (C) cross section of PU/MWCNT composite on PET foil. Double side coating. (D) Cross section of PU/MWCNT composite with measured thickness (denoted D1–D4).

Transmission electron microscopy was used to examine morphology of raw carbon nanotubes. The diameter of individual carbon nanotubes is around 25 nm and even the walls are distinguishable (Figure 3A). Carbon nanotubes have typical aggregate into bundles due to Van der Waals forces. To prevent this phenomenon, the sonication technique is used. Thus, macromolecular chains of PU are inserted between the carbon nanotubes to eliminate bundles formation.

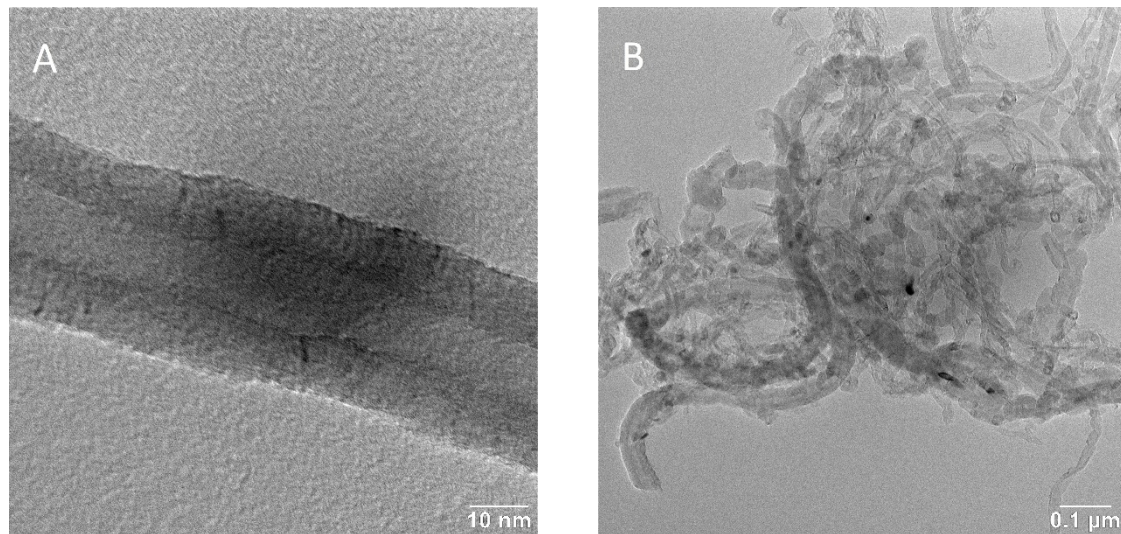


Figure 3. TEM picture of: (A) an individual multiwall carbon nanotube, (B) a bundle of multiwall carbon nanotubes.

The main binding energy peak (284.5 eV) in XPS spectra of MWCNT was assigned to the C1s- sp^2 , while the other ones were assigned to C–O (286.15 eV), C=O (287.1 eV), O–C=O (288.8–289 eV) and C1s- $\pi-\pi^*$ (291.1–291.5 eV). According to our XPS results of MWCNT total oxygen content was determined to be 18.8 at % for pure MWCNT. The sp^3/sp^2 carbon ratios are 2.50 and 1.69 for pure MWCNT (Figure 4).

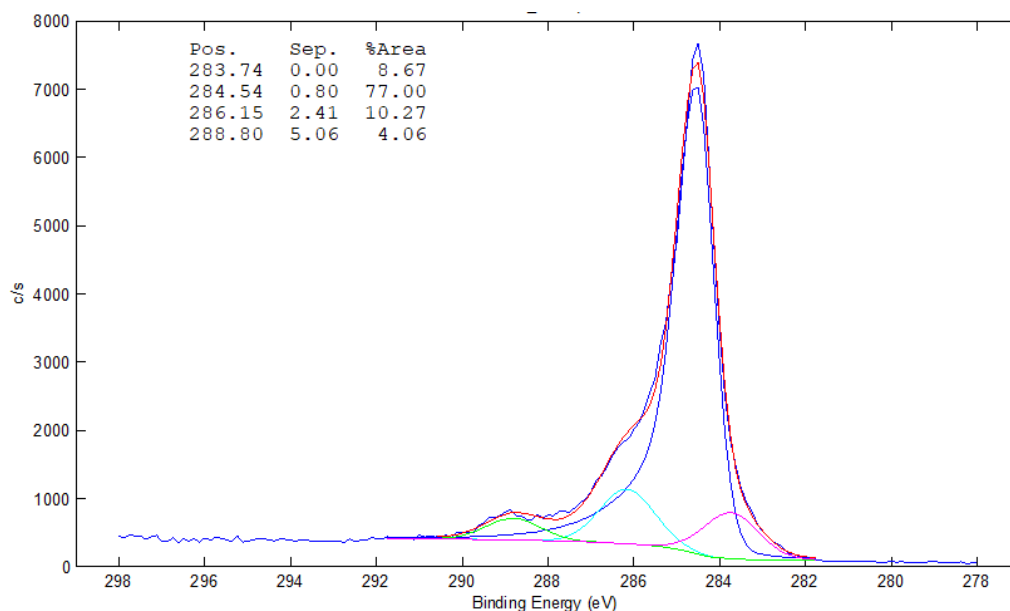


Figure 4. XPS analysis of MWCNT, raw material without any treatment.

Thermogravimetric curve presented in Figure 5 shows the weight loss during constant heating rate. Pure multiwall carbon nanotubes (MWCNT) show dramatic weight loss at 632 and 843 °C. Thermoplastic polyurethane (PU) has significant weight drop at 352 °C. Polymer composite (PU/MWCNT) shows two slight weight drops at 313 and 365 °C, respectively, both of which corresponds to polyurethane decomposition; the cumulative drop is around 30 wt % and equals to polyurethane content of the PU/MWCNT composite.

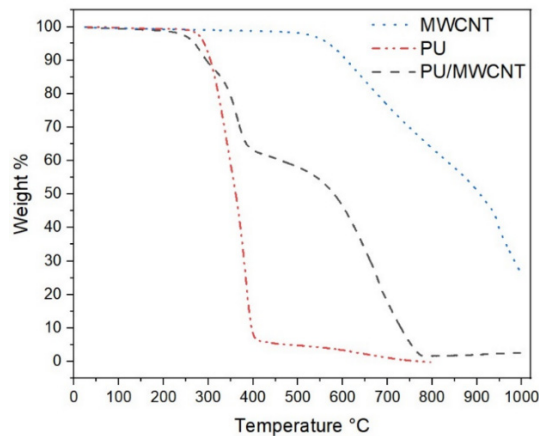


Figure 5. Thermogravimetric (TGA) curves of MWCNT (dot line), Thermoplastic polyurethane PU (dash dot dot line), PU/MWCNT composite (dash line).

The PU/MWCNT contains 30 wt % of multiwall carbon nanotubes. The high fraction of conductive filler dramatically improves electrical conductivity which is crucial point to reach high radiation efficiency and gain of prepared antenna. Measurement of DC conductivity on concentrations of MWCNT is shown in Figure 6. The percolation happens for 20 wt % of MWCNT. For 23 wt % the conductivity around 0.3 S/m was achieved. With increasing concentration of MWCNT above 23%, the conductivity of the PU/MWCNT composite further increases. For concentration 30 wt %, the conductivity 160 S/m was achieved. This point is not shown in the graph for the case of clarity. Right part of the figure shows an impact of conductivity of the composite on radiation of a simple unipole antenna (length 24.9 mm, width 4 mm, 0.5 mm thick Rogers RO4350B substrate). For conductivity 120 S/m, the radiation resistance of antenna at 2.45 GHz around 30 Ohm is obtained. However, for conductivity that is only 12 S/m, the radiation resistance becomes smaller (about 15 Ohms) and the gain of the unipole antenna is decreased. That is the reason why large filling of 30 wt % for our composite was used.

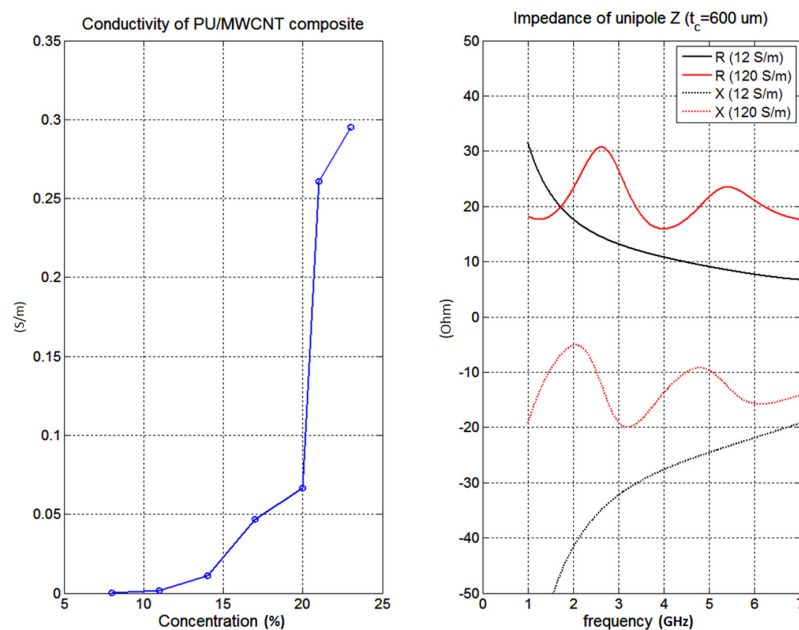


Figure 6. Left (Conductivity of PU/MWCNT composite versus concentration of CNTs), Right (Impedance of unipole antenna).

Polymer composite antennas prepared on support substrate is a very novel idea. This fact makes it very difficult to compare with the literature. The inspiration was found on the opposite end of spectra of interest in electromagnetic shielding of GHz waves. There is no exception to use 45 or 50 wt % of conductive filler [32,33].

The highly filled system has some disadvantage which is necessary to solve. The chosen of dip coating technique is one of the easy ways how to prepare very uniform layer without defects. The DMF was chosen as a solvent for PU. PU solution in DMF has very low viscosity which allow to reach relatively high MWCNT content. PU solution also allow to control and adjust viscosity of PU/MWCNT and avoid mechanical degradation of used substrate, no abrasion was observed. SEM analysis also confirm on abrasion on the surface of prepared sample.

3.2. Electrical Characterization

Measured DC conductivity of the antenna $\sigma = 160$ S/m was compared with AC conductivity extracted from waveguide measurements [30]. Despite the use of the conductive paste between the sample and the waveguide walls, the results were from measurements with the sample inside the waveguide were not acceptable. We believe that this was due to insufficient thickness of our material, which was only $70 \mu\text{m}$ thick. On the other hand, results when measuring with samples sandwiched between the flanges were better. The DC measurements of conductivity were performed by a simple two-point method since the total resistance of the measured sample was much higher than a contact resistance.

The measured dependence of the relative permittivity (ϵ_r) and permeability (μ_r) on frequency is shown in Figures 7 and 8. The real and imaginary part of permittivity of composites with CNTs is monotonically decreasing with frequency. This would be the case if the composite material was measured inside a rectangular waveguide [30]. However in our case, the measurement took place on the flange of the waveguide, but algorithms being used assumed that samples are placed inside the waveguide. This caused errors in the evaluation, which have two consequences. The first is that the functions ϵ_r and μ_r do not decrease too much with frequency within a single waveguide band. The second consequence is that discontinuities arise on the curve when moving from one frequency band to another. Validity of the first and second statements (consequences) were verified by CST microwave studio, where a synthetic composite material having smooth ϵ_r and μ_r was analyzed, resulting S-parameters were then transferred to MATLAB (Nattick, USA). Finally, ϵ_r and μ_r were extracted by algorithm described in [30]. The results obtained in MATLAB confirmed both previous statements.

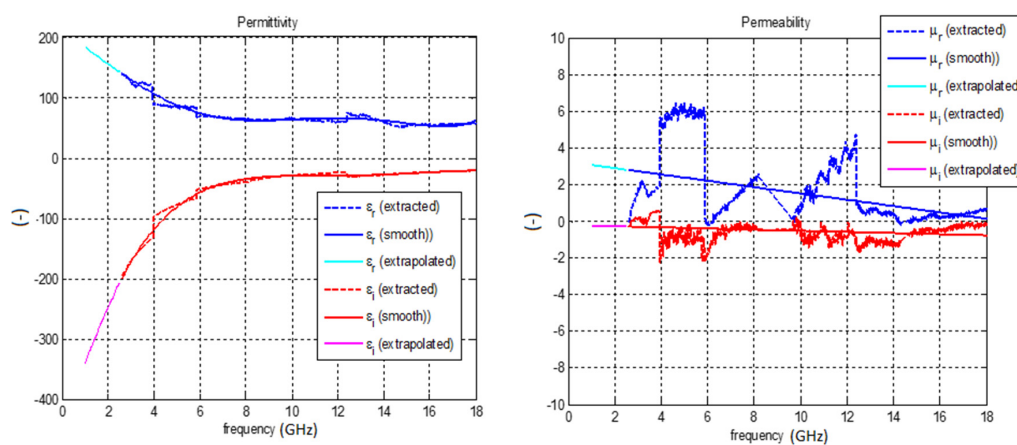


Figure 7. Measured effective permittivity (left) and magnetic permeability (right) of the polymer composite comprising carbon nanotubes and polymer matrix (measurement on the flange of the rectangular waveguide).

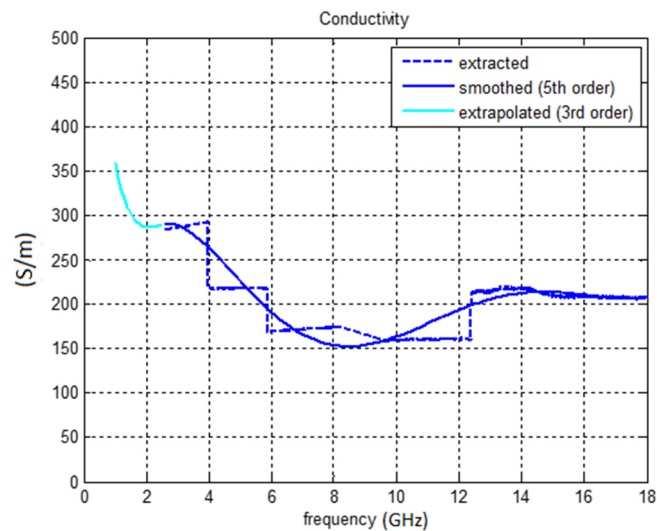


Figure 8. Measured effective conductivity of the polymer composite comprising carbon nanotubes and polymer matrix (measurement on the flange of the rectangular waveguide).

The average conductivity at 2.45 GHz is about 290 S/m and average conductivity at 5.18 GHz is around 220 S/m (Figure 8). The average permittivity at 2.45 GHz is 130 and 90 at 5.18 GHz. The behavior of permeability could not be measured too accurately since a very thin (70 μm) sample was used. The average value of the measured permeability was about 2.5 at 2.45 GHz and it decreased with frequency. Since the PU/MWCNT composite material is non-magnetic, the values of permeability should be close to 1.

Nevertheless, after the fabrication of a simple unipole composite based antenna (Rogers substrate RO4350B having thickness $h = 0.508$ mm, unipole length 24.9 mm), it was observed that the agreement between reflection coefficients of simulated and measured antenna was rather poor. The experimentally obtained values of S_{11} in dB were approximately 2 dB higher than the value predicted by the full wave simulation program (CST microwave studio). This indicates that the real effective conductivity of the composite is smaller than the value measured on the flange of the waveguide.

Due to low precision of the waveguide methods (for thin samples), the conductivity of our composite at microwave frequencies was finally measured with a microstrip line (see Figure 9). After measurements of the insertion loss S_{21} of the sample, the microstrip line was modelled in CST microwave studio (including SMA connectors) and the value of conductivity was changed by optimization in MATLAB to equal simulated and measured S_{21} (see Figure 10). The resulting conductivity of our PU/MWCNT material was equal to 120 S/m. Assuming this value of conductivity the typical agreement between measured and simulated S_{11} of a simple single layer unipole antenna improved from 2.0 to 0.5 dB.

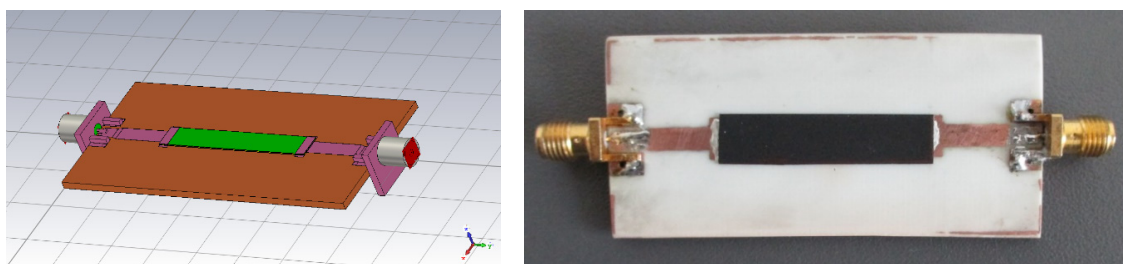


Figure 9. CST studio model of (left) and the real microstrip line (right) made from polymer composite comprising carbon nanotubes and polymer matrix for effective conductivity measurement.

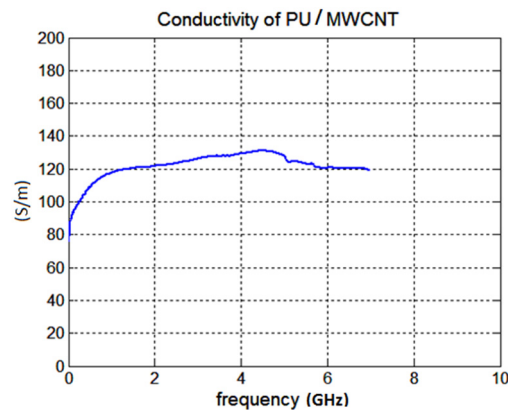


Figure 10. Measured results of the effective conductivity of the PU/MWCNT composite by a microstrip line.

3.3. Design of Antenna

In the case of the design of a grounded unipole antenna printed on a traditional dielectric substrate, the thickness of the antenna (substrate) must be considerable in order to obtain reasonable radiation resistance of the antenna. In the case of PU/MWCNT (or other carbon-based antennas such as buckypaper or PANI/MWCNT), the thickness can be smaller. Thus, low profile antennas can be realized. In Figure 11 a parametric study, performed in CST microwave studio, of a simple unipole made from PU/MWCNT composite is shown. The simulations considered that the unipole is placed on 0.508 mm thick Rogers RO4350B substrate. The length of unipole was 24.9 mm and width 4 mm. It can be seen that with increasing conductivity of the composite radiation resistance increases too; also, the reactance of the antenna starts to oscillate as is typical of antennas made from conductors.

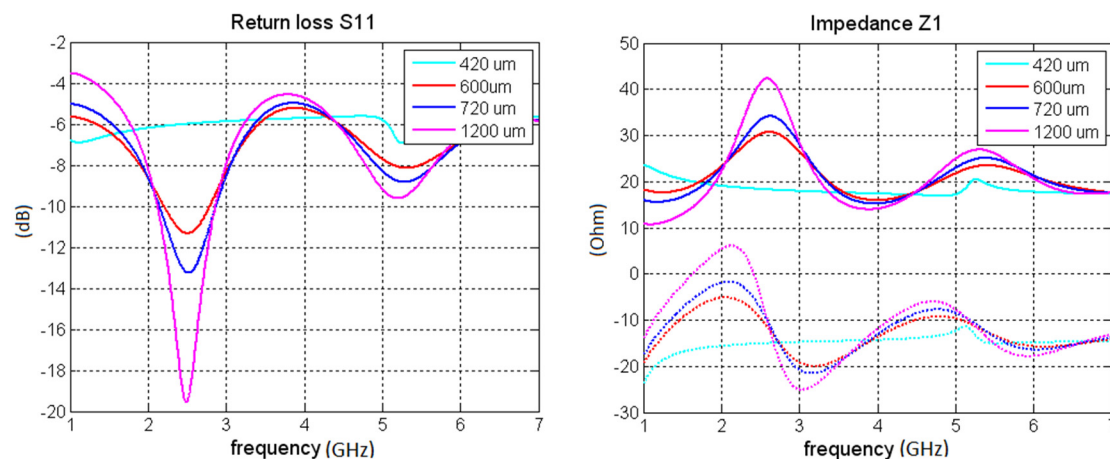


Figure 11. A simulation of characteristics of a unipole made from PU/MWCNT, input impedance as a function of conductivity.

In order to make the antenna operable and to achieve practical radiation efficiency a relatively thick composite layer (t_c layer) has to be used. Considering conductivity around 120 S/m for our operating bands, at least 600 μm thick composite has to be used. However, preparation of such a thick composite layer was not feasible from a technological point of view. Therefore, the antenna was made by stacking three layers on top of each other (Figure 12). Assuming the total thickness of the antenna $t_c = 600 \mu\text{m}$, the radiation resistance of the antenna of about 30 Ohm was achieved. With further thickness or conductivity increase, radiation resistance upwards of 50 Ohm is achievable. However, the fabrication of an antenna consisting of more than three layers would be technologically problematic.

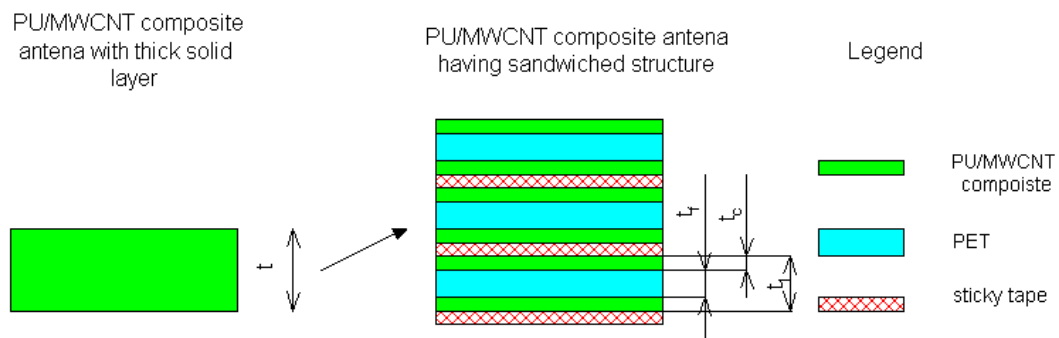


Figure 12. Detailed view of the layered structure of the polymer antenna.

Matching of the unipole antenna can be done with a LC matching circuit (Figure 13). Either a simple LC match or a double LC can be used. Use of the double LC match can guarantee independent matching in both operating bands. For the purpose of simplicity, the simple LC match was used for the unipole antenna. The length and width of C was 8 and 7 mm respectively. The length and width of L was 2.0 and 1.9 mm respectively.

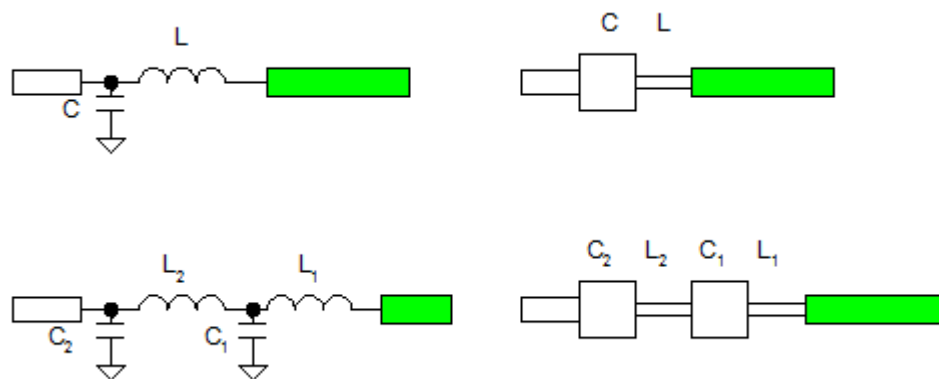


Figure 13. Schematic of the matching circuit of the antenna (top: unipole, simple match, bottom: independent matching in both operating bands).

3.4. Fullwave Simulations of the Antenna and Measurements

Based on the procedure described in the previous chapter, a unipole and an F-antenna were designed for dual band operation at 2.45 and 5.18 GHz frequency bands. The design with the F-antenna was inspired by the paper [31]. The difference between our approach and the approach described in [31] is that our design uses a ground plane. The presence of the ground plane is essential for the practical design of antenna for wearable applications.

The carrier substrate of the antennas was 2 mm thick polypropylene. The large thickness was essential in order to secure practical values of antennas' gain.

The 3D models of the antennas are shown in Figure 14. Both antennas (for dimensions see Table 1) are realized by a sandwiching technique. The dimensions of the substrate (2 mm PP layer) are 50 mm × 70 mm. The antennas were fed by a microstrip port. The reference plane of the port was placed at the beginning of the antenna. The effective permittivity of the PU/MWCNT composite was the same as given in Figure 7. The value of the effective permittivity is smoothly decreasing with frequency. The numerical value of the permittivity was 180 at 1 GHz and 70 at 7 GHz. The effective conductivity was constant and equal to 120 S/m. The permeability of 1 was assumed for the PU/MWCNT material.

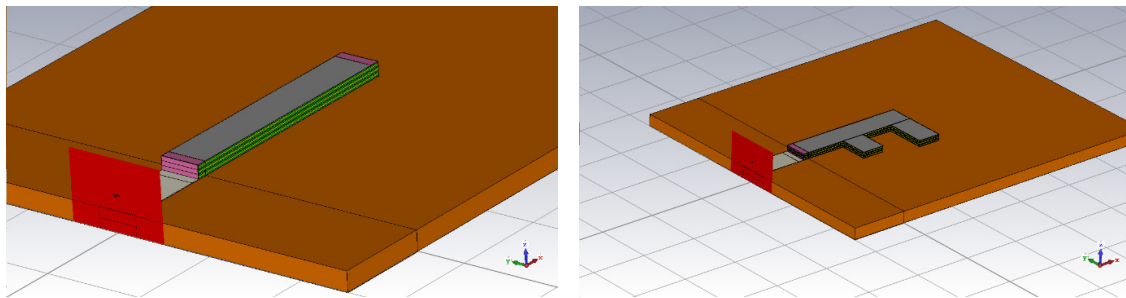


Figure 14. 3D model of unipole and F-antenna in CST microwave studio.

Table 1. Physical dimensions of the unipole and the F-antenna.

Antenna Type	Parameter	Symbol	Numerical Value
Unipole	length of unipole	l (mm)	26
	width of unipole	w (mm)	4
	thickness of single composite layer	t_c (μm)	120
	total thickness of unipole (including PET layers)	t_{tot} (μm)	1014
F-antenna	length of F-antenna	l (mm)	21
	length of first arm	l_1 (mm)	11
	length of second arm	l_2 (mm)	7
	width of F-antenna	w (mm)	4
	separation between arms	s (mm)	5.9
	thickness of single composite layer	t_c (μm)	70
	total thickness of F-antenna (including PET layers)	t_{tot} (μm)	714

The unipole and the F-antenna were manufactured in our laboratory (see Figure 15). The feeding of our antennas was realized by a short 50Ω section on the PP substrate and the 18 mm long 50Ω section on the FR4 substrate. The microstrip line and the ground layer of PP material was realized by $35 \mu\text{m}$ thick copper foil. The foil had a self-adhesive acrylic material. Electrical connection between microstrip lines on PP layer and microstrip line on the FR4 substrate was performed by a conductive silver compound. The same compound was also used for connection of PU/MWCNT composite with the feeding microstrip. The unipole antenna contained also a simple LC matching circuit to improve S_{11} of the antenna. The F-antenna does not use the matching since the 50Ω impedance can be achieved by selection of proper dimensions l , l_1 and l_2 of the antenna.

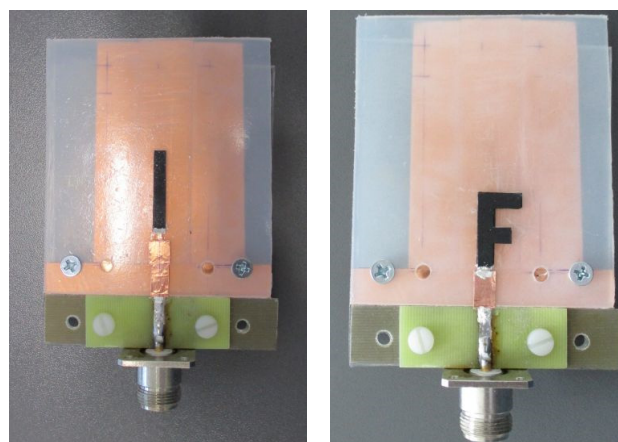


Figure 15. A photo of manufactured antennas (left: unipole; right: F-antenna).

Properties of the manufactured antenna were further examined in detail in our EMC laboratory. Firstly, the S_{11} of the antennas was measured and compared with simulations (see Figure 16). For the unipole a very good agreement between measured and simulated S_{11} was obtained inside 2.45 GHz operating band. At the 5.18 GHz the measured S_{11} resonates at lower frequency than the frequency predicted by simulation. For the F-antenna, correlation between measured and simulated S_{11} became worse but the manufactured F-antenna showed an excellent impedance match in both operating bands.

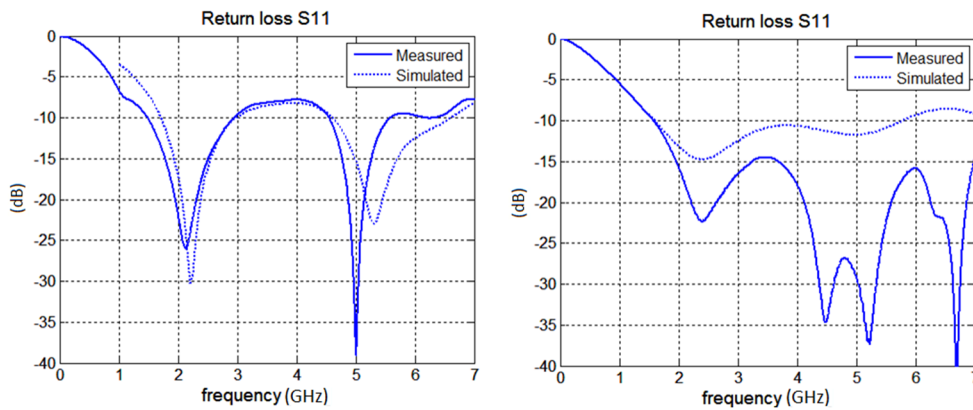


Figure 16. The measured and simulated return loss of antenna (unipole on the left; F-antenna on the right).

Secondly, radiation properties of both antennas were measured in an anechoic chamber (see Figures 17 and 18). The measured gain at the direction of main lobe is about 2 dBi larger than the gain predicted by CST. This is mainly attributed to the fact, that the model of the antennas in CST did not contained feeding microstrip on FR4 line, impedance matching circuit and the N-connector.

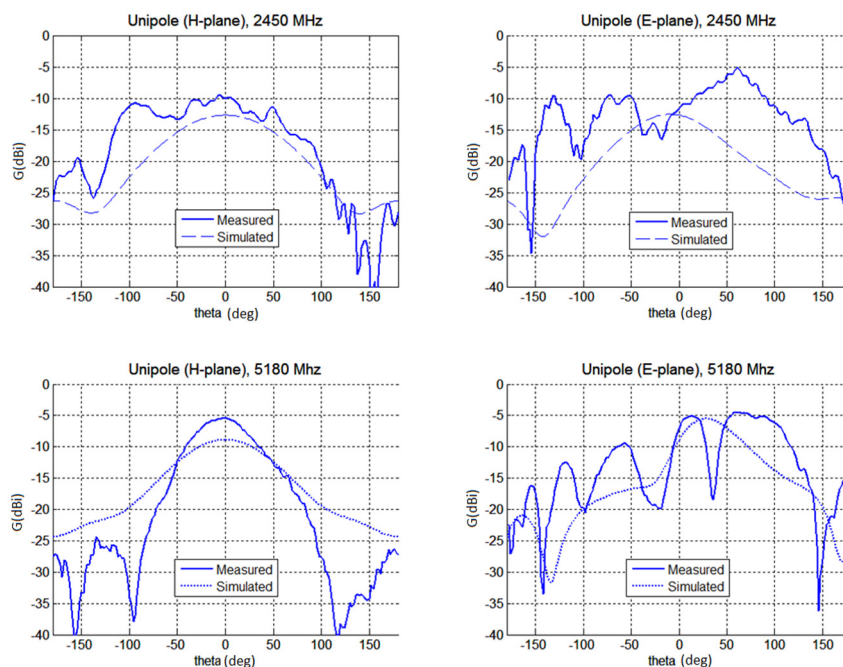


Figure 17. The measured and simulated gain of the unipole antenna (top line, absolute gain for H and E-plane at 2450 MHz, bottom line, absolute gain for H and E-plane for 5180 MHz).

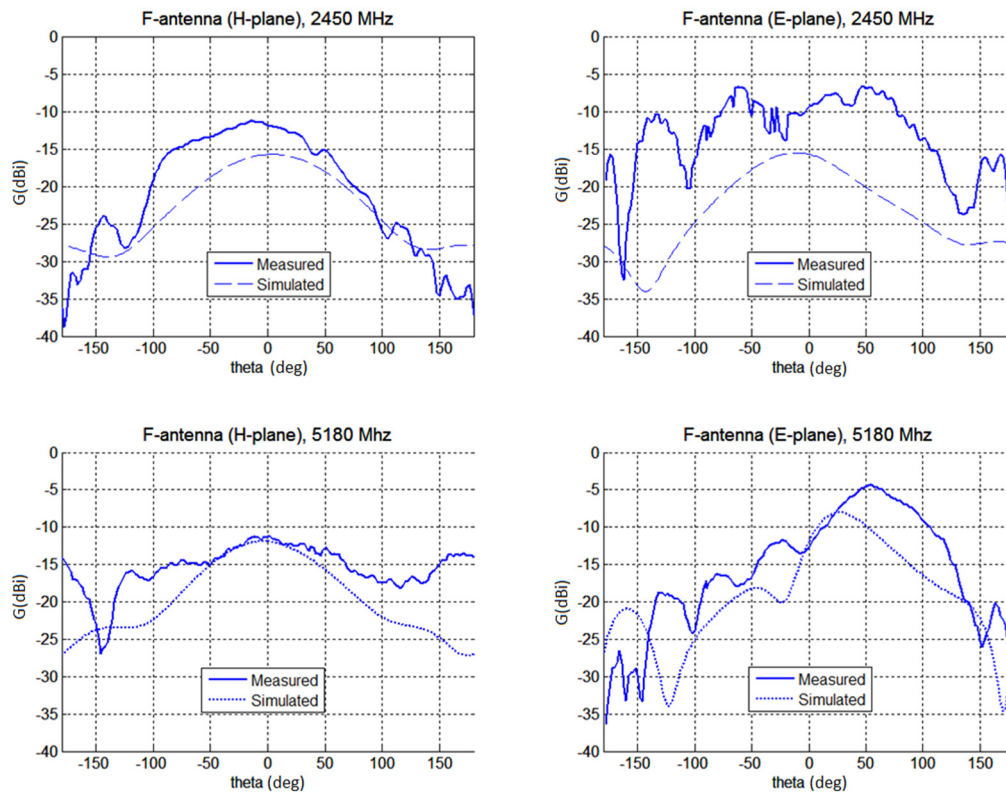


Figure 18. The measured and simulated gain of the F-antenna (top line, absolute gain for H and E-plane at 2450 MHz, bottom line, absolute gain for H and E-plane for 5180 MHz).

It was observed that both antennas achieved a very good match for both operating bands. The correlation between measured S_{11} and simulated S_{11} is also quite good.

The agreement of predicted and simulated radiation patterns is not as good as expected. The comparison of measured and simulated gains is given in Table 2. In general, the measured gain was by about 2 dB larger than the simulated values. We mainly attribute this to the fact, that simulation in CST have not assumed feeding by the microstrip on the FR substrate. The model of the antenna in CST does not account for the presence of the N panel connector.

Table 2. Simulated and measured gain of dipole and F-antenna.

Antenna Type	Frequency (MHz)	Simulated Gain (dBi)	Measured Gain (dBi)	Simulated Radiation Efficiency (%)
Unipole	2450	-12.7	-10.0	3.6
	5180	-8.9	-5.5	6.8
F-antenna	2450	-15.8	-12.0	2.2
	5180	-11.9	-11.4	4.0

The maximum measured gain of the unipole is -10 dBi and -5.5 dB for 2.45 and 5.18 GHz, respectively. The gain of the F-antenna is smaller since it used a thinner composite layer ($t_c = 70 \mu\text{m}$ only compared to $t_c = 120 \mu\text{m}$ for the unipole). Its gain is about -12 dBi at 2.45 GHz and -11.4 dBi at 5.18 GHz. By using thickness $t_c = 120 \mu\text{m}$ for F-antenna the gain would increase about 2 dBi.

Except of the gain, the radiation efficiency of the designed antennas was also monitored (Table 2). The unipole antenna ($t_c = 600 \mu\text{m}$) had radiation efficiency 3.6 and 6.8 percent for both operating bands. The radiation efficiency of the F-antenna was smaller due to a smaller thickness of the F-antenna ($t_c = 420 \mu\text{m}$).

4. Conclusions

A dual band (2.45 and 5.18 GHz) polymer composite based antenna has been designed and characterized. The antenna is made of a composite comprising polyurethane filled with multiwall carbon nanotubes (PU/MWCNT). Main benefit of used composite material is relative simplicity of its synthesis. Second benefit is flexibility of radiator of prepared antenna.

Although the absolute DC conductivity of the composite is lower ($\sigma = 160$ S/m) than for PPy or PEDOT it is still applicable for antenna design. In order to achieve the practical efficiency of radiation and to obtain practical gain the antenna, it is necessary to realize the antennas by means of thick layers.

Using the PU/MWCNT composite, a unipole and dual-band F-antenna on a 2 mm polypropylene (PP) substrate was designed and manufactured.

Measured gain of the unipole antenna is -10.0 and -5.5 dBi for 2.45 and 5.18 GHz frequency bands, The gain of F-antenna is lower than the gain of the unipole since the smaller thickness of the PU/MCNWT composite was used for the F-antenna than the thickness of the composite for the unipole. The gain of the unipole and F-antenna predicted by CST microwave studio did not agreed to much with the measured gains. This is mainly attributed to the fact, that the radiation effect of FR4 microstrip feeding line and the radiation effect of N-connector were not modeled in CST microwave studio.

In addition to the gain, the agreement of the reflection coefficient S_{11} of both antennas obtained by measurement and simulation was also monitored. A good agreement was reached for the unipole. This good agreement was caused by a precise measurement of conductivity of the PU-MWCNT composite at microwave frequencies up to 7 GHz.

The designed antennas are partially bendable and might be practically used in wearable applications. The proposed PU/MWCNT composite material can also find application in other areas than antenna design. For example microstrip matches (terminations), attenuators, as a resistive element in periodic frequency selective surfaces etc.

Author Contributions: R.O., S.G. and P.S. have been responsible for conceptual planning and writing of the paper. S.G., R.M., J.M. and R.D. have done simulations, experiments and processing of measurement data. All authors have read and agreed to the published version of the manuscript.

Funding: This work was supported by the Ministry of Education, Youth and Sports of the Czech Republic—DKRVO (RP/CPS/2020/006) and the national budget of the Czech Republic, within the framework of the project CPS-strengthening research capacity (reg. number: CZ.1.05/2.1.00/19.0409).

Conflicts of Interest: The authors declare no conflict of interest.

References

1. Qiu, Q.; Zhu, M.; Li, Z.; Qiu, K.; Liu, X.; Yu, J.; Ding, B. Highly flexible, breathable, tailorable and washable power generation fabrics for wearable electronics. *Nano Energy* **2019**, *58*, 750–758. [[CrossRef](#)]
2. Zamarayeva, A.M.; Ostfeld, A.E.; Wang, M.; Duey, J.K.; Deckman, I.; Lechêne, B.P.; Davies, G.; Steingart, D.A.; Arias, A.C. Flexible and stretchable power sources for wearable electronics. *Sci. Adv.* **2017**, *3*, e1602051. [[CrossRef](#)] [[PubMed](#)]
3. Andreu-Perez, J.; Leff, D.R.; Ip, H.M.D.; Yang, G.-Z. From Wearable Sensors to Smart Implants—Toward Pervasive and Personalized Healthcare. *IEEE Trans. Biomed. Eng.* **2015**, *62*, 2750–2762. [[CrossRef](#)] [[PubMed](#)]
4. Zhu, Z.; Liu, T.; Li, G.; Li, T.; Inoue, Y. Wearable Sensor Systems for Infants. *Sensors* **2015**, *15*, 3721–3749. [[CrossRef](#)] [[PubMed](#)]
5. Trung, T.Q.; Lee, N. Flexible and Stretchable Physical Sensor Integrated Platforms for Wearable Human-Activity Monitoring and Personal Healthcare. *Adv. Mater.* **2016**, *28*, 4338–4372. [[CrossRef](#)]
6. Parrilla, M.; Cánovas, R.; Jeerapan, I.; Andrade, F.J.; Wang, J. A Textile-Based Stretchable Multi-Ion Potentiometric Sensor. *Adv. Health Mater.* **2016**, *5*, 996–1001. [[CrossRef](#)] [[PubMed](#)]
7. Ponomarenko, A.T.; Shevchenko, V.G.; Enikolopyan, N.S. Formation processes and properties of conducting polymer composites. *Adv. Polym. Sci.* **1990**, *96*, 125–147. [[CrossRef](#)]
8. Locher, I.; Klemm, M.; Kirstein, T.; Troster, G. Design and Characterization of Purely Textile Patch Antennas. *IEEE Trans. Adv. Packag.* **2006**, *29*, 777–788. [[CrossRef](#)]

9. Salvado, L.; Loss, C.; Gonçalves, R.; Pinho, P. Textile Materials for the Design of Wearable Antennas: A Survey. *Sensors* **2012**, *12*, 15841–15857. [[CrossRef](#)]
10. Rmili, H.; Miane, J.-L.; Zangar, H.; Olinga, T. Design of microstrip-fed proximity-coupled conducting-polymer patch antenna. *Microw. Opt. Technol. Lett.* **2006**, *48*, 655–660. [[CrossRef](#)]
11. Matyas, J.; Olejnik, R.; Slobodian, P. Flexible microstrip antenna based on carbon nanotubes/(ethylene–octene copolymer) thin composite layer deposited on PET substrate. In Proceedings of the 6th International Conference on Materials and Applications for Sensors and Transducers, Athens, Greece, 27–30 September 2017; Volume 939.
12. Olejnik, R.; Slobodian, P.; Matyas, J.; Babar, D.G. High elastic polyurethane/carbon nanotube composite laminate for structure health monitoring by gain shifting of antenna sensing element. In Proceedings of the 5th International Conference on Materials and Applications for Sensors and Transducers, Mykonos, Greece, 27–30 September 2015; Volume 108.
13. Matyas, J.; Munster, L.; Olejnik, R.; Vlcek, K.; Slobodian, P.; Krcmar, P.; Urbanek, P.; Kuritka, I. Antenna of silver nanoparticles mounted on a flexible polymer substrate constructed using inkjet print technology. *Jpn. J. Appl. Phys.* **2016**, *55*, 02BB13. [[CrossRef](#)]
14. Matyas, J.; Slobodian, P.; Munster, L.; Olejnik, R.; Urbanek, P. Microstrip antenna from silver nanoparticles printed on a flexible polymer substrate. *Mater. Today Proc.* **2017**, *4*, 5030–5038. [[CrossRef](#)]
15. Hamouda, Z.; Wojkiewicz, J.-L.; Pud, A.; Belaabed, B.; Bergheul, S.; Lasri, T. Polyaniline-carbon nanotubes composites Based patch antenna. In Proceedings of the 8th European Conference on Antennas and Propagation, The Hague, The Netherlands, 6–11 April 2014; p. 2197.
16. Hamouda, Z.; Wojkiewicz, J.-L.; Pud, A.; Kone, L.; Belaabed, B.; Bergheul, S.; Lasri, T. Dual-Band Elliptical Planar Conductive Polymer Antenna Printed on a Flexible Substrate. *IEEE Trans. Antennas Propag.* **2015**, *63*, 5864–5867. [[CrossRef](#)]
17. Verma, A.; Fumeaux, C.; Truong, V.T.; Bates, B.D. A 2 GHz Polypyrrole Microstrip Patch Antenna on Plexiglas (TM) Substrate. In Proceedings of the 2009 Asia Pacific Microwave Conference, Singapore, 7–10 December 2009; p. 36.
18. Chen, S.J.; Fumeaux, C.; Talemi, P.; Chivers, B.; Shepherd, R. Progress in conductive polymer antennas based on free-standing polypyrrole and PEDOT: PSS. In Proceedings of the 2016 17th International Symposium on Antenna Technology and Applied Electromagnetics, Montreal, QC, Canada, 10–13 July 2016.
19. Kaufmann, T.; Shepherd, R.; Fumeaux, C. Modeling Conductive Polymer Antennas in the Microwave Region. In Proceedings of the 2012 IEEE International Conference on Wireless Information Technology and Systems (ICWITS), Maui, HI, USA, 11–16 November 2012; pp. 1–4.
20. Wang, Y.; Wang, T.; Wang, T.; Zhang, J.; Chen, J.; Yang, R.; Ruan, L.; Wang, B. Facile preparation of multifunctional poly(amide-imide)/polyaniline films: Combining self-cleaning, self-extinguishing, and conductive. *Polym. Eng. Sci.* **2019**, *59*, 33–43. [[CrossRef](#)]
21. Wang, Y.; Yu, H.; Li, Y.; Wang, T.; Xu, T.; Chen, J.; Fan, Z.; Wang, Y.; Wang, B. Facile Preparation of Highly Conductive Poly(amide-imide) Composite Films beyond 1000 S m⁻¹ through Ternary Blend Strategy. *Polymers* **2019**, *11*, 546. [[CrossRef](#)] [[PubMed](#)]
22. Mehdipour, A.; Sebak, A.-R.; Trueman, C.W.; Rosca, I.D.; Hoa, S.V. Reinforced Continuous Carbon-Fiber Composites Using Multi-Wall Carbon Nanotubes for Wideband Antenna Applications. *IEEE Trans. Antennas Propag.* **2010**, *58*, 2451–2456. [[CrossRef](#)]
23. Mehdipour, A.; Rosca, I.D.; Sebak, A.-R.; Trueman, C.W.; Hoa, S.V. Carbon Nanotube Composites for Wideband Millimeter-Wave Antenna Applications. *IEEE Trans. Antennas Propag.* **2011**, *59*, 3572–3578. [[CrossRef](#)]
24. Braun, H.P.; Perini, S.; Lanagan, M.T. Measurement of the surface resistivity and electrical conductivity of carbon nanotube sheets using the resonant post-method. *Mater. Lett.* **2016**, *167*, 297–299. [[CrossRef](#)]
25. Wang, Y.; Chen, J.; Shen, Y.; Wang, T.; Ni, Y.; Zhang, Z.; Sun, L.; Ji, B.; Wang, B. Control of Conductive and Mechanical Performances of Poly(Amide-Imide) Composite Films Utilizing Synergistic Effect of Polyaniline and Multi-Walled Carbon Nanotube. *Polym. Eng. Sci.* **2018**, *59*, 224–230. [[CrossRef](#)]
26. Al Moayed, N.N.; Khan, U.; Obol, M.; Gupta, S.; Afsar, M.N. Characterization of Single- and Multi-walled NCarbon Nanotubes at Microwave Frequencies. In Proceedings of the 2007 IEEE Instrumentation & Measurement Technology Conference, Warsaw, Poland, 1–3 May 2007; Volume 1, p. 1951.

27. Challa, R.K.; Kajfez, D.; Demir, V.; Gladden, J.R.; Elsherbeni, A.Z. Characterization of Multiwalled Carbon Nanotube (MWCNT) Composites in a Waveguide of Square Cross Section. *IEEE Microw. Wirel. Components Lett.* **2008**, *18*, 161–163. [[CrossRef](#)]
28. Cvelbar, U.; Markoli, B.; Poberaj, I.; Zalar, A.; Kosec, L.; Spaić, S. Formation of functional groups on graphite during oxygen plasma treatment. *Appl. Surf. Sci.* **2006**, *253*, 1861–1865. [[CrossRef](#)]
29. Cvelbar, U. Interaction of non-equilibrium oxygen plasma with sintered graphite. *Appl. Surf. Sci.* **2013**, *269*, 33–36. [[CrossRef](#)]
30. Moučka, R.; Goňa, S.; Sedlačík, M. Accurate Measurement of the True Plane-Wave Shielding Effectiveness of Thick Polymer Composite Materials via Rectangular Waveguides. *Polymers* **2019**, *11*, 1603. [[CrossRef](#)] [[PubMed](#)]
31. Panda, J.R.; Kshetrimayum, R.S. An F-shaped printed monopole antenna for dual-band RFID and WLAN applications. *Microw. Opt. Technol. Lett.* **2011**, *53*, 1478–1481. [[CrossRef](#)]
32. Chung, K.T.; Sabo, A.; Pica, A.P. Electrical permittivity and conductivity of carbon black-polyvinyl chloride composites. *J. Appl. Phys.* **1982**, *53*, 6867–6879. [[CrossRef](#)]
33. Jou, W.-S.; Cheng, H.-Z.; Hsu, C.-F. The electromagnetic shielding effectiveness of carbon nanotubes polymer composites. *J. Alloy. Compd.* **2007**, *434*, 641–645. [[CrossRef](#)]







Publisher's Note: MDPI stays neutral with regard to jurisdictional claims in published maps and institutional affiliations.



© 2020 by the authors. Licensee MDPI, Basel, Switzerland. This article is an open access article distributed under the terms and conditions of the Creative Commons Attribution (CC BY) license (<http://creativecommons.org/licenses/by/4.0/>).

Article

Wearable and Stretchable SEBS/CB Polymer Conductive Strand as a Piezoresistive Strain Sensor

Thaiskang Jamatia ¹, Jiri Matyas ¹, Robert Olejnik ^{1,*}, Romana Danova ¹, Jaroslav Maloch ¹, David Skoda ¹, Petr Slobodian ^{1,2} and Ivo Kuritka ^{1,3}

¹ Centre of Polymer Systems, Tomas Bata University in Zlín, Tr. Tomase Bati 5678, 760 01 Zlin, Czech Republic

² Department of Physics and Materials Engineering, Faculty of Technology, Tomas Bata University in Zlín, Vavrečkova 5669, 760 01 Zlin, Czech Republic

³ Department of Chemistry, Faculty of Technology, Tomas Bata University in Zlín, Vavrečkova 5669, 760 01 Zlin, Czech Republic

* Correspondence: olejnik@utb.cz

Abstract: A wearable and stretchable strain sensor with a gauge factor above 23 was prepared using a simple and effective technique. Conducting nanocomposite strands were prepared from styrene-*b*-(ethylene-co-butylene)-*b*-styrene triblock copolymer (SEBS) and carbon black (CB) through a solvent-processing method that uses a syringe pump. This novel nanocomposite preparation technique is a straightforward and cost-effective process and is reported in the literature for the first time. The work included two stages: the flexible nanocomposite preparation stage and the piezoresistive sensor stage. Depending on its molecular structure, the thermoelastic polymer SEBS is highly resilient to stress and strain. The main aim of this work is to fabricate a highly flexible and piezoresistive nanocomposite fibre/strand. Among the prepared composites, a composite corresponding to a composition just above the percolation threshold was selected to prepare the strain sensor, which exhibited good flexibility and conductivity and a large piezoresistive effect that was linearly dependent on the applied strain. The prepared nanocomposite sensor was stitched onto a sports T-shirt. Commercially available knee and elbow sleeves were also purchased, and the nanocomposite SEBS/CB strands were sewn separately on the two sleeves. The results showed a high sensitivity of the sensing element in the case of breathing activity (normal breathing, a 35% change, and deep breathing at 135%, respectively). In the case of knee and elbow movements, simultaneous measurements were performed and found that the sensor was able to detect movement cycles during walking.

Keywords: highly stretchable; wearable electronics; SEBS/CB composite strand; novel preparation technique; piezoresistive sensor; respiration activity; strain posture detection



Citation: Jamatia, T.; Matyas, J.; Olejnik, R.; Danova, R.; Maloch, J.; Skoda, D.; Slobodian, P.; Kuritka, I. Wearable and Stretchable SEBS/CB Polymer Conductive Strand as a Piezoresistive Strain Sensor. *Polymers* **2023**, *15*, 1618. <https://doi.org/10.3390/polym15071618>

Academic Editor: Andrea Pucci

Received: 11 January 2023

Revised: 28 February 2023

Accepted: 10 March 2023

Published: 24 March 2023



Copyright: © 2023 by the authors. Licensee MDPI, Basel, Switzerland. This article is an open access article distributed under the terms and conditions of the Creative Commons Attribution (CC BY) license (<https://creativecommons.org/licenses/by/4.0/>).

1. Introduction

The use of sensors has recently garnered significant attention, and its importance and need continue to grow. Sensors are transducers that transform energy from one domain into another. They convert various forms of stimuli, such as mechanical, optical or chemical signals, into electrical signals. Depending on their sensing mechanism, sensors can be classified as optic, inductive, piezoelectric, or piezoresistive. The piezoresistive sensors provide a high sensitivity with the simplest device design. Their working principle is based on the change in a material's electrical properties when it is subjected to mechanical deformation such as strain or pressure [1,2]. More precisely, the change in resistance is measured when the material flexes through exposure to pressure or strain [3].

Conventional piezoresistive sensors tend to be rigid with limited mechanical flexibility. The need exists for more versatile and robust electronic gadgets in the form of healthcare monitoring devices and lighter wearable electronic systems. Therefore, the technology of the coming era will witness the incorporation of electronic systems with more robust

technologies that integrate electronic devices into textiles, body joints, and skin. Fibre-like, flexible sensors are advantageous as they can be integrated into textiles as wearable sensors [4–10]. Wearable electronics demand that sensors be integrated into textiles by either weaving or sewing the sensor into the fabric. Since the sensor is part of the fabric, it can be bent, twisted, and stretched mechanically. Strain and pressure sensor functions are necessary to convert such mechanical stimuli into electrical signals. Moreover, electromechanical sensors with a high resistivity are desirable for recording real-time mechanical stimuli. As a result, a flexible, insulating matrix filled with conductive fillers makes for an efficient, stretchable piezoresistive sensor.

A matrix-filler system is used to achieve such a piezoresistive sensor. This nanocomposite system constitutes an organic (matrix) and an inorganic phase (filler) [11,12]. A polymer matrix was chosen for its stretchable and flexible nature. Styrene-*b*-(ethylene-co-butylene)-*b*-styrene triblock copolymer (SEBS) is one of the most commonly used thermoplastic elastomers (TPEs) due to its highly stretchable nature, processability, thermal stability, and lack of a need for vulcanisation [13–17]. Furthermore, several successful studies have been carried out on the incorporation of carbonaceous conductive fillers into SEBS matrices due to the growing interest in nanomaterials and nanotechnology. The nano-reinforcement of a polymer with carbon nanotubes (CNTs) and multiwalled CNTs (MWCNTs) has been extensively studied in the past few years [18–22]. Two-dimensional nanofillers were also employed, namely, graphene (GP) [23,24]. Moreover, combinations of CNTs and GP with zero-dimensional fullerene were investigated [25,26]. There have been extensive studies conducted on SEBS and filler nanocomposites with varying applications. Hofmann et al. blended SEBS with functionalised graphene (FG) and dispersed it in tetrahydrofuran (THF) using a melt-processing method. The SEBS/FG nanocomposites exhibited superior mechanical properties and an enhanced electrical conductivity at a lower percolation threshold. This nanocomposite has potential applications in the automotive and sealant industries [27]. Turgut et al. [28] utilised carbon nanofibres (CNFs) and SEBS to prepare nanocomposites. Similarly, CNF and an oil-swollen SEBS polymer were blended to prepare another set of nanocomposites. As expected, the increase in the filler content in both nanocomposites was accompanied by an improved tensile modulus and electrical conductivity. However, the former nanocomposites displayed a well-defined percolation threshold. The study also indicated that such composites have potential applications as strain sensors due to their high sensitivity.

Carbon black (CB) is a traditional and frequently used carbonaceous filler which does not lose its importance, is widely available in various forms, and has properties that are well known, investigated, and standardised. The addition of CB to nanocomposites with a SEBS matrix improves electrical properties and reinforces mechanical and viscoelastic behaviour [29]. In one study, Yang et al. prepared SEBS/CNT/CB nanocomposites [30]. In this work, a different volume % ratio of the fillers was investigated, and their sensing behaviours were analysed. The one-dimensional CB and the two-dimensional CNT complemented each other. CB particles filled the gaps or spacing between the conductive pathways from the CNTs. In another study, Kuester et al. [31] composed SEBS/EG (EG—expanded graphite) and SEBS/CB separately through melt-mixing, realising their application in electromagnetic interference shielding (EMI-SE). It was found that SEBS with 15 wt.% CB showed promising results for use in EMI-SE shielding applications, meaning that an elastic SEBS/CB composite with a reasonable electrical conductivity over a relatively large extent of deformation can be prepared to avoid unnecessary use of expensive nanofillers. This may be important for the safety and acceptance of these composites [32].

Moreover, wearable sensory devices are an innovative technology that has shown potential application in the field of electronic skins, such as in human health monitoring, soft robotics, and various other human–machine interfaces [33–39]. These futuristic smart devices are designed to possess a high sensitivity, high flexibility, stretchability and wide detection range. Together with a thermoplastic polymer, they form an excellent combination for use as a piezoresistive sensor. In general, sensors of this type are utilised to detect body

movements, and their largest advantage is the accuracy in measuring specific postures and movements. Based on the response from the individual sensors, it is possible to determine what kind of movement is executed and measure its intensity. There is an opportunity to use the produced SEBS/CB polymer sensor in the field of virtual reality. In virtual reality, the accuracy of movement detection is an important factor that affects the final quality of a game or other application. One of the complex detection tasks, especially during walking, is determining which foot is in front and which is behind [40–42].

Therefore, we propose the preparation of a SEBS/CB polymer conductive strand as a piezoresistive strain sensor. The advantage of our sensor lies in the direct application of the SEBS/CB polymer nanocomposite to clothing or parts of clothing. Furthermore, in using such an incorporated solution, motion detection is more accurate and can sense and detect body movements such as slow walking, brisk walking, and jogging without the need for the user to hold the monitoring device firmly in their hands or stand on it.

A specific application area for the prepared SEBS/CB polymer strand can be found in the rehabilitation techniques used in rehabilitation exercises. During rehabilitation exercises, it is very important to obtain feedback on the progress of the rehabilitated body parts [43]. In the form of a strand, a sensor is able to evaluate, for example, the bending of the limbs in the joint. Another advantage is that the weight of the SEBS/CB polymer strands used in the experimental measurements is low and therefore has a minimal effect on the load on muscles and joints. Respiration activities can also be detected during the rehabilitation process. Breathing can also refer to the oxygenation of the blood, which is one of the important indicators for medical doctors [44]. The breathing rate can also be easily measured. Identifying types of breathing can also refer to the activity performed by patients for deep breathing during heavy physical tests.

To summarize our aim and motivation, the work in this article is centred on the preparation of a flexible, conductive nanocomposite strand, SEBS/CB. An economical and eco-friendly solvent-processing method that uses a syringe pump extrusion without further heat treatment is the highlight of the nanocomposite preparation method. Additionally, the flexible, conductive nanocomposite fibre was used as a piezoresistive sensor and was integrated into a sports T-shirt and elbow and knee sleeves. This setup successfully monitored three different breathing phases and posture motions, demonstrating the sensor material's extreme versatility and usefulness.

2. Results and Discussion

2.1. Morphology (SEM)

A cross-sectional scanning electron microscopy (SEM) image shows the SEBS matrix and the carbon black particles. In Figure 1, the dark grey colour represents the SEBS polymer matrix, and the white dot particles represent the carbon black nanofiller. The solution-processing method of nanocomposite preparation is evident from the SEM micrographs. The discontinuity of the SEBS matrix can be observed in the white, granular fillers sitting on the matrix. The SEM images of the sample also depict that the filler, carbon black, was dispersed well, with some minor agglomerates. The spherical carbon black particles are spread with a homogeneous filler distribution and are incorporated into the SEBS matrix, showing a good filler–matrix interaction. This compatibility is evident from the conductivity achieved on the nanocomposite sample.

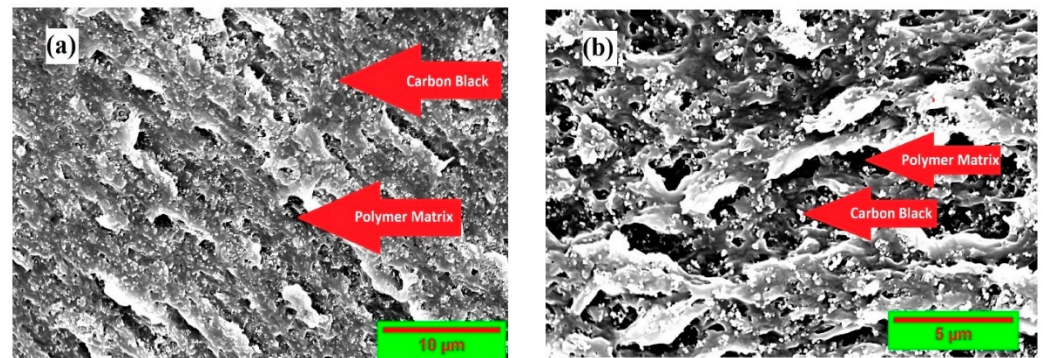


Figure 1. Scanning microscope micrograph of styrene-*b*-(ethylene-co-butylene)-*b*-styrene tri-block copolymer. (a) Surface morphology with CB nanocomposite; (b) cross-section of prepared nanocomposite.

2.2. Percolation as a Factor for Piezoresistivity Sensing Material Selection

The electrical behaviour of a conductive composite follows the percolation theory, which states that conductivity increases significantly—by many orders—when a critical volume fraction is reached: the percolation threshold. Above this value, the composite behaves as a conductor [21]. The concentration of nanofillers, their dispersions, and their processing technique are the deciding factors for the conductivity of a nanocomposite. In a polymer nanocomposite reinforced with conducting fillers, it is vital for the fillers to seep through or percolate into the polymer matrix. The network of fillers in the matrix leads to the electrical conductivity of the composite. This increases the electrical conductivity of the nanocomposite. Moreover, the connectivity of the filler particles resulting in the conductivity of the nanocomposite is either through physical contact with minimal resistance or incomplete contact with a tunnelling barrier. In general, a nanocomposite behaves as a conductor primarily due to the tunnelling of electrons through the barriers within the conductive filler network. If the conductive filler percentage is increased, the filler particles are greater in number and they are closer to each other. On the contrary, if the conductive filler percentage is decreased, the filler particles are less in number and the distance between them increases. This emphasizes the role of the mean gap size between the primary aggregates or clusters of CB particles embedded within the insulating polymer matrix. The tunnelling or hopping of charge carriers across the gaps between particles governs the conductivity of carbon-black-filled polymers above the percolation threshold [45]. The application of a strain to such a material may change the distance between the particles and influence the connectivity of the filler network, thus influencing the interparticle tunnelling. Changes in the tunnelling barriers influence the resistivity of the material, which is macroscopically manifested as a change in the measured resistance. The change in resistivity is responsible for the piezoresistive effect in nanocomposites. If the particle concentration is too high, the material has a saturated conductivity, and its resistivity may change slightly with the deformation. If the concentration of the filler is too low, the material behaves as an insulator. It should be noted that a decrease in conductivity is expected for elongation in the tensile mode. Therefore, the optimum material for making a piezoelectric strain sensor is a material with a filler concentration that just exceeds the percolation threshold. To assess the percolation behaviour of the composites, the conductivity of the SEBS/CB samples was measured as a function of the weight of the carbon black filler concentration. In accordance with the percolation theory, the composites displayed three stages of conductivity—insulation, percolation, and saturation. It is eminent from Figure 2 that the nanocomposite was insulating in the 0–10 wt.% region. From above 10 wt.% to 50 wt.% is the percolation stage when the nanocomposite begins to behave as a conductor. Finally, the 50–70 wt.% region is the saturation stage, without any significant increase in electrical conductivity. For the SEBS/CB compound, 15% is the threshold at which the

SEBS/CB behaves as a conducting material. Therefore, this composition was chosen for the preparation of the strain sensor.

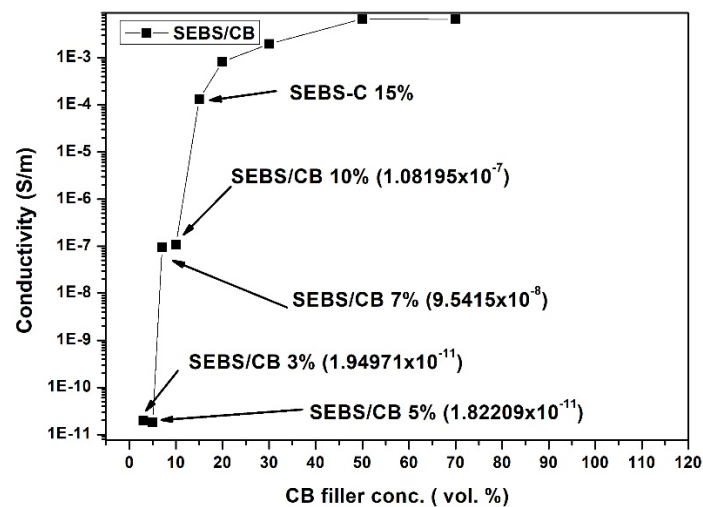


Figure 2. Percolation curve of SEBS/CB vs. conductivity. The arrow refers to chosen composite concentration for whole experimental study.

In Figure 2, which represents the percolation of the SEBS/CB vs. the conductivity samples, it can be seen that SEBS/CB 3% and the SEBS/CB 5% values are in the same exponential order. This is reflected in the graph. This can be attributed to the fact that the carbon black had just begun to percolate into the matrix. These two points display the starting or initialisation of conductivity in the matrix. The SEBS/CB 7% and SEBS/CB 10% values represent the increase in the conductivity of the nanocomposite with the increase in the amount of the carbon black conductive filler. As we observe the increase in the CB concentration, we can see a gradual increase in the conductivity.

The shape of the graph can be clearly explained by the s-like shape of a percolation curve graph from the percolation theory (as explained in Section 2.2 of the manuscript). The points from SEBS/CB 3% to SEBS/CB 5% are the insulation region in which the percolation threshold has not been reached. The points from SEBS/CB 5% to SEBS/CB 50% represent the conductivity region. This is the region in which percolation is reached, and the samples act as a conductor. The final region is the saturation phase, where the optimum electrical conductivity of the SEBS/CB composite is reached.

2.3. Mechanical Properties

A mechanical test in the form of the stress vs. strain relationship was conducted on the SEBS/CB 15% sample at two different elongation rates: 50 mm/min and 100 mm/min. As can be seen from Figure 3, at the 50 mm/min elongation rate, the elongation at break was approximately 262%. The elongation at break was approximately 300% for the 100 mm/min rate. The graph clearly demonstrates the highly stretchable property of the piezoresistive sensor at different elongation rates. This characteristic can find practical applications in wearable electrical and medical devices.

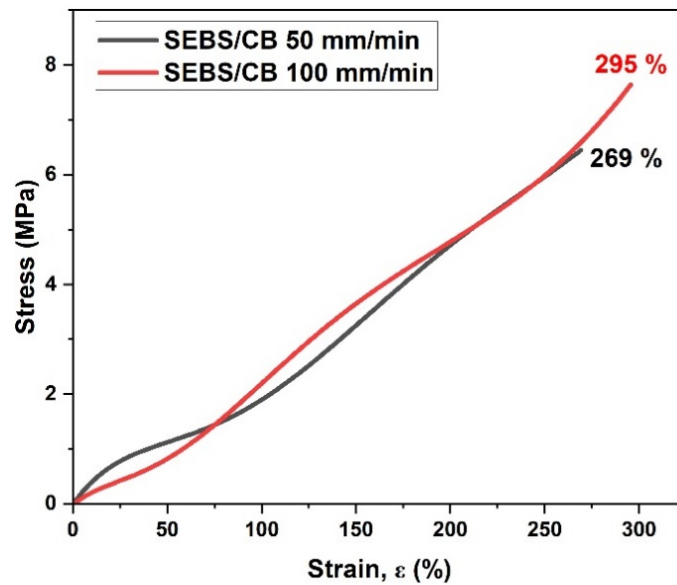


Figure 3. Stress–strain relation of the SEBS/CB 15% strand.

2.4. Electromechanical Properties

The electrical and mechanical properties of the SEBS/CB 15% conductive strand were tested. From Figure 4, it can be seen that the investigation was carried out as a function of resistance vs. the strain % and the relative response of the material $\Delta R/R_0$ vs. the strain %. The measurements were carried out in increments of elongation of 5 mm. The time difference between each measurement was 10 s. The figure below displays how stretchable the sample can be, demonstrating a strain range of up to 110%. The inset demonstrates the exponential character of the observed dependence. Therefore, a small, limited strain ranging from 0 up to a maximum of 16% strain was chosen for use in further experiments to avoid hysteresis and irreversible damage to the material.

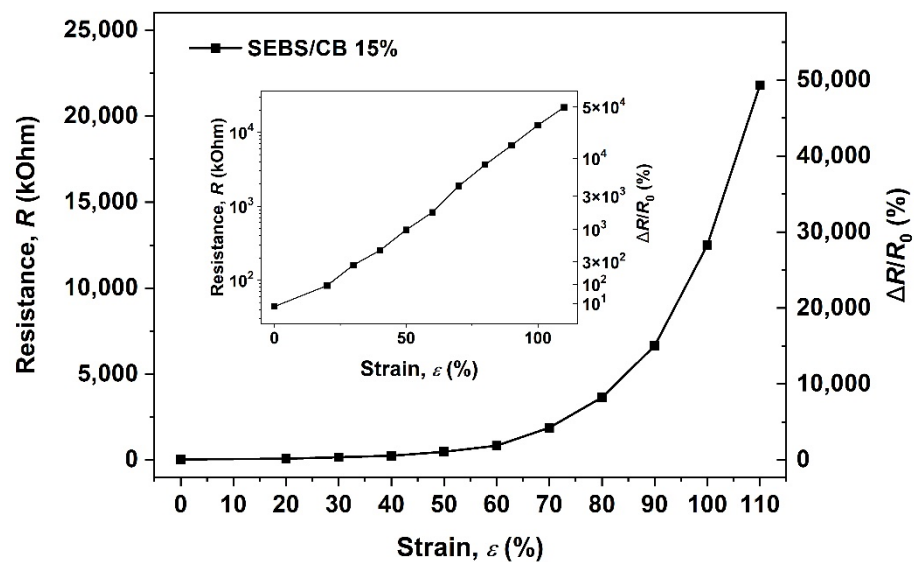


Figure 4. Electromechanical behaviour of styrene-b-(ethylene-co-butylenes)-b-styrene triblock copolymer, filled by 15 wt.% of carbon black (CB).

In the follow-up test, the SEBS/CB 15% sample underwent a similar electro-mechanical measurement at the same elongation rates of 50 mm/min and 100 mm/min. It can be seen from Figure 5 that the elongation rate of 50 mm/min reached the upper measurement limit of the multimeter at elongation above 107%. For the 100 mm/min rate, this point was

achieved above 234%. This test substantiates the highly flexible nature of the conductive SEBS/CB 15% nanocomposite strand, importantly at different elongation rates. This characteristic is essential for application in the detection of body movement, which is studied in this work.

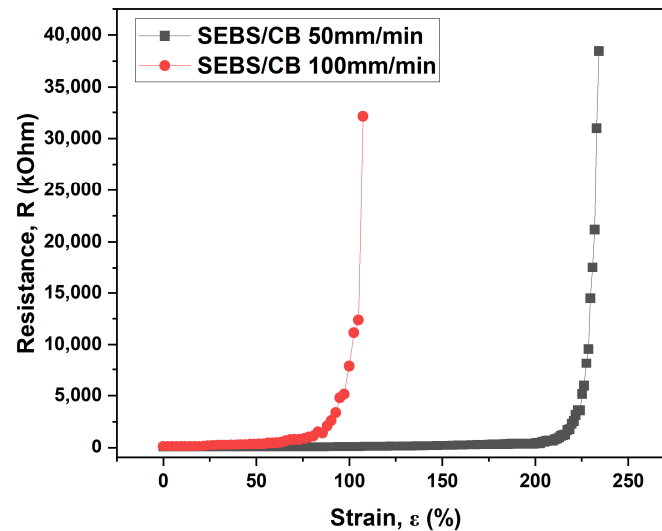


Figure 5. Electro-mechanical properties of the SEBS/CB 15% at different elongation rates.

The images depicted in Figure 6 illustrate the SEBS/CB 15% sample in (a) unstretched, (b) stretched, and (c) bent mode. This flexible and stretchable nanocomposite strand can be used to detect various human motions.

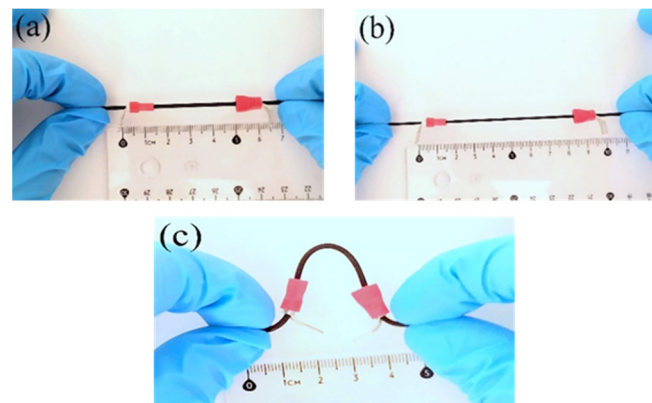


Figure 6. Pictorial representation of the SEBS/CB 15% sample in (a) unstretched, (b) stretched, and (c) bent form.

In another demonstration in Figure 7, the SEBS/CB 15% piezoresistive sensor was subjected to a cyclic loading–unloading test (lasting up to almost 5000 cycles). It can be seen from Figure 7 that the sensor exhibited a high flexibility and durability. Moreover, insets (a) and (b) in the figure show that the conductive SEBS/CB 15% strand demonstrated a good endurance limit, long working life, and stability. Finally, in inset (c), it is evident that the mechanical stimuli corresponded to the electromechanical response of the sensor in the form of a sine wave (1 Hz frequency) with $\pm 3\%$ strain.

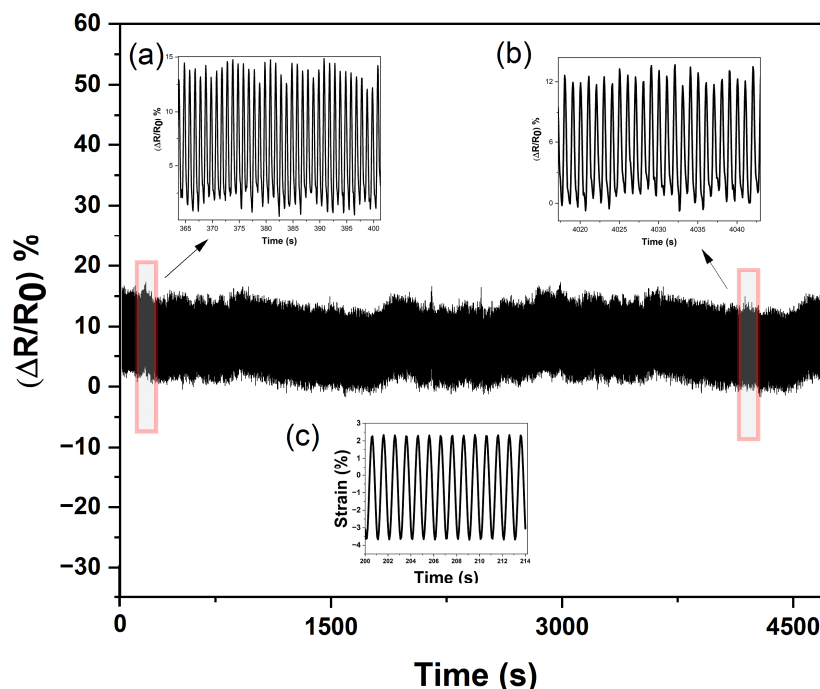


Figure 7. Durability and endurance test of the SEBS/CB 15% sensor. Insets (a,b) are the enlarged cyclic loading–unloading response, and (c) is the mechanical stimuli with respect to the electromechanical response.

2.5. Gauge Factor and Piezoresistivity Analysis

One crucial parameter that is considered in evaluating the performance of a sensor is its sensitivity in the form of a gauge factor (*GF*). Simply put, this is the ratio of the change in resistance per unit to the change in length per unit. The *GF* is usually used to evaluate the sensitivity of a sensor with strain variation. Mathematically, *GF* is defined by the ratio of the relative difference of the measured relative resistance change ($\Delta R/R_0$) to the applied mechanical strain (ϵ):

$$GF = \frac{(\Delta R/R_0)}{\epsilon} \tag{1}$$

where R_0 represents the initial specimen resistance and ΔR represents the resistance change, $R - R_0$.

Figure 8a depicts the gauge factor vs. strain relationship for the nanocomposite strand SEBS/CB 15%. The *GF* ranges from 28 to 23 upon elongation from 0 to 15%. Moreover, the relation shows an almost linear piezoresistive response.

A gauge factor of a piezoresistive strand strain sensor may be expressed as

$$GF = 1 + 2\nu + \frac{(\Delta\rho/\rho_0)}{\epsilon} \tag{2}$$

where ν represents Poisson’s ratio, ρ_0 represents the initial material resistivity, and $\Delta\rho$ represents the resistivity change, $\rho - \rho_0$. The last term is the simplest form of a piezoresistivity coefficient and is usually considered constant [46].

Elastomers are generally considered to be practically incompressible, with Poisson’s ratio value nearly equal to 0.5 (for a cylindrical shape). Although Poisson’s ratio depends on the chemical structure of the elastomer and on the filler concentration, these dependencies are very weak over a broad range of the filler content. Hence, the value of 0.5 is a sufficiently good guess in our case, especially with respect to the experimental error, which is shown later. If there is no piezoresistivity effect, the value of the *GF* is just 2, i.e., $1 + 2\nu$. Indeed, the value of *GF* is 2 for many materials, typically metals. The exception for this is platinum,

which demonstrates a $GF \approx 6$ [47]. It is evident that GF values above 20 indicate a strong piezoelectric effect comparable with that of semiconductors [1].

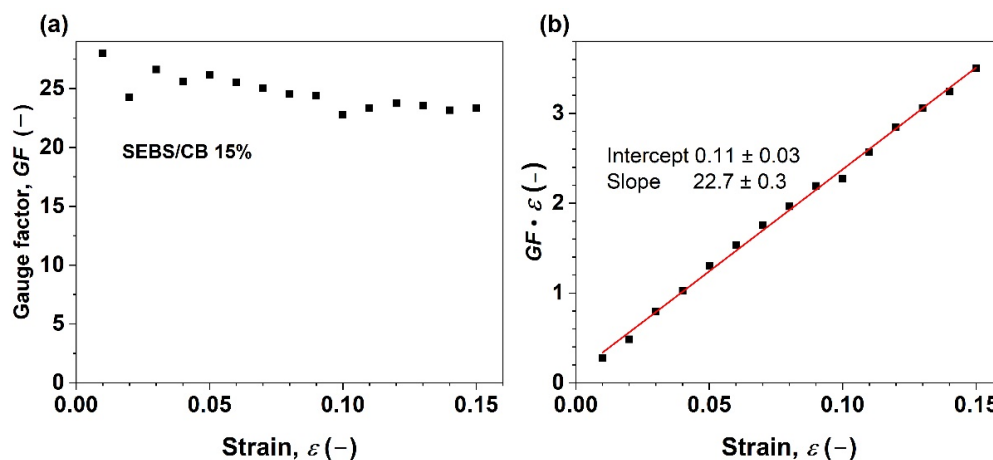


Figure 8. (a) Gauge factor vs. elongation of styrene-*b*-(ethylene-co-butylene)-*b*-styrene triblock copolymer filled with 15 wt.% of carbon black (CB); (b) analysis of the resistivity change responsible for the piezoresistive effect. The red line represents a linear fit to the experimental data.

In order to analyse the piezoelectric effect, Equation (2) was rearranged, multiplying both sides by the applied mechanical strain (ε):

$$GF \cdot \varepsilon = (1 + 2\nu) \cdot \varepsilon + (\Delta\rho/\rho_0) \quad (3)$$

The product $GF \cdot \varepsilon$ was then plotted against ε in Figure 8b. In no way does the slope of the line have a value of 2. Instead, a value of 22.7 ± 0.3 is found. A small positive intercept is also observed. This implies a linear dependence of the term $\Delta\rho/\rho_0$ on ε , as in the following equation:

$$\Delta\rho/\rho_0 = \frac{d(\Delta\rho/\rho_0)}{d\varepsilon} \cdot \varepsilon + const = const_1 \cdot \varepsilon + const_2 \quad (4)$$

Yielding an expanded equation:

$$GF \cdot \varepsilon = (1 + 2\nu + const_1) \cdot \varepsilon + const_2 \quad (5)$$

From the above, it is evident that the linear component of the piezoresistivity coefficient, $const_1$, is approximately 20.7, indicating a linear dependency of the material's resistivity change on the applied strain. In other words, $\Delta\rho/\rho_0$ increases 20.7 times when $\varepsilon = 100\%$. This observation explains the exponential shape of the electromechanical behaviour curve in Figure 4. On the other hand, the small intercept of $const_1$ with the value of 0.11 ± 0.03 does not change with the applied strain. Therefore, it most likely corresponds to the contribution of a small, inevitable systematic error to the measured values due to the resistance of the measuring wires, contact electrodes, and contact resistances as only a two-point method was used for the resistance measurement with the aid of the digital multimeter.

2.6. Thermal Properties (TGA-DSC)

The thermogravimetric (TGA) analysis was measured in air, in the temperature range of room temperature to 1000 °C at a 5 °C min⁻¹ heating rate. The weight loss was analysed in weight percentage. The TGA curves of pure SEBS, carbon black, and SEBS/CB 15% are plotted in the upper graph window of Figure 9. It can be observed that the pure SEBS sample followed a degradation with poorly resolved steps. The TGA of SEBS/CB 15% shows that its thermal resistance was increased due to the carbon black filler. The

onset degradation temperature of the nanocomposite was increased by approximately 50 °C when compared to pure SEBS. As can be seen, the 15% loading of carbon black (by mass) is evident from the last mass loss step of the SEBS/CB 15%, which corresponds to the loading percentage of the filler in the matrix. The DSC thermogram is shown in the lower graph window and matches well with the TG steps observed for the composite and its components. No phase change is indicated in the material at expectable application temperatures. The polymer matrix degradation began at above 200 °C and proceeded in several steps. The slight jump in the DSC thermogram at ca. 380 °C may be associated with the evolution of a bubble from the molten polymer. The maximum mass loss rate was achieved at ca 433 °C, whereas the last degradation step of the polymer matrix ended at approximately 560 °C. The remaining 15% of the CB oxidized completely below 740 °C.

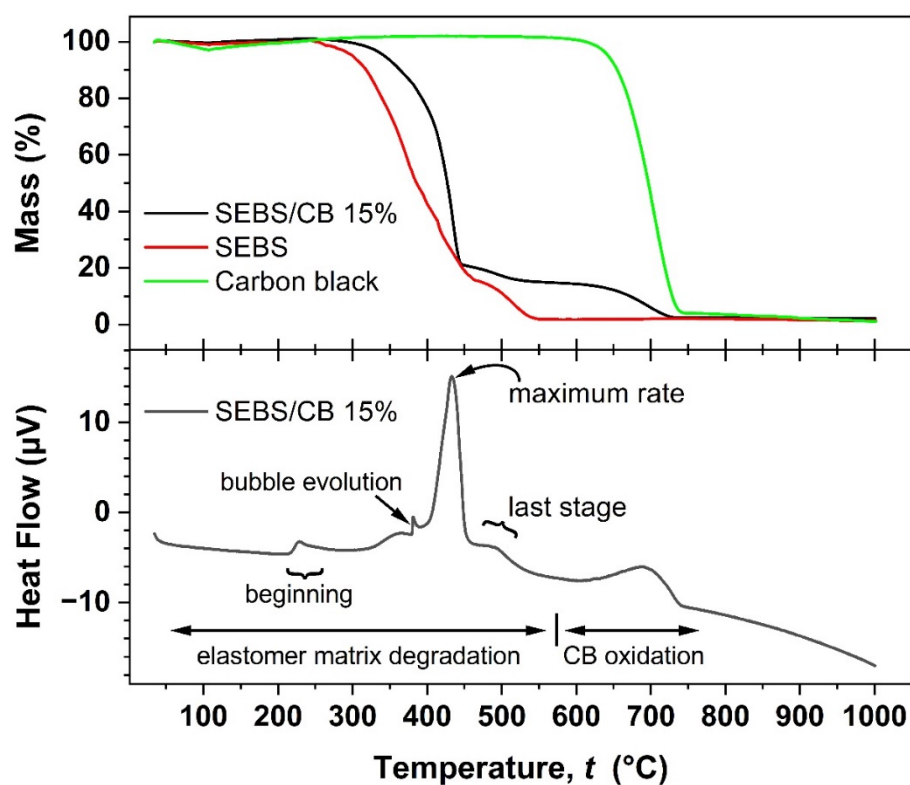


Figure 9. TGA analysis of SEBS, carbon black, and SEBS/CB 15% samples (upper graph window) and simultaneous DSC analysis of the SEBS/CB 15% sample (lower graph window).

2.7. Piezoresistive Wearable Sensor

In order to study the usability of the SEBS/CB nanocomposite strand, the SEBS/CB 15% sample was stitched on a sports T-shirt, and three different modes of breathing were monitored: normal breathing, deep breathing and inhale–hold–exhale. The test was conducted on an individual wearing the body-fit tee with the stretchable fibre stitched around the chest of the clothing. The three different modes of breathing were monitored as an electrical resistance response to the sensor. The real-time reading of the sensor was observed and was used for ten cycles. In another instance, the nanocomposite fibre was sewn onto the knee and elbow sleeves. These sleeves were worn by the volunteer on the right elbow and right knee. A brisk walk was conducted to test the piezoresistive response of the SEBS/CB 15% conductive fibre. The idea was to apply the sensing element to the T-shirt, knee sleeves, and elbow sleeves with minor modifications, as shown in Figure 10.

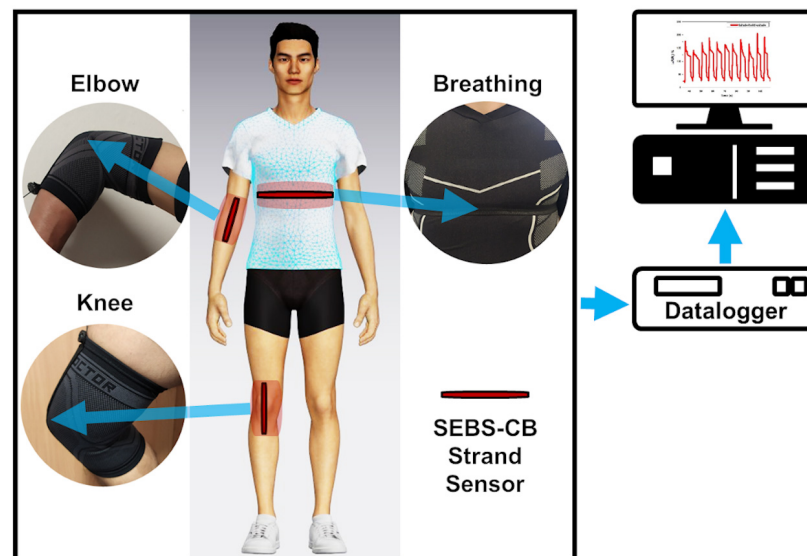


Figure 10. Schematic illustration of the position of the sensors on the chest, elbow, and knee.

The sample calibration was performed based on the initial value of R_0 for each experimental sample. For all measurements, the samples with an initial value equal to or close to the R_0 value were used. The results are shown in Figures 10 and 11 as a percent-age change in the relative resistance.

$$\Delta R/R_0 = \frac{(R - R_0)}{R_0} \quad (6)$$

where R_0 is the electrical resistance of the measured sample before the first elongation, R is the resistance during elongation, and strain is the relative change in specimen length.

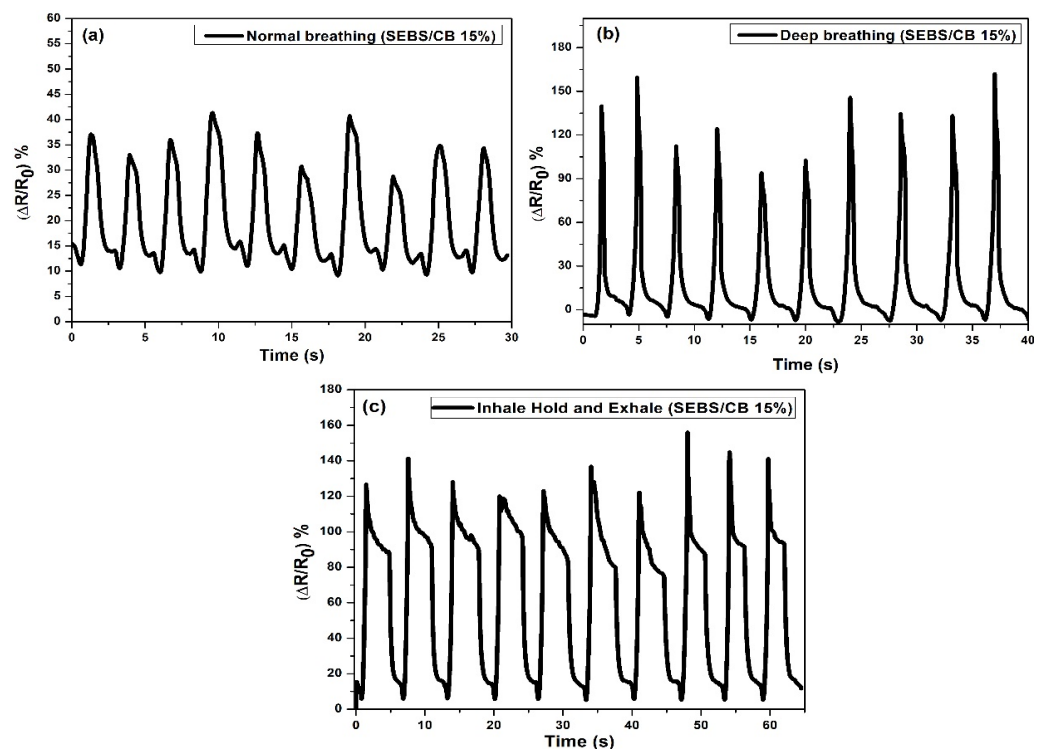


Figure 11. Different types of normal breathing represent by change of resistivity. (a) Normal breathing, (b) deep breathing, and (c) inhale–hold–exhale. Ten cycles were performed.

Subsequently, the cloth and the sleeves with the sensor incorporated were worn by a volunteer. The sensor was pre-strained by 10% of the initial length of the sensor. The pre-strain of the sensor ensured the acquisition of relevant data from the sensor. On the ends, there were outputs for contacts connected to the datalogger via cables. The maximum change in electrical resistance was 25% with normal breathing. The maximum change in electrical resistance was 150% with deep breathing (Figure 11). The response of the sensor to electrical resistance was very sensitive to deformation, reversible, and able to detect breathing in real time.

The stabilizing effect on the resistance extension loops and the residual normalized resistance change was constant from the beginning. The structure of the curves remained more or less the same regardless of the number of deformation cycles. In addition, the shape of the recorded peaks and curves was maintained irrespective of the number of deformation cycles. This mechanical stabilization is advantageous for using the sensor as an elongating sensing element. In the next section, the application of the sensor to the knee and elbow is described in Figure 12. The sensor on the sleeves was pre-strained by 10% of the initial length of the sensor, similar to the T-shirt. The cavity with the sensor was located on the axis of the measured joint. The volunteer wore the sleeves with sensors, and the movement of the knee and elbow on an elliptical trainer was simulated.

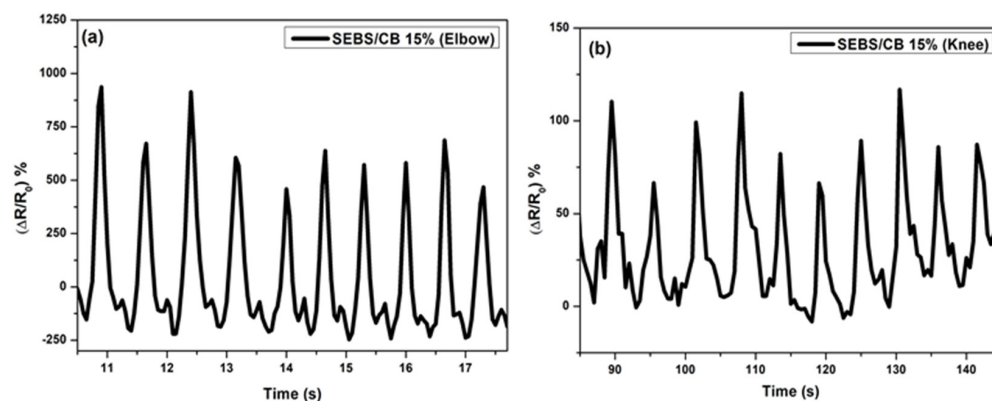


Figure 12. Change of resistivity vs. time for walking sensors: (a) elbow response and (b) knee response. The responses were measured simultaneously.

3. Materials and Methods

3.1. Materials

Polystyrene-block-poly(ethylene-ran-butylene)-block-polystyrene (SEBS) powder, average $M_w = 118,000$ was purchased from Sigma-Aldrich (Sigma-Aldrich St. Louis, MO, USA), and carbon black, Super P[®] Conductive 99% (carbon black) was purchased from Alfa Aesar (Alfa Aesar, Heysham, Lancashire, UK). The solvent toluene (p.a.) was procured from PENTA (PENTA s.r.o., Prague, Czech Republic). The extrusions were conducted with a New Era NE-1000 one-channel (New Era Pump Systems, Inc., Farmingdale, NY, USA), programmable syringe pump. The knee and elbow sleeves were purchased from Shock Doctor (size: XS) (Shock Doctor, Taiwan), and the sports T-shirt (size: S) (Decathlon, France), was purchased from Decathlon.

3.2. SEBS/CB Nanocomposite Preparation

To prepare the 15 wt.% nanocomposite (denoted as SEBS/CB 15%), 1 g of SEBS and 0.15 g of carbon black were added separately to a 25 mL beaker. Toluene was separately added to the beaker containing SEBS and CB. The beaker containing toluene and SEBS was stirred in a magnetic stirrer at 500 rpm for 30 min. In another 25 mL beaker on a magnetic stirrer, CB and toluene were mixed together for two hours. This was followed by the addition of the SEBS solution to the beaker containing CB (about 8 h) to properly mix the composite dispersion. This dispersion was then poured into a Petri dish (15 cm

diameter), and the composite was allowed to dry overnight at room temperature. The dried SEBS/CB 15% composite was peeled off with tweezers, mixed with toluene, and loaded into a 6 mL syringe. A New Era NE-1000 one-channel, programmable syringe pump was utilised for the extrusion of the composite. The syringe opening served as the extrusion die. The extrusion velocity was 2.5 mL/h. An illustration of the solution-processing nanocomposite preparation is depicted in Figure 13. The extruded SEBS/CB fibre/strand was dried overnight at room temperature. The diameter of the extruded strand was 1.65 mm on average.

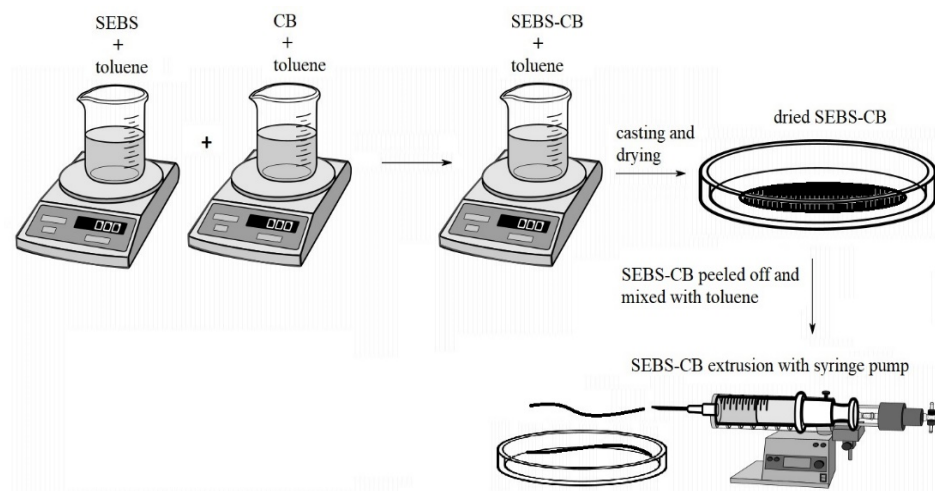


Figure 13. Illustration of a stretchable and flexible SEBS/CB strand preparation.

Similarly, the remaining composites were prepared with varying CB filler concentrations, summarized in Table 1.

Table 1. SEBS/CB different filler conc.

Sample	SEBS (g)	CB (g)
SEBS/CB 3%	1	0.03
SEBS/CB 5%	1	0.05
SEBS/CB 7%	1	0.07
SEBS/CB 10%	1	0.10
SEBS/CB 15%	1	0.15
SEBS/CB 20%	1	0.20
SEBS/CB 30%	1	0.30
SEBS/CB 50%	1	0.50
SEBS/CB 70%	1	0.70

3.3. Scanning Electron Microscopy (SEM)

The SEBS/CB 15% strand was dipped in liquid nitrogen and fractured to achieve a flat surface of the sample suitable for SEM analysis. To avoid charge build-up and artefacts on the sample, the fracture surfaces were coated with a conductive metal (Au/Pd) with a sputtering device. The sputtering process created a very thin conductive layer on the sample surface. This process rapidly increased the sample conductivity, which was crucial for obtaining SEM images. It was followed by placing the sample on a metal stub using carbon tape. The Nova NanoSEM 450 (FEI) microscope (Thermo Fisher Scientific, Hillsboro, Oregon, USA) was used with a Schottky field emission electron source and operated at 0.02–30 keV.

3.4. Thermogravimetric Analysis (TGA)

The thermogravimetric analysis (TGA) was performed on a Setaram LabSys Evo (SETARAM Instrumentation, Caluire, France) instrument to analyse the SEBS polymer and SEBS/CB nanocomposite degradation. The test was carried out to quantify and verify the concentration of the carbon black filler. The composite strand was sliced into a small piece (10 mg) and placed in an Al₂O₃ crucible. The samples were heated in an air atmosphere (60 mL min⁻¹) up to 1000 °C at a heating rate of 5 °C min⁻¹.

3.5. Percolation Measurement

The percolation curve of the SEBS/CB nanocomposite strands was measured on a KEITHLEY 6517B, TEKTRONIX, INC (Artisan Technology Group, Champaign, Illinois, USA). Each sample was connected using the two-point method. The length between the clamps was 100 mm. All samples had the same diameter of 1.65 mm. The technique was implemented to measure the conductivity of the composites with different concentrations of carbon black filler, Table 1.

3.6. Mechanical and Electromechanical Test

The Testometric M350-5CT (Testometric, Lancashire, UK) mechanical testing machine was employed to study the mechanical test of the SEBS/CB nanocomposite strands. Pieces were sliced from a long-extruded SEBS/CB sample at 10 cm. The cut 10 cm sample was equipped with two metal electrode holders placed at 5 cm distance apart. The sample was fixed at two terminals of the Testometric M350-5CT instrument and connected to a digital multimeter UNI-T 71C (UNIT-T, Dongguan City, Guangdong Province, China). The analysis was carried out by stretching the strand in 5 mm increments, and the registered change in resistivity was noted. The test continued until the flexible SEBS/CB sample disintegrated during the testing process, Figure 4. The cyclic response of the SEBS/CB15% was conducted on an Instron 8871.

3.7. Sensor Test

A sensor test was performed using the Keysight 34980A (Keysight, Santa Rosa, CA, USA) multifunctional switch/measure unit data-logger device. The sampling rate was adjusted to 50 ms. For monitoring different modes of breathing, one channel was used. Similarly, for the elbow and knee movement measurement, two channels with the same 50 ms sampling rate were used. The data-logging system was able to measure these multiple channels simultaneously. Sensors were connected by wires with alligator clamps to eliminate transition resistance. The position of the breathing sensor was carefully chosen in order to place the sample on the most sensitive part of the chest. The reading of the breathing motion process consisted of two aspects: the chest deformation during the breathing process and the durability of the T-shirt under normal wear and the comfort during its usage.

The process of choosing a sensor location can be divided into two stages. First, the dimension of the chest was measured using a conventional method to obtain the percentage change during the breathing process. The simulation of the chest deformation was performed by Avatar software. The software was able to simulate the deformation and show the deformation of the chest (while inhaling and exhaling) and identify the most effective location of the sensor with respect to its wearability. A garment-design software, CLO 3D, was employed for the simulation of bodily movements and tensions on the sports T-shirt. The virtual, 3D person in this software is called the "Avatar", and the personal dimension features can be tailored according to, for example, height, chest circumference, waist circumference, arm length, leg length, etc. The Avatar model shows the distribution of deformation from the front and back parts of the chest, Figure 14.

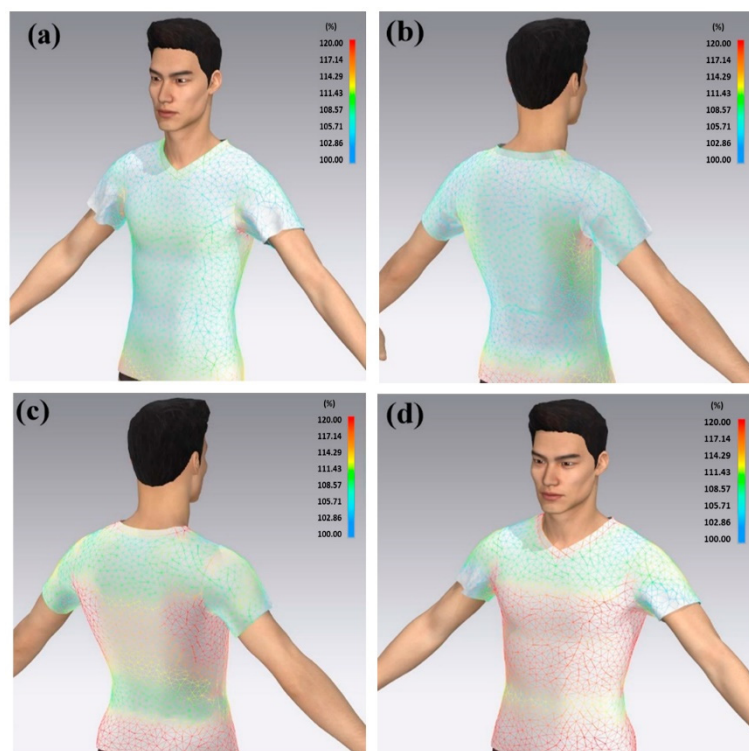


Figure 14. Tension simulation during breathing process. (a) Exhale—front view, (b) exhale—back view, (c) inhale—back view, and (d) inhale—front view. Colour scale shows the expansion of chest.

4. Conclusions

This work demonstrates two things: firstly, the nanocomposite preparation was successful using a solvent-processing method of mixing the SEBS and CB, casting, drying, and finally extruding using a syringe pump. After surveying the literature across journals, we can confirm that this extrusion of nanocomposite samples using a syringe pump is the first of its kind. In the following observation, the as-prepared SEBS/CB nanocomposite strand was highly flexible and conductive due to the presence of the superconductive carbon black filler. After preparing a series of SEBS/CB nanocomposites (Table 1), a percolation threshold was achieved at SEBS/CB 15%. Moreover, this sample also exhibited good stretchability and durability, with a loading–unloading cyclic response of up to almost 5000 (Figure 7). The conducting fibre could be stretched up to 21 cm from its original length of 10 cm, which is an elongation of approximately 110%, Figure 4. This makes it feasible to utilise the strand as a flexible piezoresistive sensor that is also wearable. The proof-of-concept was observed when the SEBS/CB 15% strand was stitched on a sports T-shirt, elbow sleeve, and ankle sleeve and three modes of breathing and bodily motion (walking) were successfully monitored and measured. The good sensing performance, with a GF larger than 23, was attributed to a strong piezoresistive effect (Figure 8b) due to the presence of the conductive filler, carbon black, in a properly selected concentration above the percolation threshold, and the thermoplastic copolymer, SEBS, which provided the flexibility and stretchability properties. Moreover, the piezoresistive coefficient depended linearly on the applied strain. We presented a key wearable sensor with applications that can be extended to healthcare, robotics, and smart textiles, with some possible scope for improvement.

In summary, the following are the highlights of our work with the SEBS/CB nanocomposite:

- The solution-processing technique for preparing the SEBS/CB sensors is the first of its kind;
- The high flexibility of the sensor measured up to 300% (Figure 3);

- The highest sensitivity of the SEBS/CB was achieved at a CB concentration of 15% (by volume);
- A wearable piezoresistive sensor was demonstrated with the SEBS/CB 15% sensor.

Author Contributions: Conceptualization, T.J., R.O. and I.K.; methodology, P.S., J.M. (Jiri Matyas), R.O. and I.K.; software, J.M. (Jaroslav Maloch); validation, P.S. and I.K.; formal analysis, T.J. and I.K.; investigation, T.J., J.M. (Jiri Matyas), R.O., R.D. and D.S.; writing—original draft preparation, T.J., R.O., R.D. and J.M. (Jiri Matyas); writing—review and editing, I.K.; visualization, T.J., J.M. (Jaroslav Maloch), R.O., D.S. and I.K.; supervision, P.S. and I.K.; funding acquisition, I.K. and R.D. All authors have read and agreed to the published version of the manuscript.

Funding: This research was funded by The Ministry of Education, Youth and Sports of the Czech Republic within the framework of DKRVO (project numbers RP/CPS/2022/006 and (RP/CPS/2022/007). In addition, Romana Danova explicitly acknowledges the support of the Internal grant agency of Tomas Bata University, project number IGA/CPS/2020/008.

Institutional Review Board Statement: Not applicable.

Informed Consent Statement: Not applicable.

Data Availability Statement: Not applicable.

Acknowledgments: The Tomas Bata University in Zlin is acknowledged for all the support provided in kind.

Conflicts of Interest: The authors declare no conflict of interest. The funders had no role in the design of the study; in the collection, analyses, or interpretation of data; in the writing of the manuscript; or in the decision to publish the results.

References

1. Nguyen, T.; Dinh, T.; Phan, H.P.; Pham, T.A.; Dau, V.T.; Nguyen, N.T.; Dao, D.V. Advances in ultrasensitive piezoresistive sensors: From conventional to flexible and stretchable applications. *Mater. Horiz.* **2021**, *8*, 2123–2150. [[CrossRef](#)] [[PubMed](#)]
2. Fiorillo, A.S.; Critello, C.D.; Pullano, A.S. Theory, technology and applications of piezoresistive sensors: A review. *Sens. Actuators A Phys.* **2018**, *281*, 156–175. [[CrossRef](#)]
3. Fraden, J. *Handbook of Modern Sensors: Physics, Designs, and Applications*, 5th ed.; Springer: Berlin/Heidelberg, Germany, 2016. [[CrossRef](#)]
4. Liu, X.; Miao, J.; Fan, Q.; Zhang, W.; Zuo, X.; Tian, M.; Zhu, S.; Zhang, X.; Qu, L. Recent Progress on Smart Fiber and Textile Based Wearable Strain Sensors: Materials, Fabrications and Applications. *Adv. Fiber Mater.* **2022**, *4*, 361–389. [[CrossRef](#)]
5. Leal-Junior, A.; Avellar, L.; Frizzera, A.; Marques, C. Smart textiles for multimodal wearable sensing using highly stretchable multiplexed optical fiber system. *Sci. Rep.* **2020**, *10*, 13867. [[CrossRef](#)]
6. Lin, S.; Hu, S.; Song, W.; Gu, M.; Liu, J.; Song, J.; Liu, Z.; Li, Z.; Huang, K.; Wu, Y.; et al. An ultralight, flexible, and biocompatible all-fiber motion sensor for artificial intelligence wearable electronics. *Npj Flex. Electron.* **2022**, *6*, 27. [[CrossRef](#)]
7. Zeng, W.; Shu, L.; Li, Q.; Chen, S.; Wang, F.; Tao, X.M. Fiber-based wearable electronics: A review of materials, fabrication, devices, and applications. *Adv. Mater.* **2014**, *26*, 5310–5336. [[CrossRef](#)]
8. Jin, H.; Abu-Raya, Y.S.; Haick, H. Advanced Materials for Health Monitoring with Skin-Based Wearable Devices. *Adv. Healthc. Mater.* **2017**, *6*, 1700024. [[CrossRef](#)]
9. Gao, L.; Zhu, C.; Li, L.; Zhang, C.; Liu, J.; Yu, H.D.; Huang, W. All Paper-Based Flexible and Wearable Piezoresistive Pressure Sensor. *ACS Appl. Mater. Interfaces* **2019**, *11*, 25034–25042. [[CrossRef](#)]
10. Zheng, Q.; Lee, J.; Shen, X.; Chen, X.; Kim, J.-K. Graphene-based wearable piezoresistive physical sensors. *Mater. Today* **2020**, *36*, 158–179. [[CrossRef](#)]
11. Dios, J.R.; Gonzalo, B.; Tubio, C.R.; Cardoso, J.; Gonçalves, S.; Miranda, D.; Correia, V.; Viana, J.C.; Costa, P.; Lanceros-Méndez, S. Functional Piezoresistive Polymer-Composites Based on Polycarbonate and Polylactic Acid for Deformation Sensing Applications. *Macromol. Mater. Eng.* **2020**, *305*, 2000379. [[CrossRef](#)]
12. Nath, K.; Khanal, S.; Krause, B.; Lach, R. Electrically conductive and piezoresistive polymer nanocomposites using multiwalled carbon nanotubes in a flexible copolyester: Spectroscopic, morphological, mechanical and electrical properties. *Nano-Struct. Nano-Objects* **2022**, *29*, 100806. [[CrossRef](#)]
13. Shen, Z.; Feng, J. Mass-produced SEBS/graphite nanoplatelet composites with a segregated structure for highly stretchable and recyclable strain sensors. *J. Mater. Chem. C* **2019**, *7*, 9423–9429. [[CrossRef](#)]
14. Cetin, M.S.; Karahan Toprakci, H.A. Flexible electronics from hybrid nanocomposites and their application as piezoresistive strain sensors. *Compos. Part B Eng.* **2021**, *224*, 109199. [[CrossRef](#)]






15. Costa, P.; Oliveira, J.; Horta-Romarís, L.; Abad, M.J.; Moreira, J.A.; Zapiráin, I.; Aguado, M.; Galván, S.; Lanceros-Mendez, S. Piezoresistive polymer blends for electromechanical sensor applications. *Compos. Sci. Technol.* **2018**, *168*, 353–362. [[CrossRef](#)]
16. Padovano, E.; Bonelli, M.E.; Veca, A.; De Meo, E.; Badini, C. Effect of long-term mechanical cycling and laser surface treatment on piezoresistive properties of SEBS-CNTs composites. *React. Funct. Polym.* **2020**, *152*, 104601. [[CrossRef](#)]
17. Ma, L.; Lei, X.; Li, S.; Guo, S.; Yuan, J.; Li, X.; Cheng, G.J.; Liu, F. A 3D flexible piezoresistive sensor based on surface-filled graphene nanosheets conductive layer. *Sens. Actuators A Phys.* **2021**, *332*, 113144. [[CrossRef](#)]
18. Njuguna, M.K.; Yan, C.; Hu, N.; Bell, J.M.; Yarlalagadda, P.K.D.V. Sandwiched carbon nanotube film as strain sensor. *Compos. Part B Eng.* **2012**, *43*, 2711–2717. [[CrossRef](#)]
19. Akhtar, I.; Chang, S.H. Radial alignment of carbon nanotubes for directional sensing application. *Compos. Part B Eng.* **2021**, *222*, 109038. [[CrossRef](#)]
20. Akhtar, I.; Chang, S.H. Highly aligned carbon nanotubes and their sensor applications. *Nanoscale* **2020**, *12*, 21447–21458. [[CrossRef](#)]
21. Zeng, J.; Ma, W.; Wang, Q.; Yu, S.; Innocent, M.T.; Xiang, H.; Zhu, M. Strong, high stretchable and ultrasensitive SEBS/CNTs hybrid fiber for high-performance strain sensor. *Compos. Commun.* **2021**, *25*, 100735. [[CrossRef](#)]
22. Sam-daliri, O.; Faller, L.; Farahani, M.; Roshanghias, A. MWCNT-Epoxy Nanocomposite Sensors for Structural Health Monitoring. *Electronics* **2018**, *7*, 143. [[CrossRef](#)]
23. Enrique-Jimenez, P.; Quiles-Díaz, S.; Salavagione, H.J.; Wesner, D.; Schönherr, H.; González-Casablanca, J.; García-Quismondo, R.; Martínez, G.; Gómez-Fatou, M.; Ania, F.; et al. Control of the structure and properties of SEBS nanocomposites via chemical modification of graphene with polymer brushes. *Eur. Polym. J.* **2017**, *97*, 1–13. [[CrossRef](#)]
24. Costa, P.; Gonçalves, S.; Mora, H.; Carabineiro, S.A.C.; Viana, J.C.; Lanceros-Mendez, S. Highly Sensitive Piezoresistive Graphene-Based Stretchable Composites for Sensing Applications. *ACS Appl. Mater. Interfaces* **2019**, *11*, 46286–46295. [[CrossRef](#)] [[PubMed](#)]
25. Pan, S.; Pei, Z.; Jing, Z.; Song, J.; Zhang, W.; Zhang, Q.; Sang, S. A highly stretchable strain sensor based on CNT/graphene/fullerene-SEBS. *RSC Adv.* **2020**, *10*, 11225–11232. [[CrossRef](#)]
26. Ghabezi, P.; Farahani, M. *Effects of Nanoparticles on Nanocomposites Mode I and II Fracture: A Critical Review*; Mittal, K.L., Ed.; Scrivener Publishing LLC: Beverly, MA, USA, 2018; Volume 4, pp. 391–411. [[CrossRef](#)]
27. Hofmann, D.; Thomann, R.; Mülhaupt, R. Thermoplastic SEBS Elastomer Nanocomposites Reinforced with Functionalized Graphene Dispersions. *Macromol. Mater. Eng.* **2018**, *303*, 1700324. [[CrossRef](#)]
28. Turgut, A.; Tuhin, M.O.; Toprakci, O.; Pasquinelli, M.A.; Spontak, R.J.; Toprakci, H.A.K. Thermoplastic Elastomer Systems Containing Carbon Nanofibers as Soft Piezoresistive Sensors. *ACS Omega* **2018**, *3*, 12648–12657. [[CrossRef](#)]
29. Moreno, I.A.E.; Diaz, A.D.; Duarte, M.E.M.; Gómez, R.I. Strain effect on the electrical conductivity of CB/SEBS and GP/SEBS composites. *Macromol. Symp.* **2009**, *283–284*, 361–368. [[CrossRef](#)]
30. Yang, X.; Sun, L.; Zhang, C.; Huang, B.; Chu, Y.; Zhan, B. Modulating the sensing behaviors of poly(styrene-ethylene-butylene-styrene)/carbon nanotubes with low-dimensional fillers for large deformation sensors. *Compos. Part B Eng.* **2019**, *160*, 605–614. [[CrossRef](#)]
31. Kuester, S.; Merlini, C.; Barra, G.M.O.; Ferreira, J.C.; Lucas, A.; De Souza, A.C.; Soares, B.G. Processing and characterization of conductive composites based on poly(styrene-*b*-ethylene-*ran*-butylene-*b*-styrene) (SEBS) and carbon additives: A comparative study of expanded graphite and carbon black. *Compos. Part B Eng.* **2016**, *84*, 236–247. [[CrossRef](#)]
32. Commission EU. Commission recommendation of 18 October 2011 on the definition of nanomaterial (2011/696/EU). *Off. J. Eur. Communities Legis* **2011**, *275*, 38.
33. Jeong, Y.; Park, J.; Lee, J.; Kim, K.; Park, I. Ultrathin, Biocompatible, and Flexible Pressure Sensor with a Wide Pressure Range and Its Biomedical Application. *ACS Sens.* **2020**, *5*, 481–489. [[CrossRef](#)] [[PubMed](#)]
34. Aziz, S.; Chang, S.H. Smart-fabric sensor composed of single-walled carbon nanotubes containing binary polymer composites for health monitoring. *Compos. Sci. Technol.* **2018**, *163*, 1–9. [[CrossRef](#)]
35. Yang, T.; Deng, W.; Chu, X.; Wang, X.; Hu, Y.; Fan, X.; Song, J.; Gao, Y.; Zhang, B.; Tian, G.; et al. Hierarchically Microstructure-Bioinspired Flexible Piezoresistive Bioelectronics. *ACS Nano* **2021**, *15*, 11555–11563. [[CrossRef](#)] [[PubMed](#)]
36. Salavagione, H.J.; Shuttleworth, P.S.; Fernández-Blázquez, J.P.; Ellis, G.J.; Gómez-Fatou, M.A. Scalable graphene-based nanocomposite coatings for flexible and washable conductive textiles. *Carbon* **2020**, *167*, 495–503. [[CrossRef](#)]
37. Chen, T.; Wu, G.; Panahi-Sarmad, M.; Wu, Y.; Xu, R.; Cao, S.; Xiao, X. A novel flexible piezoresistive sensor using superelastic fabric coated with highly durable SEBS/TPU/CB/CNF nanocomposite for detection of human motions. *Compos. Sci. Technol.* **2022**, *227*, 109563. [[CrossRef](#)]
38. Qin, Z.; Chen, X.; Lv, Y.; Zhao, B.; Fang, X.; Pan, K. Wearable and high-performance piezoresistive sensor based on nanofiber/sodium alginate synergistically enhanced MXene composite aerogel. *Chem. Eng. J* **2023**, *451*, 138586. [[CrossRef](#)]
39. Olivieri, F.; Rollo, G.; De Falco, F.; Avolio, R.; Bonadies, I.; Castaldo, R.; Cocca, M.; Errico, M.E.; Lavoragna, M.; Gentile, G. Reduced graphene oxide/polyurethane coatings for wash-durable wearable piezoresistive sensors. *Cellulose* **2023**, *30*, 2667–2686. [[CrossRef](#)]
40. Parger, M.; Tang, C.; Xu, Y.; Twigg, C.D.; Tao, L.; Li, Y.; Wang, R.; Steinberger, M. UNOC: Understanding Occlusion for Embodied Presence in Virtual Reality. *IEEE Trans. Vis. Comput. Graph.* **2021**, *2626*, 4240–4251. [[CrossRef](#)]
41. Jiang, F.; Yang, X.; Feng, L. Real-time full-body motion reconstruction and recognition for off-the-shelf VR devices. In Proceedings of the VRCAI 2016 15th ACM SIGGRAPH Conference on Virtual-Reality Continuum and Its Applications in Industry, Zhuhai, China, 3–4 December 2016; Volume 1, pp. 309–318. [[CrossRef](#)]

42. Caserman, P.; Garcia-Agundez, A.; Gobel, S. A Survey of Full-Body Motion Reconstruction in Immersive Virtual Reality Applications. *IEEE Trans. Vis. Comput. Graph.* **2020**, *26*, 3089–3108. [[CrossRef](#)]
43. Matheve, T.; Brumagne, S.; Demoulin, C.; Timmermans, A. Sensor-based postural feedback is more effective than conventional feedback to improve lumbopelvic movement control in patients with chronic low back pain: A randomised controlled trial. *J. Neuroeng. Rehabil.* **2018**, *15*, 85. [[CrossRef](#)]
44. Nicolò, A.; Massaroni, C.; Passfield, L. Respiratory frequency during exercise: The neglected physiological measure. *Front. Physiol.* **2017**, *8*, 922. [[CrossRef](#)] [[PubMed](#)]
45. Klüppel, M. The Role of Disorder in Filler Reinforcement of Elastomers on Various Length Scales. *Adv. Polym. Sci.* **2003**, *164*, 1–86. [[CrossRef](#)]
46. Beckwith, T.G.; Buck, N.L.; Marangoni, R.D. *Mechanical Measurements*; Addison-Wesley Pub. Co.: Reading, MA, USA, 1982.
47. Pallas-Areny, R.; Webster, J.G. *Sensors and Signal Conditioning*; John Wiley & Sons: New York, NY, USA, 2012.

Disclaimer/Publisher’s Note: The statements, opinions and data contained in all publications are solely those of the individual author(s) and contributor(s) and not of MDPI and/or the editor(s). MDPI and/or the editor(s) disclaim responsibility for any injury to people or property resulting from any ideas, methods, instructions or products referred to in the content.

Article

Pressure-Driven Piezoelectric Sensors and Energy Harvesting in Biaxially Oriented Polyethylene Terephthalate Film

Romana Stepancikova ¹, Robert Olejnik ¹, Jiri Matyas ¹, Milan Masar ¹, Berenika Hausnerova ^{1,2} and Petr Slobodian ^{1,3,*}

¹ Centre of Polymer Systems, University Institute, Tomas Bata University, Trida T. Bati 5678, 76001 Zlin, Czech Republic; danova@utb.cz (R.S.); olejnik@utb.cz (R.O.); matyas@utb.cz (J.M.); masar@utb.cz (M.M.); hausnerova@utb.cz (B.H.)

² Department of Production Engineering, Faculty of Technology, Tomas Bata University in Zlin, Vavreckova 5669, 76001 Zlin, Czech Republic

³ Department of Physics and Materials Engineering, Tomas Bata University in Zlin, Vavreckova 5669, 76001 Zlin, Czech Republic

* Correspondence: slobodian@utb.cz

Abstract: This study reports the possibility of using biaxially oriented polyethylene terephthalate (BOPET) plastic packaging to convert mechanical energy into electrical energy. Electricity is generated due to the piezoelectricity of BOPET. Electricity generation depends on the mechanical deformation of the processing aids (inorganic crystals), which were found and identified by SEM and EDAX analyses as SiO₂. BOPET, as an electron source, was assembled and tested as an energy conversion and self-powered mechanical stimuli sensor using potential applications in wearable electronics. When a pressure pulse after pendulum impact with a maximum stress of 926 kPa and an impact velocity of 2.1 m/s was applied, a voltage of 60 V was generated with short-circuit current and charge densities of 15 μAcm^{-2} and 138 nCm^{-2} , respectively. Due to the orientation and stress-induced crystallization of polymer chains, BOPET films acquire very good mechanical properties, which are not lost during their primary usage as packaging materials and are beneficial for the durability of the sensors. The signals detected using BOPET sensors derived from pendulum impact and sieve analyses were also harvested for up to 80 cycles and up to 40 s with short-circuit voltages of 107 V and 95 V, respectively. In addition to their low price, the advantage of sensors made from BOPET plastic packaging waste lies in their chemical resistance and stability under exposure to oxygen, ultraviolet light, and moisture.

Keywords: flexible sensor; piezoelectricity; harvesting; biaxially oriented polyethylene terephthalate



Citation: Stepancikova, R.; Olejnik, R.; Matyas, J.; Masar, M.; Hausnerova, B.; Slobodian, P. Pressure-Driven Piezoelectric Sensors and Energy Harvesting in Biaxially Oriented Polyethylene Terephthalate Film. *Sensors* **2024**, *24*, 1275. <https://doi.org/10.3390/s24041275>

Academic Editor: Tian-Bing Xu

Received: 19 January 2024

Revised: 11 February 2024

Accepted: 14 February 2024

Published: 17 February 2024



Copyright: © 2024 by the authors. Licensee MDPI, Basel, Switzerland. This article is an open access article distributed under the terms and conditions of the Creative Commons Attribution (CC BY) license (<https://creativecommons.org/licenses/by/4.0/>).

1. Introduction

Piezoelectric materials convert mechanical energy into electrical energy. Among the most promising materials, piezoelectric ceramics, polymers, and polymer composites are notable for their versatility. They possess key attributes, such as flexibility, lightweight nature, effective processability through polymer processing, adaptability in design, and recyclability. This flexibility and adaptability render polymer composites particularly well-suited for applications such as sensors and energy harvesting devices [1–5]. Sensors constructed from these materials exhibit sensitivity to mechanical stimuli and can be integrated into self-powered systems and smart devices for various technical applications [2], including medical diagnostics [3], structural health monitoring [4], and wearable applications [5].

The concept of piezoelectric polymer materials represents the use of piezoelectric polymers such as poly(vinylidene fluoride) (PVDF) [6–8] or copolymers such as poly(vinylidene fluoride-trifluoroethylene) (P(VDF-TrFE)) [9] or poly(vinylidene fluoride-co-hexafluoropropylene)

(P(VDF-HFP)) [10]. In addition, the piezoelectric polymer can be mixed with a non-piezoelectric polymer, such as polyborosiloxane, to improve flexibility for detecting stimuli such as bending, shock, vibration, and breathing [11]. Another possibility is the preparation of piezoelectric composites consisting of piezoelectric ceramic particles distributed in a polymer matrix [12]. The polymer matrix can represent both piezoelectric polymers with added piezoelectric particles and common non-piezoelectric polymers with active piezoelectric particles. The first group can be represented by a PVDF matrix embedded with $\text{Cs}_2\text{AgBiBr}_6$ [13], nanostructured Zn- Fe_2O_3 nanoparticles [14], PVDF loaded with ZnO/ZnS core-shell nanoparticles for sustainable, wearable self-powered electrical devices [15], and BaTiO_3 particles dispersed in a piezoelectric polymeric PVDF-TrFE matrix providing flexibility and processability [16], all working as self-powered devices. The second group includes quasi-static pressure sensors or switches made from a polyamide-6 matrix with piezoelectric lead zirconate titanate (PZT) [17], PZT-porous polyurethane (PU) composites [2], calcium-modified lead titanate ceramics, and the thermoplastic polymer polyether ketone [18]. In this respect, a promising potential lies in the plastic waste that contains piezoelectric particles as the process or functional additives, as recently reported [19].

Piezoelectric generators, known as PENG, which are employed in various sectors, serve for energy harvesting and simultaneous deformation detection. Their applications include consumer goods, medical devices, engineering, automotive, aerospace, industrial settings, and security [20,21], as well as non-traditional applications such as piezoelectric harvesting generators for oceanic vehicles [22]. Polymer-based harvesting systems can incorporate PVDF thin films [8] as piezoelectric nanogenerators with an open-circuit voltage of 0.41 V, which is approximately 12 times greater than that of neat PVDF films [14] or elastic ultrathin PVDF-TrFE films applied as wearable remote devices for monitoring human body movements [23]. Polymer composites can also be applied as flexible and easy polymer processing to fabricate BaTiO_3 particles in PVDF-TrFE polymeric matrix composites, which provide an output voltage of 59.5 V and an output current of 6.52 μA of the PENG generator [16]. If PVDF was filled with $\text{Cs}_2\text{AgBiBr}_6$, an open-circuit voltage of 126 V, short-current density of 4.67 mA m^{-2} , output power density of 0.39 W m^{-2} , and the ability to light up at least 86 LED and power electronic devices such as a timer were obtained [13]. The conversion sensitivity of pure PVDF was 0.091 V/N compared to 0.153 V/N for the PVDF-ZnO/ZnS composite [15]. P(VDF-HFP) filled with polyaniline and methylammonium lead iodide ($\text{CH}_3\text{NH}_3\text{PbI}_3$) exhibited an open-circuit piezoelectric voltage output of 5 V and an output power of 8.2 nW [10].

Biaxially oriented polyethylene terephthalate (BOPET) is produced by blown extrusion into films intended for the flexible packaging of food and technical products. Plastics are always manufactured using processing aids and additives to adjust the properties of the final product. For BOPET films, mainly SiO_2 is used in small quantities in order to reduce friction during winding and handling. Currently, only the triboelectricity of BOPET is considered for the generation of nanogenerators [24,25]. In this study, BOPET containing SiO_2 particles is considered as a piezoelectric composite to construct self-powered sensors of mechanical stimuli and as a source of effective electrical energy harvesting, thereby generating electrical signals.

2. Materials and Methods

2.1. Material

A Tenolan[®] biaxially oriented polyethylene terephthalate (BOPET) film with a thickness of 50 μm was obtained from Fatra a.s., Napajedla, Czech Republic.

Fourier Transform Infrared (FTIR) spectroscopy analysis of the BOPET film was performed (FTIR Nicolet iS 5) using the Attenuated Total Reflectance (ATR) technique with a germanium crystal. The CO_2 background spectra were subtracted and each spectrum represented an average of 64 scans. The obtained spectra (Figure 1) were compared with the HR Polymer Additives and Plasticizers library using the Omnic software (version 8), which resulted in a match of 91%.

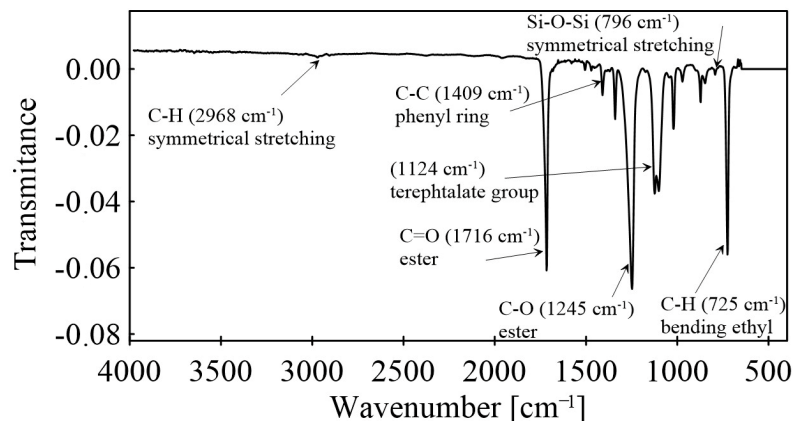


Figure 1. Fourier Transform Infrared (FTIR) spectroscopy spectra of BOPET film.

Dielectric thermal analysis (DETA) was conducted using a broadband dielectric/impedance analyzer (Concept 50, Novocontrol Technologies GmbH & Co. KG, Montabaur, Germany). The BOPET specimen was interposed between two gold-plated electrodes with a diameter of 20 mm. The measurements of relative permittivity and dielectric loss were then carried out across a frequency range of 1 Hz to 1 MHz at room temperature.

Dielectric thermal analysis was performed to determine the relative permittivity of the BOPET film. The results are presented in Figure 2 as frequency-dependent permittivity and dielectric loss values. The stable relative permittivity at low frequencies was 3.2. The results for our BOPET are consistent for the commercially well-known oriented polyester with the trade name Mylar[®] with a typical BOPET film dielectric constant value of 3.2 film at 20 °C and 1 kHz [26]. Mylar, which according to a datasheet is coated with SiO₂, was also investigated for its piezoelectric properties with a respective piezoelectric constant of 42.02 ± 10^{-12} m/V [27]. The dielectric constant of the piezoelectric layer improves the electrical output performance of piezoelectric nanogenerators [28].

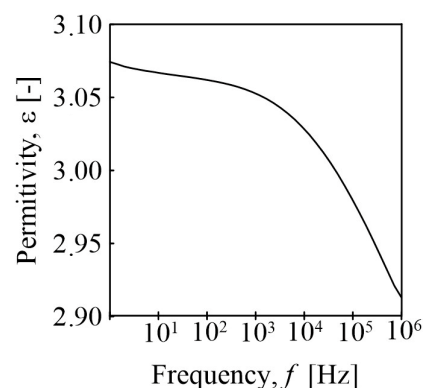


Figure 2. Dielectric relative permittivity of BOPET as a function of frequency at room temperature.

The determination of the crystalline content in BOPET involved X-ray diffraction (XRD) analysis using a MiniFlexTM diffractometer (Malvern Panalytical, Malvern, UK) with CoK β radiation at 40 kV and 15 mA. After scanning the sample in the 2 θ range of 10–90°, the collected data, initially obtained using a cobalt source, were converted to a copper source using PowDLL software.

The XRD analysis was aimed at validating the presence of a crystalline phase in the BOPET film, and the corresponding spectra are depicted in Figure 3. The crystallinity, denoted by X_c , was calculated using the following formula [29]:

$$X_c = \frac{\sum A_{cr}}{\sum A_{cr} + \sum A_{amr}} \times 100 [\%] \quad (1)$$

where ΣA_{amr} and ΣA_{cr} are the total integral areas of the amorphous and crystalline diffraction peaks, respectively.

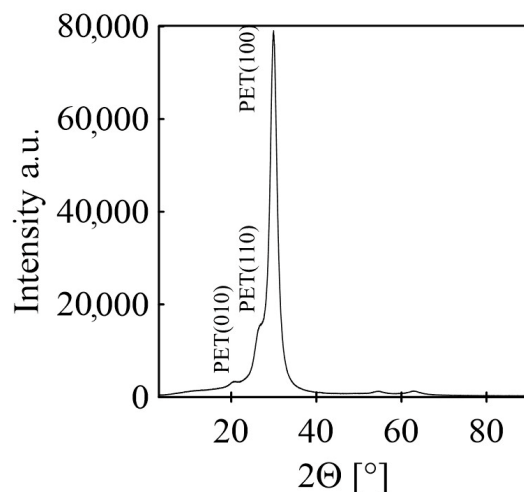


Figure 3. XRD analysis of the BOPET film.

According to this analysis, the crystallinity of the BOPET was approximately 71.5%. The spectrum of the BOPET film revealed a distinctive and well-defined peak. This characteristic feature signifies meticulously organized polymer chains with a notable crystalline phase. The crystallite size calculated according to the Scherrer equation [30] for peak 100 is 34.1 Å.

Differential scanning calorimetry (DSC) analysis (DSC 1, Perkin Elmer, Waltham, MA, USA) was used to analyze the BOPET film and amorphous PET prepared by subjecting molten PET to a rapid temperature drop in ice water (Figure 4). The samples weighed approximately 10 mg each. The BOPET film and amorphous PET were heated from 50 to 300 °C at a heating rate of 10 °C/min.

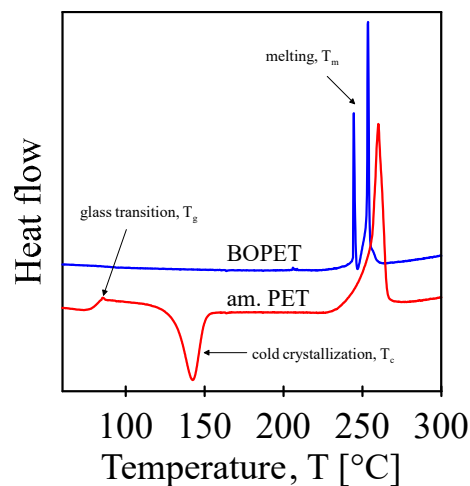


Figure 4. DSC analysis of BOPET film and BOPET film melted at 300 °C and then cooled by temperature jump to iced water at 0 °C.

DSC analysis confirmed that the BOPET used in this study was a semicrystalline polyethylene terephthalate polymer with parallel-oriented straight polymer chains. This was indirectly confirmed by the first measured thermo-analytical DSC curve of the BOPET film (see Figure 4), since only the melting of the crystalline phase can be observed, and no glass transition and cold crystallization were detected.

Moreover, the melting peak is bimodal, which means that there is melting of two fundamentally different types of crystals, where their structure determines the melting

temperature. A thermodynamically perfect crystal has a higher melting temperature. This corresponds with the results of the XRD diffractogram, which also describes the bimodal nature of the BOPET crystalline structure. The found melting temperatures defined as the peak temperatures are 245 °C and 254 °C, with melting enthalpies 9.3 and 23.0 J/g, respectively.

The sample for the second scan prepared as amorphous PET, apart from melting, exhibited two other thermal phenomena. It is a glass transition temperature of 85 °C with a transition enthalpy of 0.4 J/g, and exothermic cold crystallization at 142 °C with -24.4 J/g. These transitions were finally followed by a simple PET melting peak at 260 °C with 44.6 J/g.

2.2. Characterization Methods

The examination of processing aid distribution within packing plastics involved a comprehensive analysis conducted with a scanning electron microscope (SEM), specifically the NOVA NanoSEM 450 (FEI Co., Hillsboro, OR, USA) operating at an accelerating voltage of 10 kV. Energy-dispersive X-ray spectroscopy (EDX) was employed to determine the chemical composition of the solid particles observed on the surface.

2.3. BOPET Self-Powered Mechanical Stimuli Sensor

Figure 5 illustrates the schematics and photographs of the experimental setup designed for mechano-electrical piezo-electrification through the pressure loading of the BOPET film. Pressure pulses were administered using a rubber impact flexibility measurement apparatus (Polymer Test, Versta, Zlin, Czech Republic). In this setup, the BOPET film was positioned between two 25 mm \times 25 mm copper electrodes. The applied impact energy was 0.5 J, and the impact velocity was consistently maintained at 2.1 m/s.

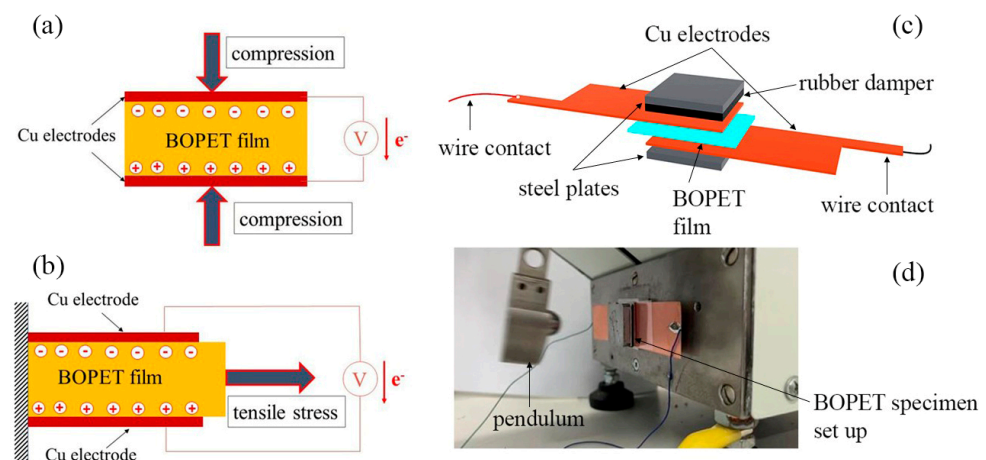


Figure 5. Schematic illustration of sensing systems for measuring the response of BOPET film to piezoelectric deformation by mechanical pressure stimuli (a) and tensile stress pulls (b), experimental setup for pressure mechanical loading (c), and arrangement of measurement (d).

A strain gauge (L6D-C3-40 kg, Zemic Europe B.V., Etten-Leur, The Netherlands) integrated into the apparatus effectively gauged the force applied during pendulum impact. The strain gauge was powered by an analog converter (TZA11410, VTS Zlin s.r.o., Zlin, Czech Republic) with a ± 20 mA output and 24V DC supply.

To monitor the generated piezoelectric voltage, an oscilloscope (Infinivision 1000 x-series, 4ch, 100 MHz, DSOX1204A, Keysight, Santa Rosa, CA, USA) with an input impedance of 1 M Ω was employed. To calculate the short-circuit current, Ohm's law was applied as one cycle discharged through electrically resistive loads of 10 k Ω , measured by an oscilloscope connected in parallel to the load. Finally, the charge generated per cycle was measured using an electro-scope (GRG-BTA charge sensor) connected to a LabQuest

interface system (Vernier, Edu-for s.r.o., Prague, Czech Republic). The measurement for different types of mechanical loading—applied tensile stress pulls—is shown in Figure 5b.

A schematic illustration of the experimental setup for the mechanical pressure loading of the BOPET film is shown in Figure 5c. The BOPET film was sandwiched between the two copper electrodes. The electrodes were protected by metal plates (25 mm × 25 mm) against damage from pendulum strikes induced by the equipment to test the impact flexibility of the rubbers. The photograph in Figure 5d shows the arrangement of measurements. The capacitance of the sensor was approximately 18 nF.

The BOPET film was stressed under tension when the stress pulls were derived from the defined free fall of the weight. The BOPET film was placed between two copper electrodes with a width of 20 mm and a length of 40 mm, with the possibility of free movement via deformations along the electrode length. The tensile pulse in the film was derived by free-falling weights along a 20 cm track with weights of 103, 237, and 325 g, respectively. The fall velocity was 2 m/s, and the maximum tensile stresses achieved by the free fall were 30.3, 46.7, and 76.6 MPa, respectively.

Further testing of the arrangement with the potential to be a self-powered mechanical stimulus sensor was performed in the following four arrangements. The first example is the tapping of a finger onto a sensor. Second, an analytical sieve shaker (Retsch AS200; Verder Scientific, Haan, Germany) was used as the vibration source. The third example represents the response to the impact of a glass ball weighing 52 g at a speed of 4.1 m/s. Finally, the vibrational pressure stress derived from the sonotrode of the Dr. Hielscher GmbH apparatus, UP200S (200 W, 24 kHz), was tested.

2.4. Energy Harvesting

The Graetz bridge incorporates a quartet of Schottky diodes with a diode opening voltage of 1.5 V, as shown in Figure 6 (according to [19]). These diodes played a pivotal role in transforming the piezoelectric AC voltage into a DC voltage. Subsequently, the accumulated charge was harvested into an 8 nF mica capacitor. Following the charge of the capacitor, the circuit underwent a brief transformation, redirecting its energy either towards an oscilloscope or illuminating a sequential series of seven LED diodes via a short circuit.

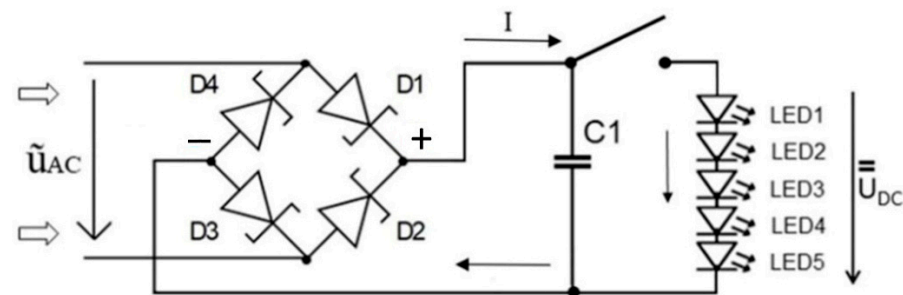


Figure 6. Schematic diagram of energy harvester incorporating the Graetz bridge based on Schottky diodes with storage capacitor and five LED diodes.

3. Results

The SEM analysis revealed that the particles of the processing aid were distributed in the BOPET film, while EDAX analysis was used to determine their chemical composition. The filler particles on the surface of the BOPET film were observed as light spots (Figure 7a). The different intensities of the emitted light indicate the different chemical natures of the dispersed particles. They have a broad distribution of diameters, ranging from units of micrometers to approximately 500 nm. Particular solid particles were also observed in its cross-section (Figure 7b), which means that they were distributed in the bulk, and thus were admixed into the polyester melt.

The details of the two typical types of particles found in the BOPET film are presented in the lower parts of Figure 7c,d. The first represents one solid particle and the other is an agglomerate formed by the clustering of smaller particles.

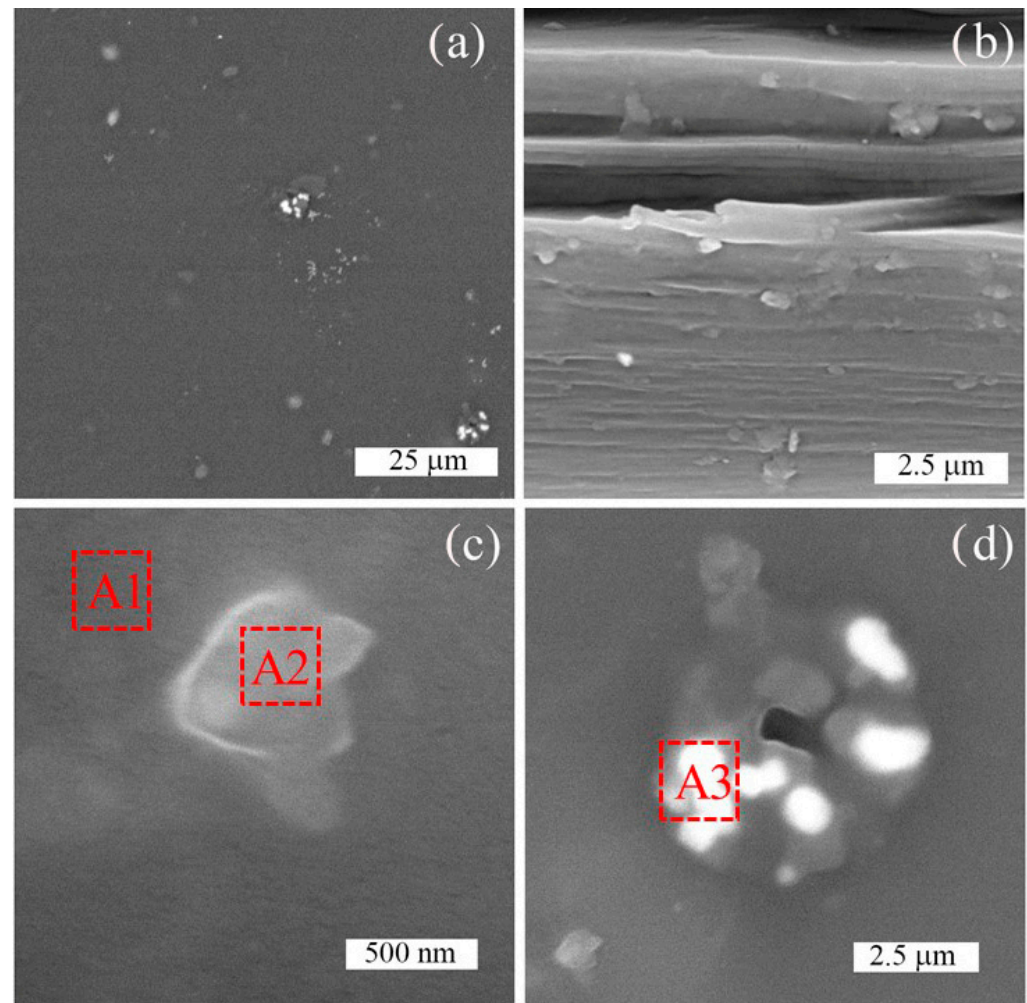


Figure 7. SEM analysis of (a) surface, (b) cross-section, and (c,d) detailed views of two particulate fillers identifiable in the polymer matrix. The red numbered squares show the places where the EDAX analysis was performed.

The results of the EDAX analysis are depicted in Table 1; in area A1, only C and O elements were found, corresponding to the pure polymer matrix, and area A2 contained silicon as evidence of SiO_2 . There were also traces of other elements, such as F, Na, Cl, and K. A3 areas showed significant representation of elements, such as F, Na, Cl, and K, and traces of Si and Ca. These can represent other process ingredients, such as antiblockers and sliding additives such as waxes, as well as surfactants (CaCO_3), for better sliding properties. Therefore, from the perspective of piezoelectric properties, BOPET can be considered as a polymer composite containing piezoelectric SiO_2 particles distributed in a polyester polymer matrix.

The electrical reaction of BOPET to mechanical compressive stress was produced by employing a pendulum to create mechanical vibrations. In a single impact of the pendulum, the subject sample experienced compression, leading to an initial voltage of approximately 16 V (the maximum measured pressure during the impact was ~ 148 kPa, and the impact velocity was ~ 2.1 m/s). As the pendulum recoils, the BOPET film relaxes, producing a voltage of the opposite polarity. The subsequent diminishing elastic vibrations of the film also resulted in voltage oscillations, which dissipated within 7 ms, as shown in Figure 8a. Furthermore, the effect of the amount of applied compression on the piezoelectric response was investigated. Figure 8b shows two (148 kPa and 926 kPa) of the seven tested pressures. The effect of the thickness of the BOPET film for a maximum applied pressure of 551 kPa

(Figure 8c) resulted in 38 V for the 50 μm film, 32 V for the 125 μm film, and 16 V for 150 μm the thick film.

Table 1. Results of EDAX analysis of particulate fillers found in the tested polymer waste packaging analyzed in areas A1–A3 depicted in Figure 7.

Area in SEM	Element	Weight %	Atomic %
A1	C	90.76	92.9
	O	9.24	7.1
A2	C	82.88	89.08
	O	8.36	6.74
	Si	5.56	2.6
	traces F, Na, Cl, K	-	-
A3	C	80.52	90.5
	O	3.19	2.69
	F	1.41	1
	Na	1.36	0.8
	Cl	5.67	2.16
	K	6.65	2.29
	Traces Si, Ca	-	-

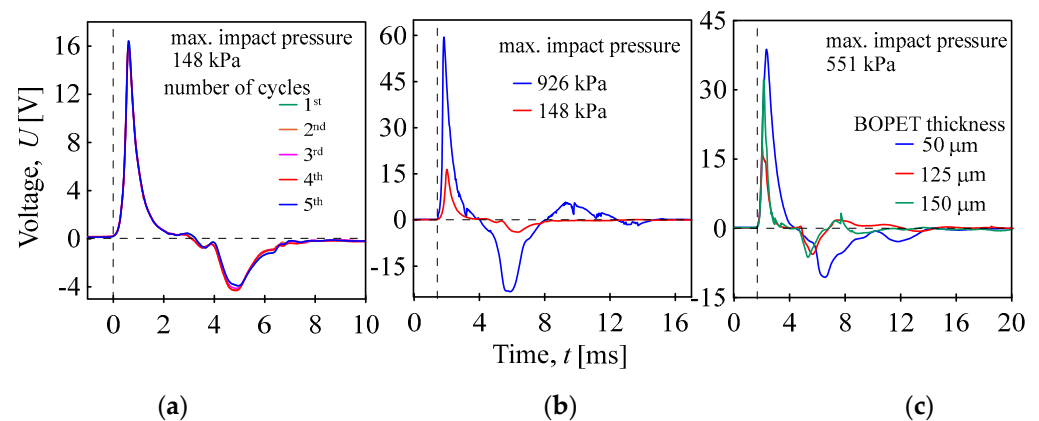


Figure 8. Piezoelectric responses of the BOPET film to pressure pulses after pendulum impact; five identical cycles (a), two different maximum pendulum impact pressures (b), and thickness of BOPET film (c).

The measurement confirms the assumption that by increasing the amount of compressive stress, the piezoelectric response increases from 16 V at 148 kPa to 60 V at 926 kPa. A greater level of deformation of the SiO_2 crystals leads to a higher piezoelectric voltage. The dependence of the maximum piezoelectric voltage on the maximum mechanical pressure caused by pendulum impact is shown in Figure 9. The generated voltage does not correspond linearly to the applied pressure, but the effect of pressure gradually decreases from values around 0.1 V/kPa to 0.05 V/kPa. A typical polymer compressive stress curve (dependence of strain on the applied stress) is also nonlinear. As the pressure increases, the influence of the pressure on the deformation decreases, and the material resists the deformation more. The piezoelectric properties are determined by the deformation of the crystalline SiO_2 lattice when the deformation of the polymer matrix is transferred. Thus, when the deformation of the polymer matrix is smaller, the effect of pressure on the piezoelectric response is also reduced.

The electrical reaction of BOPET to mechanical tensile stress pulls for different applied maximal stresses is presented in Figure 10. The specimen was elongated, followed by relaxation in length with time dependency as vibrations. The initial voltage of approximately 2.4 V for ~ 30.3 MPa and a velocity of ~ 2 m/s was measured.

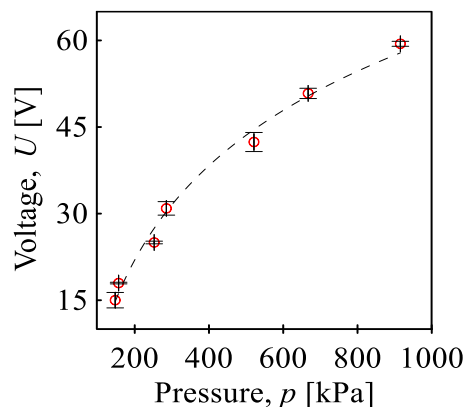


Figure 9. Generated maximum piezoelectric voltage on the maximum mechanical pressure caused by the pendulum impact on BOPET film.

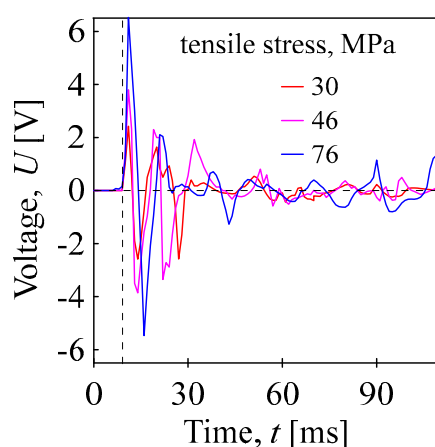


Figure 10. Piezoelectric responses of the BOPET film to tensile stress pulses for different stresses indicated.

Similar to the case of compressive stress, the piezoelectric response increased with the magnitude of the applied stress and the applied tensile stress, as shown in Figure 11. However, the BOPET sensor prepared in this way was much less sensitive to applied stress than it was in the case of pressure stress. The measured tensile stress dependency was linear, with a slope of approximately 0.09 V/MPa.

The BOPET film can serve as a mechanical–electrical transducer, as illustrated in Figure 9, showing its application in pendulum impact detection. Additional examples of this self-powered mechanical stimuli sensor are shown in Figure 12. The BOPET sensor, assembled according to the scheme in Figure 5a, was subjected to mechanical stimuli such as vibrations by a sieve analyzer, free-fall impact of a glass ball, or vibrational pressure stress induced by the sonotrode. In all scenarios, BOPET efficiently converted mechanical stimuli into a corresponding electrical signal, demonstrating sensitivity, real-time responsiveness, reversibility, and reproducibility. The response to the free fall impact of a glass ball weighing 52 g at a speed of 4.1 m/s attained 9.6 V, as shown in Figure 12a. In the other responses, the subsequent impacts of the ball caused by elastic rebound from the sensor with subsequent attenuation during repeated impacts were recorded. Figure 12b shows the response to a mechanical pressure stimulus derived using a sieve analysis machine. The sequences of cyclically repeating vibrations were observed with an approximate sequence frequency of ~17 Hz. A highly sensitive response of the sensor was recorded both during its compression and subsequent relaxation within a range of maximum voltages of 8 V. Finally, the vibrational pressure stress from the ultrasound region derived by the sonotrode was measured. The measurement was performed in pulse mode; Figure 12c depicts one pulse

with a converted electrical signal with a frequency of 22 kHz and a maximum amplitude of approximately ± 60 mV.

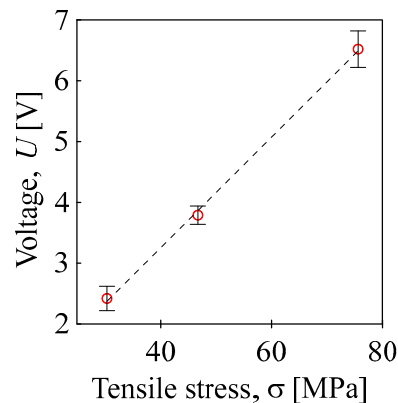


Figure 11. Maximum piezoelectric voltage generated on the tensile stress of BOPET sensor.

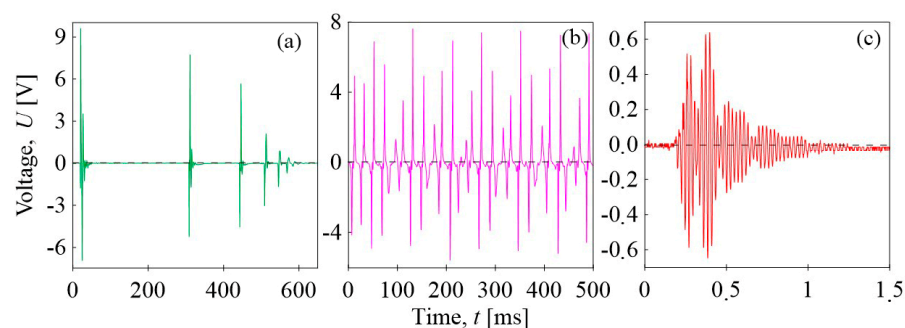


Figure 12. Electromechanical conversion by the BOPET film as a self-powered polymer sensor transforming mechanical stimuli into corresponding electrical signals: (a) free fall impact of a glass ball, (b) vibration by sieving machine, and (c) the vibrational pressure stress derived by the sonotrode.

Examples of self-powered mechanical stimulus sensors for wearable flexible electronics are shown in Figure 13. The response of the sensor to the tapping of the finger is sensitive and reversible, and the maximum generated electric voltage is approximately 5 V; when steps are taken with the sensor placed under the heel, it generates a voltage of more than 2 V.

The pendulum impact on the BOPET film and vibrations delivered by sieve analysis was converted into an electric signal. This energy can be stored simultaneously, turning mechanical energy into electricity through mechano-electrical conversion. The generated piezoelectric voltage is in the form of AC, and for effective utilization, it must be rectified into DC. This was achieved using the Graetz Bridge, a full-bridge rectifier. The final DC charge can then be stored in the capacitor. After charging the capacitor, it can be short-circuited. Figure 14 shows the time-dependent short-circuited voltage, which was stored in the capacitor for varying durations of the sieve analysis apparatus vibration detection/conversion, different numbers of pressure pulses after pendulum impact, and tensile stress pulses. After the short circuit, the voltage response reaches a significant maximum and then decays exponentially to zero over time. The discharge times for all harvesting times ranged up to 350 ms after a short circuit. The lowest values were obtained for tensile stress pulses (above 20 V after 80 cycles). The size of the peaks increased with the number of pendulum impacts, reaching approximately 107 V for 80 impact cycles, and the duration of the sieve analysis vibration was 95 V for 40 s. The demonstration of the potential to utilize stored energy is evident in the flashing of seven yellow LED diodes connected in series for impact cycles, seven green LED diodes for energy from vibrations, and five red LED diodes for tensile pulses with a lighting duration of approximately 10 ms.

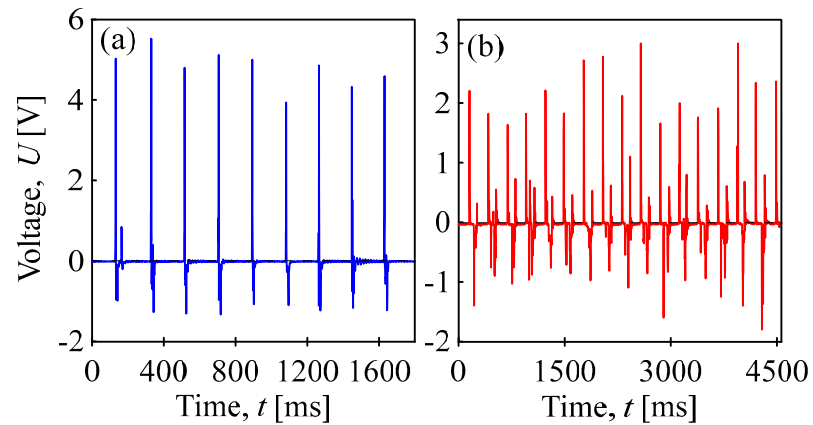


Figure 13. Electromechanical conversion by the BOPET film as a self-powered polymer sensor transforming mechanical stimuli into corresponding electrical signals applied in the area of wearable electronics: (a) tapping of finger, blue; (b) steps taken with the sensor placed under the heel, red.

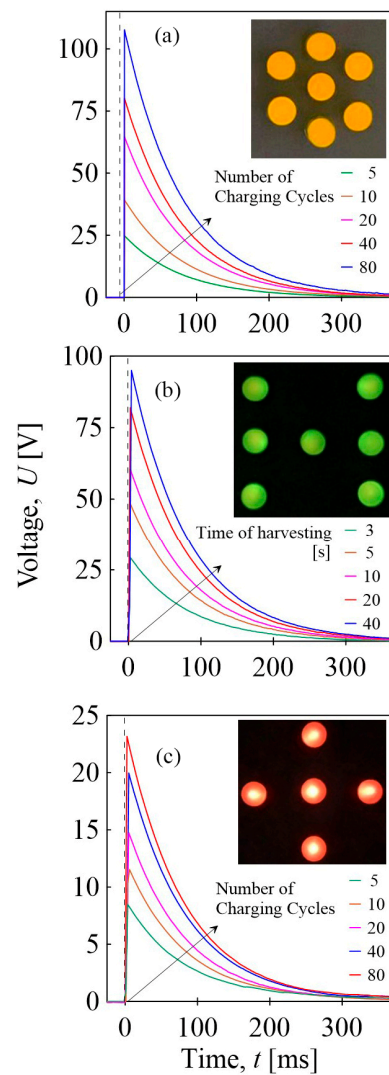


Figure 14. The short-circuited voltage of the charged capacitor by: (a) pressure pulses after pendulum impact onto BOPET foil, (b) vibrations delivered by sieve analysis apparatus, and (c) tensile stress pulses. Light flash of seven yellow LED diodes connected in series after 10 impact cycles, seven green ones after 10 s of vibration harvesting, and five red diodes after 80 tensile pulse cycles.

4. Discussion

This article reports an important finding that polymer packaging materials can have unexpected properties, and their waste can be further employed in the area of sensors and energy harvesting.

The idea that polymeric packaging waste can be converted into electrical energy should be understood as a way to produce renewable energy. A renewable energy source is defined as energy that can renew itself on a human timescale. In connection with this, various types of waste have been considered, especially those leading to caloric utilization. This is how biomass, biogas, and waste incineration are used, or hydrogen is produced by the pyrolysis of waste plastics [31]. Solid municipal waste is also a source of renewable energy instead of being landfilled [32]. Alternatively, fuel for ignition engines is produced from waste plastics [33].

The intricate process of the production of biaxially oriented polyethylene terephthalate films, primarily intended for food packaging applications, unfolds through the biaxial stretching of amorphous polyethylene terephthalate and its subsequent crystallization under tension within the heat exposed. The heat-setting stage is crucial to prevent the film from reverting to its initial unstretched state and firmly anchoring the alignment of the polymer chains in the film direction. Notably, this molecular alignment triggers the initiation and growth of the embryonic crystals.

Examination of the structure revealed a consistent edge-on crystalline orientation between the rigid amorphous fraction and mobile amorphous fraction [34]. The presence of the rigid fraction in BOPET plays a crucial role in reducing the polymer chain mobility, consequently impacting the potential conductivity of the charge carriers. All the lamellar crystals in the BOPET films exhibited an edge-on configuration. This characteristic minimizes the hindrance of charge-carrier conduction imposed by these crystals [35].

Additives are incorporated into polyethylene terephthalate and other thermoplastics to modify their processing properties. However, in this study, it is demonstrated that they can have a different function in the recycling of polymer packaging.

In the case of the BOPET film, SiO₂ was added to pure polyethylene terephthalate as an additive to reduce the generation of unwanted static electricity during film winding. Using BOPET waste, we obtained a polymer composite with a PET matrix, in which the piezoelectric filler was distributed. Therefore, the entire packaging polymer film was piezoelectric.

When the film is mechanically stimulated, mechanical energy is converted into electricity. This conversion is highly sensitive, and the response is reversible in real-time deformation. Moreover, it is a function of the applied mechanical stress, and the generated electrical voltage increases with increasing stress. In this way, the waste material is applicable as a self-powered sensor of mechanical stimuli, where the further generated signal can serve as effective electrical energy through the harvesting process.

As previously mentioned, poly (vinylidene fluoride) is a rare polymer material that serves as a piezoelectric energy harvester. The PVDF-based nanogenerators usually provide very good output values; a piezoelectric organic–inorganic hybrid PVDF-TrFE nanocomposite film with BaTiO₃ nanoparticles showed output voltages of 59.5 V, but at a low compression pressure of 100 N [16], P(VDF-HFP) filled with polyaniline and (CH₃NH₃PbI₃) has an excellent output power of 8.2 nW at a pressure amplitude of ~14 kPa [10].

However, these materials are purpose-built, expensive, toxic, and chemically unstable. However, the material proposed in this paper, where approximately 60 V for a pendulum impact with a pressure of 926 kPa was obtained, solves some of the drawbacks associated with PVDF-based nanogenerators, as BOPET is a harmless material intended for contact with food.

Currently, flexible materials can effectively serve as self-powered sensors for signaling external stimuli. Due to their convenient elastic properties, they can be utilized in high-tech areas, such as soft robotics [36] and wearable electronics [37]. As a source of energy based on ever-improving methods of harvesting, innovative procedures can be applied

to obtain higher-energy performance from low-energy sources, for example, by grouping and connecting them in series and blocks. Examples with a potential perspective in this area include piezoelectricity for the conversion of wind energy [38] or the conversion of mechanical energy of vehicles on highway power supply systems [39].

5. Conclusions

The aim of this study was to use a waste BOPET film to prepare a mechanical stimuli sensor and provide mechano-electrical conversion for useful electrical energy generation. Due to its orientation and stress-induced crystallization of polymer chains, BOPET acquires very good mechanical properties, which are beneficial for the durability of sensors and the long-term generation of electrical energy from sources such as (otherwise wasted) vibrations of machines. Due to the flexibility of BOPET, such sensors are suitable for wearable electronics. The SiO₂ particles added to BOPET as a technological additive during the production of films for the packaging of food as well as technical products, including electronics, bring piezoelectricity to BOPET. The aforementioned possibility of contact with food shows that it is a polymer composite, which is not toxic or harmful to human health. This is another great advantage of BOPET sensors if one considers that a number of solutions for piezoelectric polymer composites are based on harmful inorganic fillers. In addition to its excellent mechanical properties, BOPET shows good temperature stability, and according to DSC, the material shows no changes up to the melting temperature of the crystalline phase of approximately 245 °C; thus, it can be considered a high-temperature resistant material. Its chemical resistance should also be mentioned, as it dissolves only in strong solvents, such as trifluoroethanol or fluoroacetic acid. Finally, it is stable when exposed to oxygen, ultraviolet light, and moisture.

Author Contributions: Conceptualization, P.S.; methodology, P.S., R.O. and J.M.; validation, P.S., R.S., R.O. and J.M.; formal analysis, P.S.; investigation, P.S., R.S. and M.M.; resources, P.S.; data curation, P.S. and M.M.; writing—original draft preparation, P.S. and R.S.; writing—review and editing, B.H.; visualization, P.S. and B.H.; supervision, P.S.; project administration, P.S. and B.H.; funding acquisition, P.S. and B.H. All authors have read and agreed to the published version of the manuscript.

Funding: This work was supported by the Ministry of Education, Youth, and Sports of the Czech Republic within the framework of DKRVO, authors P.S., R.O., J.M.—RP/CPS/2022/007, and B.H.—RP/CPS/2022/003.

Institutional Review Board Statement: Not applicable.

Informed Consent Statement: Not applicable.

Data Availability Statement: Data obtained throughout the study were stored according to the TBU Data Management Plan and are available upon request from the corresponding author.

Conflicts of Interest: The authors declare no conflicts of interest.

References

1. Sappati, K.K.; Bhadra, S. Piezoelectric Polymer and Paper Substrates: A Review. *Sensors* **2018**, *18*, 3605. [\[CrossRef\]](#)
2. Khanbareh, H.; de Boom, K.; van der Zwaag, S.; Groen, W.A. Highly sensitive piezo particulate-polymer foam composites for robotic skin application. *Ferroelectrics* **2017**, *515*, 25–33. [\[CrossRef\]](#)
3. Ali, F.; Koc, M. 3D Printed Polymer Piezoelectric Materials: Transforming Healthcare through Biomedical Applications. *Polymers* **2023**, *15*, 4470. [\[CrossRef\]](#) [\[PubMed\]](#)
4. Ghadarah, N.; Ayre, D. A Review on Acoustic Emission Testing for Structural Health Monitoring of Polymer-Based Composites. *Sensors* **2023**, *23*, 6945. [\[CrossRef\]](#) [\[PubMed\]](#)
5. Chang, S.-M.; Hur, S.; Park, J.; Lee, D.-G.; Shin, J.; Kim, H.S.; Song, S.E.; Baik, J.M.; Kim, M.; Song, H.-C.; et al. Optimization of piezoelectric polymer composites and 3D printing parameters for flexible tactile sensors. *Addit. Manuf.* **2023**, *67*. [\[CrossRef\]](#)
6. Slobodian, P.; Olejnik, R.; Matyas, J.; Hausnerova, B.; Riha, P.; Danova, R.; Kimmer, D. Electrical Detection of Vibrations of Electrospun PVDF Membranes. *Int. J. Mol. Sci.* **2022**, *23*, 14322. [\[CrossRef\]](#) [\[PubMed\]](#)

7. He, Z.; Mohsenzadeh, E.; Zhang, S.; Rault, F.; Salaün, F. Development of high-sensitive piezoelectric nanogenerators of all-organic PVDF multilayer nanofibrous membrane with innovative 3D structure via electrohydrodynamic processes. *J. Polym. Res.* **2023**, *30*, 1–15. [[CrossRef](#)]
8. Li, S.; Crovetto, A.; Peng, Z.; Zhang, A.; Hansen, O.; Wang, M.; Li, X.; Wang, F. Bi-resonant structure with piezoelectric PVDF films for energy harvesting from random vibration sources at low frequency. *Sens. Actuators A Phys.* **2016**, *247*, 547–554. [[CrossRef](#)]
9. Oh, S.R.; Yao, K.; Zhang, L.; Tay, F.E.H. Asymmetric electrode design for significant performance enhancement of piezoelectric P(VDF-TrFE) polymer microcantilevers. *Smart Mater. Struct.* **2015**, *24*, 045035. [[CrossRef](#)]
10. Barman, P.S.; Garain, S.; Adhikary, P. A self-powered mechanical energy harvester based on CH₃NH₃PbI₃ doped P(VDF-HFP)/PANI composite films. *Phys. Chem. Chem. Phys.* **2023**, *25*, 30583–30595. [[CrossRef](#)]
11. Zhou, Z.; You, C.; Chen, Y.; Xia, W.; Tian, N.; Li, Y.; Wang, C. Piezoelectric sensing performance of flexible P(VDF-TrFE)/PBDM porous polymer materials. *Org. Electron.* **2022**, *105*, 106491. [[CrossRef](#)]
12. Lushcheikin, G.A. New polymer-containing piezoelectric materials. *Phys. Solid State* **2006**, *48*, 1023–1025. [[CrossRef](#)]
13. Wang, M.; Wang, X.; Xu, Y.; Chai, S.; Zhao, Z.; Li, Q.; Wu, J.; Chen, J.; Zhu, Z.; Bae, B.S.; et al. Enhanced nanogenerator by embedding lead-free double perovskite Cs₂AgBiBr₆ in polymer matrix for hybrid energy harvesting. *J. Mater. Chem. C* **2023**, *12*, 207–220. [[CrossRef](#)]
14. Yempally, S.; Magadia, P.; Ponnamma, D. Effect of Zn-Fe₂O₃ nanomaterials on the phase separated morphologies of polyvinylidene fluoride piezoelectric nanogenerators. *RSC Adv.* **2023**, *13*, 33863–33874. [[CrossRef](#)]
15. Ali, N.; Kenawy, E.-R.; Wadoud, A.A.; Elhadary, M.I. Wearable Electrospun Piezoelectric Mats Based on a PVDF Nanofiber-ZnO@ZnS Core-Shell Nanoparticles Composite for Power Generation. *Nanomaterials* **2023**, *13*, 2833. [[CrossRef](#)]
16. Cho, Y.; Jeong, J.; Choi, M.; Baek, G.; Park, S.; Choi, H.; Ahn, S.; Cha, S.; Kim, T.; Kang, D.-S.; et al. BaTiO₃@PVDF-TrFE nanocomposites with efficient orientation prepared via phase separation nano-coating method for piezoelectric performance improvement and application to 3D-PENG. *Chem. Eng. J.* **2022**, *427*, 131030. [[CrossRef](#)]
17. Van Den Ende, D.A.; Groen, W.A.; Van Der Zwaag, S. Development of temperature stable charge based piezoelectric composite quasi-static pressure sensors. *Sens. Actuators A Phys.* **2010**, *163*, 25–31. [[CrossRef](#)]
18. Marin-Franch, P.; Martin, T.; Tunnicliffe, D.; Das-Gupta, D. PTCa/PEKK piezo-composites for acoustic emission detection. *Sens. Actuators A Phys.* **2002**, *99*, 236–243. [[CrossRef](#)]
19. Slobodian, P.; Olejnik, R.; Matyas, J.; Riha, P.; Hausnerova, B. A coupled piezo-triboelectric nanogenerator based on the electrification of biaxially oriented polyethylene terephthalate food packaging films. *Nano Energy* **2023**, *118*, 108986. [[CrossRef](#)]
20. Peng, Y.; Xu, Z.; Wang, M.; Li, Z.; Peng, J.; Luo, J.; Xie, S.; Pu, H.; Yang, Z. Investigation of frequency-up conversion effect on the performance improvement of stack-based piezoelectric generators. *Renew. Energy* **2021**, *172*, 551–563. [[CrossRef](#)]
21. Zhou, L.; Sun, J.; Zheng, X.; Deng, S.; Zhao, J.; Peng, S.; Zhang, Y.; Wang, X.; Cheng, H. A model for the energy harvesting performance of shear mode piezoelectric cantilever. *Sens. Actuators A Phys.* **2012**, *179*, 185–192. [[CrossRef](#)]
22. Li, Z.; Peng, Y.; Xu, Z.; Peng, J.; Xin, L.; Wang, M.; Luo, J.; Xie, S.; Pu, H. Harnessing energy from suspension systems of oceanic vehicles with high-performance piezoelectric generators. *Energy* **2021**, *228*, 120523. [[CrossRef](#)]
23. Bae, J.; Song, J.; Jeong, W.; Nandanapalli, K.R.; Son, N.; Zulkifli, N.A.B.; Gwon, G.; Kim, M.; Yoo, S.; Lee, H.; et al. Multi-deformable piezoelectric energy nano-generator with high conversion efficiency for subtle body movements. *Nano Energy* **2022**, *97*, 107223. [[CrossRef](#)]
24. Syamini, J.; Chandran, A. Mylar Interlayer-Mediated Performance Enhancement of a Flexible Triboelectric Nanogenerator for Self-Powered Pressure Sensing Application. *ACS Appl. Electron. Mater.* **2023**, *5*, 1002–1012. [[CrossRef](#)]
25. Bhavya, A.S.; Varghese, H.; Chandran, A.; Surendran, K.P. Massive enhancement in power output of BoPET-paper triboelectric nanogenerator using 2D-hexagonal boron nitride nanosheets. *Nano Energy* **2021**, *90*, 106628. [[CrossRef](#)]
26. DuPont Tijin Films. Available online: <http://www.dupontteijinfilms.com> (accessed on 2 January 2024).
27. Zúñiga, V.T.; Carmona, S.G.; Saavedra, O.G.M. Electromechanical characterization of didactical piezoelectric sensors based on crystalline grade PET. *J. Phys. Conf. Ser.* **2019**, *1221*, 012059. [[CrossRef](#)]
28. Amangeldinova, Y.; Aben, D.; Ma, X.; Ahn, H.; Kim, K.; Shin, D.-M.; Hwang, Y.-H. Enhancing Electrical Outputs of Piezoelectric Nanogenerators by Controlling the Dielectric Constant of ZnO/PDMS Composite. *Micromachines* **2021**, *12*, 630. [[CrossRef](#)] [[PubMed](#)]
29. Slobodian, P. Rigid amorphous fraction in poly(ethylene terephthalate) determined by dilatometry. *J. Therm. Anal. Calorim.* **2008**, *94*, 545–551. [[CrossRef](#)]
30. Holzwarth, U.; Gibson, N. The Scherrer equation versus the ‘Debye-Scherrer equation. *Nat. Nanotechnol.* **2011**, *6*, 534. [[CrossRef](#)] [[PubMed](#)]
31. Kothari, R.; Tyagi, V.; Pathak, A. Waste-to-energy: A way from renewable energy sources to sustainable development. *Renew. Sustain. Energy Rev.* **2010**, *14*, 3164–3170. [[CrossRef](#)]
32. Hossain, H.Z.; Hossain, Q.H.; Monir, M.U.; Ahmed, T. Municipal solid waste (MSW) as a source of renewable energy in Bangladesh: Revisited. *Renew. Sustain. Energy Rev.* **2014**, *39*, 35–41. [[CrossRef](#)]
33. Bukkarapu, K.R.; Gangadhar, D.S.; Jyothi, Y.; Kanasani, P. Management, conversion, and utilization of waste plastic as a source of sustainable energy to run automotive: A review. *Energy Sources A Recover. Util. Environ. Eff.* **2018**, *40*, 1681–1692. [[CrossRef](#)]

34. Li, Y.; Makita, Y.; Zhang, G.; Rui, G.; Li, Z.-M.; Zhong, G.-J.; Miyoshi, T.; Huang, H.-D.; Zhu, L. Effects of Rigid Amorphous Fraction and Lamellar Crystal Orientation on Electrical Insulation of Poly(ethylene terephthalate) Films. *Macromolecules* **2020**, *53*, 3967–3977. [[CrossRef](#)]
35. Badia, J.; Strömberg, E.; Karlsson, S.; Ribes-Greus, A. The role of crystalline, mobile amorphous and rigid amorphous fractions in the performance of recycled poly (ethylene terephthalate) (PET). *Polym. Degrad. Stab.* **2012**, *97*, 98–107. [[CrossRef](#)]
36. Pan, M.; Yuan, C.; Liang, X.; Zou, J.; Zhang, Y.; Bowen, C. Triboelectric and Piezoelectric Nanogenerators for Future Soft Robots and Machines. *iScience* **2020**, *23*, 101682. [[CrossRef](#)] [[PubMed](#)]
37. Zhao, B.; Qian, F.; Hatfield, A.; Zuo, L.; Xu, T.-B. A Review of Piezoelectric Footwear Energy Harvesters: Principles, Methods, and Applications. *Sensors* **2023**, *23*, 5841. [[CrossRef](#)] [[PubMed](#)]
38. Sun, C.; Shang, G. Research Status of Wind Energy Piezoelectric Generator. *Energy Power Eng.* **2018**, *10*, 487–507. [[CrossRef](#)]
39. Yang, H.; Wang, L.; Zhou, B.; Wei, Y.; Zhao, Q. A preliminary study on the highway piezoelectric power supply system. *Int. J. Pavement Res. Technol.* **2017**, *11*, 168–175. [[CrossRef](#)]

Disclaimer/Publisher’s Note: The statements, opinions and data contained in all publications are solely those of the individual author(s) and contributor(s) and not of MDPI and/or the editor(s). MDPI and/or the editor(s) disclaim responsibility for any injury to people or property resulting from any ideas, methods, instructions or products referred to in the content.

Ing. Romana Štěpančíková

Polymerní kompozitní materiály pro nositelnou elektroniku

Polymer composite materials for wearable electronic

Disertační práce

Publikováno: Univerzita Tomáše Bati ve Zlíně

nám. T. G. Masaryka 5555, 760 01 Zlín.

Editace: publikováno elektronicky

Sazba: Romana Štěpančíková

Tato publikace neprošla žádnou korekturou ani redakční kontrolou

Rok: 2024